UNIVERSIDADE FEDERAL DE SANTA CATARINA
CENTRO DE CIÊNCIAS BIOLÓGICAS
PROGRAMA DE PÓS-GRADUAÇÃO EM BIOTECNOLOGIA E BIOCIÊNCIAS

Bruna Rodrigues Moreira

Algas vermelhas como fonte de compostos bioativos: estratégias de regulação, cultivo e aplicação

Florianópolis
2023

Bruna Rodrigues Moreira

Algas vermelhas como fonte de compostos bioativos: estratégias de regulação, cultivo e aplicação

Tese submetida ao Programa de Pós-Graduação em Biotecnologia e Biociências da Universidade Federal de Santa Catarina como requisito parcial para a obtenção do título de Doutora em Biociências e Biotecnologia.

Orientador: Prof. José Bonomi Barufi, Dr.
Coorientadores: Prof. Marcelo Maraschin, Dr., e Prof. Félix López Figueroa, Dr.

Florianópolis

2023

Moreira, Bruna Rodrigues
Algas vermelhas como fonte de compostos bioativos : estratégias de regulação, cultivo e aplicação / Bruna Rodrigues Moreira ; orientador, José Bonomi Barufi, coorientador, Marcelo Maraschin, coorientador, Félix López Figueroa, 2023.
202 p.

Dissertação (mestrado profissional) - Universidade Federal de Santa Catarina, Centro de Ciências Biológicas, Programa de Pós-Graduação em Biotecnologia e Biociências, Florianópolis, 2023.

Inclui referências.

1. Biotecnologia e Biociências. 2. Macroalgas. 3. Prospecção. 4. Fotossíntese. 5. Atividades biológicas. I. Barufi, José Bonomi. II. Maraschin, Marcelo . III. Figueroa, Félix López IV. Universidade Federal de Santa Catarina. Programa de Pós-Graduação em Biotecnologia e Biociências. V. Título.

Bruna Rodrigues Moreira

Algas vermelhas como fonte de compostos bioativos: estratégias de regulação, cultivo e aplicação

O presente trabalho em nível de Doutorado foi avaliado e aprovado, em 17 de julho de 2023, pela banca examinadora composta pelos seguintes membros:

Prof. Leonardo Rubi Rorig, Dr.
Instituição: Universidade Federal de Santa Catarina

Prof.(a) Nathalie Korbee Peinado, Dr.(a)
Instituição: Universidad de Málaga

Prof. Eduardo Walter Helbling, Dr.
Instituição: Estación de Fotobiología Playa Unión

Prof.(a) Helen Treichel
Instituição: Universidade Federal de Santa Catarina

Dra. Paula Celis Plá
Instituição: Centro de Ciências Ambientales

Certificamos que esta é a versão original e final do trabalho de conclusão que foi julgado adequado para obtenção do título de Doutora em Biotecnologia e Biociências.

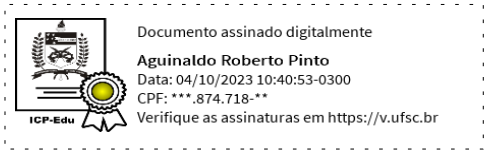

Coordenação do Programa de Pós-Graduação

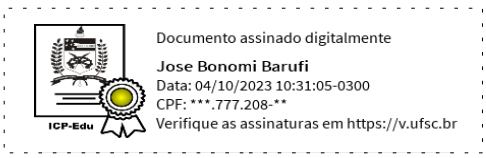

Prof. José Bonomi Barufi, Dr.

Orientador

Florianópolis, 2023

Dedico este trabalho as minhas avós Iracilda e Anésia (in memoriam), as matriarcas da família.

AGRADECIMENTOS

Primeiramente agradeço à minha família: aos meus pais Dainie e Moacir, e aos meus irmãos Mariana e Higor, por sempre me apoiarem em todos os momentos que me fizeram chegar até aqui. Em especial à Mariana, por estar sempre presente para a nossa família, me permitindo morar longe, mas com o coração mais tranquilo.

Agradeço, de todo meu coração, ao meu orientador e amigo Prof. José Bonomi, que mesmo sem me conhecer me recebeu de braços abertos em Florianópolis e me orientou nesta trajetória tão bonita. Meus agradecimentos também são aos professores Leonardo Rorig e Paulo Horta, pelo companheirismo e o cuidado de sempre. Sem essa tríade de "paizões" o LAFIC definitivamente não seria esta grande família que é.

Agradeço aos meus coorientadores por abrirem as portas de seus laboratórios em momentos tão importantes do meu doutorado. O professor Marcelo Maraschin que me recebeu tão bem no início de tudo, incluindo o início da pandemia. Agradeço especialmente ao professor Félix Figueroa, que me possibilitou viver uma das maiores oportunidades da minha vida pessoal e profissional: o intercâmbio de um ano na Espanha, no auge da pandemia, e que agregou importantemente a este doutorado.

Agradeço, especialmente, aos amigos que fiz nos laboratórios em que trabalhei: LAFIC, LMBV e FYBOA. Muito obrigada a todos por fazerem este caminho mais leve e mais divertido. Obrigada por sempre ajudarem nos momentos de crise, nas contribuições científicas, por estarem sempre prontos para o bar de sexta e para o "*perreo*" do final de semana.

Agradeço à minha família e aos meus amigos goianos que estão espalhados por este mundão. Obrigada por entenderem e me apoiarem em cada momento, apesar da distância física. Agradeço também a todas os meus amigos e companheiros de estadia aqui em "Flonopix" e em Málaga, com quem tive o prazer de dividir oito casas diferentes. Agradeço às mulheres/amigas do grupo Cores de Aidê, do qual eu faço parte, e que me enchem de amor e alegria através do batuque.

Agradeço à minha fé, que independente de religião, me ajuda a seguir todos os dias acreditando que estou contribuindo para um futuro melhor, baseado na ciência e no progresso para uma sociedade mais justa e igualitária.

Por fim, agradeço à Universidade Federal de Santa Catarina e Universidad de Málaga, que me deram todo o suporte estrutural e técnico que precisei. Agradeço a todos os membros do Laboratório de Ficologia, Laboratório de Morfologia e Biotecnologia Vegetal, Laboratório

de Fotobiología e Biotecnología de Organismos acuáticos (FYBOA - UMA), a empresa Five Rabbits e aos Servicios Centrales de Apoyo a la Investigación (SCAI - UMA). Agradeço ao suporte financeiro fornecido pela Coordenação de Aperfeiçoamento de Pessoal de Nível Superior (CAPES), pela bolsa vigente no Brasil (DS no 88882.438333/2019-01) e a bolsa de doutorado sanduíche (edital/ PRINT no 88887.578926/2020-00), que me permitiram realizar este trabalho.

Finalizo este agradecimento citando uma frase sempre dita pela minha mãe: “Bruna, você é muito sortuda por sempre encontrar pessoas maravilhosas no seu caminho”. Então, agradeço a todos vocês (sem citar nomes para não esquecer de ninguém), que sabem que fizeram parte desta trajetória. Durante estes quatro anos conheci muito mais do que colegas de trabalho, conheci amigos, criei vínculos e até mesmo familiares, por onde passei. Muito obrigada a todos do fundo do meu coração!

“Que nada nos limite. Que nada nos defina. Que nada nos sujeite. Que a Liberdade seja a nossa própria substância”.

Simone de Beauvoir

RESUMO

A ampla biodiversidade das macroalgas as coloca em uma posição de destaque como fontes promissoras de moléculas com atividades biológicas interessantes. Em uma perspectiva biotecnológica, estes compostos podem ser utilizados como princípios farmacológicos, cosméticos e nutracêuticos. Visando a produção sustentável destas moléculas, desenvolver estratégias de cultivo de algas em laboratório é de extrema importância para garantir o escalonamento da produção destas moléculas. Para este estudo, foram escolhidas seis macroalgas vermelhas: *Phycocalidia acanthophora*, *Porphyra linearis*, *Plocamium cartilagineum*, *Chondracanthus teedei*, *Osmundea pinnatifida* e *Gracilaria cornea*. Para uma caracterização inicial, extratos aquosos e hidroalcoólicos de cada espécie foram preparados e avaliados em relação a seu conteúdo bioquímico e atividades biológicas de capacidade antioxidante, atividade inibitória da enzima colagenase e atividade fotoprotetora. Considerando o estado da arte apresentado na literatura e os resultados observados no experimento anterior, a espécie *P. cartilagineum* foi escolhida para os estudos de regulação ecofisiológica. Visando entender os mecanismos de fotoaclimatação desta alga em seu ambiente natural, um estudo de campo foi realizado, contendo amostras de lugares com maior e menor exposição solar durante um ciclo diário. A modulação da potencial atuação de fotorreceptores também foi analisada por meio de um experimento submetendo as algas a diferentes qualidades de luz e concentrações de nutrientes, simulando o padrão lumínico de um ciclo diário. Por fim, avaliou-se também o perfil químico de polissacarídeos sulfatados de *P. cartilagineum* e seu potencial anticâncer em diferentes linhagens celulares. Analisando os extratos das diferentes macroalgas, as espécies *P. acanthophora* e *P. lineares* foram as que mais se destacaram, apresentando as maiores concentrações de compostos fenólicos e aminoácidos tipo micosporinas (MAAs). Além disso, apresentaram capacidade antioxidante e elevado potencial para inibição da enzima colagenase. Ao serem incorporados a uma formulação cosmética, os extratos aquosos destas duas algas não foram citotóxicos para células da pele e melhoraram os fatores de proteção associados às atividades biológicas. No experimento de campo com a espécie *P. cartilagineum*, observou-se que as algas situadas em locais com maior exposição às radiações PAR e UV não sofriam fotoinibição ao longo do dia e acumulavam uma maior concentração de compostos fotoprotetores. O experimento para a modulação dos fotorreceptores evidenciou que as radiações UV e azul, associadas a uma maior concentração de nutrientes, foram as mais eficientes para aumentar as concentrações dos compostos de interesse. A extração e caracterização do polissacarídeo sulfatado de *P. cartilagineum* resultaram num polissacarídeo composto majoritariamente por galactose e com potencial citotóxico *in vitro* para a linhagem U-937, uma linhagem humana de leucemia. Além disso, o polissacarídeo demonstrou uma alta seletividade em relação às células saudáveis testadas. Como destaques do trabalho, constatou-se a ausência de toxicidade celular e um elevado potencial de extratos ricos em MAAs na inibição da enzima colagenase, colocando estas moléculas como potenciais agentes cosméticos. Por outro lado, o polissacarídeo de *P. cartilagineum* destacou-se na área farmacológica por sua citotoxicidade em células de leucemia. Por fim, a possibilidade de modulação da produção de compostos contribui com as perspectivas de escalonamento das moléculas de interesse.

Palavras-chave: macroalgas vermelhas, atividade biológica, cultivo, fotorreceptores, biotecnologia.

ABSTRACT

The wide macroalgae biodiversity stands the seaweeds as promisor source of molecules presenting interesting biological activities. In a biotechnological perspective, these compounds may be used as pharmaceutical, cosmetic and nutraceutical molecules. Aiming to ensure a sustainable production of these molecules, to develop strategies for algae cultivation in laboratory conditions is extremely important to guarantee the scale up for biocompounds production. For this study, six red macroalgae were chosen: *Phycocalidia acanthophora*, *Porphyra linearis*, *Plocamium cartilagineum*, *Chondracanthus teedei*, *Osmundea pinnatifida* and *Gracilaria cornea*. To an initial characterization, aqueous and hydroethanolic extracts of each species were prepared and evaluating regarding their biochemical content and biological activities as antioxidant capacity, potential to inhibit the enzyme collagenase and photoprotective potential. Considering the state of the art and the results observed in the screening study mentioned before, the specie *P. cartilagineum* was chosen to ecophysiological regulation studies. Aiming to understand the photoacclimation mechanisms of this alga in its natural environmental, a field study was performed, evaluating samples from different sites placed under higher and lower solar exposition during a daily cycle. The modulation of a potential action of photoreceptors was also analyzed through an experiment exposing the algae to different light qualities and nutrient concentrations, simulating a luminous pattern of a sunny daily cycle. Finally, the chemical profile of sulphated polysaccharides extracted from *P. cartilagineum* and anticancer potential in different cell lines were also evaluated. Analyzing the extracts of different macroalgae, the species *P. acanthophora* and *P. linearis* stand out when compared to the others, presenting the highest content of polyphenol content and mycosporine-like amino acids (MAAs). Furthermore, they also presented antioxidant capacity and the highest potential to inhibit the enzyme collagenase. When incorporated to a cosmetic formulation, the aqueous extracts from these two algae were not cytotoxic to epithelial cells and also enhanced the photoprotection factors associated to the biological activities. In the field study with *P. cartilagineum*, the algae placed in sites with higher exposition to PAR and UV radiations did not suffer photoinhibition throughout the day and accumulated a higher concentration of photoprotective compounds. The experiment to evaluate the modulation of photoreceptors evidenced that UV and Blue radiations, associated to a higher nitrate concentration, were the most efficient condition to increase the production of the interest compounds. The extraction and characterization of the sulphated polysaccharide from *P. cartilagineum* resulted on the obtention of a sulphated galactan, which presented an in vitro cytotoxic potential to U-937 cell line. Moreover, the polysaccharide exhibited a high selectivity comparing to health cell lines. As highlights of this thesis, it was verified the absence of cytotoxicity and a potential of aqueous extracts rich in MAAs in inhibit collagenase, standing out these molecules by their cosmetic potential. On another hand, the polysaccharide from *P. cartilagineum* was highlighted on pharmacological field by its cytotoxicity on leukemia cells. Finally, the possibility to modulate the production of these compounds contributes to the perspectives of scale up.

Keywords: red macroalgae, biological activity, cultivation, photoreceptors, biotechnology.

RESUMEN

La gran diversidad de macroalgas se consideran fuentes prometedoras de moléculas bioactivas. En una perspectiva biotecnológica, estos compuestos pueden ser utilizados como principios farmacológicos, cosmecéuticos y nutracéuticos. Teniendo como objetivo la producción sostenible de estas moléculas, desarrollar estrategias de cultivo de algas en laboratorio es de extrema importancia para garantizar el escalado de su producción. Para esta investigación, fueron elegidas seis especies de macroalgas rojas: *Phycocalidia acanthophora*, *Porphyra linearis*, *Plocamium cartilagineum*, *Chondracanthus teedei*, *Osmundea pinnatifida* y *Gracilaria cornea*. Para la caracterización inicial, se realizaron extractos acuosos e hidroetanolicos y se analizó su composición bioquímica y diversas actividades biológicas como la capacidad antioxidante, actividad inhibitoria de la enzima colagenasa y capacidad fotoprotectora. Teniendo en cuenta el estado del arte y los resultados obtenidos en el estudio anterior, la especie *P. cartilagineum* fue elegida para los estudios de regulación ecofisiológica. Para comprender la fotoaclimatacción de esta alga en su hábitat natural, se realizó un estudio en campo, evaluando la capacidad fotosintética de algas de sitios con mayor y menor exposición solar durante un ciclo solar diario. También se estudió la modulación de la potencial actuación de fotoreceptores en *P. cartilagineum*, mediante un experimento en laboratorio, sometiendo las algas a diferentes calidades de luz y concentraciones de nutrientes, y simulando el patrón luminoso de un ciclo diario. Finalmente, fue evaluado el perfil químico de los polisacáridos sulfatados del *P. cartilagineum* y su potencial antitumoral en diferentes líneas celulares. Analizando los extractos de las diferentes macroalgas, las especies *P. acanthophora* y *P. linearis* fueron las que más destacaron, presentando las concentraciones más altas de compuestos fenólicos y aminoácidos tipo micosporinas (MAAs). Además, presentaron capacidad antioxidante y un elevado potencial para inhibir la enzima colagenasa. Al incorporar los extractos a una formulación cosmética, estos no presentaron toxicidad para las células de la piel y mejoraron los factores de protección asociados a distintas actividades biológicas. En el experimento en campo con la especie *P. cartilagineum*, se observó que las algas que se encontraban en sitios con mayor exposición solar no sufrían fotoinhibición a lo largo del día y acumulaban concentraciones más altas de compuestos fotoprotectores. El experimento para la modulación de los fotoreceptores de *P. cartilagineum* evidenció que la radiación UV y azul, asociadas a una mayor concentración de nutrientes, fueron las más eficientes para incrementar las concentraciones de los compuestos de interés. La extracción y caracterización del polisacárido sulfatado de *P. cartilagineum* resultó en un polisacárido compuesto principalmente por galactosa, y con potencial citotóxico in vitro para la línea celular U-937, una línea celular humana de leucemia. Además, el polisacárido demostró una elevada selectividad en relación a las células sanas. En este trabajo se puede destacar, que se determinó la ausencia de citotoxicidad y un alto potencial para inhibir la enzima colagenasa de los extractos de algas rojas ricos en MAAs, poniendo a estas moléculas como potenciales agentes cosmecéuticos. Por otro lado, el polisacárido de *P. cartilagineum* se destaca en el área farmacológica por su citotoxicidad en células de leucemia. Finalmente, la posibilidad de modular la producción de compuestos de interés contribuye con las perspectivas futuras de cultivo a gran escala de esta especie.

Palabras clave: macroalgas rojas, actividad biológica, cultivo, fotoreceptores, biotecnología

LISTA DE FIGURAS

LISTA DE TABELAS

LISTA DE ABREVIATURAS E SIGLAS

αETR: Eficiência fotossintética

AC: Capacidade antioxidante

AHA: Alfa-hidroxiácidos

APC: Aloficocianina

BEPF: Fator de proteção biologicamente efetivo

CAT: Catalase

Chl *a*: Clorofila a

CO_2: Dióxido de Carbono

Da: Dalton

DNA: Ácido desoxirribonucleico

DW: Peso seco

E_K: Irradiância de saturação

ETR: Taxa de Transporte de Elétrons

ETR_{max}: Taxa de Transporte de Elétrons máxima

F_v/F_m: Rendimento quântico máximo do fotossistema II

FW: Peso fresco

GSH-Px: Glutationa Peroxidase

H_2O_2: Peróxido de Hidrogênio

HEPG: Human hepatocellular carcinoma

HPLC: Cromatografia líquida de alta eficiência

MAA: Aminoácido tipo Micosporina

MEC: Matrix Extracelular

MPP: Metaloproteinases

NADPH: Fosfato de Dinucleotídeo de Adenina e Nicotinamida

nm: nanômetros

NO: Óxido Nítrico

NO_3^-: íon Nitrato

O_2^-: Radical Superóxido

OH^-: Radical Hidroxila

$ONOO^-$:Peroxinitrito

PAM: Pulso de Amplitude Modulada

PAR: Radiação Fotossinteticamente Ativa

PC: Ficocianina

PE: Ficoeritrina

PEC: Ficoeritrocianina

pH: Potencial hidrogeniônico

PO_4^{2-}: íon Fosfato

PSII: Fotossistema II

RLC: Curva rápida de luz

RPM: Rotações por minuto

sp.: Espécie

SOD: Superóxido Dismutase

SOX: Lâmpada de sódio de baixa pressão

SPF: Fator de proteção solar

UV: Radiação Ultravioleta

UV-A: Radiação Ultravioleta do tipo A

UV-B: Radiação Ultravioleta do tipo B

UV-C: Radiação Ultravioleta do tipo C

SUMÁRIO

1 INTRODUÇÃO GERAL

A seguinte revisão bibliográfica abordará conceitos relacionados aos principais temas apresentados nesta tese. De um modo geral, este trabalho contém aspectos fisiológicos, bioquímicos e biotecnológicos de macroalgas vermelhas. Algas são organismos que apresentam distintas morfologias e graus de complexidade, capazes de desenvolver diferentes mecanismos de aclimatação em relação aos ambientes em que se encontram (VEGA et al., 2021). Um dos principais fatores ambientais associados as estratégias de fotoaclimatação é a radiação solar, composta por radiação ultravioleta, visível e infravermelho. Para se aclimatarem aos diferentes ambientes, as algas podem realizar modulações em pigmentos fotossintetizantes, fotorreceptores e moléculas fotoprotetoras como por exemplo compostos fenólicos e aminoácidos tipo micosporinas (FIGUEROA et al., 2009; MARQUARDT et al., 2009). De um ponto de vista biotecnológico, moléculas produzidas por algas podem apresentar atividades biológicas interessantes para as indústrias farmacêutica, cosmética e nutracêutica. Pensando-se em um possível aumento de escala da produção destas moléculas de uma maneira sustentável, é de extrema importância o desenvolvimento de técnicas de cultivo que permitam o escalonamento das algas em laboratório (VEGA et al., 2020b). Sendo assim, a revisão a seguir trará conceitos relacionados aos temas mencionados anteriormente.

1.1 RADIAÇÃO

Organismos vivos são constantemente submetidos a diversos fatores ambientais, sendo a radiação solar um fator de extrema relevância. A luz solar que incide sobre Terra é composta de um amplo espectro eletromagnético, sendo 81% desta energia composta pelas radiações que variam entre 200 a 4000 nm, dividida em radiação ultravioleta (100-400 nm), radiação visível (400 a 750 nm) e infravermelho (750-4000 nm), como representado na Figura 1.

Figura 1. Espectro de radiação emitido pelo Sol.

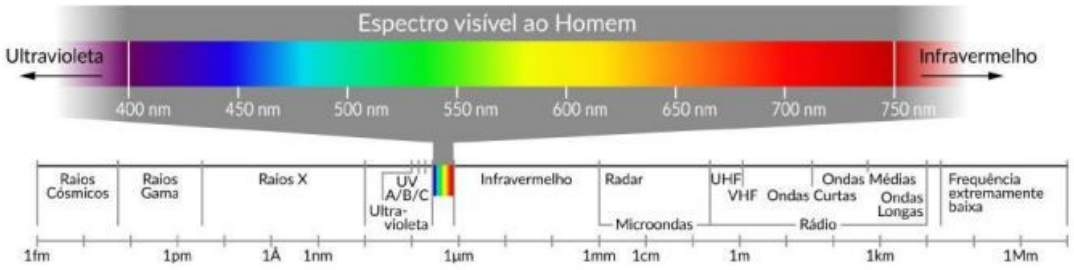

Fonte: Atlas Brasileiro de Energia Solar, 2017.

Para melhor compreensão dos mecanismos de fotoaclimatação desenvolvidos pelas algas, bem como a necessidade pela busca de compostos fotoprotetores que diminuam os impactos negativos da radiação ultravioleta (UV) na pele, é necessário conhecer determinadas características associadas a radiação UV e o espectro de luz visível. A radiação UV pode ser definida como parte da radiação eletromagnética emitida entre 100 e 400 nm. Dentre esta faixa, a radiação UV é dividida em: ultravioleta C (UV-C), entre 100 e 280 nm, ultravioleta B (UV-B), entre 280 e 320 e ultravioleta A (UV-A) entre 320 e 400 nm. Por definição, quanto menor o comprimento de onda maior a quantidade de energia contida na radiação e consequentemente maior o poder de reação destas partículas com outras moléculas. Em organismos fotossintetizantes, a radiação UV influencia diretamente em aspectos morfológicos, reprodutivos, fotossíntese e respostas metabólicas, dependendo da intensidade ou da dose de exposição (PROUTSOS et al., 2022). Em humanos, a radiação UV está associada à síntese de vitamina D3, bem como a processos relacionados à produção de radicais livres e alteração da homeostasia de células da pele (ABDULRAHMAN, 2023).

A radiação ultravioleta pode causar diversos efeitos negativos quando disponibilizada em excesso para organismos vivos. Em humanos, a pele é o órgão que mais sofre os efeitos desta exposição, visto que é a camada mais externa e reveste todo o corpo. Os principais efeitos, diretos e indiretos, associados a esta exposição à radiação UV, são inflamação, imunossupressão, danos no DNA, geração de espécies reativas de oxigênio, carcinogênese e fotoenvelhecimento (PÉREZ-SÁNCHEZ et al., 2018). Os três tipos de radiação UV mencionados anteriormente penetram de maneira distinta na pele humana, como pode ser observado na Figura 2. Em geral, se descartam os efeitos da UV-C na pele, pois embora seja a mais potencialmente danosa, esta radiação é retida na camada de ozônio e não atinge a superfície terrestre. Já a UV-B atinge a pele no nível da epiderme, sendo associada principalmente às reações de escurecimento da pele e formação de eritemas. Por fim, a UV-A

é considerada a radiação de maior poder de penetração e é associada às reações de fotoenvelhecimento, causando alterações celulares e na matriz extracelular da derme.

Figura 2. Penetração da radiação ultravioleta em diferentes camadas da pele.

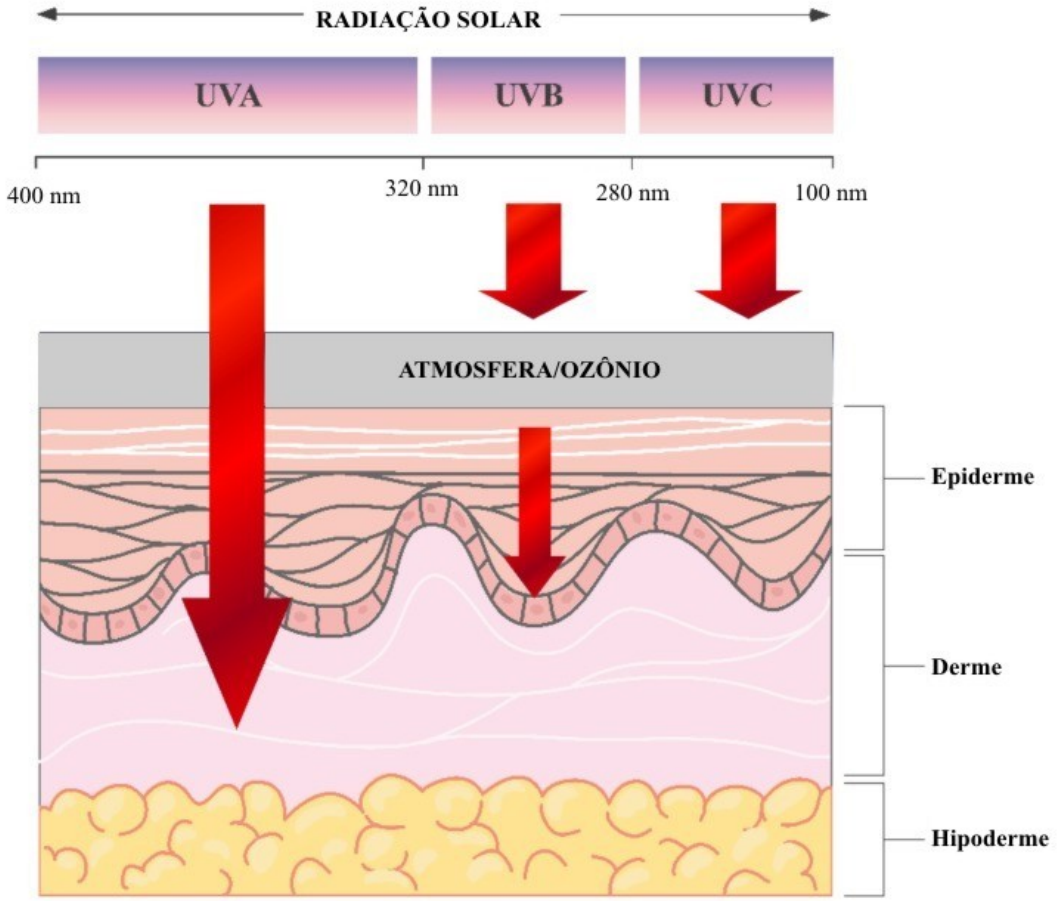

A espessura das flechas está associada com a intensidade dessas radiações, considerando uma redução da UV-B ao atravessar a camada de ozônio, por exemplo. Adaptado de Pérez-Sánchez et. al (2018).

Parte da radiação visível é denominada radiação fotossinteticamente ativa (PAR), de 390 a 760 nm, e é fundamental para a vida dos organismos fotossintetizantes como plantas e algas. A incidência da radiação PAR, bem como da radiação UV, depende diretamente de fatores astronômicos como a posição do Sol em relação à Terra, assim como fatores meteorológicos como a presença de nuvens, por exemplo. Além disso, os efeitos biológicos resultantes da incidência da radiação dependem do seu respectivo poder de penetração e dos mecanismos evolutivos desenvolvidos pelos organismos para adaptação ao ambiente, como a presença de fotorreceptores e a produção de compostos que absorvem e convertem o sinal

luminoso em um sinal químico (ALLORENT; PETROUTSOS, 2017; PROUTSOS et al., 2022).

1.2 PELE HUMANA E INTERAÇÕES COM A RADIAÇÃO

A pele é o maior órgão do corpo humano, podendo alcançar até 16% do peso corporal e recobrindo uma superfície de até 2 m^2. Este órgão desempenha inúmeras funções, sendo inicialmente destacado como barreira física e mecânica por fazer uma interface entre o corpo e o ambiente, auxiliando no controle da temperatura corporal, proteção contra desidratação, percepção de estímulos externos por terminações nervosas, entre outras funções (JUNQUEIRA; CARNEIRO, 2018; PESSOA, 2014). Estruturalmente, a pele é dividida em três camadas, a epiderme, a derme e a hipoderme (camada subcutânea). No esquema a seguir (Figura 3), podem ser observadas além destas três camadas, outras estruturas que compõem este órgão e estão diretamente envolvidas nas funções estruturais e homeostáticas mencionadas anteriormente.

Figura 3. Esquema representativo da pele, apontando as diferentes camadas da pele, sendo estas: epiderme, derme e camada subcutânea ou hipoderme.

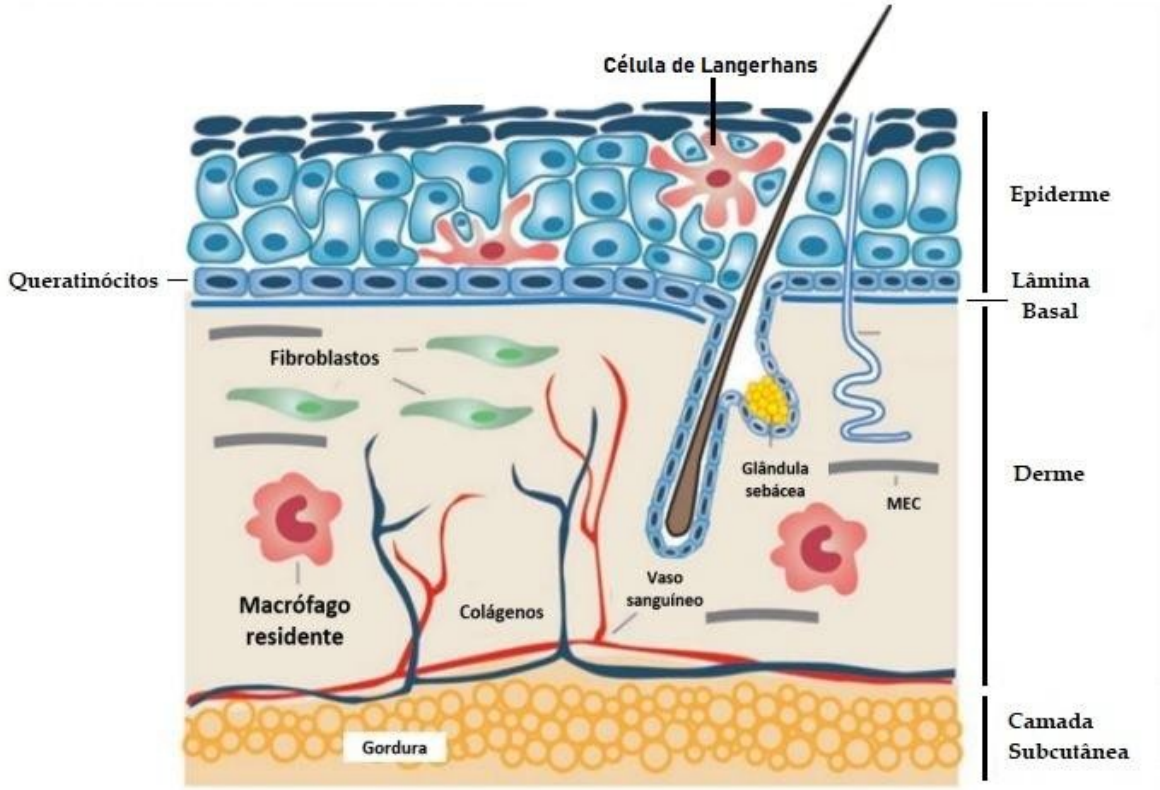

Além das diferentes camadas é possível observar também diferentes componentes celulares e estruturais em cada camada como: epiderme formada por tecido epitelial estratificado contendo em sua maioria queratinócitos em diferentes estágios de desenvolvimento; derme constituída por tecido conjuntivo contendo fibroblastos, células de defesa e matriz extracelular; hipoderme, ou camada subcutânea, formada por células de tecido adiposo. Fonte: Carmo (2019).

A epiderme é formada por 4 camadas sendo estas as camadas basal, espinhosa, granulosa, lúcida e córnea, formadas por queratinócitos em diferentes estágios de desenvolvimento (CARMO, 2019; JUNQUEIRA; CARNEIRO, 2018). Abaixo da epiderme encontra-se a derme, cuja função principal é a sustentação nutricional e estrutural da epiderme. Estruturalmente esta região é subdividida em duas camadas, a derme superficial ou papilar e a derme reticular profunda, que se diferenciam pelo grau de compactação e espessura das fibras. Quando comparados os cortes histológicos pode se observar na derme superficial a presença de tecido conjuntivo frouxo, com a presença de fibras de colágeno, fibras elásticas, fibrócitos, vasos sanguíneos e terminações nervosas com menor grau de compactação e organização. Já na derme reticular observa-se um tecido conjuntivo denso, com maior grau de compactação, organização e fibras elásticas mais espessas. Em ambas, o principal tipo celular encontrado corresponde aos fibroblastos, que são células achatadas e alongadas produtoras de colágeno e outras glicoproteínas da matriz extracelular (MEC). Esta

matriz é constituída principalmente por colágeno do tipo I e III, fibronectina, lamininas, glicosaminoglicanos, proteoglicanos e fibras elásticas. Quanto ao componente celular, além de fibroblastos, na derme também são encontradas células do sistema imune como mastócitos, macrófagos e células dendríticas. Os vasos sanguíneos encontrados nesta região é que fornecem a quantidade necessária de nutrientes e gases para a derme e epiderme, já que esta última é um tecido avascular. Por fim, a hipoderme é formada majoritariamente por adipócitos, células que armazenam gordura (CARMO, 2019).

Compreender a estrutura da pele e seus componentes celulares é de extrema importância para intervir em possíveis doenças ou fatores externos que possam influenciar na homeostase e no bem-estar do indivíduo. O processo de envelhecimento da pele é um processo biológico complexo que envolve fatores intrínsecos e extrínsecos ao ser humano. Os fatores intrínsecos levam ao envelhecimento natural, que ocorre como resultado da degeneração dos tecidos bem como a diminuição dos processos de reparo. Este processo natural do envelhecimento humano resulta no aparecimento de rugas, perda de elasticidade da pele e perda do tecido adiposo subcutâneo. Por outro lado, o envelhecimento extrínseco, é o processo de envelhecimento acelerado pela exposição a fatores externos, dentre eles, radiação ultravioleta, poluição e tabagismo. Dentre as fontes mencionadas, a radiação é considerada uma das mais importantes no envelhecimento precoce da pele, também denominado fotoenvelhecimento, podendo levar em casos mais graves ao surgimento de câncer de pele (MORA HUERTAS et al., 2016).

O termo fotoenvelhecimento foi inicialmente proposto em Kligman em 1986, definindo que este processo correspondia a uma aceleração do processo de envelhecimento natural da pele porém com características celulares e moleculares específicas ao fotoenvelhecimento. Como mencionado anteriormente, a UV-B possui menor poder de penetração na pele afetando principalmente a epiderme, causando vermelhidão da pele, perda de água por danos no extrato córneo e redução das propriedades elásticas da pele. A UV-A por outro lado é capaz de penetrar camadas mais profundas da pele, atingindo a derme, causando a maioria das reações associadas ao fotoenvelhecimento. Como características histológicas do fotoenvelhecimento estão a formação de fibras elásticas mais finas, redução da produção de colágeno tipo I, aumento da produção de colágeno tipo III, aumento de proteoglicanos e glicosaminoglicanos na matriz extracelular (TANVEER; RASHID; TASDUQ, 2023).

Pesquisadores sugerem alterações em duas vias decorrentes da incidência da radiação ultravioleta sobre a pele: via de sinalização MAPK e via de sinalização TGF-β/Smad. A primeira via mencionada, ativação da MAPK se inicia pela ativação de receptores celulares de Interleucina 1 (IL-1), fator de crescimento da epiderme (EGF) e fator de necrose tumoral (TNF-α), que desencadeia a fosforilação das proteínas quinases. A ativação das quinases leva a uma série de eventos de transcrição e ativação proteica que resultam no aumento da expressão de metaloproteinases de matriz (MMPs), que aumentam a degradação de componentes da matriz extracelular como colágeno, elastina e ácido hialurônico, levando a formação de rugas e perda da elasticidade. A segunda via envolvida no processo de fotoenvelhecimento é a via de TGF-β/Smad. Neste cenário, e a radiação UV regula negativamente a expressão do receptor TGF-β do tipo II (TβRII), reduzindo a ativação dos fatores de transcrição Smad2 e Smad3 e reduzindo a produção do prócolageno tipo I, precursor do colágeno tipo I, tipo de colágeno mais abundante na pele (LV et al., 2022).

1.3 MECANISMOS DE PROTEÇÃO AO FOTOENVELHECIMENTO

Entre as estratégias mais clássicas para evitar o processo de fotoenvelhecimento podem-se citar: evitamento da exposição solar, o uso de roupas e acessórios que protejam a pele e o uso de protetores solares. Os protetores solares comerciais são geralmente divididos em inorgânicos e orgânicos, dependendo das moléculas que os constituem e da forma de dissipação da radiação. Protetores inorgânicos, ou físicos, são aqueles que refletem e dispersam a radiação, sendo que dióxido de titânio e óxido de zinco os ingredientes mais utilizados em formulações desse tipo. Em geral, são muito estáveis e eficientes, porém o processo de micronização destes compostos, para evitar o efeito “embranquecido” associados a eles, pode reduzir a eficiência de absorção de UV-A e do espectro visível, além de poder representar um risco por inalação para os trabalhadores que produzem estes produtos. Em contrapartida, filtros orgânicos, absorvem a radiação UV e a dissipam em forma de calor, evitando assim os danos diretos a moléculas da pele. Embora sejam considerados eficientes, estudos indicam que o uso destes compostos orgânicos pode exercer impactos negativos a saúde do consumidor e ao meio ambiente (ANTONIOU et al., 2010; REALI, 2023).

Uma vez que o indivíduo seja exposto sem a devida proteção à luz solar ou radiação UV, é necessário pensar em estratégias para reduzir o impacto da radiação. Compostos antioxidantes também são utilizados como a estratégia para a prevenção aos danos que levam

ao fotoenvelhecimento. Como mencionado anteriormente, raios UV-A e UV-B podem causar danos diretos ou indiretos a moléculas da pele. Os danos indiretos ocorrem pelo estímulo do aumento da produção de radicais livres, que posteriormente reagem com moléculas como proteínas, lipídeos e ácidos nucleicos. Sendo assim, produtos tópicos contendo compostos antioxidantes devem ser considerados para a redução dos danos causados pela radiação UV. Dentre os compostos com capacidade antioxidante pode-se citar a vitamina C, vitamina E, ubiquinonas e α-hidroxiácidos (AHA) (ANTONIOU et al., 2010). Diversas pesquisas avaliam a obtenção de compostos antioxidantes provenientes de fontes naturais, como algas e plantas, por exemplo. Nestes organismos, é possível encontrar diferentes classes de compostos que exercem esta função como por exemplo compostos fenólicos, carotenoides, aminoácidos tipo micosporinas (MAAs), licopeno e antocianinas. Outra abordagem a ser utilizada é a aplicação de enzimas antioxidantes, que convertem os radicais livres a moléculas com menor poder de reação, como por exemplo as enzimas catalase, glutationa peroxidase e superóxido dismutase (PANDEL et al., 2013).

1.4 ESTRESSE OXIDATIVO

Como mencionado anteriormente, um dos efeitos biológicos da incidência da radiação sobre organismos vivos é o aumento da produção de espécies reativas e consequentemente estimulação do estresse oxidativo, fenômeno decorrente do desbalanço entre as espécies reativas e mecanismos/moléculas antioxidantes. O estresse oxidativo resulta em danos às moléculas biológicas, como a desnaturação de proteínas, degradação de vitaminas e alterações em ácidos nucleicos, podendo levar a condições mais graves como o aparecimento de câncer de pele. As espécies reativas são produzidas naturalmente pelos organismos, por uma série de reações enzimáticas durante a peroxidação lipídica nos peroxissomos, fosforilação oxidativa nas mitocôndrias, por oxidases citoplasmáticas, ciclooxigenases e NADPH oxidases na membrana plasmática. Dentre os principais grupos de espécies reativas encontram-se as Espécies Reativas de Oxigênio (Superóxido - O_2^-, radical hidroxila - OH^-, peróxido de hidrogênio - H_2O_2) e Espécies Reativas de Nitrogênio (Óxido nítrico - NO, peroxinitrito - $ONOO^-$) (YUBERO-SERRANO et al., 2014).

Assim como as espécies reativas, seres humanos, animais, algas e plantas também produzem naturalmente moléculas antioxidantes, que podem ser enzimas, como a catalase (CAT), superóxido dismutase (SOD), tiorredoxina redutase (Trr), glutationa peroxidase

(GSH-Px) ou não-enzimáticas como vitamina C e vitamina E (Srivastava et al.,2023). Além de serem produzidas pelos próprios organismos, estas moléculas podem também ser adquiridas por meio da alimentação, com preferência para antioxidantes obtidos de fontes naturais (DENG et al., 2023).

Várias classes de moléculas podem apresentar capacidade antioxidante sendo os mais comumente listados as vitaminas como vitamina C e E, carotenoides como carotenos e xantofilas, e compostos fenólicos como, por exemplo, flavonoides, ácidos fenólicos e lignanas. Estas moléculas podem apresentar diversos mecanismos de ação para exercer sua capacidade antioxidante, incluindo sequestro de radicais livres, quelação de metais e ativação de vias de moléculas antioxidantes endógenas (OROIAN; ESCRICHE, 2015). Considerando a alta diversidade ambiental e os diferentes mecanismos de adaptação desenvolvidos por diferentes organismos frente a estressores ambientais, diversos organismos podem ser fontes de antioxidantes naturais. No grupo das algas, os principais grupos de antioxidantes correspondem a: ficobiliproteínas, fluorotaninos, carotenoides, polissacarídeos sulfatados, scitonemina e MAAs (SONANI; RASTOGI; MADAMWAR, 2017).

Outro mecanismo desencadeado durante a exposição solar da pele é aumento da expressão de metaloproteinases de matriz (MMPs), como por exemplo colagenases e elastases, resultando no aumento da degradação das fibras presentes na matriz extracelular. PITTAYAPRUEK e colaboradores (2016) indicam o potencial das radiações UV-A e UV-B em potencializar a produção de colagenases (MMP-1 e MMP-13), gelatinases (MMP-2 e MMP-9), estromelisinas (MMP-3 e MMP-10), matrilisina (MMP-7) e elastase (MMP-12). Sendo assim, é possível pensar em produtos que atuem na inibição destas enzimas, evitando com que ocorra esta desestruturação da matriz (QUAN et al., 2009). Extratos ricos em compostos fenólicos e MAAs vem sendo estudados em relação ao seu potencial para inibição destas enzimas (MOREIRA et al., 2022).

1.5 MACROALGAS VERMELHAS (RHODOPHYTA)

As macroalgas marinhas representam um grupo diverso responsável por parte da produção primária dos oceanos e ecologicamente, desempenham papéis importantes associados à fixação de carbono, proteção e alimentação de animais marinhos. Estes organismos, distribuídos ao longo da zona costeira, desenvolvem constantemente diferentes estratégias de adaptação em relação à variação de fatores ambientais, como diferenças de

salinidade, temperatura, exposição à radiação ultravioleta, força de cisalhamento, e também contra as alterações climáticas aceleradas pelo processo antropológico como por exemplo ondas de calor, acidificação dos oceanos e aumento da temperatura (JI; GAO, 2021).

As macroalgas são classificadas em três Filos, sendo estes Rhodophyta, Chlorophyta e Ochrophyta. Uma das principais características que os distingue é a presença e a concentração de diferentes pigmentos fotossintetizantes, ainda que todos os grupos contemplem a presença do pigmento essencial para a fotossíntese que é a clorofila *a*. As macroalgas vermelhas (Rhodophyta) possuem como pigmentos acessórios as ficobiliproteínas. A clorofila *a* absorve de modo eficiente a energia luminosa entre 400 e 500 nm e entre 650 e 720 nm. Porém, as algas podem apresentar diferentes complexos de pigmentos auxiliares que otimizem a captação de fótons, como os ficobilissomos, que capturam de modo eficiente a energia de fótons entre 450–650 nm (Figura 4), a qual pode ser transferida entre moléculas do complexo antena, aumentando assim a capacidade de aproveitamento de energia pela fotossíntese nesses organismos (DAGNINO-LEONE et al., 2022).

As ficobiliproteínas são classificadas em quatro tipos: ficoeritrina (PE), ficocianina (PC), aloficocianina (APC), e ficoeritrocianina (PEC). Possuem em sua estrutura cromóforos de cadeia aberta tetrapirrólica denominados ficobilinas, que conferem o espectro de absorção de cada pigmento e consequentemente sua coloração característica. Quando extraídos, estes pigmentos podem apresentar potencial biotecnológico como marcadores biofluorescentes, elevada capacidade antioxidante, ação anti-inflamatória, potencial antiviral e incremento da imunidade (LI et al., 2019).

Figura 4. Espectro de absorção entre 400 e 700 nanômetros apresentados pelos principais pigmentos fotossintetizantes encontrados em algas vermelhas.

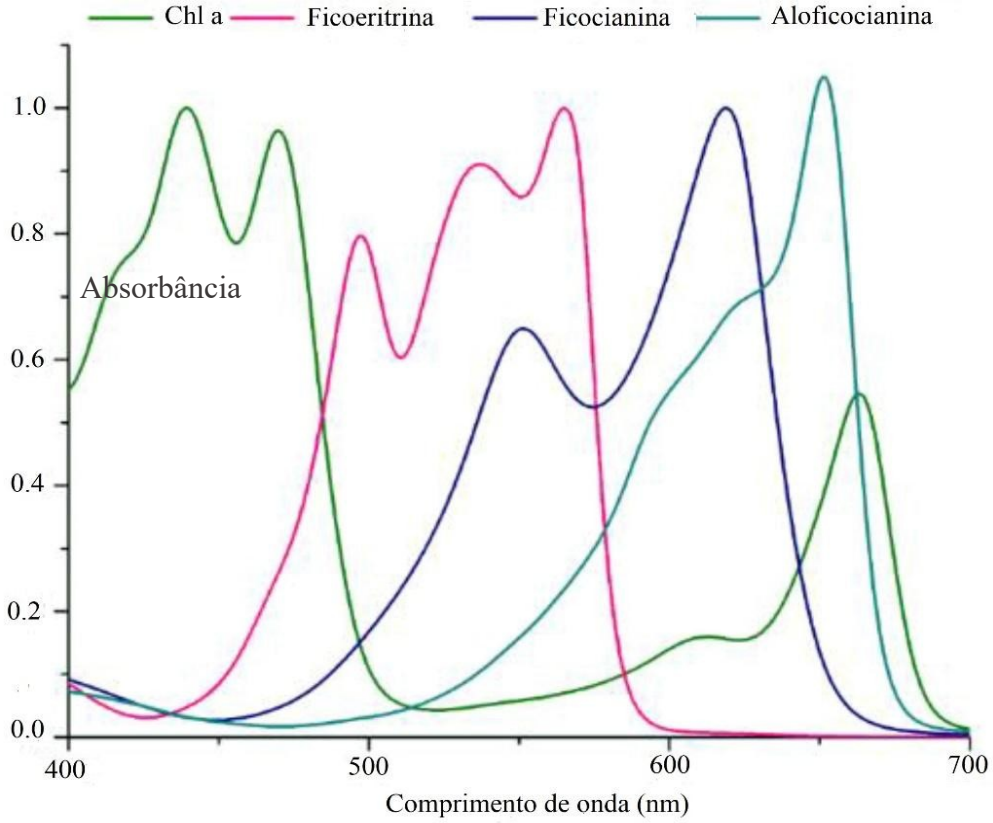

Fonte: Dagnino-Leone et al. (2022).

Os experimentos conduzidos nesta tese abordaram seis espécies de macroalgas vermelhas, representadas na Figura 5. Em seguida, se apresentam aspectos específicos de cada uma delas.

Figura 5. Algas utilizadas nos experimentos relacionados na presente tese. A – *Phycocalidia acanthophora*, B – *Porphyra linearis*, C – *Plocamium cartilagineum*, D – *Chondracanthus teedei*, E – *Gracilaria cornea* e F – *Osmundea pinnatifida*.

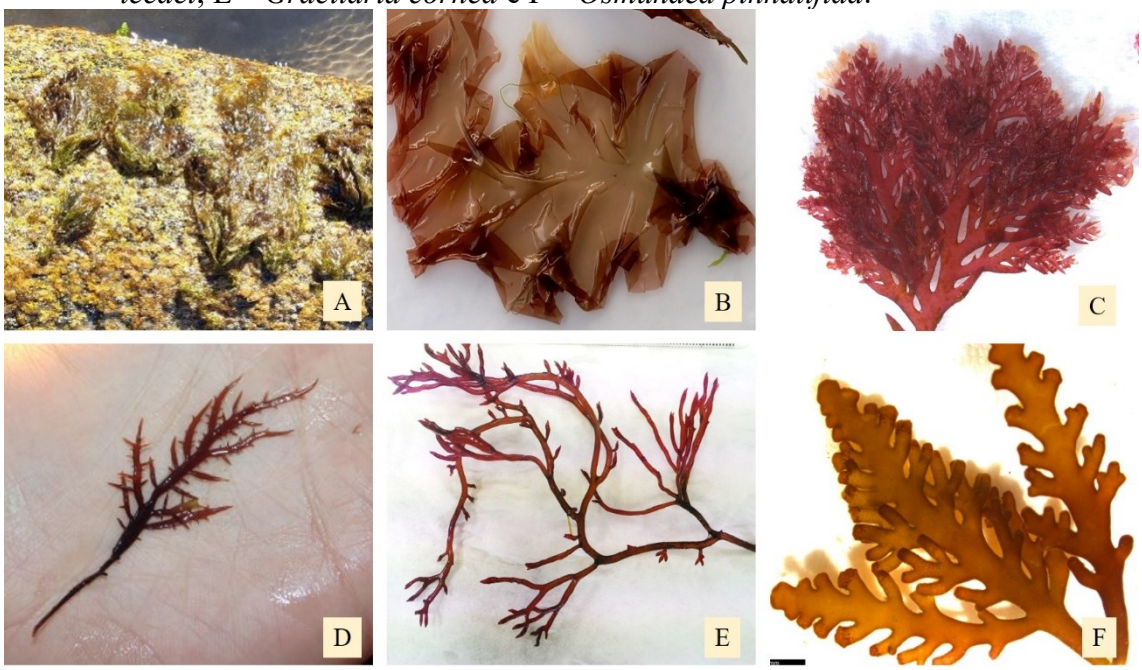

Fonte: A e C – imagens da autora, B – iNaturalist, E e F – Schneider et al. (2020a, 2022)

Phycocalidia acanthophora é atualmente conhecida como *Phycocalidia acanthophora* var. *brasiliensis* E.C. Oliveira & Coll (anteriormente *Pyropia acanthophora*, e ainda antes outrora chamada de *Porphyra acanthophora*) e pertence à família Bangiaceae. Corresponde a uma macroalga vermelha que apresenta duas fases principais em seu ciclo de vida, sendo que a fase gametófito é uma etapa foliácea composta por uma lâmina constituída por uma camada de células, e o esporófito uma etapa filamentosa, usualmente associada a conchas de moluscos (designada como *Conchocelis*). Essa alga ocorre na região entre marés e por isso se desenvolve sob influência de vários estressores locais como dessecação, alta incidência de radiação ultravioleta, força de cisalhamento e variações na temperatura. Assim, esta espécie consiste num organismo de estudo muito interessante para a biotecnologia, já que produz diferentes moléculas para auxiliar nos mecanismos de adaptação a estressores em grande amplitude de ocorrência e potencial impacto (PEREIRA et al., 2020). Devido a sua alta exposição à radiação ultravioleta durante o período de maré baixa, esta alga produz elevadas concentrações de aminoácidos tipo micosporinas, que são moléculas capazes de absorver radiação entre 310 e 360 nm. Estas moléculas devido a sua alta estabilidade térmica e baixa toxicidade, são compostos interessantes para o desenvolvimento de formulações

fotoprotetoras, além de apresentarem capacidade antioxidante e potencial para inibição de enzimas associadas ao processo de envelhecimento da pele (MOREIRA et al., 2022).

A espécie *Porphyra linearis* Greville, também pertencente à família Bangiaceae, compartilha diversas características descritas para a espécie *Phycocalidia acanthophora*, já que também apresenta uma fase gametofítica haploide foliácea monoestromática. Assim como a espécie mencionada anteriormente, *P. linearis* também apresenta elevadas concentrações de MAAs em sua composição (MOREIRA et al., 2022). As algas do gênero *Porphyra* possuem uma grande importância econômica na indústria alimentícia, e estima-se que no ano de 2015 foram produzidos 1.2 milhões de toneladas. São popularmente conhecidas como "Nori" e recebem grande atenção pelo seu uso no preparo do sushi (MACHADO et al., 2020). Além de ser apreciada na culinária oriental, as algas também se destacam pelo seu conteúdo nutricional, contendo elevadas concentrações de aminoácidos essenciais ao ser humano.

A espécie *Plocamium cartilagineum* (Linnaeus) P.S.Dixon, pertencente à família Plocamiaceae, é uma espécie de macroalga marinha encontrada principalmente em zonas de águas temperadas, em profundidades que variam de 2 a 26 metros. *P. cartilagineum* é constituída por um talo pseudoparenquimatoso corticado, altamente ramificado. É muito destacada na literatura por ser fonte de terpenos halogenados, moléculas associadas a potenciais efeitos citotóxicos, antifúngico, moluscicida e inseticida (SABRY et al., 2017; VALENTÃO et al., 2010). Além disso, esta alga possui em sua composição polissacarídeos sulfatados, que podem agir como agentes virucidas e apresentar potencial atividade antitumoral (HARDEN et al., 2009; YU et al., 2018).

Chondracanthus teedei (Mertens ex Roth) Kützing é uma alga pertencente à família Gigartinaceae, amplamente distribuída pela Europa, África, América do Norte e América do Sul e em alguns países asiáticos (GUIRY, 2017). A espécie possui talos cilíndricos e achatados, com até 5 cm de comprimento, apresentando ramificações em apenas um plano, dando um aspecto triangular ao talo (NASSAR, 2012). Em sua composição, se destaca pelo grande acúmulo de carragenana, a qual é constituída por polissacarídeos sulfatados, e são presentes na parede celular de algas pertencentes à ordem Gigartinales. Estes polissacarídeos podem variar em sua composição, dependendo das algas produtoras e das etapas do ciclo de vida em que se encontram. Carragenanas podem ser utilizadas como agentes espessantes e gelificantes na indústria alimentícia (PEREIRA; MESQUITA, 2004).

Gracilaria cornea J.Agardh é uma macroalga vermelha pertencente à família Gracilariaceae. Essa espécie é encontrada em zonas entre marés e possui textura cartilaginosa,

com eixos cilíndricos em mais de um plano, talo de estrutura sólida e pseudoparenquimatosa, com ramificações irregulares, de coloração variada, de acordo com as condições ambientais às quais está exposta (SCHNEIDER et al., 2022). *G. cornea* recebe atenção econômica devido à alta produção comercial de ágar, um polissacarídeo sulfatado muito utilizado como agente gelificante nas indústrias alimentícias e farmacológicas e com potencial para aplicações na indústria cosmética e farmacêutica (CHEN et al., 2019).

Osmundea pinnatifida (Hudson) Stackhouseé uma espécie de alga marinha vermelha, pertencente à Família Rhodomelaceae. Esta alga é encontrada em regiões entre marés no litoral da Espanha, Portugal e região da Macaronésia. *O. pinnatifida* é uma alga utilizada na culinária por ter um sabor característico doce-apimentado (SCHNEIDER et al., 2020a). Esta espécie, por ser comestível e ser uma fonte rica em fibras, proteínas e ácidos graxos, é um interessante alimento funcional para a produção de suplementos alimentícios. Além disso, esta alga produz elevadas quantidades de manitol, um monossacarídeo utilizado na indústria farmacêutica como excipiente para a produção de comprimidos e como princípio ativo para a prevenção de falência renal aguda (MELO et al., 2021).

1.6 POLISSACARÍDEOS

Algas marinhas possuem em sua constituição elevadas concentrações de polissacarídeos, podendo estes ser tanto estruturais, estabilizando a parede celular, quanto estocados como componentes de reserva energética. Por definição, polissacarídeos são macromoléculas formadas pela junção de monossacarídeos através de ligações glicosídicas. A presença de determinados grupos químicos nas cadeias de polissacarídeos pode alterar propriedades estruturais e bioquímicas destas moléculas, afetando suas atividades biológicas. Polissacarídeos sulfatados apresentam grupos sulfatos ligados a hidroxilas dos monossacarídeos. Diversos estudos indicam que polissacarídeos sulfatados geralmente apresentam melhores atividades biológicas que os não-sulfatados (CASTRO-VARELA et al., 2023; SHAO; CHEN; SUN, 2013; TERUYA et al., 2007).

Do ponto de vista biotecnológico, polissacarídeos sulfatados e não-sulfatados, apresentam diversas atividades biológicas de grande relevância incluindo capacidade antioxidante, atividade antitumoral, antiviral, antienvelhecimento, imunomoduladora e probiótica. Dentre os polissacarídeos extraídos de algas mais comumente estudados e explorados estão: alginato (encontrado em *Sargassum* spp., *Ascophyllum nodosum*,

Saccharina latissima), ágar (que pode ser obtido a partir de *Gracilaria* spp., *Gelidium*), carragenana (derivados dos talos de *Hypnea musciformis*, *Chondrus crispus, Kappaphycus alvarezii*), ulvanos (*Ulva* spp.), fucoidanos (*Sargassum*, *Laminaria digitata*, *Fucus vesiculosus*) e laminarina (*Laminaria* spp.) (HENTATI et al., 2020).

Uma das bioatividades mais destacadas para os polissacarídeos de algas é a atividade antitumoral, sendo que suas características químicas como peso molecular, composição de monossacarídeos e ligações glicosídicas, estão intrinsecamente ligadas a esta atividade biológica (NIGAM et al., 2022). Estatísticas indicam que o câncer é um problema de saúde mundial, estando atrelado a eventos epidemiológicos, demográficos, tecnológicos e de estilo de vida. O último relatório produzido pela Agência Internacional para Pesquisa em Câncer em 2020 estimou que em 2020 foram diagnosticados 19,3 milhões de novos casos de câncer e aproximadamente 10 milhões de mortes associadas a 36 tipos de câncer em todo o mundo. De acordo com a agência, os tipos de câncer mais frequentes são câncer de mama em mulheres (11,7%), câncer de pulmão (11,4%), câncer de próstata (7,3%), câncer de pele não-melanoma (6,2%) e câncer de cólon (6%). Também de elevada importância ressalta-se uma incidência de 2,5% de leucemia e 1,7 % de melanoma nos casos avaliados (SUNG et al., 2021).

Diferentes abordagens são usadas no tratamento de câncer, sendo a mais tradicional o uso da quimioterapia. Como ideia central do tratamento, os agentes quimioterápicos matam rapidamente as células tumorais, que são mais susceptíveis ao tratamento. Em contrapartida, de um modo geral, estes tratamentos não apresentam alta seletividade e matam também células saudáveis, podendo afetar células da pele, medula óssea, neurônios e células sanguíneas por exemplo. Esta toxicidade para células saudáveis desencadeia uma série de efeitos colaterais no paciente, que muitas vezes os levam a desistir do tratamento (YANG et al., 2023).

Considerando os fatos mencionados anteriormente em relação às desvantagens do tratamento quimioterápico, é de extrema importância a prospecção de novos compostos que apresentem uma elevada seletividade de células tumorais em relação às células saudáveis. Devido à alta biodiversidade que existe no planeta, moléculas extraídas de fontes de origem natural como algas e plantas vem sendo muito destacadas em literatura, como por exemplo os polissacarídeos mencionados anteriormente (MAZEPA et al., 2022). Diferentes mecanismos pelos quais ocorrem a atividade antitumoral dos polissacarídeos extraídos de algas são mencionados na literatura. Um trabalho de revisão de YAO et al. (2022) elenca os seguintes mecanismos possíveis pelos quais podem ocorrer esta bioatividade: inibição da proliferação

celular e formação de colônias, indução de apoptose mediada por caspases, apoptose mediada por alterações no retículo endoplasmático, apoptose mediada por produção de espécies reativas de oxigênio, indução de alterações no ciclo celular, inibição de angiogênese e metástase, sequestro de radicais livres, modulação da resposta imune do organismo e regulação da microbiota intestinal.

1.7 COMPOSTOS FOTOPROTETORES

1.7.1 Aminoácidos tipo micosporinas

Os aminoácidos tipo micosporinas (MAA) correspondem a metabólitos secundários produzidos por fungos e algas. Ocasionalmente, estes compostos podem ser detectados em baixas quantidades em animais, porém acredita-se que este fato ocorre por ingestão na cadeia trófica ou pela presença de organismos simbiontes (ROSIC, 2019). Estas moléculas apresentam como características elevada polaridade, peso molecular inferior a 400 Da, alta solubilidade em água e espectro de absorção máxima entre 310 e 360 nm. Suas características físico-químicas conferem a estas moléculas as capacidades de fotoproteção, antioxidante, osmorregulação e termorregulação nos organismos que as produzem (VEGA et al., 2021).

O primeiro relato destas moléculas foi feito em 1961 por Tsujino e Saito que identificaram uma molécula que absorve a radiação ultravioleta (UV) em 334 nm, identificando-a como “substância 334”. Atualmente, mais de 30 tipos de MAAs já foram identificados e caracterizados. Os MAAs são compostos nitrogenados que possuem em sua estrutura central um anel de ciclohexamina ou ciclohexanona, responsáveis pela absorção da radiação ultravioleta. Dezenove MAAs identificados em algas e suas respectivas estruturas químicas estão representados na Figura 6. A presença dos MAAs está associada então a um mecanismo natural de fotoproteção contra a radiação UV, onde estas moléculas absorvem a radiação emitida pelo sol e a dissipam em forma de calor, evitando assim danos diretos em biomoléculas e formação de radicais livres (CONDE; CHURIO; PREVITALI, 2007).

Em algas, as espécies com maior potencial para a produção de MAAs pertencem ao grupo das rodófitas. Diversos estudos indicam que os gêneros *Porphyra/Pyropia* são os que concentram as maiores quantidades destes compostos (BRIANI et al., 2018; HUOVINEN et al., 2004; SCHNEIDER et al., 2020b). Além do papel fundamental da radiação UV na produção destes compostos, outros fatores parecem afetar a quantidade e os tipos de MAAs

produzidos. Avaliando o efeito de diferentes qualidades de luz visível em talos de *Porphyra leucosticta*, Korbee e colaboradores (2005) evidenciaram que o cultivo desta alga em luz azul aumenta a produção de MAAs em relação ao controle utilizando luz branca, enquanto os usos das radiações amarela e vermelha provocaram uma redução da concentração de MAAs em relação ao controle. Os diferentes tipos de luz também modularam os tipos de MAAs produzidos, como por exemplo a significativa redução do teor de shinorina quando a luz azul foi utilizada, em comparação com todas as outras qualidades de radiação usadas no experimento (branca, verde, amarela e vermelha). A disponibilidade de nitrogênio também afeta diretamente a produção de MAAs, sendo que, de modo geral, concentrações maiores de nitrogênio levam a produção de maiores quantidades de MAAs (KORBEE et al., 2004; NAVARRO et al., 2014a).

Devido à sua capacidade de absorver radiação no espectro de radiação ultravioleta, associado à sua baixa citotoxicidade e elevada estabilidade, os MAAs são moléculas de elevado potencial para o desenvolvimento de formulações fotoprotetoras (DE LA COBA et al., 2019). O grupo Mibelle AG Cosmetics desenvolveu o primeiro protetor solar comercial contendo o aminoácido tipo micosporina porphyra-334 extraído da espécie *Porphyra umbilicalis*. A formulação desenvolvida pelo grupo indicou a efetividade do produto pela redução nos danos ao DNA de fibroblastos causados por radiação UV *in vitro*. Além disso o estudo realizado com mulheres entre 36 e 54 anos indicou que o novo protetor também é eficiente para reduzir a peroxidação lipídica, estimular o aumento da firmeza e suavidade da pele além de reduzir a profundidade das rugas (SCHMID et al., 2003)

Um estudo recente de De La Coba et al. (2019) evidenciou propriedades distintas dos MAAs além da capacidade fotoprotetora de prevenir a formação de eritema na pele. Nesse trabalho, os autores determinaram diferentes fatores de proteção de atividades biológicas (BEPFs do inglês “Biological Effective Protection Factors”). A partir de espectros de ação de diferentes atividades biológicas, os pesquisadores evidenciaram potenciais atividades de proteção de danos ao DNA, fotocarcinogênese, imunossupressão sistemática, fotoisomerização do ácido urocânico, formação do radical singleto e fotoenvelhecimento de diferentes formulações contendo MAAs, sendo estes porphyra-334, shinorina e micosporina-serinol.

Figura 6. Estrutura química e ʎ máximo de 19 tipos de aminoácidos tipo micosporinas detectados em algas.

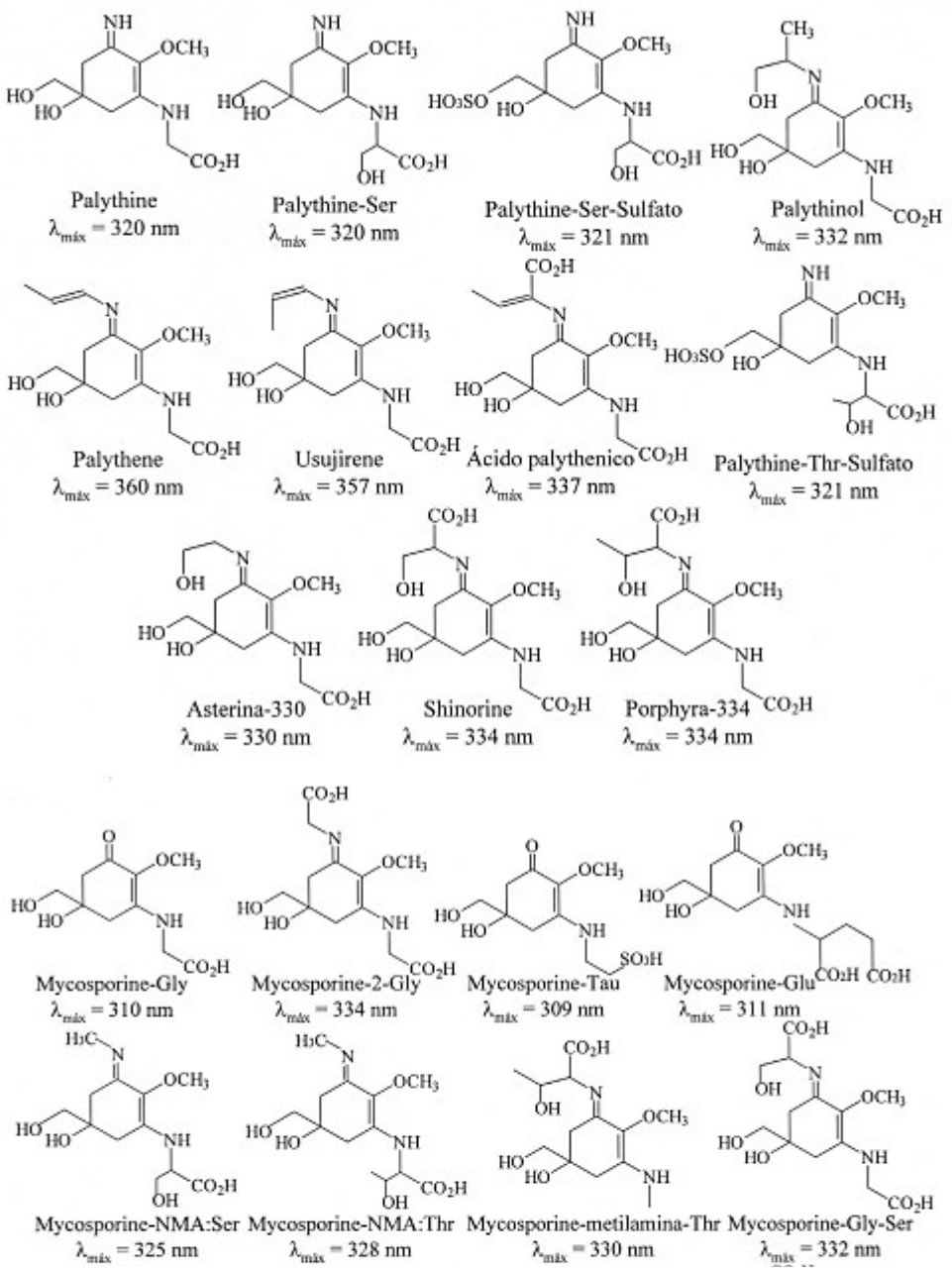

Ser = serina, Thr = treonina, Gly = glicina, Tau = taurina. Adaptado de Korbee et al. (2006).

1.7.2 Compostos fenólicos

Compostos fenólicos correspondem a um grande e diverso grupo de metabólitos secundários produzidos principalmente por algas e plantas como mecanismo de defesa contra predadores. Por definição, para ser considerada um composto fenólico, a molécula deve conter em sua estrutura química um radical hidroxila ligado diretamente a um grupo

hidrocarboneto aromático, apresentando normalmente também grupos metoxi e glicosil. Esta característica química confere a este grupo uma elevada capacidade antioxidante por sequestro de radicais livres e atividade quelante de metais (JIMENEZ-LOPEZ et al., 2021). De acordo com sua estrutura molecular, compostos fenólicos podem ser divididos em flavonoides ou não-flavonoides. Embora sejam produzidos em maiores quantidades por algas pardas (Ochrophyta), estes compostos também são produzidos por algas vermelhas. Os compostos fenólicos mais comumente descritos em algas vermelhas são os bromofenóis, flavonoides, ácidos fenólicos e terpenóides (COTAS et al., 2020).

Além da capacidade antioxidante direta pelo sequestro de radicais livres, compostos fenólicos também são capazes de ativar vias de mecanismos antioxidantes endógenos via ativação dos fatores Nrf/ARE. Estas propriedades vêm sendo associadas a um elevado potencial de neuroproteção visto que pacientes com doença de Alzheimer possuem uma disfunção mitocondrial que resulta em um aumento da expressão e liberação de espécies reativas de oxigênio. Além disso, pacientes com Alzheimer também apresentam elevadas quantidades de cobre e ferro no cérebro, que podem potencialmente formar espécies reativas através de reações de Fenton. Sendo assim, por apresentar atividade quelante de metais, compostos fenólicos estão associados a múltiplos mecanismos de neuroproteção (CHOI et al., 2012).

1.7.3 Carotenoides

Carotenoides são metabólitos secundários, de natureza lipofílica, produzidos por algas, plantas, algumas bactérias e fungos. Os carotenoides desempenham papel muito importante nos organismos fotossintetizantes, visto que apresentam potencial para captação de luz e transferência de elétrons para a cadeia transportadora de elétrons. Além de auxiliar no processo de fotossíntese, alguns carotenoides estão relacionados a mecanismos de fotoproteção, destinando elétrons excedentes para o ciclo de xantofilas. Estruturalmente, estas moléculas podem ser divididos em carotenos (formados por cadeias de hidrocarbonetos), e xantofilas (uma forma oxigenada dos carotenos). A eficiência destas moléculas em exercer sua capacidade antioxidante está diretamente relacionada a sua estrutura química, variando de acordo com a quantidade de ligações duplas presentes e os radicais químicos acoplados ao esqueleto de hidrocarbonetos. A natureza hidrofóbica dos carotenoides permite que eles sejam

bons antioxidantes via mecanismo de proteção de membranas celulares contra peroxidação lipídica (SONANI; RASTOGI; MADAMWAR, 2017).

Em relação a sua funcionalidade, carotenoides podem ser classificados em primários e secundários. Os carotenoides primários são aqueles que compõem o aparato fotossintético e auxiliam na captação de luz para a realização da fotossíntese. Já os carotenoides secundários estão associados a mecanismos de proteção contra estressores ambientais, como por exemplo fotoproteção destinando parte do fluxo de elétrons que sobrecarregaria o aparato fotossintético para o ciclo de xantofilas (ZAREKARIZI; HOFFMANN; BURRITT, 2023).

As algas são consideradas importantes fontes de diversos carotenoides. Exemplos de alta eficiência para a produção destes compostos são *Haematococcus pluvialis, Chlorella zofingiensis* e *Chlorococcum* sp. como produtores de astaxantina. β-caroteno pode ser encontrado em *Arthrospira platensis*, *Chlorella vulgaris*, e *Dunaliella salina*, enquanto que *Phaeodactylum tricornutum, Laminaria japonica, Undaria pinnatifida, Hizikia usiformis, Sargassum* spp. e *Fucus* spp. podem ser utilizadas como fonte de fucoxantina (ASHOKKUMAR et al., 2023). Sabe-se também que as condições de cultivo das algas interferem diretamente na síntese destes compostos, sendo afetada por fatores como temperatura, salinidade, quantidade e qualidade de luz (ZAREKARIZI; HOFFMANN; BURRITT, 2023).

Carotenoides recebem grande destaque na indústria alimentícia pois além de possuírem cores intensas e serem candidatos a bons corantes, ainda podem ser utilizados como ingredientes funcionais para enriquecimento do alimento devido a seu potencial antioxidante e por serem precursores da síntese de vitamina A. Embora apresentem elevado potencial nutracêutico, existem algumas limitações do uso dos carotenoides, incluindo baixa estabilidade na presença de luz, presença de oxigênio e temperaturas elevadas. Para solucionar estes problemas, vários estudos focam no desenvolvimento de carreadores que aumentem a estabilidade, a solubilidade e a bioatividade dos carotenoides (CARVALHO DE QUEIROZ et al., 2022; ZIMMER; MENDONÇA; ZAMBIAZI, 2022)

1.8 FOTOSSÍNTESE A PARTIR DA FLUORESCÊNCIA DA CLOROFILA A.

A fotossíntese corresponde ao processo de formação de moléculas orgânicas a partir da fixação de CO_2 atmosférico, H_2O e energia luminosa pela captação de fótons, podendo esta ser dividida em fase fotoquímica e bioquímica. Durante a primeira etapa da fotossíntese, a

radiação PAR atinge os organismos fotossintetizantes e é absorvida pelos pigmentos fotossintetizantes, localizados nos complexos antenas. Estes pigmentos são moléculas proteicas que possuem em sua extremidade cromóforos, os quais determinam sua coloração. Em algas, os principais pigmentos encontrados são clorofilas a, b e c, ficobiliproteínas e carotenoides. O processo de captura de energia resulta na excitação e ressonância de moléculas que são transferidos entre moléculas no complexo antena. Essa transferência se finaliza ao atingir os centros de reação dos fotossistemas I e II, dentro dos quais ocorre a transferência não apenas de energia mas também de elétrons entre moléculas, permeando um processo de óxido-redução, que resulta então na cadeia transportadora de elétrons na membrana dos tilacóides. Os fotossistemas I e II contém as moléculas de clorofila P680 e P700, respectivamente (LEISTER, 2023).

Um dos métodos mais consolidados para a determinação da fotossíntese em algas e plantas é o uso de pulsos de saturação contendo amplitude modulada (PAM). O método tem por princípio calcular indiretamente as taxas de fotossíntese considerando que a energia da radiação incidente sobre as algas pode percorrer três caminhos: (1) ser absorvida pela clorofila *a* no fotossistema II (PSII), (2) ser absorvida pela clorofila *a* e ser descartada como fluorescência (em um comprimento de onda maior que o absorvido) ou (3) ser perdida em forma de calor. Considerando que a perda de calor é mínima, o PAM é capaz de medir a fluorescência emitida pela clorofila *a* situada no fotossistema II (PSII) (WHITE; CRITCHLEY, 1999). A partir das variações de fluorescência, são calculados parâmetros descritores do comportamento da fotossíntese dos organismos, tais como os rendimentos quânticos efetivo e máximo, e também taxas de transporte de elétrons. Para calcular estas taxas, se utilizam os seguintes conceitos apresentados na Figura 7:

F_0: fluorescência basal mínima detectada pelo equipamento em algas aclimatadas ao escuro;

F_m: fluorescência máxima em uma alga aclimatada ao escuro, emitida após um pulso de saturação;

F_V: Fluorescência variável calculada através da diferença entre F_m e $F_{0;}$

F_m': fluorescência máxima em uma alga aclimatada a determinada fonte de iluminação, emitida após um pulso de saturação;

F_s: fluorescência detectada pelo equipamento em algas em estado estacionário aclimatadas a determinada fonte de iluminação.

Figura 7. Medidas da fluorescência emitida pela clorofila a utilizando-se um fluorímetro PAM em (a) organismos aclimatados ao escuro e (b) organismos aclimatados a determinada fonte de luz.

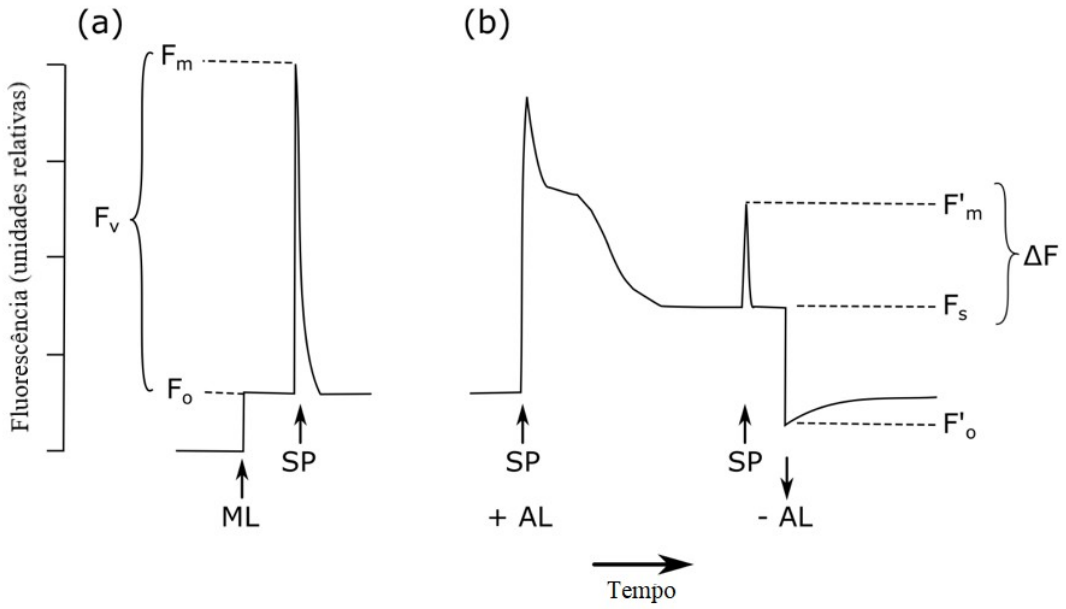

AL = Luz actínica, SP = Pulso de Saturação, ML = Luz de Medida. Adaptado de Kooten e Snel (1990).

A partir dos parâmetros apresentados na Figura 7a, relacionados aos organismos pré-aclimatados ao escuro, é possível calcular o rendimento quântico máximo (F_v/F_m), momento em que é detectado o maior potencial para fotossíntese porque todos os centros de reação encontram-se oxidados neste momento. O F_v/F_m pode ser calculado por meio da seguinte fórmula:

$$\frac{F_v}{F_m} = \frac{(F_m - F_0)}{F_m}$$

Utilizando-se os parâmetros apresentadas na Figura 7b, com as algas aclimatadas a uma determinada fonte de luz, se calcula o rendimento quântico efetivo (YII), utilizando a seguinte fórmula:

$$Y(II) = \frac{(F_m' - F_s)}{F_m'}$$

Outro importante parâmetro que pode ser calculado utilizando-se os dados calculados a partir da fluorescência da clorofila é a taxa de transporte de elétrons (ETR), que permite calcular o fluxo de elétrons ao longo da cadeia transportadora. O cálculo do ETR se realiza a partir da equação descrita a seguir:

$ETR = Y(II) * Abst * I * F_{II}$, sendo:

Abst: absortância do talo

I: irradiância incidente sob o talo

F_{II}: fator de proporção de clorofilas *a* associadas ao fotossistema II, sendo adotado valor de 0.15 para algas vermelhas (JOHNSEN; SAKSHAUG, 2007).

Outra técnica importante que pode ser realizada utilizando-se o PAM, é a realização de curvas rápidas de luz (RLC), que permitem o cálculo de distintos parâmetros fotossintetizantes utilizados para avaliar o estado fisiológico e possíveis estados de fotoaclimatação dos organismos fotossintetizantes (CRUZ; SERÔDIO, 2008). Um modelo de RLC contendo alguns possíveis parâmetros a serem calculados, está apresentado na Figura 8. A realização de curva de luz nos permite calcular parâmetros fotossintetizantes importantes tanto para avaliar o estado fisiológico da alga quanto para planejar as melhores condições de cultivo específicas para cada alga. Por meio destas curvas é possível calcular o valor do ângulo alfa (α) que permite calcular a eficiência fotossintética da alga, bem como o valor de β que indica um coeficiente de inibição, o valor da $E_{k,}$ referente a irradiância mínima que causa a saturação do fotossistema e o valor de ETR_{max}, que representa a taxa máxima de transporte de elétrons (RALPH; GADEMANN, 2005).

Figura 8. Modelo de curva rápida de luz (RLC) representando os valores da taxa de transporte de elétrons (ETR) em função do aumento da irradiância PAR (µmol de fótons m^{-2} s^{-1}).

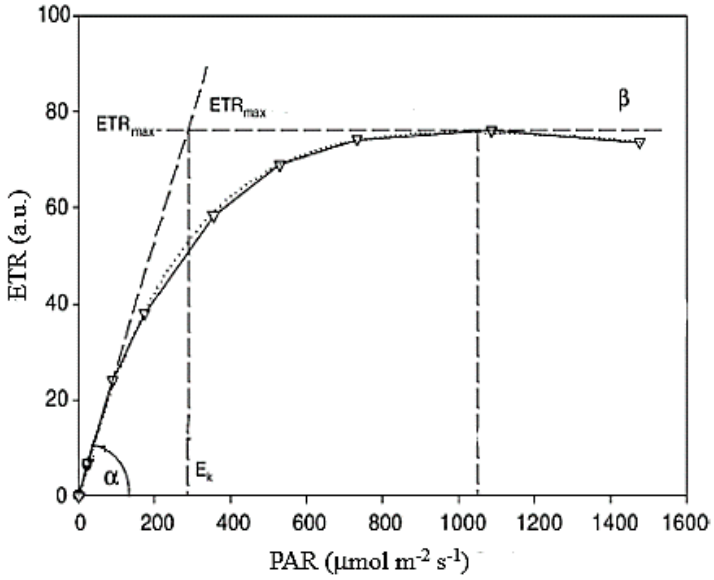

Os parâmetros apresentados na figura correspondem a α = tangente do ângulo que indica a eficiência fotossintética, Ek = irradiância de saturação mínima, ETRmax = taxa de transporte de elétrons máxima e β = coeficiente de fotoinibição. Adaptado de Ralph & Gademann (2005).

1.9 FOTORREGULAÇÃO/ FOTORRECEPTORES

Como já mencionado anteriormente, diferentes qualidades de luz exercem importante efeito em organismos fotossintetizantes. Radiações absorvidas pelos pigmentos direcionam o fluxo de elétrons pela cadeia transportadora de elétrons desencadeando o processo da fotossíntese. Por outro lado, a radiação pode interagir também com outras moléculas capazes de desencadear outros processos fisiológicos, como os fotorreceptores. Fotorreceptores são moléculas proteicas unidas a um cromóforo não-proteico, sensíveis à radiação, que ao detectarem variações na intensidade, qualidade e padrões da mesma, desencadeiam cadeias de transdução de sinais e geram consequentemente respostas moleculares e fisiológicas no organismo. Dentre as funções influenciadas pelos fotorreceptores, podem-se citar alterações morfológicas, controle do ciclo circadiano, formação de gametas, fotoaclimatação e fotoproteção (KOTTKE et al., 2017).

Os principais fotorreceptores descritos em algas são fitocromos (absorvem radiação no espectro identificados como as cores vermelho e vermelho longo), criptocromos (radiação azul e UV-A) e rodopsinas. Compreender estas relações de modulação dos fotorreceptores permite o desenvolvimento de estratégias de cultivo para aumentar ou suprimir a produção de compostos de interesse (KIANIANMOMENI; HALLMANN, 2014).

Vários experimentos com macroalgas evidenciam o aumento da produção de determinados compostos por meio da fotobiologia. Os primeiros experimentos desta área foram realizados utilizando-se alface como modelo de estudo. Em um experimento inovador, Flint (1934), evidenciou o efeito de várias irradiâncias na germinação de brotos de alface, indicando que as radiações amarela, laranja e vermelha promoviam a germinação, enquanto violeta, azul e verde inibiam o processo. A partir deste primeiro relato, outros estudos foram sendo realizados utilizando diferentes estratégias para tentar esclarecer os mecanismos de ação pelo qual estes efeitos ocorriam (BORTHWICK et al., 1954; FLINT; MCALISTER, 1935). Uma das possíveis maneiras de se analisar a ação de fotorreceptores em algas é a exposição de algas a diferentes tipos de radiação, normalmente monocromáticas, em fotoperíodos definidos (BONOMI BARUFI; FIGUEROA; PLASTINO, 2015; FIGUEROA; AGUILERA; NIELL, 1995; KORBEE; FIGUEROA; AGUILERA, 2005). Alguns autores utilizam também a estratégia de utilizar quantidades de luz, utilizando lâmpadas SOX, suficiente para saturar a fotossíntese e adicionam pequenas quantidades de luz complementar para estimular a ação dos fotorreceptores (PAGELS et al., 2020; SCHNEIDER et al., 2020a, 2022).

Atualmente, experimentos de fotobiologia são realizados utilizando-se tanto a estratégia clássica proposta por Flint, expondo os organismos a radiações monocromáticas, quanto com abordagens mais complexas, a fim de se entender a modulação de respostas morfológicas, fisiológicas e bioquímicas desencadeadas por fotorreceptores.

1.10 JUSTIFICATIVA

A Figura 9 apresenta os principais temas abordados nesta tese e que justificam a realização deste trabalho. O esquema apresentado a seguir representa as diferentes etapas do processo biotecnológico desenvolvido, incluindo a prospecção de compostos em espécies distintas, a avaliação do funcionamento da alga em campo, a regulação da síntese dos diferentes compostos, a purificação do produto e testes de aplicabilidade. A diversidade no mundo das algas é um grande indicador biológico da variedade de compostos químicos que podem ser encontrados nestes organismos. Dessa forma, realizar uma prospecção das substâncias que podem ser alvo de interesse aplicado sempre é pertinente, dado que essas substâncias podem estar presentes em grupos diversos com capacidade aplicada também variada. Considerando os compostos descritos na literatura, sabe-se que algas vermelhas apresentam em sua composição alto teor de polissacarídeos, proteínas e as maiores concentrações de aminoácidos tipo micosporinas, moléculas que se destacam por sua capacidade fotoprotetora. Estas moléculas, numa vertente biotecnológica, podem ser utilizadas para o desenvolvimento de diversos produtos em diferentes setores industriais. Como exemplos, podemos citar que pigmentos fotossintetizantes e compostos fenólicos apresentam elevada capacidade antioxidante, que podem ser utilizados na indústria cosmética e para preservação de alimentos. Polissacarídeos são muito utilizados como agentes emulsificantes na indústria alimentícia e apresentam potencial atividade virucida e antitumoral. Diante deste fato, a multidisciplinaridade da biotecnologia permite o entendimento e potencial exploração sustentável desses compostos.

Considerando que recursos naturais devem ser explorados de modo consciente e sustentável, é de extrema importância adquirir o conhecimento para o cultivo das algas, a fim de se produzir biomassa suficiente sem causar maiores impactos ambientais. Além disso, utilizando-se cultivos em ambientes controlados, é possível desenvolver estratégias para estimular a produção dos compostos de interesse, considerando modulações do crescimento, fotossíntese, e reprodução, tendo em conta a atividade de pigmentos e fotorreceptores. Assim, as abordagens experimentais analisam o comportamento bioquímico e fisiológico das algas em ambiente natural durante um ciclo diário e usam estas informações como subsídios para a realização dos cultivos de algas em condições de laboratório.

Figura 9. Esquema representativo dos principais temas e estratégias abordados neste trabalho.

•

1.11 HIPÓTESES

- Uma maior concentração de compostos fotoprotetores em algas vermelhas inibe as metaloproteinases.
- *P. cartilagineum* sintetiza diferentes MAAs e pigmentos em curto espaço de tempo durante um ciclo diário.
- A interação entre a presença de nutrientes e a radiação azul que atinge maiores profundidades na coluna de água modula as respostas bioquímicas e fisiológicas de *P. cartilagineum*.
- Um composto isolado de *Plocamium cartilagineum* causa toxicidade em células humanas.

1.12 OBJETIVOS

1.12.1 Objetivo geral

O objetivo deste trabalho foi analisar um processo biotecnológico em macroalgas constituído por diferentes etapas, a saber: prospecção, cultivo, regulação, extração e aplicabilidade de compostos de macroalgas vermelhas

1.12.2 OBJETIVOS ESPECÍFICOS

- Realizar a caracterização bioquímica de extratos aquosos e hidroetanólicos de diferentes algas vermelhas, analisado o espectro UV-Vis dos extratos, rendimento de extração, teor de carbono, nitrogênio, hidrogênio e enxofre, compostos fenólicos e aminoácidos tipo micosporinas.
- Analisar as atividades biológicas dos extratos de algas por meio de sua capacidade antioxidante, inibição da enzima colagenase e potencial fotoprotetor.
- Analisar a fotossíntese *in situ* de *P. cartilagineum* de acordo com sua localização no ambiente aquático e variações ao longo do dia.
- Verificar o teor de pigmentos fotossintetizantes e aminoácidos tipo micosporinas *in situ* de *P. cartilagineum* de acordo com sua localização no ambiente aquático e variações ao longo do dia.
- Avaliar a modulação fotossintetizante e de fotorreceptores em *P. cartilagineum* em um experimento associando diferentes radiações monocromáticas (UV, azul e verde) e assimilação de diferentes concentrações de nitrato.
- Caracterizar quimicamente o polissacarídeo extraído de *P. cartilagineum* por meio de análises do teor de carbono, hidrogênio, nitrogênio e enxofre, cromatografia gasosa associada a espectrômetro de massas e Espectroscopia no infravermelho por transformada de Fourier.
- Avaliar o potencial citotóxico do polissacarídeo extraído de *P. cartilagineum* em células de linhagem tumoral (HCT-116, U-937 e G-361) e em células saudáveis (HACAT e 1064sK).

2 CAPÍTULO 1

Manuscript published by *Algal Research*

Antioxidant and anti-photoaging properties of red marine macroalgae: Screening of bioactive molecules for cosmeceutical applications

Bruna Rodrigues Moreira [a,*] , Julia Vega [b] , Angela Daniela Alarcón Sisa [c] , Joan Steban Bohórquez Bernal [c] , Roberto T. Abdala-Díaz [b] , Marcelo Maraschin [d] , Félix L. Figueroa [b] , José Bonomi-Barufi [a]

[a] Programa de Pos-Graduação em Biociências e Biotecnologia, Laboratório de Ficologia, Departamento de Botânica, Universidade Federal de Santa Catarina, 88040-900 Florianópolis, Brazil.

[b] Universidad de Málaga, Instituto Universitario de Biotecnología y Desarrollo Azul (IBYDA), Departamento de Ecología, Campus Universitario de Teatinos s/n, 29071 Málaga, Spain.

[c] Grupo de Investigación en Compuestos Funcionales, Facultad de Ciencias Exactas y Naturales, Universidad de Antioquia, 050010 Medellín, Colombia.

[d] Laboratório de Morfogênese e Bioquímica Vegetal, Centro de Ciências Agrárias, Universidade Federal de Santa Catarina, 88034-000 Florianópolis, Brazil.

2.1 ABSTRACT

Oxidative stress generated by UV exposition plays an important role on photoaging. Understanding the cell physiological responses due to the action of oxidative molecules process helps to develop approaches to reduce its impact on skin cells. In this context, algae can be source of biomolecules with antioxidant, inhibition of metalloproteinases and photoprotective capacities, such as mycosporine-like amino acids and phenolic compounds. This study focuses on the characterization of aqueous and hydroethanolic extracts of six red marine macroalgae: *Phycocalidia acanthophora*, *Porphyra linearis*, *Condracanthus teedei*, *Gracilaria cornea*, *Osmundea pinnatifida* and *Plocamium cartilagineum* (from two different sites). Besides their biochemical characterization, we also evaluated antioxidant capacity, potential to collagenase inhibition, and photoprotective capacity by different biological effective protection factors (BEPFs). Results evidenced a better correlation among the compounds of interest and bioactivity when using water as solvent rather than hydroethanolic solution. *P. acanthophora* and *P. linearis* aqueous extracts were highlighted in all analyses. Considering this fact, these two extracts were incorporate onto a cosmeceutical formulation. BEPFs evidenced that the incorporation of the extracts increased the photoprotection factors when compared to the control without physical filters. According to the findings herein described, the potential of red macroalgae as source of bioactive compounds with antiaging potential is reinforced.

Keywords: Antiaging, collagenase inhibition, mycosporine-like amino acids, screening, red macroalgae

2.2 INTRODUCTION

The skin is the largest organ of the human body and corresponds to the first mechanical barrier that protects it against external factors, helping on thermoregulation, protection against dehydration and pathogen infections (LAI-CHEONG; MCGRATH, 2021). The skin has been an important target of both cosmetic and pharmaceutical industries due to increasing populational and commercial concerns with aging and beauty. Some authors define the skin as a "social organ", because it reflects directly on social contact and factors as skin disorders, aging or a personal displeasure with self-appearance may reduce life quality and trigger psychological disorders (CORTÉS et al., 2021; MORAIS et al., 2022).

Anatomically, skin can be divided into epidermis, dermis, and hypodermis. Epidermis corresponds to a layered squamous epithelium differentiated in four layers: stratum basale, stratum spinosum, stratum granulosum, and stratum corneum. The epidermis is composed mainly by keratinocytes, melanocytes, Langerhans and Merkel cells, and the stratum corneum correspond to the main obstacle to the transport of bioactive ingredients due to the presence of a lipidic layer. Otherwise, dermis is composed mostly by fibroblasts and the extracellular matrix (ECM), containing collagen (70%), elastin, glycoproteins, proteoglycans, water, and hyaluronic acid. This layer plays an important role on skin's structural support. Finally, the hypodermis is the inner layer of skin and it is composed by adipocytes containing carotenoids with antioxidant capacity (ABDO; SOPKO; MILNER, 2020; ITA, 2020).

The intrinsic aging, a natural process over time, and photoaging (extrinsic aging), due to the unprotected exposition to ultraviolet (UV) radiation, are characterized mainly by alterations on dermal ECM and lead to the appearance of wrinkles, flaccidity, and hyperpigmentation. Both processes present different physiological responses that result in the aging process, but both exhibit reduction in the collagen production and increasing fibril fragmentation (MCCABE et al., 2020). Although intrinsic aging is a natural and inevitable genetically predetermined process, the study of processes and factors associated to the intrinsic aging and photoaging allows a greater understand on ways to minimize visible signs of aging and guides the development of specific treatment products (CHIEN et al., 2018).

Oxidative stress, defined as an unbalance between oxidative molecules and antioxidants, is frequently associated to aging process. Naturally, the human body possesses different antioxidant mechanisms, including non-enzymatic ones as ascorbic acid, α-tocopherol, uric acid, glutathione, as well as enzymatic mechanisms such as superoxide

dismutase (SOD), catalase (CAT), glutathione peroxidase (GPx) and glutathione reductase (GR). In case of reduction on antioxidant mechanisms and/or an increase of free radicals as Reactive Oxygen Species (ROS) and Reactive Nitrogen Species (RNS), a series of reactions may occur, resulting on damage of lipids, proteins and nucleic acids (PERES et al., 2011). Considering the aging process, the oxidative stress is associated to the reduction of collagen and increase of metalloproteinase (as collagenase, elastase, and hyaluronidase) production, resulting on the degradation of ECM compounds, reduction of the proteoglycan content, organization of the fibers, and increase of inflammatory processes (GANGULY; HOTA; PRADHAN, 2021; GU et al., 2020).

Approaches to diminish the generation and impact of free radicals on skin cells are frequently highlighted on cosmetic and pharmaceuticals. In this context, the search for bioactive ingredients from natural sources, instead of synthetic ingredients, set algae as a promising source of bioactive compounds (RESENDE et al., 2021). Macroalgae exhibit many adaptative mechanisms which allow them to survive in distinct environments, including areas with high ultraviolet radiation exposition. Part of this physiological and biochemical plasticity comes from the production of biocompounds with both UV-screen and antioxidant capacities (NAVARRO et al., 2018; VEGA et al., 2020b). Such compounds have a high biotechnological potential (CHRAPUSTA et al., 2017; VEGA et al., 2021). Red macroalgae are described on literature as sources of sulfated polysaccharides, proteins, antioxidant pigments, polyphenols, and for presenting the highest content of mycosporine-like amino acids (MAAs) among the algal groups (BRIANI et al., 2018; SCHNEIDER et al., 2020b).

Many authors reported antioxidant capacity of extracts and compounds purified of red macroalgae (RANGEL et al., 2020; SUWAL et al., 2019; VEGA et al., 2020a, 2020b). Besides their antioxidant capacity, the potential of phenolic compounds and MAAs to inhibit metalloproteinases have been investigated. Ethanolic extract from *Jania rubens* exhibited potential to inhibit collagenase, elastase, and hyaluronidase enzymes, reducing the degradation of the main components of the ECM (FAYAD et al., 2018). Hartmann *et al.* (HARTMANN et al., 2015) showed the potential of MAAs shinorine, porphyra-334, and palythine isolated from *Palmaria palmata* and *Porphyra* sp. on collagenase inhibition.

Based on the information mentioned previously, the goal of this study was to characterize the aqueous and hydroethanolic extracts of six red macroalga species, in order to evaluate their antioxidant capacity and potential to inhibit the collagenase activity. Considering all analyses, the most promising extracts from *P. linearis* and *P. acanthophora*

were incorporated into a dermocosmetic prototype and evaluated for their *in vitro* cytotoxicity. In addition, four Biological Effective Protection Factors (BEPFs) from these two formulations were determined according to de la Coba et al. (2019)

2.3 MATERIAL AND METHODS

2.3.1 Algal Material

The algae samples used in this study were collected at sites in Brazil and Spain (Table 1**)**. *Phycocalidia acanthophora* and *Porphyra linearis* were harvested from intertidal zones, meanwhile, *Condracanthus teedei, Osmundea pinnatifica* and *Plocamium cartilagineum* from subtidal zones. These species were detached from rocky shores, considering that they were attached by holdfast in hard substrates. *Gracilaria cornea* thalli were obtained from algal cultures in tanks performed by the Spanish Bank of Algae, in Canary Islands. The species is originally from Caribe but has been cultivated by vegetative reproduction over the past 30 years in outdoor tanks. All different species were sampled and moved to the laboratory, where their thalli were cleaned with seawater to remove the impurities and finally submitted to a quickly distilled water bath in order to remove the salt excess. The samples were lyophilized, milled, and stored with silica at room temperature. Freeze-dried material was utilized in the diverse analyses described below.

Tabela 1. Macroalgae species utilized in this study and their collection sites.

	Longitude and latitude	Collection place	Period of Collection
Phycocalidia acanthophora	27°34’25’’S, 48°25’16’’W	Florianópolis/Brazil	August/2020
Chondracanthus teedei	28°20’17’’S, 48°42’12’’W	Imbituba/Brazil	August/2020
Gracilaria cornea	28°07’50’’N, 15°26’50’’ W	Gran Canaria/Spain	June/2020
Osmundea pinnatifida	36° 42’ 42’’N, 4° 19’35’’ W	Málaga/Spain	May/2020
Plocamium cartilagineum	36° 03’45’’ N, 5°42’00’’ W	Tarifa/Spain	Februray/2021
Plocamium cartilagineum	36°44’17’’N, 3°45’15’’W	La Herradura/Spain	March/2021
Porphyra linearis	42°24’22’’N, 8°41’06’’ W	Galicia /Spain	April/2021

Samples were obtained from two countries, at different periods.

2.3.2 Extraction

In order to evaluate the potential of the extracts in cosmeceutical field, two extractions using eco-friendly solvents were performed, being that water and a hydroethanolic solution (1: 1). For this purpose, to each below described assay, 20 mg of dried algae were homogenized with 1mL of solvent. The extracts were incubated during 2 hours, at 45°C under agitation. After incubation, the extracts were centrifuged (10 min, 4000 rpm, 4°C) and the supernatant collected and stored at -20°C.

For quantification of MAAs, three different extracts were utilized. In this case, in addition to the aqueous and hydroethanolic ones, a methanolic extract was also prepared as described by Korbee-Peinado et al. (KORBEE; FIGUEROA; AGUILERA, 2005). Shortly, 20 mg dried algae were homogenized with 1 mL of methanol 20% (v/v). The extracts were incubated during 2 hours, at 45°C, under agitation. After incubation, the extracts were centrifuged (10 min, 4000 rpm, 4°C) and the supernatant collected and evaporated using a vacuum centrifuge during 18 h. The pellet was resuspended in 1 mL methanol (HPLC grade), and filtered (0.22μm).

2.3.3 UV-vis Absorption Spectrum

The absorbances of aqueous and hydroethanolic extracts were determined using a UV–visible spectrophotometer (Shimadzu UV Mini-1240), with a spectral window from 280 to 700 nm and resolution of 1 nm.

2.3.4 Yield of Extraction

To evaluate the extraction yield, the algal extracts were prepared as above mentioned (item 2.2), with an initial known biomass (Initial Biomass). Further, the supernatants were collected, transferred to falcon tubes previously weighed (Tubes weight, TW), and then placed in a stove at 60°C during 48 h, when they were weighed again (Tubes with dried extract weight, TDEW). Biomass extraction yield was calculated as the following equation:

$$\text{Extraction Yield (\%)} = \frac{(TDEW - TW)}{Initial\ biomass} x\ 100$$

2.3.5 Total Carbon, Nitrogen, Hydrogen, and Sulfur content

Total Carbon (C), Nitrogen (N), Hydrogen (H) and Sulfur (S) contents from the dry algal biomass were evaluated using a CNHS LECO-932 elemental analyzer (St. Joseph, MI, USA) in the Research Support Central Services (SCAI, University of Málaga, Málaga, Spain). Only one sample of each species was used to conduct this analysis, considering a descriptive perspective.

2.3.6 Antioxidant capacity

2.3.6.1 ABTS+

Antioxidant capacity was evaluated using the ABTS method (RE et al., 1999). Previously, ABTS reagent was prepared by mixing a solution of ABTS (2, 2′-azino-bis (3-ethylbenzothiazoline-6-sulphonic acid, 7 mM), potassium persulfate ($K_2S_2O_8$, 2.45 mM), and sodium phosphate buffer (0.1 M, pH 6.5). The reagent was incubated in darkness at room temperature for 16 h. The reaction was done by adding 900 µL of the ABTS solution and 100 µL of algal extract. The samples were shaken and absorbance (abs) was recorded by a UV–visible spectrophotometer (Shimadzu UV Mini-1240) at 727 nm at the beginning of the reaction (T0) and after 8 min of incubation (T8). Phosphate buffer was used as blank. The antioxidant capacity (AC) was calculated according to the formula:

$$AC\% = [(absT0 - absT8)/abs\ T0] * 100$$

The antioxidant compounds concentration was calculated using a standard curve of Trolox (6-hydroxy-2, 5, 7, 8-tetramethylchroman-2-carboxylic acid), using the linear fitting $y = 0.1185x + 0.004$ ($r^2 = 0.99$), and the results expressed in µM of TE (Trolox equivalent) per g of algal dry weight (DW).

2.3.6.2 Catalase

Catalase activity of aqueous and hydroethanolic extracts of the red macroalgae investigated was determined based on the decay of hydrogen peroxide at 240 nm (BARROS et al., 2003). For this, 50 µL of lyophilized extracts (20 mg. mL^{-1} resuspended in water) were added to 1 mL of PBS containing 20 mM of hydrogen peroxide. The absorbance was measured during 7 min, with intervals of 15 s, at 240nm. One unit of catalase is defined as the amount of enzyme which hydrolyzes 1 µmol of H_2O_2 per minute, at 25°C. The results were expressed as U. CAT per milligram of soluble protein. The determination of the soluble protein content in the extracts was done based on the Bradford methodology using the Coomassie Brilliant blue G-250 reagent (BRADFORD, 1976).

2.3.7 Phenolic Compounds

The quantification of phenolic compounds on the algal extracts was performed using the Folin-Ciocalteau reagent (FOLIN; CIOCALTEU, 1927). Briefly, for this assay 100 µL of algal extract were mixed to 700 µL of distilled water and 50 µL of Folin-Ciocalteau reagent. The reaction is started by the addition of 150 µL of 20% sodium carbonate (Na_2CO_3). The tubes were stirred and the reaction incubated at 4 °C during 2 h. At the end of the incubation time, the absorbance was determined at 760 nm using a UV–visible spectrophotometer (Shimadzu UV Mini-1240). Distilled water was used as a blank. The total content of phenolic compounds was calculated using a standard curve with phloroglucinol (Sigma P-3502) (6-hydroxy-2, 5, 7, 8-tetramethylchroman-2-carboxylic acid), considering the linear fitting y=0.0757x-0.021
(r^2 = 0.99), and the results expressed in mg g^{-1} of equivalent of phloroglucinol per g of algal dry weight (DW).

2.3.8 Collagenase Inhibitory Activity

The inhibition of collagenase activity was performed according to the methodology described by Widowati et al. (2016), with slight modifications, using FALGPA (Furylacroloyl-LEU-GLY-PRO- ALA) as substrate. For this purpose, 20 µL of collagenase

(1.6 $U.mL^{-1}$) was incubated during 20 min with 50µL of the different algal extracts (5 $mg\ mL^{-1}$). After incubation, 70 µL of 50 mM tricine buffer (pH 7.5) and 100 µL of a 1 mM FALGPA in 50 mM tricine buffer (pH 7.5) were added, and the reaction started immediately. The absorbance (abs) was measured using a microplate reader at 335nm, at 0 min (T0) and after 5 min (T5) of incubation at room temperature. Epigallocatechin gallate (EGCG) was used as positive control and the collagenase inhibitory activity calculated as follows:

$$\text{Inhibition \%} = [(\text{abs T0} - \text{abs T5})/\text{abs T0}] * 100$$

2.3.9 Mycosporine-Like Amino acids (MAAs) Composition and Concentration

The MAA content was analyzed according to the methodology described by Chaves-Peña et al. (2019). In addition to above mentioned extract, a methanolic extract of each species was prepared, to serve as reference and compare with previous studies. Then, aqueous, hydroethanolic and methanolic extracts were filtered (0.2µm membrane filter) and injected in a Waters 600 UHPLC system (Waters Chromatography, Barcelona, Spain). Aliquots (20µL) of the samples were injected into a reverse-phase Luna C8 column (5µm particle size, 4.06 mm×250 mm - Phenomenex, Aschaffenburg, Germany) coupled to a pre-column (C8, Octyl, MOS; Phenomenex). As UHPLC eluent, a 1.5% methanol (v/v) plus 0.15% acetic acid (v/v) solution was used in an isocratic flux, during 30 min. The peaks of the analytes of interest were compared with analytical standards of porphyra-334 (P334), shinorine, and palythine, previously purified in a periodic counter-current chromatograph apparatus (VEGA et al., 2023).

In the case of aqueous extracts, the MAAs were also further identified by electrospray ionization mass spectrometry (ESI-MS) with a high-resolution mass spectrometer (model Orbitrap Q-Exactive, Thermo Scientific S.L., Bremen,Germany) in the Central Service for Research Support (SCAI, University of Málaga, Málaga, Spain). The equipment was configured in positive mode with a voltage of 3.5 kV.

2.3.10 Cell Culture and Maintenance

To evaluate the effect of the extracts on the viability of skin cells, human fibroblasts (1064sk, CIC-UGA, ES) and immortalized human keratinocytes (HACAT, ATCC, USA) cell lines were used. To maintain the cells, HACAT cells were grown in RPMI-1640 medium (BioWhittaker, ref. BE12-167F) supplemented with 10% fetal bovine serum (Biowest ref. S1810-500), 1% penicillin–streptomycin solution 100×, and 0.5% of amphotericin B. 1064sk fibroblasts were previously cultured using Dulbecco's modified Eagle's medium (DMEM) (Capricorn Scientific, ref. DMEM-HPSTA) supplemented with 10% fetal bovine serum (Biowest, ref. S1810-500), 1% penicillin–streptomycin solution 100× (Capricorn Scientific, ref. PS-B), and 0.5% of amphotericin B (Biowest ref. L0009-100). The cells were kept at an atmosphere-controlled incubator, with 5% CO_2, at 37 °C.

2.3.11 Cell Viability Determination Using the MTT Assay

The cell viability assay used in this study is based on the reduction of 3-(4, 5-dimethylthiazol-2-yl)-2, 5-diphenyltetrazolium bromide (MTT, Sigma-Aldrich) to the corresponding water insoluble purple formazan by the mitochondrial dehydrogenase in living cells. The experiment was conducted using 96-well plates, containing 10000 1064sk cells/well and 6000 HACAT cells/well, with different concentrations of the extracts, ranging from 0.009 to 10 mg mL^{-1}. The solutions were incubated during 72 h, at the same conditions as the maintenance protocol. At the end of incubation time, 10 µL of the MTT solution (5 mg mL^{-1} in phosphate buffered saline) and 100 µL of culture medium were added to each well. The plates were incubated at 37 °C for 4 h, and finally the formazan crystals produced were solubilized with 150 µL of 0.04 M HCl - 2-propanol and the absorbance measured spectrophotometrically at 550 nm (Micro Plate Reader Synergy HTX, BIOTEK, USA). The results are expressed as IC_{50}, that corresponds to the amount of the compound required to reduce 50% of the cell survival (ABDALA DÍAZ et al., 2019).

2.3.12 Development of the Base Cream Formulation

The cosmeceutical formulation was elaborated from scratched and consists on an oil-in-water (O/W) emulsion according to the requirements of natural cosmetics (Table 2). The

algal extracts utilized to prepare cosmeceutical formulation were done with the species *P. acanthophora* and *P. linearis*.

Tabela 2. Cosmeceutical ingredients (%) in the formulation utilized in the assays performed in this study.

Ingredient	**%**
Oily phase	
Cetearyl alcohol	0.5
Estearyl alcohol	0.5
Cetearyl alcohol and cetearyl glucoside (Montanov 68)	4
Cetearyl olivate and sorbitan olivate (Olivem 1000)	4
Isopropyl miristate	1.5
Coco caprylate	1.5
Ricinus communis seed oil (Castor oil)	5
Sesamm indicum seed oil	5
Titanium dioxide	7.5
Zinc oxide	7.5
Aqueous phase	
Algal extract	10
Glycerin	10
Distilled water	Q. s
Additional Ingredient	
Benzyl alcohol, *Cymbopogon flexuosus* leaf oil, tocopherol (Euxyl Eco)	< 1

Q.s as quantity sufficient.

To obtain a stable emulsion, the two phases were prepared separately and homogenized at an UNGUATOR 2100 homogenizer.

2.3.13 Biological Effective Protection Factors (BEPFs)

After assessing biochemical composition and extracts activities, we decided to test the inclusion of our aqueous extracts into sunscreens formulations. In this way, the biological effective protection factors (BEPFs) of these compositions were calculated according to de la Coba *et al.* (DE LA COBA et al., 2019).

In the standard method reported by ISO24443, photoprotection coefficients of SPF and UVAPF are calculated using a polymethylmethacrylate (PMMA) plate (Schönberg, Hamburg, Germany) with roughness (Ra) of 6 µm. In our procedure, different PMMA plates, with an acceptable surface of 50 mm x 50 mm and a different roughness (Ra), in the range of

3.5–4.5 μm, were adopted. The utilization of a lower roughness in the PMMA plates produces different photoprotection indices, increasing the SPF and UVAPF values (FERRERO et al., 2007). To estimate how much our data would be overestimated when compared to the standard procedure, a correction factor (CF) using a reference standard cream was obtained. This cream was applied in the PMMA plate with appropriate roughness (Ra = 6), obtaining a SPF = 16 (Sun Protection Factor, with the application of 1.3 $mg.cm^{-2}$ of cream in the correct PMMA plate with Ra=6 μm. In the case of a plate with 25 cm^2, a total amount of 32.5 mg of cream should be applied, as described by ISO24443.

Different amounts of cream Ref.SPF#16 were spread on the PMMA plate surface (15, 20, 22.5, 25, and 30 mg) with a gloved fingertips for 30 s (approx.). Then, the plates remained in darkness to dry for 30 min, and transmittance through plates was measured using a spectrophotometer (UV-2700i, Shimadzu, Duisburg, Germany) with an integrating sphere. Erythema action spectrum was used to calculate the SPF and PPD action spectra was applied in the calculation of UVAPF, as the following equation:

$$\text{SPF or UVAPF} = \frac{\Sigma_{290}^{400} Act.Sp(\lambda) * E(\lambda)}{\Sigma_{290}^{400} Act.Sp(\lambda) * E(\lambda) * T(\lambda)}$$

Where,

Act.Sp (λ) = action spectra (SCHNEIDER et al., 2020b)

E (λ) = spectral irradiance of a sunny midday in a summer day (June) in Malaga (W m^{-2});

T (λ) = transmittance values at each wavelength (0–1);

A (λ) = absorptance values at each wavelength (0–1).

Then, a calibration curve was created, using SPF values vs. cream quantities spread in the PMMA plates. The linear fitting as y=2.6083x-29.979 (r^2=0.96) was obtained and allowed the estimation of SPF that would be obtained if 32.5 mg were applied on the PMMA plate with roughness of 3.5-4.5, resulting in the $SPF_{roughness3.5\text{-}4.5}$ of 54.79. When dividing $SPF_{roughness3.5\text{-}4.5}$ by $SPF_{roughness\ 6}$, the CF was 3.42.

After obtaining CF, the following formulations were prepared: BC, Base cream; BC+PF, Base cream plus 15% physical filters (ZnO and TiO_2); BC+A_{Pl}, Base cream plus 10% of *P. linearis* aqueous extract; BC+A_{Pa}, Base cream plus 10% of *P. acanthophora* aqueous extract; BC+PF+A_{Pl}, Base cream and 15% physical filters (ZnO and TiO_2) plus 10% of *P. linearis* aqueous extract; BC+PF+A_{Pa}, Base cream and 15% physical filters (ZnO and TiO_2)

plus 10% of *P. acanthophora* aqueous extract. Thirty mg of each cream separately were applied in the PMMA plates with Ra=3.5-4.5 mm. The transmittance was measured as above, and after, plates were moved to a Solar Simulator Oriel Spectra Physics lamp, remained there by 30 min, receiving UV radiation (70W m^2, 290-400 nm). After, transmittances were measured again, allowing the understanding about creams stability against UV-radiation. Besides SPF, other protection factors were calculated with these 30 mg-applied creams. The following action spectra (Erythema, Permanent Pigment Darkening, Elastosis, Photoaging and Singlet oxygen production) were obtained from Schneider *et al.* (SCHNEIDER et al., 2020b). They were used to calculate the Sun Protection Factor (SPF, as described above), UV-A Protection Factor (UVAPF), Elastosis Protection Factor (EPF), Photoaging Protection Factor (PPF), and Singlet Oxygen Protection Factor (SOPF), respectively. The five indices (SPF, UVAPF, EPF, PPF, SOPF) were calculated following the same equation above, using their specific action spectra, respectively.

2.3.14 Statistical Analysis

All tests were conducted in three replicates and the results are presented as the mean value ± standard deviation. The statistical significance of the means was evaluated by one-factor Analysis of Variance (ANOVA), followed by the Tukey's test. Pearson's correlation was performed among the dependent variables, performed using the software Statistic 7.0. A level of significance of 95% ($p < 0.05$) was established for all analyses. The *t*-student test was used to compare on BEPFS analysis, the groups containing the extracts with its respective control. Principal component analysis (PCA) was done by using the Software Primer 6.

2.4 RESULTS

2.4.1 UV-vis Absorption Spectrum

The UV absorption spectra (280-400 nm) indicate the presence of absorption peaks between 320 and 340 nm for all extracts investigated, highlighting the extracts of *P. linearis* and *P. acanthophora* (Figure 10). A clear pattern of absorbance profiles among all extracts on the visible absorption spectra (400-700 nm, Figure 11) was not detected. *P. linearis* and *G.*

cornea presented aqueous extracts with major peaks between 500 and 650 nm. The pigment contents detected in aqueous extract of *P. linearis* correspond to 7.01 ± 0.12 mg of R-phycoerythrin per gram of dry biomass and 6.94 ± 0.2 mg of R-phycocyanin per gram of dry biomass. For *G. cornea*, 7.92 ± 0.44 mg of R-phycoerythrin per gram of dry biomass was found, and lower amounts (0.38 ± 0.04 mg of R-phycocyanin per gram of dry biomass) were detected (Table S1). The other species also presented phycobiliproteins in lower amounts.

Figura 10. UV absorption spectra (λ = 280–400 nm) of the aqueous and hydroalcoholic (1:1 v/v) extracts for six species of red macroalgae.

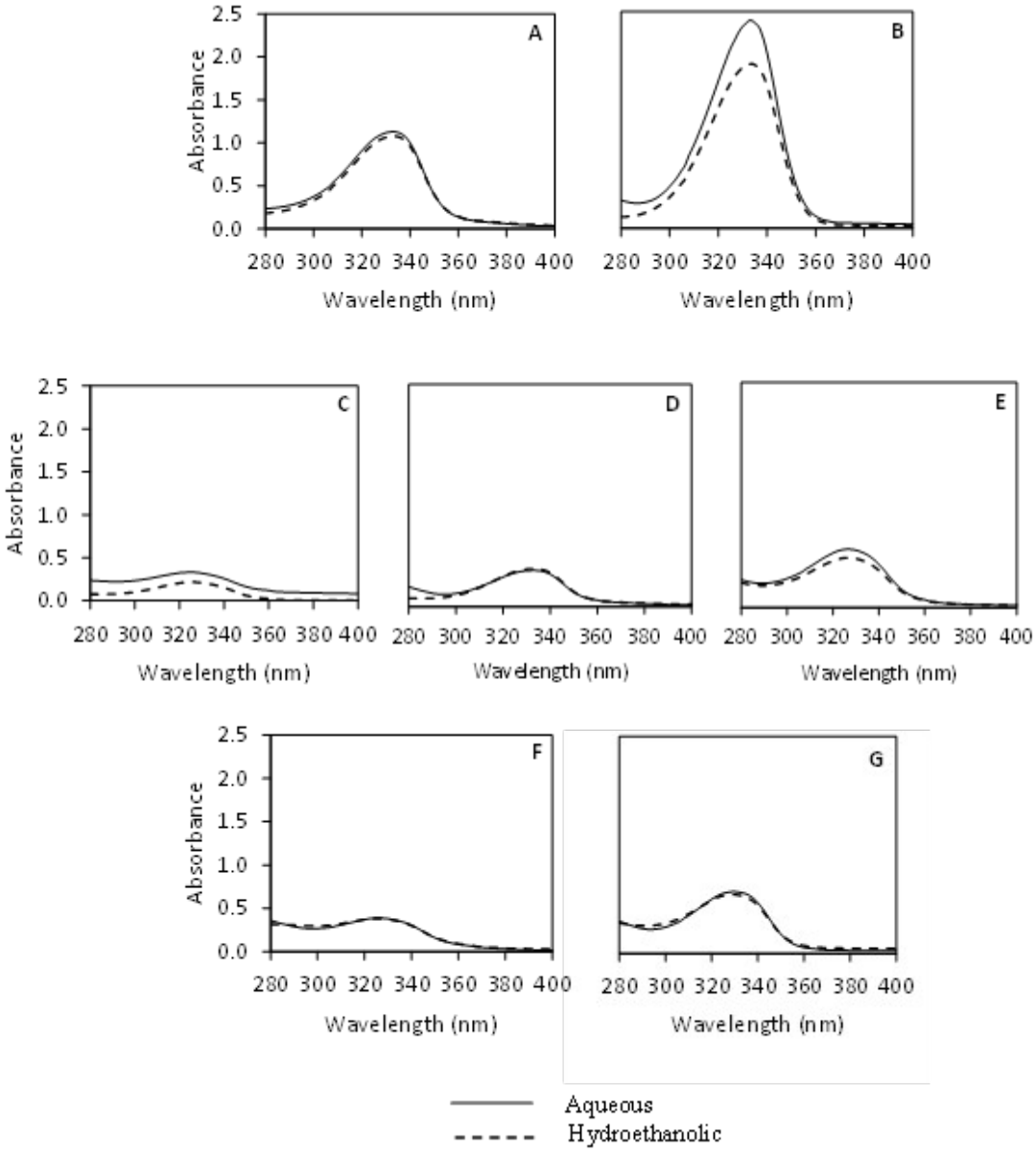

Each graph corresponds to the extracts of: A, *Phycocalidia acanthophora*; B, *Porphyra linearis*; C, *Condracanthus teedei*; D, *Gracilaria corne*; E, *Osmundea pinnatifida*; F, *Plocamium cartilagineum* (TA); G,

Plocamium cartilagineum (LH). The species Plocamium cartilagineum was sampled in two sites: La Herradura (LH) and Tarifa (TA).

Figura 11. Absorption spectra in the visible region (λ = 400-700 nm) of the aqueous and hydroalcoholic (1:1 v/v) extracts for each species of the red macroalgae in study.

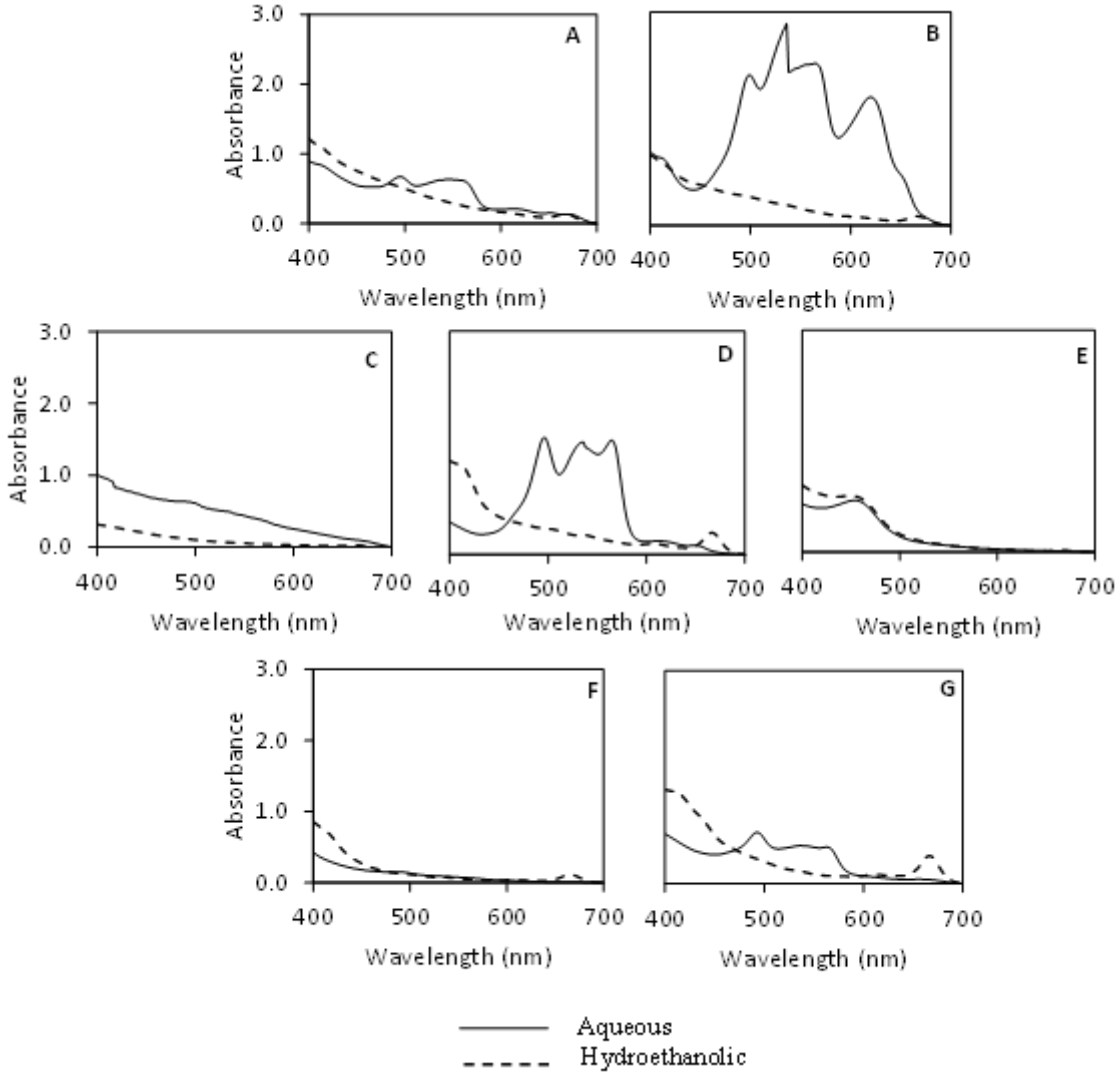

Each graph corresponds to the extracts of: A, *Phycocalidia acanthophora*; B, *Porphyra linearis*; C, *Condracanthus teedei*; D, *Gracilaria corne*; E, *Osmundea pinnatifida*; F, *Plocamium cartilagineum* (TA); G, *Plocamium cartilagineum* (LH). The species Plocamium cartilagineum was sampled in two sites: La Herradura (LH) and Tarifa (TA).

2.4.2 Yield of Extraction

The use of different solvents impacted directly on the extraction yield (Table S2 - ANOVA). The extraction yield (Figure 12) was statistically higher with water as solvent

comparatively to the hydroethanolic solution (water/ ethanol) ($p < 0.05$) in all evaluated species. Aqueous extracts yield varied from 21 to 86%, while hydroethanolic yield ranged from 12 to 67%, indicating water a better solvent for extraction of metabolites. Besides, the highest yields were obtained with *G. cornea* extracts.

Figura 12. Extraction yield of the aqueous and hydroalcoholic extracts (ethanol: water, 1:1) of six red macroalgae species.

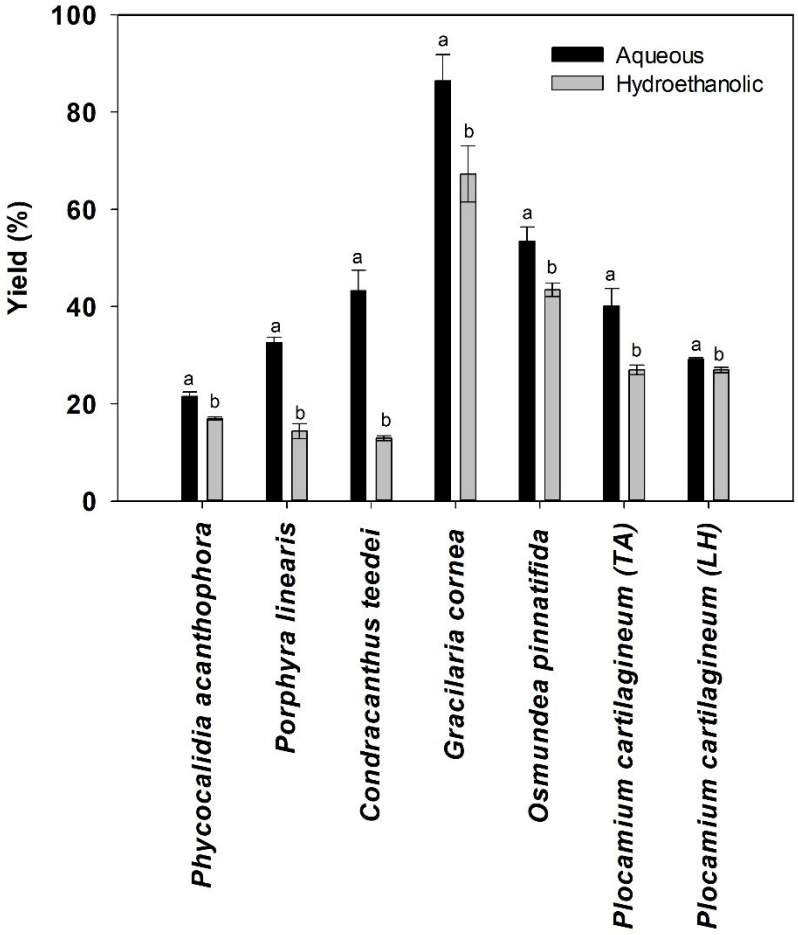

The results are expressed as percentage of extraction yield (%). Different letters indicate significantly differences between the solvents used ($p < 0.05$). Data are represented as means ± standard- deviation ($n = 3$). The species *Plocamium cartilagineum* was sampled in two sites: La Herradura (LH) and Tarifa (TA).

2.4.3 Total Carbon, Nitrogen, Hydrogen, and Sulfur content

The biomass of *P. acanthophora* and *P. linearis* presented the highest percentage of carbon and hydrogen. In fact**,** *P. linearis* can be highlighted by its high content of nitrogen when compared to the others. Meanwhile, *C. teedei* biomass presented the highest percentage in sulfur (Table 3).

Tabela 3. Descriptive elemental composition of the dry biomass of Phycocalidia acanthophora, Porphyra linearis, Condracanthus teedei, Gracilaria cornea, Osmundea pinnatifida and Plocamium cartilagineum.

	% C	% H	% N	% S
Phycocalidia acanthophora	37.9	5.8	1.4	1.4
Porphyra linearis	37.9	5.7	6.5	1.5
Condracanthus teedei	26.5	4.4	1.6	6.5
Gracilaria cornea	22.1	3.5	2.5	4.3
Osmundea pinnatifida	23.2	3.8	1.7	2.1
Plocamium cartilagineum (TA)	28.1	4.9	3.1	3.4
Plocamium cartilagineum (LH)	28.4	4.7	4.3	3.7

The species *Plocamium cartilagineum* was sampled in two sites: La Herradura (LH) and Tarifa (TA). Data are presented as percentage of Carbon, Nitrogen, Hydrogen and Sulfur (CHNS). Only one replicate was done, and the data are purely descriptive.

2.4.4 Antioxidant Capacity

The antioxidant capacity was evaluated by a non-enzymatic ($ABTS^{+}$) and an enzymatic (catalase activity) method (Table 4). Aqueous extracts were more efficient to scavenge the radical $ABTS^{+}$ when compared to the hydroethanolic ones (Table S2 - ANOVA). Aqueous extract of *P. linearis* presented the highest antioxidant capacity (5.93±0.07 µM TE g^{-1}DW) among all extracts. Regarding the enzymatic method, hydroethanolic extracts did not exhibit catalase activity, while aqueous extracts of *C. teedei* presented the highest values (2.2±0.4 units of catalase per mg of soluble proteins), followed by aqueous extract of *P. linearis* (1.38±0.1 U cat mg^{-1} soluble proteins).

Tabela 4. Antioxidant capacity of aqueous and hydroethanolic extracts (ethanol: water, 1:1) of six red alga species, determined by the $ABTS^{+}$ and catalase methodologies.

	Non-enzymatic		**Enzymatic**	
	$ABTS^{+}$ (µM TE g^{-1})		**Catalase (Ucat mg^{-1} SP)**	
	Aqueous	Hydroethanolic	Aqueous	Hydroethanolic
Phycocalidia acanthophora	$1.13^{a} \pm 0.04$	$0.95^{b} \pm 0.06$	$0.86^{a} \pm 0.1$	0
Porphyra linearis	$5.93^{a} \pm 0.07$	$2.35^{b} \pm 0.07$	$1.38^{a} \pm 0.1$	0
Condracanthus teedei	$1.09^{a} \pm 0.07$	$0.65^{b} \pm 0.04$	$2.2^{a} \pm 0.4$	0
Gracilaria cornea	$1.85^{a} \pm 0.09$	$1.4^{b} \pm 0.03$	0	0
Osmundea pinnatifida	$0.45^{a} \pm 0.02$	$0.53^{a} \pm 0.06$	$0.44^{a} \pm 0.09$	0
***Plocamium cartilagineum* (TA)**	$1.57^{a} \pm 0.05$	$1.55^{a} \pm 0.03$	$0.19^{a} \pm 0.06$	0
***Plocamium cartilagineum* (LH)**	$2.06^{a} \pm 0.11$	$1.87^{b} \pm 0.03$	0	0

Values are expressed in µg of Trolox Equivalents (TE) per mg of algae dry weight (DW) for the ABTS+ experiment, and catalase activity is expressed in Units of catalase (Ucat) per mg of soluble proteins (SP). Different letters indicate significant differences between aqueous and hydroethanolic extracts, according to a Tukey test ($p < 0.05$). Data are represented as means ± standard- deviation ($n = 3$). The species *Plocamium cartilagineum* was sampled in two sites: La Herradura (LH) and Tarifa (TA).

2.4.5 Phenolic Compounds

Except for *G. cornea*, all aqueous extracts exhibited higher or equal content of polyphenols than hydroethanolic extracts (Table S2 – ANOVA). Aqueous extract of *P. linearis* showed the highest amount of phenolic compounds, containing 14 mg phloroglucinol per g dry algal biomass ($mg \cdot g^{-1}$ DW) (Figure 13).

Figura 13. Concentration of polyphenolic compounds (mg phloroglucinol per g algal biomass - dry weight) in aqueous and hydroethanolic extracts (ethanol: water, 1:1) of red macroalgae.

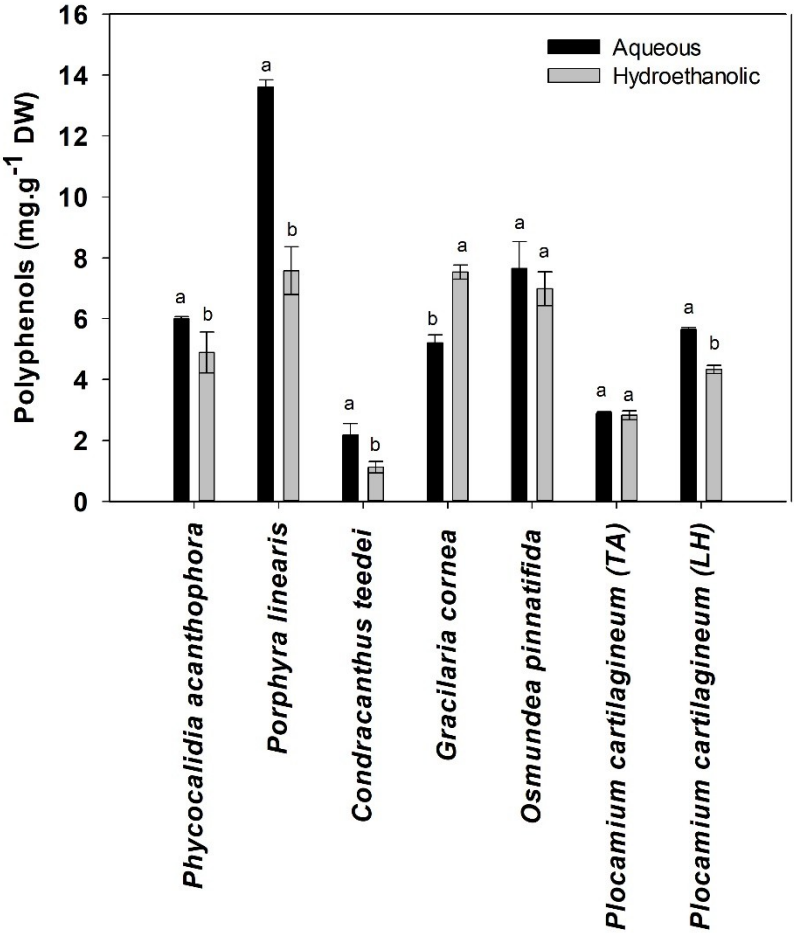

Different letters indicate significant differences between aqueous and hydroethanolic extracts, according to a Tukey test ($p < 0.05$). Data are represented as means ± standard- deviation ($n = 3$). The species *Plocamium cartilagineum* was sampled in two sites: La Herradura (LH) and Tarifa (TA).

2.4.6 Mycosporine-Like Amino acids (MAAs) Composition and Concentration

The concentrations of mycosporine-like amino acids (MAAs) measured on algae extracts are presented in Figure 14. MAAs contents were quantified using UHPLC in the three types of extracts (aqueous, hydroethanolic and methanolic). In the case of hydroethanolic extracts, the results are not presented here because the obtained chromatographic peaks did not show a satisfactory resolution, avoiding efficient identification and separation of MAA types. Aqueous extracts *P. linearis* and *P. acanthophora* exhibited the highest amount of total MAAs, with values over 8 mg per g of algal biomass dry weight.

Figura 14. Mycosporine-like amino acids (MAAs) detected in aqueous and 20% methanolic extracts (methanol: water, v/v) of six red macroalga species.

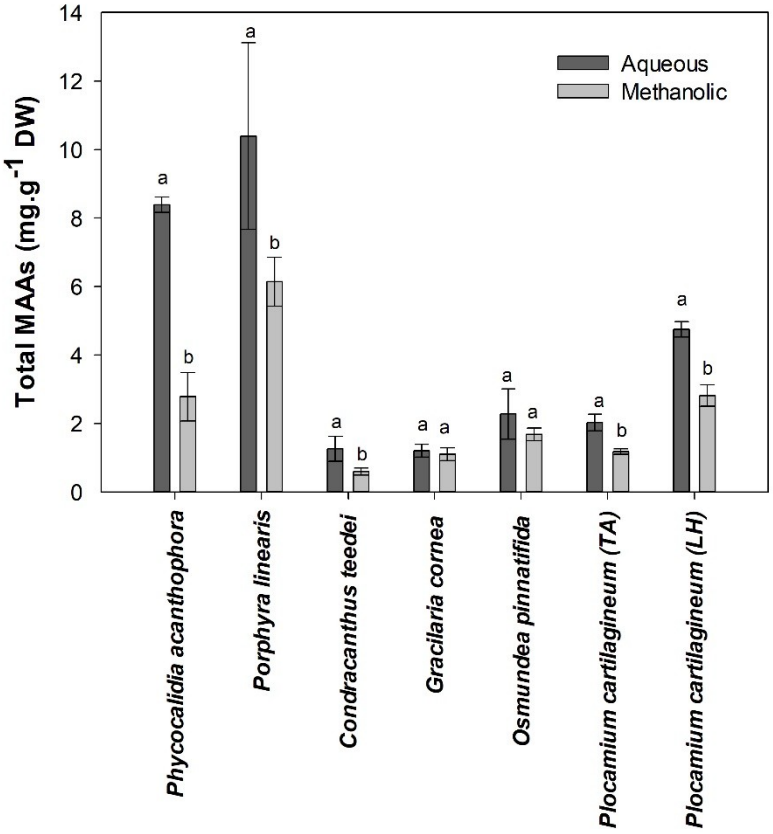

MAA concentration is expressed in mg of MAAs by g of dry algal biomass. Different letters indicate significant differences between aqueous and methanolic extracts, according to a Tukey test ($p < 0.05$). Data are represented as means ± standard- deviation ($n = 3$). The species *Plocamium cartilagineum* was sampled in two sites: La Herradura (LH) and Tarifa (TA).

ESI-MS analysis indicated the presence of different MAAs profiles in the aqueous extracts of the red macroalgae investigated (Table 5). The results revealed the presence of porphyra-334, shinorine, palythine, and asterine-330. These are MAAs usually described in red marine macroalgae species. The following molecular formulas, which can be common to more than one MAAs, were also detected in some extracts: $C_{13}H_{20}N_2O_5$ corresponding to the molecular formula of usurjirine and palythene, $C_{13}H_{22}N_2O_6$ presenting the molecular formula of palythinol, mycosporine-glutinol, mycosporine-methylamine:threonine and Aplysiapalythine B and $C_{12}H_{20}N_2O_6$ equivalent to the molecular formula of mycosporine-2-glycine, palythine-threonine and mycosporine-methylamine:serine.

Tabela 5. Mycosporine-like amino acid composition characterized by ESI mass spectrometry for the aqueous extracts of the analyzed species.

	Aplysiapalythine B	Asterine-330	$C_{13}H_{20}N_2O_5$	$C_{13}H_{22}N_2O_6$	Mycosporine-Glutamine	$C_{12}H_{20}N_2O_6$	Palythine	Shinorine	Mycosporine-2-glycine	Porphyra-334	Palythine-Serine
Phycocalidia acanthophora	x	x	x	x	x					x	
Porphyra linearis	x		x	x		x	x	x	x	x	
Condracanthus teedei					x	x	x	x	x	x	
Gracilaria cornea			x	x		x					
Osmundea pinnatifida	x			x		x	x				
***Plocamium cartilagineum* (TA)**				x		x	x	x			x
***Plocamium cartilagineum* (LH)**					x	x	x	x	x		x

The species *Plocamium cartilagineum* was sampled in two sites: La Herradura (LH) and Tarifa (TA). C13H20N2O5 is the molecular formula of usurjirine and palythene. C13H22N2O6 is the molecular formula of palythinol, mycosporine-glutinol, mycosporine-methylamine:threonine and Aplysiapalythine B. C12H20N2O6 is the molecular formula of mycosporine-2-glycine, palythine-threonine and mycosporine-methylamine:serine.*All ESI-MS spectra are presented in supplementary material (Figures S1-S7).

2.4.7 Collagenase Inhibitory Activity

The experiments regarding the inhibition of the collagenase activity revealed that all six tested macroalgae extracts were able in to inhibit that enzyme, at least by 15%. However, two species must be highlighted for both extracts assessed. Following the pattern observed for total MAAs, the species with more potential to inhibit collagenase activity were *P. acanthophora* and *P. linearis* (Figure 15). Importantly, the ethanolic extract of *P. linearis* inhibited by 100% the enzyme activity.

Figura 15. Inhibitory collagenase activity by the aqueous and hydroethanolic extracts of the six red macroalgae investigated.

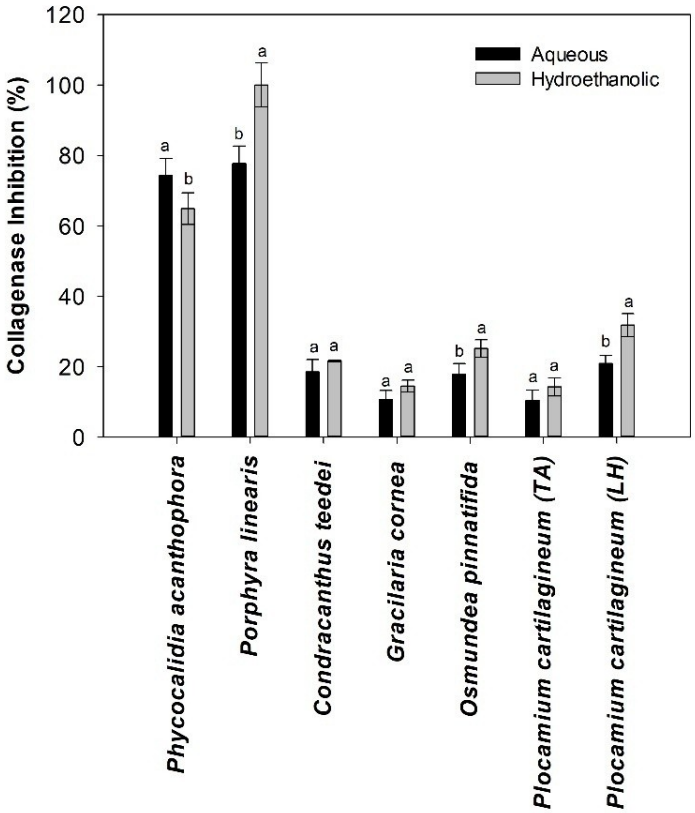

The results are expressed in percentage of inhibition (%). Different letters indicate significant differences between aqueous and hydroethanolic extracts, according to a Tukey test ($p < 0.05$). Data are represented as means ± standard- deviation (n = 3). The species *Plocamium cartilagineum* was sampled in two sites: La Herradura (LH) and Tarifa (TA).

Pearson's correlation among the different biochemical compounds and bioactivities on aqueous extracts are shown in Table S4. All correlations observed are positive ones. The antioxidant activity by quenching of the radical $ABTS^+$ was correlated to the polyphenols, MAAs, PE, PC contents, and also the inhibition of collagenase. Besides $ABTS^+$, the polyphenol content was also positively correlated to collagenase inhibition, PE and PC. PC was positively correlated to all factors and R-PE to all factors, except to collagenase inhibition. Similarly, Pearson's correlation values for the variables analyzed in the hydroethanolic extracts are shown in Table S5. The $ABTS^+$ antioxidant activity was positively correlated to the inhibition of collagenase. Phycocyanin was positively correlated to the polyphenol content and also with the collagenase inhibition. Considering that aqueous extracts were more correlated to biochemical factors than hydroethanolic, the data was also analyzed using a PCA analysis (Figure 16). The plot indicated that the two principal axes explained 95.2% of the variation, where the first principal component analysis (PC1)

explained 86.7% of total variation and the second (PC2) accounted for 8.5% of the variation. Based on PCA graph, the species *P. linearis* and *P. acanthophora* were grouped negatively in quadrant 3 and are more correlated to the dependent variables, except for phycoerythrin amounts. *P. cartilagineum* (LH) and *G. cornea*, both grouped in the quadrant 1, could be associated to this last parameter.

Figura 16. Principal Component Analysis (PCA) for biochemical parameters obtained from aqueous extracts of the six red macroalgae investigated.

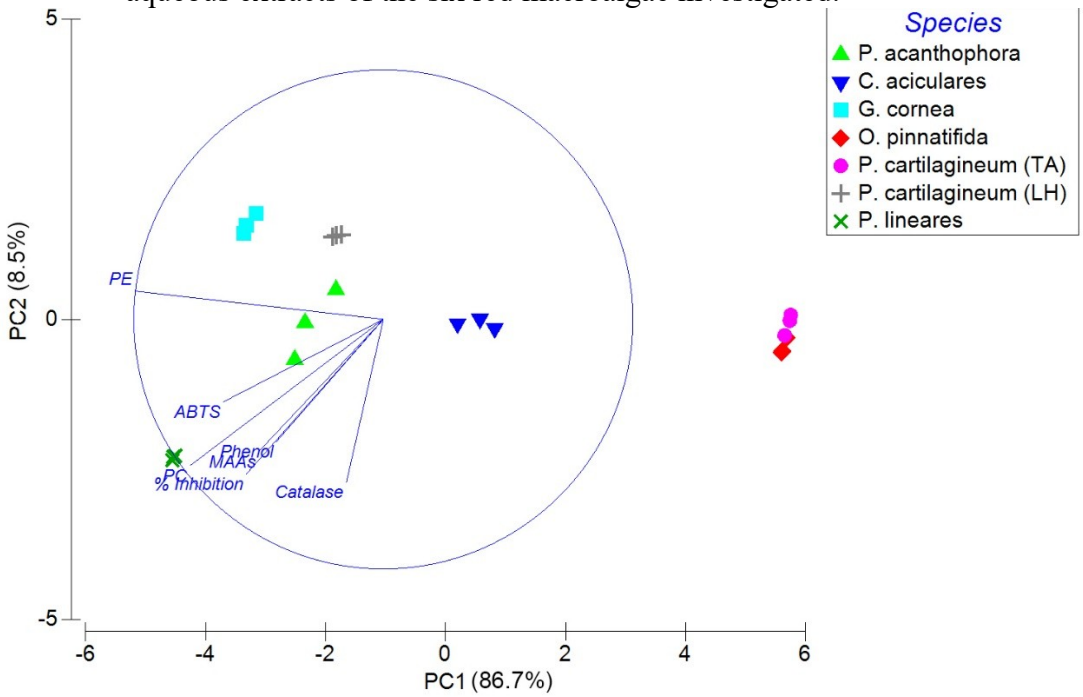

Plots of axis PC1 vs axis PC2 representing the position of the 21 samples are included in the analysis. Q1, Q2, Q3 and Q4 correspond to the different quadrants in the graph. Mycosporine-Like amino acids as MAAs. Phycoerythrin as PE. Phycocyanin as PC.

2.4.8 Cell Viability Determination Using the MTT Assay

The cell viability measured using the MTT reagent indicated that cell proliferation depends on the alga extracts concentration. Cells presented higher survival when extract concentration decreased (Figure 17). It is also observed a sharp decreasing on cell viability in lowest concentrations. Using the values obtained from those curves, IC_{50} values were calculated for both extracts. The IC_{50} value in HACAT cells was 3610 ± 0.08 µg mL^{-1} for the *P. linearis* aqueous extract and 3920 ± 0.08 µg mL^{-1} for *P. acanthophora* extract. In the case of 1064sk fibroblast cell line, the IC_{50} obtained treating the cells with *P. linearis* aqueous

extract from was equivalent to 6520 ± 0.51 µg mL^{-1}, with a lower value (1950 ± 0.92 µg mL^{-1}) for *P. acanthophora* extract.

Figura 17. Survival (%) of human cells following exposure to algal extracts.

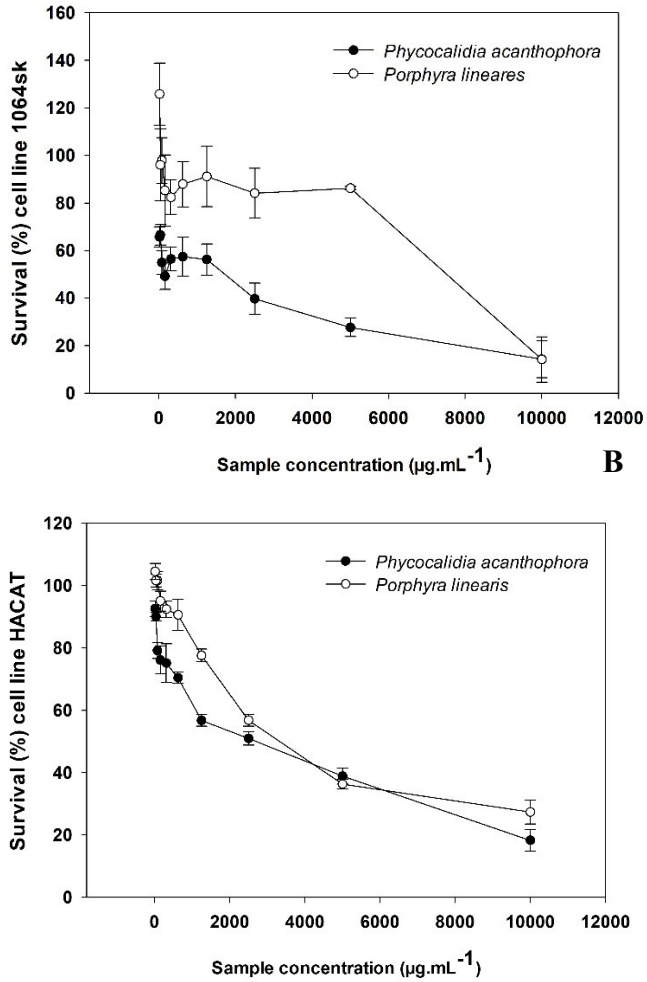

A. keratinocytes HACAT and B. Fibroblasts 1064sk exposed to different concentrations (19 to 10000 µg mL^{-1}) of *Porphyra linearis* and *Phycocalidia acanthophora* extracts. Data are presented as means ± standard deviation (n = 4).

2.4.9 Biological Effective Protection Factors (BEPFs)

Table 6 presents the results of different photoprotection indices, including Sun Protection Factor (SPF) and Biological Effective Protection Factors (BEPFs). The addition of *P. linearis* and *P. acanthophora* aqueous extracts to the base cream increased the values obtained in all factors calculated, when compared to base cream control (BC), especially in SOPF (1.92 ± 0.23 and 1.70 ± 0.07, respectively). When considering the addition of the

extracts to the base cream containing physical filters, significant differences ($p < 0.05$) were not detected between the new formulations and control (BC+PF). Irradiating the plates with the UV radiation of the solar simulator reduced the values found for all biological factors in both formulations, base cream containing the extract of *P. acanthophora* (BC+A_{Pa}) and the base cream containing physical filters and the extract of *P. linearis* (BC+PF+A_{Pl}).

Tabela 6. SPF and BEPFs values for the tested formulations.

	SPF		UVAPF		EPF		PPF		SOPF	
	BI	AI	BI	AI	BI	AI	BI	AI	BI	AI
BC	0.98 ± 0.01	-	0.97 ± 0.003	-	0.97 ± 0.003	-	0.97 ± 0.003	-	0.96 ± 0.003	-
BC+A_{Pl}	1.60* ± 0.15	1.43 ± 0.14	1.53* ± 0.12	1.38 ± 0.11	1.45* ± 0.1	1.32 ± 0.1	1.62* ± 0.14	1.45 ± 0.13	1.92* ± 0.23	1.65 ± 0.21
BC+A_{Pa}	1.49^{*a} ± 0.03	1.37^{b} ± 0.04	1.44^{*a} ± 0.04	1.34^{b} ± 0.04	1.44^{*a} ± 0.04	1.29^{b} ± 0.03	1.51^{*a} ± 0.05	1.39^{b} ± 0.05	1.70^{*a} ± 0.07	1.53^{b} ± 0.07
BC+PF	6.16 ± 1.03	6.03 ± 0.03	4.9 ± 0.64	4.91 ±0.06	4.63 ± 0.57	4.7 ± 0.06	6.03 ± 0.1	5.92 ± 0.04	6.28 ± 1.06	6.12 ± 0.03
BC+PF+A_{Pl}	7.13^{a} ± 0.64	6.05^{b} ± 0.2	5.81^{a} ± 0.39	5.02^{b} ± 0.15	5.41^{a} ± 0.34	4.72^{b} ± 0.13	7.15^{a} ± 0.61	6.05^{b} ± 0.21	7.81^{a} ± 0.73	6.43^{b}± 0.25
BC+PF+A_{Pa}	7.11 ± 1.06	6.69 ± 0.81	5.74 ± 0.7	5.37 ± 0.52	5.34 ± 0.61	5.02 ± 0.46	7.09 ± 1.04	6.63 ± 0.78	7.73 ± 1.2	7.13 ± 0.88

Data are represented as means ± standard- deviation (n = 4). Different letters indicate significant differences ($p < 0.05$) between the same formulation before (BI) and after (AI) irradiation. (*) indicate significant differences ($p < 0.05$) between the formulations and their respective control without the extracts calculated with t-student test. BC, Base cream; BC+PF, Base cream plus physical filters; BC+A_{Pl}, Base cream plus 10% of alga *Porphyra linearis* aqueous extract; BC+A_{Pa}, Base cream plus 10% of alga *Phycocalidia acanthophora* aqueous extract; BC+PF+A_{Pl}, Base cream and 15% physical filters plus 10% of alga *Porphyra linearis* aqueous extract; BC+PF+A_{Pa}, Base cream and 15% physical filters plus 10% of alga *Phycocalidia acanthophora* aqueous extract.

2.5 DISCUSSION

In this study, extractions using water and a hydroethanolic solution (water/ethanol, 1:1) were performed using biomass samples of six red macroalgae species, in order to biochemically characterize them and evaluate their antiaging potential. Photoprotective compounds of the red algae such as MAAs and phenolic compounds were strongly correlated with antioxidant capacity and collagenase inhibition, regardless of the species utilized. This reinforce the relevance of understanding what type of compounds in an algal extract can be responsible for causing determined response, and also strongly argue for utilization of red algal extracts into cosmeceutical formulations, focusing on a larger range of photoprotection activities in addition to the more known approach of SPF values (ÁLVAREZ-GÓMEZ et al., 2019).

The extraction yield of aqueous extracts was significantly higher ($p < 0.05$) than all hydroethanolic extracts. Farvin and Jacobsen (SABEENA FARVIN; JACOBSEN, 2013) observed the same for 16 different species from Danish coast, indicating that the yield of extraction increases with the solvent polarity. The polarity also plays an important role on the molecules to be extracted and consequently on their bioactivities, as the antioxidant capacity for example. Water and ethanol are solvents widely used due to their low toxicity and higher extraction yield when compared to other less polar solvents as acetone, methanol and ethyl acetate according to the requirements of natural cosmetics (PLAZA et al., 2010). As a disadvantage, the use of polar solvents may reduce the extraction of antioxidants with low polarity as carotenoids for example (FRANCO et al., 2008).

As can be observed in Pearson's correlation, the biochemical parameters are more closely correlated when using water as solvent, indicating that the use of water was more efficient on extraction of compounds with antioxidant capacity and collagenase inhibition. Mancini-Filho et al. (MANCINI-FILHO; VIDAL-NOVOA; SILVA, 2013) reinforces that the antioxidant capacity of marine macroalgae is mostly determined by their polar compounds, such as MAAs and polyphenols (cinnamic acids, phlorotannins, and bromophenols).

The absorption spectra recorded helped to elucidate UV- and visible-absorbing compounds in different wavelengths. Red macroalgae are described as sources of

mycosporine-like amino acids, UV-absorbing compounds which intensively absorb radiation in the 310 to 360 nm spectral windows, depending on the MAA type (VEGA et al., 2021). The absorption peak observed in 320-340 nm for both aqueous and ethanolic extracts in all species was associated to the imino-MAAs palythine, palythinol, porphyra-334, shinorine, and asterina-330. The same pattern was observed by Álvarez-Gomez et al (ÁLVAREZ-GÓMEZ; KORBEE; FIGUEROA, 2016). This was an expected fact because shinorine and palythine are the most commonly MAA found in subtidal red algae and porphyra-334 the main MAA in genera *Bangia* and *Porphyra* (DIEHL et al., 2019). In addition, ESI-MS analysis (Table 5) showed the presence of other MAAs in the red macroalgae utilized in our study, such as mycosporine-glutamine, mycosporine-2-glycine, palythine-serine, and aplysiapalythine B. Complementary chemical analysis are necessary to identify with accuracy the MAAs mentioned before, not usually described in those species. An innovative study of Orfanoudaki and Hartmann described for the first time in macroalgae the isolation of four unusual MAAs, mycosporine-methylamine-threonine, mycosporine-alanine-glycine, aplysiapalythine A, and aplysiapalythine B (ORFANOUDAKI et al., 2019). Although we do not have the purified standards of these MAAs for further UHPLC quantification, this achievement may indicate new algal species as source of those MAAs.

It was possible to observe that water was more efficient to MAAs extraction when compared to a 20% methanolic solution, considering that using water we obtained the same or higher total MAA content. The same fact was observed by Chaves-Peña et al. (CHAVES-PEÑA et al., 2019). This is an important achievement because it allows the use of water as solvent for MAAs for purpose of application of those secondary metabolites in cosmetic products, reducing its cytotoxicity to humans, as well as the impact on nature by using an eco-friendly solvent. Schneider et al. (SCHNEIDER et al., 2020b), investigating 22 species of macroalgae (red, green and brown macroalgae) and 1 marine lichen, observed the highest MAA content in the *P. umbilicalis*, *B. arthropurpuea, F. rayssiae* and *P. longate* species, with values ranging from 4 to 10 mg g^{-1} DW. Interestingly, similar amounts were found in our analysis for *P. acanthophora* and *P. linearis*. In our study, the antioxidant capacity of both aqueous and hydroethanolic extracts determined by ABTS in *O. pinnatifida* was much lower than that reported by Schneider et al. (2020a), what might be related to its smaller contents of

MAAs, polyphenols and biliproteins. The specimens were collected in the same site, but in different years and seasons. In our study, high antioxidant capacity was detected by using water as solvent, whereas Schneider et al. did extracted the metabolites with hydro-methanolic solvent(SCHNEIDER et al., 2020b). Thus, our extract seems to be more suitable for purposed of developing natural cosmetic products due to absence of methanol.

According to Gnaiger and Bittcrlich (1984), a linear relationship among carbon, hydrogen and nitrogen contents with the carbohydrate, lipid, and protein compositions seems to exist. *P. linearis* and *P. acanthophora* can be highlighted according to the CHNS elemental analysis by its high content of carbon. Literature describes the presence of a polysaccharide called porphyrans, sulfated galactans found on *Porphyra*-like species cell wall, presenting antioxidant, hypolipidemic, anti-inflammatory, anticoagulant and antitumor activities (BHATIA et al., 2013; CHEN et al., 2021; WU et al., 2015). On the other hand, the sulfur content can also be associated to the presence of sulfur polysaccharides. The high sulfur content in *C. teedei* can be explained by the presence of carrageenans in this genus. This polysaccharide is composed by sulfated galactans found in the cell walls of that red algae (WANG et al., 2012). In contrast, the genus *Gracilaria* present agar as cell wall polysaccharide (LONG et al., 2021). Differences on monosaccharide composition, sulfation degree, molecular weight, conformation, and dynamic stereochemistry determine the different bioactivities of the polysaccharides i.e., antioxidant capacity, immunomodulatory, antiproliferative, antiviral (NGO; KIM, 2013). On the other hand, nitrogen content is related to the protein composition. In this context, the highest percentage of nitrogen in *P. linearis* and *P. cartilagineum* (collected in La Herradura beach) biomasses may indicate abundance of compounds such as phycobiliproteins and soluble proteins (data not shown) in these species, respectively. These molecules have been recorded as potential antioxidant compounds (DAGNINO-LEONE et al., 2022; RODRIGUES et al., 2020).

Phenolic compounds are secondary metabolites with the capacity of capture free radicals and chelate metal ions, resulting in an elevated antioxidant capacity. Among algae, brown algae (Ochrophyta) are the major producers of these molecules, but it is also possible to find them in red algae (JIMENEZ-LOPEZ et al., 2021). The amount of polyphenols detected on aqueous extract of *P. linearis* (13.6 $mg.g^{-1}$ DW) was

higher than the described in two brown and four green species by Schneider (SCHNEIDER et al., 2020b). The types of phenolics usually described in red algae are bromophenols, flavonoids, phenolic acids, and phenolic terpenoids (COTAS et al., 2020; LIU; HANSEN; LIN, 2011).

In this study, *P. linearis* and *P. acanthophora* extracts were the most efficient in inhibiting the enzyme collagenase and presented the highest contents of MAAs, and these two variables were strongly correlated. Corroborating with this data, Hartmann et al. (HARTMANN et al., 2015) also point out the relation between MAAs and collagenase inhibition. The authors purified the MAAs shinorine, porphyra-334, and palythine, and showed the IC_{50} values for collagenase inhibition by these compounds, being respectively 104.0 ± 3.7, 105.9 ± 2.3, and 158.9 ± 3.2 μM of purified MAA. *In silico* simulations have indicated a direct interaction between the MAAs tested and native peptide's P1′-P3′ region of the collagenase catalytic center. Besides antioxidant and enzyme inhibition, MAAs may play different roles on skin protection (LEANDRO; PEREIRA; GONÇALVES, 2020; VEGA et al., 2021). Suh et al.(2014) suggest an antiaging potential of the MAAs shinorine and Mycosporine-glycine throughout an anti-inflammatory activity by modulation of COX-2 expression.

Taking into account the results found, *P. linearis* and *P. acanthophora* aqueous extracts, that showed higher antioxidant capacity and potential to inhibit collagenase activity, were selected to be incorporated into a cosmeceutical formulation and calculate the biological effective protection factors (BEPFs).

To determine the cytotoxicity of new formulations is important to prevent adverse toxic effects, and it can be realized by *in vitro* testing the ingredients of the formulations using cytotoxicity assays with normal human skin cell lines. By calculating the IC_{50} values is possible to determine safe concentrations to be incorporated into the formulation. In our study, a low cytotoxicity of both extracts on human fibroblasts and keratinocytes was found, considering that the IC_{50} values obtained are over 1.9 mg mL^{-1}. Studies show that MAAs such as shinorine, porphyra-334, and mycosporine-glycine are not toxic to human lung fibroblasts. The same MAAs presented low cytotoxicity in keratinocytes at high concentrations, as in lower concentrations cell proliferation was stimulated, an interesting trait that can be associated to an eventual wound healing potential of that compound (ÁLVAREZ-GÓMEZ et al., 2019; CHOI et al., 2015). It is important to highlight these facts because

the use of natural extracts and/or natural-derived compounds are considered safer and more sustainable alternatives to commercial photoprotectors (SEN; MALLICK, 2021).

The BEPFs are relevant to represent the photoprotection data in a broader level than only SPF. Using the transmittance measures and the action spectrum it is possible to calculate several biological factors and then to plan biochemical assays in order to reinforce the results obtained. However, as the BEPFs are still low explored, the biggest bottleneck of the analysis is the availability of the action spectra associated to the effective response to be evaluated. Although the difference is not high, it was observed a significant increase on the BEPFs ($p < 0.05$) when adding both extracts to the base cream without physical filters. The same was not observed using the base cream with physical filters. We believe that the effect of the extracts was masked by the limited dispersion related to titanium dioxide and zinc oxide (REINOSA et al., 2016) and also that the final bioactive compounds into the cream formulations were too low and then, new approaches must be taken into account allowing their increment and potential higher bioactivity of the final lotion in a photoprotective perspective.

2.6 CONCLUSION

Red macroalgae can be source of different molecules with biotechnological potential. Among the species chosen in this study, *P. acanthophora* and *P.linearis* extracts were the most interesting extracts with antiaging potential due to their positively correlated antioxidant capacity, mycosporine content, and inhibition of the activity of the enzyme collagenase. Finding MAAs considered unusual in macroalgae was another important achievement of this study. Regarding the BEPFs, although the results were not the as expected, we highlight the functionality of the analysis to calculate different biological responses and the relevance of evaluating new formulations photostability.

Acknowledgements

We would like to thanks to Ingrid Palica and Juan Camilo Mejía Giraldo for all the support on the development of the base cream used in this work. We also want to

thanks Nathalie Korbee for the technical support during the Mycosporine-like amino acids analyses.

Funding

This work was supported by Coordenação de Aperfeiçoamento de Pessoal de Nível Superior – Brasil (CAPES) [grant numbers 88882.438333/2019-01] and the internalization program CAPES-PRINT [grant numbers 88887.578926/2020-00]. The financial support by Junta de Andalucia, the projects (1) FACCO- UMA18-FEDER JA-162 and (2) NAZCA- PY20-00458-FR is thankful. We are also thankful to the Program Jóvenes Investigadores e Innovadores from Colombia (grant number 2019-25210).

3 CAPÍTULO 2

Manuscript submitted to Journal *Phycologia*

Daily variations on photosynthesis, pigmentation and photoprotection of *Plocamium cartilagineum* (Plocamiaceae, Rhodophyta)

Bruna Rodrigues Moreira[1*], Daniela Rodrigues Fernandes[2], Julia Vega[3], Félix Álvarez Gómez[3], Pablo Castro Varela[3], José Bonomi-Barufi[1], Félix López Figueroa[3]

[1] Laboratório de Ficologia, Departamento de Botânica, Universidade Federal de Santa Catarina, Florianópolis, 88049-900, SC, Brasil; *bruna.rm01@gmail.com; + 55 62981524237 - corresponding author.

[2] Universidade Federal do Estado do Rio de Janeiro, CCBS, Instituto de Biociências, Departamento de Botânica. Avenida Pasteur, 458. Urca, Rio de Janeiro, 22290-255, RJ, Brazil.

[3] Universidad de Málaga, Instituto Andaluz de Biotecnología y Desarrollo Azul (IBYDA), Departamento de Ecología, Campus Universitario de Teatinos s/n - Centro Experimental Grice Hutchinson, Lomas de San Julián 2, 29004 Málaga, España.

3.1 ABSTRACT

Field studies are a useful tool to understanding how seaweeds develop protection mechanisms against the variability of environmental conditions. The present paper comprises a short-term study during a daily cycle by evaluating *Plocamium cartilagineum* photosynthesis and biochemistry under different radiation and temperature conditions. Then, four work Sites were chosen at La Herradura beach, Spain. Higher values of irradiance and temperature at Sites #3 and #4 directly reflected on $ETR_{in\ situ}$ values. Algae from Site #1 exhibited a dynamic photoinhibition when compared to algae from Site #4. A lower content of pigments was observed to the algae that received higher irradiances, indicating photoacclimation. Samples found at Site #3 presented the highest concentrations of mycosporine-like amino acids (MAAs) between 15:30h and 19:30h. MAAs proportion varied among the sites and the daily collection period. We conclude that environmental conditions have influenced photosynthetic parameters and the accumulation of pigments and MAAs in *P. cartilagineum*, evidencing its high plasticity.

Keywords: algae, marine ecology, field study, short-term, *Plocamium cartilagineum*, photosynthesis, biochemical compounds.

3.2 INTRODUCTION

Environmental conditions, mainly radiation and temperature, constantly change throughout the day, depending on the presence of clouds and the Sun angle, directly affecting photosynthetic organism performance (CONDE-ÁLVAREZ et al., 2002; FIGUEROA et al., 2010). Considering this context, *in situ* measurements on field studies help to comprehend the relation between environmental conditions and algal physiology, and it is important to develop strategies for algal cultivation under laboratory conditions. Evaluating short-term variations of the algae during a daily cycle period helps to elucidate photosynthetic and biochemical strategies developed by the algae during the day, so they can adapt to different conditions of irradiance, temperature, desiccation, and salinity (FIGUEROA; GÓMEZ, 2001).

Field studies evaluate the adaptation mechanisms through photosynthetic parameters and production of pigments and photoprotector compounds (CONDE-ÁLVAREZ et al., 2002; FIGUEROA et al., 2003; FLORES-MOYA et al., 1999; HADER et al., 1996). López-Figueroa (1992) evaluated the content of chlorophyll *a*, phycoerythrin, and phycocyanin in *Condrus crispis* and *Pophyra laciniata* by associating the pigment production to light quantity and quality during a daily cycle. Betancor et al. (2015) carried out analysis to determine photosynthetic activity and photoprotector compounds in *Cystoseira humilis* and *Digenea simplex* in an intertidal rock pool. The authors evidenced a daily and seasonal fluctuation of photosynthetic pigments, phenolic compounds and mycosporine-like amino acids (MAAs) (ABDALA-DÍAZ et al., 2006; BARCELÓ-VILLALOBOS et al., 2017; FIGUEROA et al., 1997).

In addition to pigment content, Flores-Moya et al. (1998) noticed a fluctuation of nitrate reductase and carbonic anhydrase activities, enzymes associated to nutrient assimilation, in *Rissoella verruculosa* throughout the day.

Macroalgae from southern Spain, on Mediterranean coast, are constantly submitted to high doses of UV radiation, due to the high irradiance and water transparency (HÄDER; FIGUEROA, 1997). *Plocamium cartilagineum* is a red macroalgae (family *Plocamiaceae*, order *Gigartinales*) characterized by the accumulation of phycoerythrin and secondary metabolites i.e, halogenated monoterpenes (WU; KRAUSS; VETTER, 2020). This species, which contains high levels of phycobiliproteins, also modulates pigment rates and the synthesis of UV-absorbing compounds, as mycosporine-like amino acids and polyphenols. Mycosporine-like amino acids are UV absorbing compounds in the 310 to 360 nm range, with

low molecular weights (200-400 Da). The accumulation of MAAs is regulated by both UV radiation and inorganic nitrogen supply (BONOMI BARUFI et al., 2012; HUOVINEN et al., 2006; PEINADO et al., 2004). Most of ecophysiological studies have been conducted under laboratory conditions by using artificial photosynthetic active radiations (PAR, λ= 400-700 nm) and UV radiation (λ=280-400 nm) (ÁLVAREZ-GÓMEZ; KORBEE; FIGUEROA, 2019; FIGUEROA et al., 2003; NAVARRO et al., 2014a).

The effects of UV radiation and nitrate or ammonium on the accumulation and productivity has also been conducted under solar radiation in algae suspended in tanks (BARCELÓ-VILLALOBOS et al., 2017; FIGUEROA et al., 2008, 2010). However, most of the works have been conducted in algae exposed to longer periods, 48 h to several weeks. Field studies on the accumulation of photosynthetic pigments in red macroalgae have been conducted in both the short and long-term periods (FIGUEROA et al., 1997; FLORES-MOYA et al., 1999; JIMÉNEZ et al., 1998; LÓPEZ-FIGUEROA, 1992; QUINTANO et al., 2018); however, studies in the natural accumulation environment of MAAs and phenolic compounds in the short term are scarce (ABDALA-DÍAZ et al., 2006; BETANCOR et al., 2015; GÓMEZ et al., 1998). The short-term variation of pigments has been related to short variation on photosynthetic performance including photoinhibition at noon periods (BETANCOR et al., 2015; FIGUEROA et al., 1997; FLORES-MOYA et al., 1999). In red macroalgae *Pyropia columbina* and *Mazaeella laminaroides*, the short-term variation of MAAs in the natural field are not only related to solar radiation, including increased UVB radiation by ozone depletion, but also due to nitrate availability (NAVARRO et al., 2021, 2014a, 2014b). Those compounds mentioned before, besides their directly photoprotection properties, are also correlated to an antioxidant capacity, which reduces the negative impact of UV radiation on algae cells (VEGA et al., 2021).

Plocamium cartilagineum also modulates the biochemical synthesis of UV-absorbing compounds, as MAAs and polyphenols, also pigment rates, including phycobiliproteins and halogenated monoterpenes (HOYER et al., 2001; V. BRITO et al., 2016; WU; KRAUSS; VETTER, 2020)(WU; KRAUSS; VETTER, 2020). The production of MAAs from *P. cartilagineum* was proportionally inverse to the water depth (Hoyer et al. 2000). This species is a fleshy cartilaginous species, with a light-red iridescent prominent color and has a worldwide distribution, especially in temperate and polar regions (GUIRY, 2017). It can be found at low intertidal and sublittoral oligotrophic waters of the Mediterranean Sea, where it

is exposed to different intensities and qualities of light depending on daily and seasonal light cycles (BOTTALICO; ALONGI; PERRONE, 2016; JIMÉNEZ et al., 1998).

This study aimed to evaluate photosynthetic pigment and MAAs production, and also the antioxidant capacity related to photosynthetic response in *Plocamium cartilagineum* exposed to different irradiances during a daily-cycle period in a rock shore at Mediterranean Spanish coast. The main purpose was to comprehend the physiological and protection adaptations mechanisms developed by macroalgae related to daily light fluctuation.

3.3 MATERIAL AND METHODS

3.3.1 Biological material and experimental design

The study was conducted in the field with the red macroalga *Plocamium cartilagineum* (Linnaeus) P.S.Dixon (Plocamiales, Rhodophyta. Four different collection sites, namely as Sites #1, #2, #3 and #4, were selected at La Herradura Beach (Figure 18), Granada, Spain (36°44'17"N, 3°45'01" W). Measurement and samples were taken at the light phase of the day in May 2015, during spring season, in order to follow short-term variation in both photosynthetic activity and biochemical compounds. Sites #1 and #2 was located at 1.5 m depth and Sites #3 and #4 was located at 0.25 m.

Figura 18. Rocky shore area where in situ measurements were conducted and samples were collected to biochemical analyses

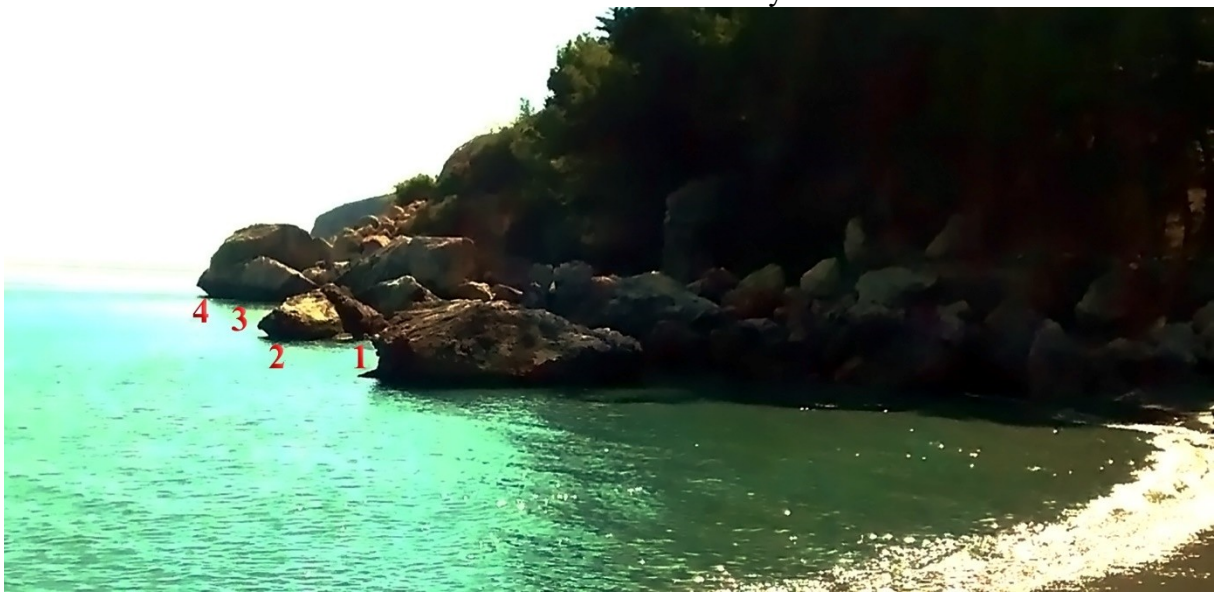

Collection sites: La Herradura beach, (36°44'17"N, 3°45'01" W). Four sites (numbered from 1 to 4) were chosen.

Photosynthetic active radiation (PAR, λ=400-700 nm) and ultraviolet-A radiation (UVA, λ=315-400 nm) were monitored during the daily cycle by using an underwater data logger ZIPPO-HOBBO-U12-UV with a PAR sensor (SQ-212) and a UV sensor (LPUVA01). Temperature was determined by using underwater Hobo thermometer sensor. The different data-logger sensors registered information during the day of the experiment and were positioned beside the area where photosynthetic parameters measurements and samples were taken. For comparison, daily values of radiation were obtained from NILU UV-6 equipment, on May 12, 2015 located in a weather station at SCAI – University of Málaga, Spain (36°43'12.6'' N 4°25.22' W).

During the daily period, at each different *P. cartilagineum* occurrence site, different procedures were taken in the following time periods: 9:00, 11:30, 13:00, 15:30, 17:00 and 19:00 (GMT+1). Photosynthetic parameters were recorded *in situ* with an underwater fluorometer Diving-PAM (Walz, Effeltrich, Germany). Algal samples were collected to conduct biochemical analyses of photosynthetic pigments, mycosporine-like amino acids (MAAs), and antioxidant capacity. The collected samples were frozen in liquid nitrogen at the beach and transferred to a -80°C freezer at laboratory. Furthermore, at two different sites (Site #1 and #4), algal thalli samples were collected to evaluate ETR on light curves with incubations at different solar irradiances. These analyses are detailed below.

3.3.2 Photosynthesis estimated by in vivo chlorophyll a fluorescence of PSII

Three different procedures were done for estimating photosynthetic activity of *P. cartilagineum.* Firstly, six different thalli attached to the rocky shores had *in vivo* chlorophyll *a* fluorescence accessed by using a Diving PAM (Walz GmbH Effletrich, Germany). The thalli received a saturating pulse (0.8 s with intensity > 4,000 μmol photons $m^{-2} \cdot s^{-1}$) allowing the measurement of steady state fluorescence (Ft) and maximum fluorescence of light acclimated samples (Fm'). With these values, effective quantum yield (YII, that is equivalent to $\Delta F/F_m$' or ϕ_{PSII}, as per (KROMKAMP; FORSTER, 2003), was calculated according to Genty et al. (1989): $Y(II) = (F_m'/F_t)/F_m'$. This measurement was taken six times for each site along the daylight period.

The second procedure was ETR vs. irradiance in a Rapid light curve performed at field with recent collected thalli from Sites #1 and #4. Those two places were chosen for presenting different irradiation patterns. Samples were previously acclimated in darkness for

15 min. Then, the thalli received a saturating pulse, (0.8 s with intensity >4,000 μmol photons $m^{-2} \cdot s^{-1}$), obtaining of F_o and F_m values, which were used for the calculation of maximum quantum yield,

$$F_v/F_m=(F_m-F_o)/F_m.$$

In sequence, the thalli were incubated in trays containing seawater covered by layers of mesh of gray neutral filters. At each 5 min, one mesh layer was removed, and sequentially 8 solar irradiances were obtained: 60, 86, 148, 252, 314, 606, 1,058 and 1,661 μmol photons.$m^{-2} \cdot s^{-1}$. Light irradiance was measured with the Diving-PAM-coupled underwater light sensor. Also, before the remotion of one mesh layer, effective quantum yield Y(II) was measured, as previously explained, using the Diving-PAM optic fiber (5 mm diameter).

Y(II) values obtained in both procedures were used for calculating the electron transport rates (ETR), estimating photosynthetic capacity, as the following formula:

$$ETR(II) = Y(II) \times E_{PAR} \times A \times F_{II} \ (1) \ \mu mol \ electrons \ m^{-2} \cdot s^{-1}.$$

Where E_{PAR} is the incident irradiance of PAR (photosynthetically active radiation, λ=400–700 nm); A is the Absorptance; and F_{II} is the fraction of cellular chlorophyll *a* associated with LHCII (Light Harvesting Complex associated to PSII); recorded as 0.15 for red macroalgae (FIGUEROA; CONDE-ÁLVAREZ; GÓMEZ, 2003; JOHNSEN; SAKSHAUG, 2007); Absorptance, was determined as A=1-T, as reported by Figueroa et al. (2009) where T is the estimated transmittance, as shown in equation $T = E_t/E_o$. E_o is the incident irradiance of solar radiation determined by a cosine corrected sensor Li-189 (LI-COR Ltd, Nebraska, USA) connected to a radiometer Li-250 (LI-COR Ltd, Nebraska, USA), and E_t is the transmitted irradiance, measured by placing a small thallus piece above the PAR sensor (FIGUEROA et al., 2009).

Light curves were fitted according to the model by Eilers and Peeters (1988) to obtain the maximum ETR (ETR_{max}), the initial slope of the curves (α_{ETR}), and the irradiance of ETR saturation (E_k).

3.3.3 Photosynthetic pigments

The concentration of photosynthetic pigments (chlorophyll *a* and phycobiliproteins) was evaluated in the samples collected from the four sites. Chlorophyll *a* was extracted from frozen 60-80 mg of fresh weight biomass, grinded in a mortar with 2.5 mL acetone 90 % with purified sand. Phycobiliproteins were quantified from 60-80 mg of fresh weight biomass, macerated in a mortar with 3 mL of buffer phosphate 0.1 M pH 6.5. All these extractions were conducted overnight, at 4 °C, in the dark. After this period, samples were centrifuged at 2,683x g, 4 °C per 10 minutes. The concentration of these pigments was estimated by spectrophotometric methods and followed calculation formulae for Chlorophyll *a* (RITCHIE, 2008) and phycoerythrin (SAMPATH-WILEY; NEEFUS, 2007). All determinations were carried out in triplicate.

3.3.4 Mycosporine-like amino acids (MAAs)

MAAs were extracted from 20 milligrams of dry biomass with 1 mL of 20% aqueous methanol (v/v) for 2 hours in water bath at 45 °C. After that, 0.7 mL of the extract was transferred to an Eppendorf and evaporated in a rotary evaporator. The dry extracts were resuspended in 100 % methanol and filtrated through a 0.2 µm membrane filter before running the analysis on HPLC (Waters 600 HPLC). The mobile phase was a mixture of aqueous methanol 2.5 % (v/v) and acetic acid 0.1 % (v/v) in water. The extracts (10 µL) were injected in a C8 chromatographic column with a 0.5 ml · min^{-1} flow rate, and a run time of 20 minutes per sample. The MAAs peaks were detected in a PDA photodiode detector at 330 nm wavelength and with absorption spectra between 290 nm to 400 nm. MAAs extraction, identification, and quantification of MAAs followed Korbee et al. (2004).

MAAs were also identified with the use of positive and negative electrospray ionization mass spectrometry (70-700 m/z) (ESI-MS) (Orbitrap Q-Exactive, Thermo Scientific S.L., Bremen, Germany) in the Research Support Central Services (SCAI, University of Malaga, Spain). All analyses were performed in triplicate.

3.3.5 ABTS Assays

The antioxidant capacity was characterized by scavenging hydrosoluble free radicals, based on the absorbance decreasing at 734 nm (decolorization) of ABTS (2,2'-azinobis (3-

ethylbenzothiazoline 6-sulfonate) cation radical, generated by the oxidation of ABTS with potassium persulfate, following Re et al. (1999) protocol. The stock solution of ABTS (7 mM) was prepared with distilled water and then added the potassium persulfate (2.45 mM, final concentration). This mixture was maintained in the darkness at ambient temperature for 16h before use in order to secure the $ABTS^+$ formation and stability. The $ABTS^+$ solution was diluted to 5-6% with phosphate buffer saline-PBS (0.1 M, pH 7.4) generating an initial absorbance of 0.7 - 0.75 at 734 nm. To obtain the antioxidant capacity of the samples, aqueous extracts were prepared as follows: 1 g of seaweed was grinded in a mortar with a solution of 14.85 mL of buffer phosphate saline – PBS (0.1 M, pH 7.4) plus 0.15 ml EDTA (60 mM) to inhibit the protease action. This extraction occurred overnight, in the dark at 4 °C. After that period, the mixture was centrifuged for 25 min at 4000 RPM and 4 °C. The supernatant was kept in the dark at 4 °C and the pellet were dried and weighted.

The assay was performed with spectrophotometer (UVMini-1240 model, Shimadzu) in a 1 mL cuvette containing 960 µL ($ABTS^+$ + PBS) + 40 µL sample. The final concentrations of the aqueous extract were diluted 25 X at the spectrophotometer readings, whereas the dry methanolic extract had 25 mg diluted 10 X in PBS and reached a final concentration of 0.1 mg · ml^{-1} in the cuvette.

The antioxidant calibration curve were taken with six concentrations of Trolox (Sigma Aldrich) ranging from 0.625 to 20 µM · mL^{-1} after 6 min of incubation in $ABTS^+$ at room temperature (RE et al., 1999). The decay percentage of absorbance at 734 nm was calculated and expressed as TEAC mg^{-1} of extract, whereas the values of antiradical activity followed the formulae:

$$AA\% = \frac{(|control| - |sample|)}{|control|} x\,100$$

All determinations were carried out in triplicate.

3.3.6 Statistical analysis

All statistical analyses were performed using Statistic 7.0 Software. The homogeneity analysis of variance was assessed conducting Cochran's test. Results were also analyzed by factorial ANOVA, using the collection site and time period as independent factors, with a $p < 0.05$ significance level. To determine differences among the samples, post

hoc comparisons were made with Newman-Keuls test. Correlations among the dependent factors were stablished using Pearson's correlation analysis and among independent and dependent factors, using a linear regression analysis. Significant differences between two independent groups were determined by using Student's t test. All biochemical analyses were conducted using three replicates.

3.4 RESULTS

3.4.1 Characterization of local abiotic factors

Maximum total irradiance in Malaga (Spain) on May 12, 2015 was reached around 14h (Figure 19). On this site, at this time, the photosynthetic active radiation (PAR) reached 432 W · m^{-2}, and ultraviolet A (UV-A) and ultraviolet B (UV-B) radiation, 35.1 W · m^{-2} and 2.63 W · m^{-2}, respectively (Table 7).

Figura 19. Air irradiance of PAR, UVA and UVB radiations in the air

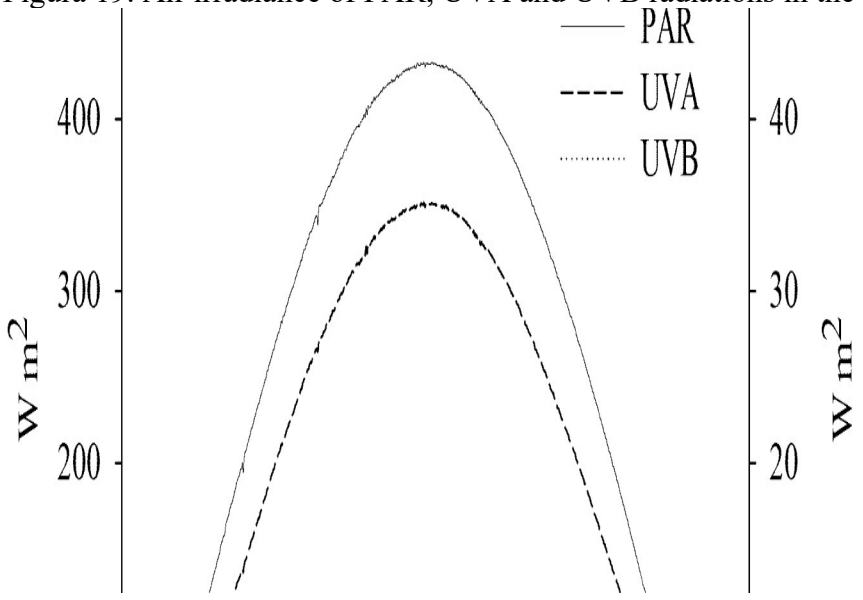

Data measured in Malaga Station during the daily light cycle of May 12, 2015.

Tabela 7. Daily integrated irradiance, average irradiance and irradiation at 12:00 GMT detected in Malaga Station during the daily light cycle of May 12, 2015.

	PAR	UV-A	UV-B
Daily Integrated Irradiance (KJ · m^{-2})	12745.23	979	64.81
Average Irradiance (W · m^{-2})	255.00	19.58	1.29
Irradiance at 12:00 GMT (W · m^{-2})	430.85	34.96	2.62

The sites chosen to evaluate photosynthetic and biochemical parameters of *P. cartilagineum* presented distinct patterns of PAR, UV-A and UV-B, as observed in Figure 20. Daily-integrated irradiance at Site #3 and #4 were higher than Site #1 and #2, corresponding to maximal irradiance of 1,049.1 µmol photons $m^{-2} \cdot s^{-1}$ of PAR and 0.09 $W \cdot m^{-2}$ of UVA in Site #3, and 1,121 µmol $m^{-2} \cdot s^{-1}$ of PAR and 0.05 $W \cdot m^{-2}$ of UVA in Site #4. Although Sites #3 and #4 presented a similar luminosity pattern, algal samples at Site #3 were exposed to a higher dose of UV-A than those at Site #4. Sites #1 and #2 were located in places with shadow during certain part of the day, presenting different patterns of irradiance throughout the day. Site #1 showed maximum irradiance after 14:00h decreasing during the afternoon; meanwhile, at Site #2 the maximum light time was observed between 9:00h and 13:30h, with maximum irradiance around 13:30h. *In situ* temperature was also higher in Sites #3 and #4, reaching almost 30 °C and 27 °C, respectively (Figure 21). Sites #1 and #2 presented a peak of temperature around 9:00h but it remained stable during the day, around 18 °C.

Figura 20. In situ underwater PAR (µmol photons $m^{-2} \cdot s^{-1}$) and UV-A radiation ($W \cdot m^{-2}$) during the daily cycle period of May 12, 2015, at the four sites of collection of *Plocamium cartilagineum* in la La Herradura beach, Granada, Spain.

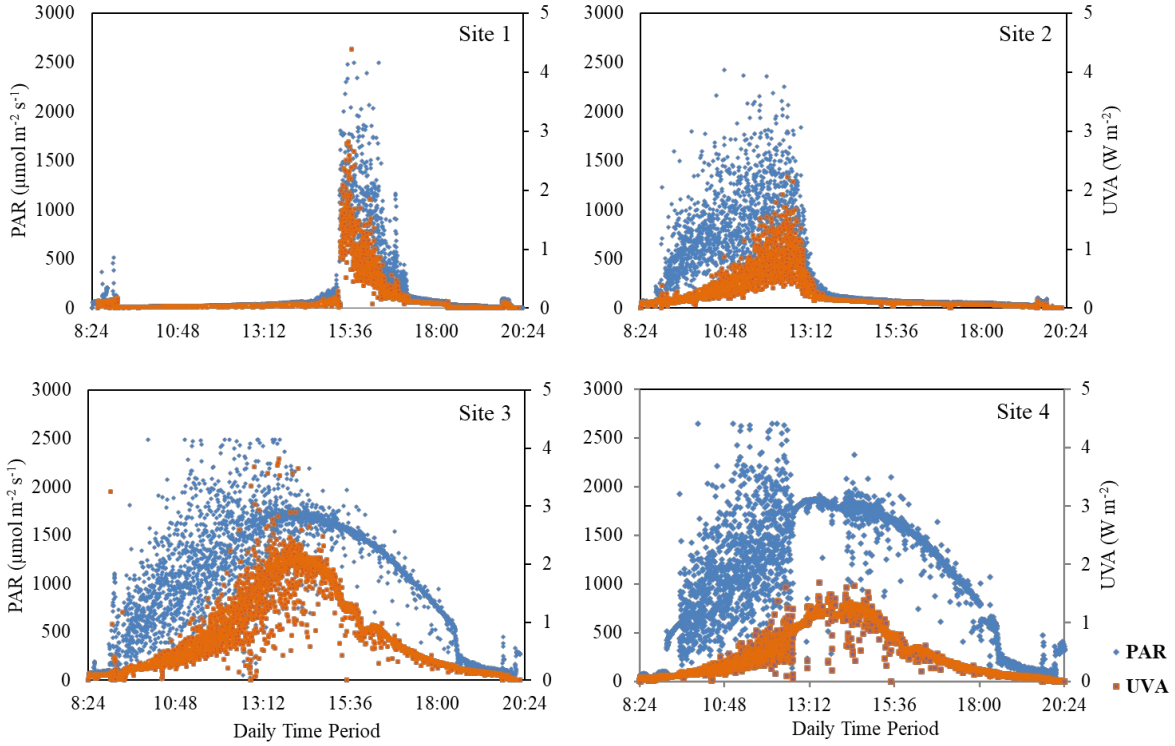

Figura 21. In situ underwater temperature (°C) during the daily cycle period of May 12, 2015, in the four sites of collection of *Plocamium cartilagineum* in la La Herradura beach, Granada, Spain.

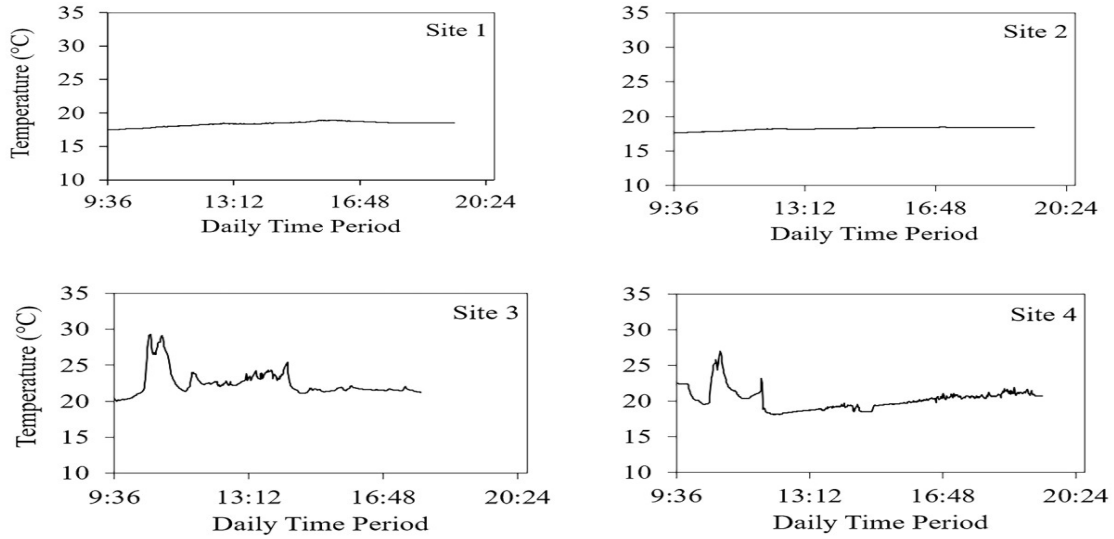

3.4.2 Photosynthesis estimated by in vivo chlorophyll a fluorescence of PSII

Electron transport rate (ETR) values were significantly influenced by the interaction between the collection site and the daily time period (ANOVA – Table S6, $p < 0.05$). The highest ETR values were detected at Site #3 at 13:00h and Site #4 at 13:00h and 15:30h. In both sites, the ETR pattern followed the sunlight variation (Figure 20, Figure 22). The ETR increased during the morning, reached its maximum at midday and reduced through the rest of the day. In the Site #1, the maximum ETR value was obtained at 15:30h (86.3 ± 17.9 µmol electrons $m^{-2} \cdot s^{-1}$) and for Site #2 at the morning period, from 9:30h to 13:00h (Figure 22).

Figura 22. In situ ETR measurements obtained from attached thalli from the different sites, during the daily cycle period

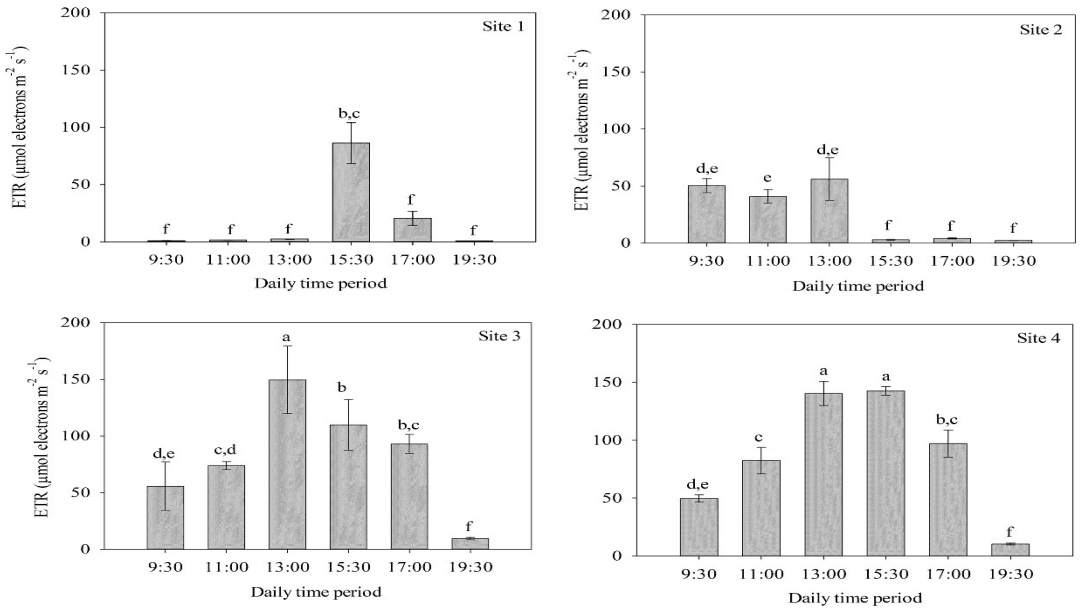

Different letters indicate significant differences among ETR values throughout the day in the four sites of collection. Results were expressed as mean ± standard-deviation (n=6).

Considering the ETR vs. irradiance curves obtained with nine different irradiances, we observed that *P. cartilagineum* from Sites #1 and #4 presented the same light curve pattern until irradiances close to 500 µmol photons $m^{-2} \cdot s^{-1}$ (Figure 23). The fitting pattern was slightly different between both places, because at the last light intensity evaluated (1,661 µmol photons $m^{-2} \cdot s^{-1}$) electron transport rate values were statistically different. Thalli from Site 4 enhanced ETR achieving 48.8 µmol electrons $m^{-2} \cdot s^{-1}$, whereas those one from Site 1 presented an ETR decay pattern at this same light intensity (11.1 µmol electrons $m^{-2} \cdot s^{-1}$).

Figura 23. Electron transport rates (ETR) obtained with exposure of *Plocamium cartilagineum* to increasing solar PAR

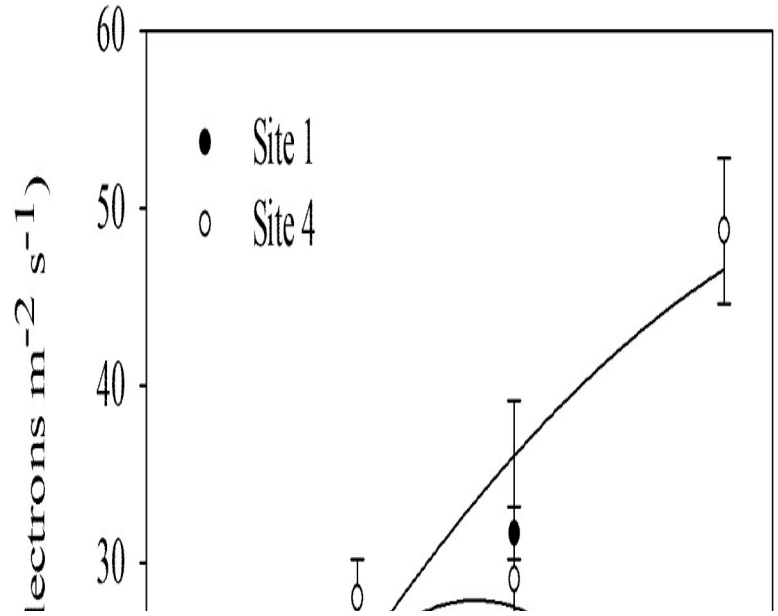

The samples evaluated were collected at site #1 and site #4. Data are mean +/- SD (n=4).

Photosynthetic parameters were calculated from the mentioned light curve (Figure 23). The maximal quantum yield (F_v/F_m) was reduced at the thalli from Site #1 (0.48 ± 0.04^b) in comparison to thalli from site #4 (0.62 ± 0.03^a). Photosynthetic efficiency (α_{ETR}) and ETR_{max} did not present significant differences between thalli from both sites (Table S7). The saturation irradiance (E_k) was around 3 times higher on thalli from Site #4 (716.8 ± 329.8^a) in comparison to those from Site #1 (247.2 ± 42.4^b).

3.4.3 Photosynthetic pigments

The pigment content of chlorophyll *a* (Chl *a*) and phycoerythrin (PE) were significantly influenced by the two independent factors, i.e., site of collection and daily time period, but not by the interaction between both factor, i.e., collection site and daily time period, but not by the interaction between both factors (ANOVA – Table S6, $p < 0.05$). Regarding this fact, the statistical analysis was performed considering the comparison among the collection sites and the daily time period independently. Firstly, we noticed that the content of both, Chl *a* and PE, was higher in Sites #1 and #2 than in Sites #3 and #4. Considering the daily fluctuation of Chl *a*, the highest level of the pigment was obtained at 17:00h, equivalent to 219.5 ± 80.9 µg per gram of fresh weight. For phycoerythrin, except for

the slightly reduction at 19:30h, the levels of PE were maintained constant throughout the day (Figure 24).

Figura 24. Chlorophyll a (Chl *a*) and Phycoerythrin (PE) content measured in *P. cartilagineum* extracts from the four sites of collection during the daily cycle period

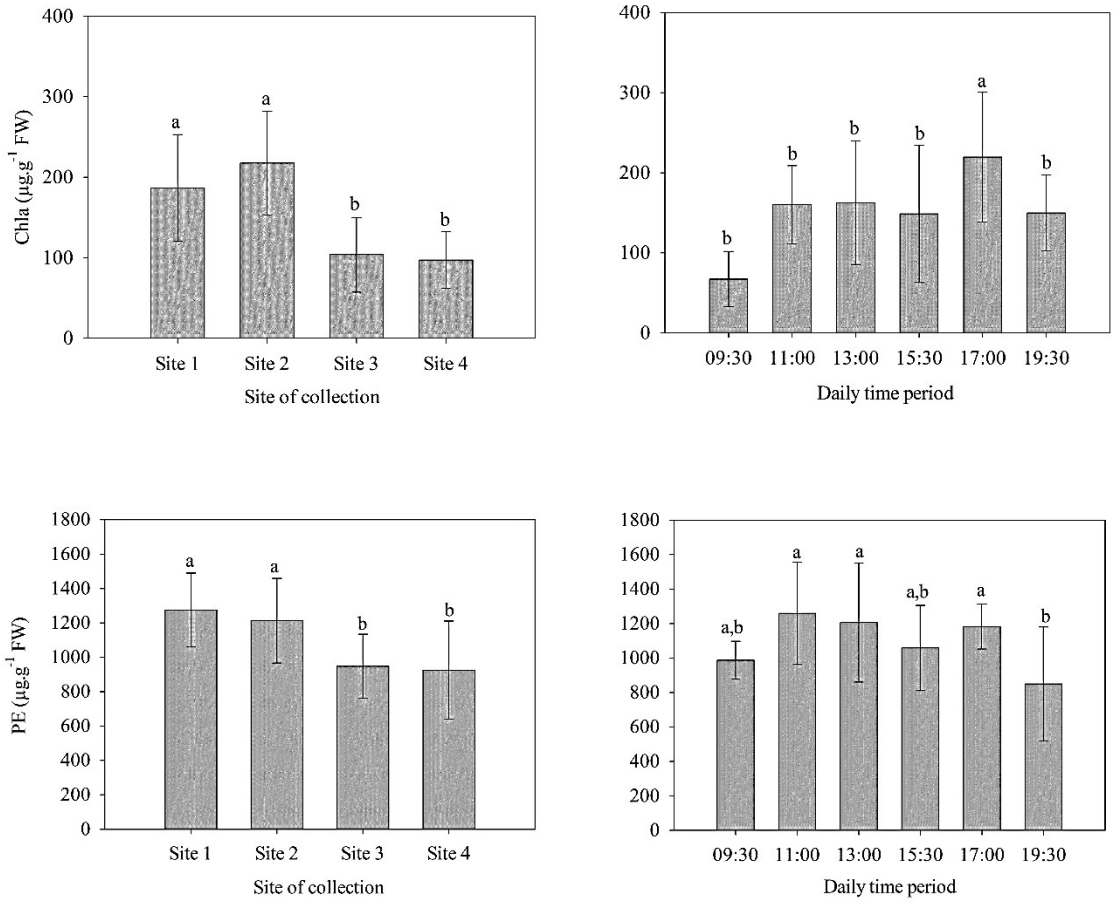

Pigment levels were expressed in µg pigment (Chl a or PE) per g of fresh weight. Different letters indicate significant differences among de sites of collection and the daily time period independently.

3.4.4 Mycosporine-like amino acids

The interaction between the variables collection site and daily time period significantly influenced the mycosporine-like amino acid content (ANOVA – Table S6, $p < 0.05$). In this context, algae from Site #3 presented the highest levels of MAAs, showing an increasing pattern of MAAs level during the day. For the remaining three sites, the content of MAAs in *P. cartilagineum* did not show a significant variation during the day (Figure 25). Palythinol was the main MAA found in *P. cartilagineum*, with the maximum absorption peak at 332 nm, followed by shinorine (Figure 26). We also observed that thalli from Sites #3 and

#4 present a higher proportion of palythine when compared to samples collected in the Sites #1 and #2.

Figura 25. Mycosporine-like amino acids (MAAs) measured in *Plocamium cartilagineum* extract in the different sites of collection during the daily cycle period

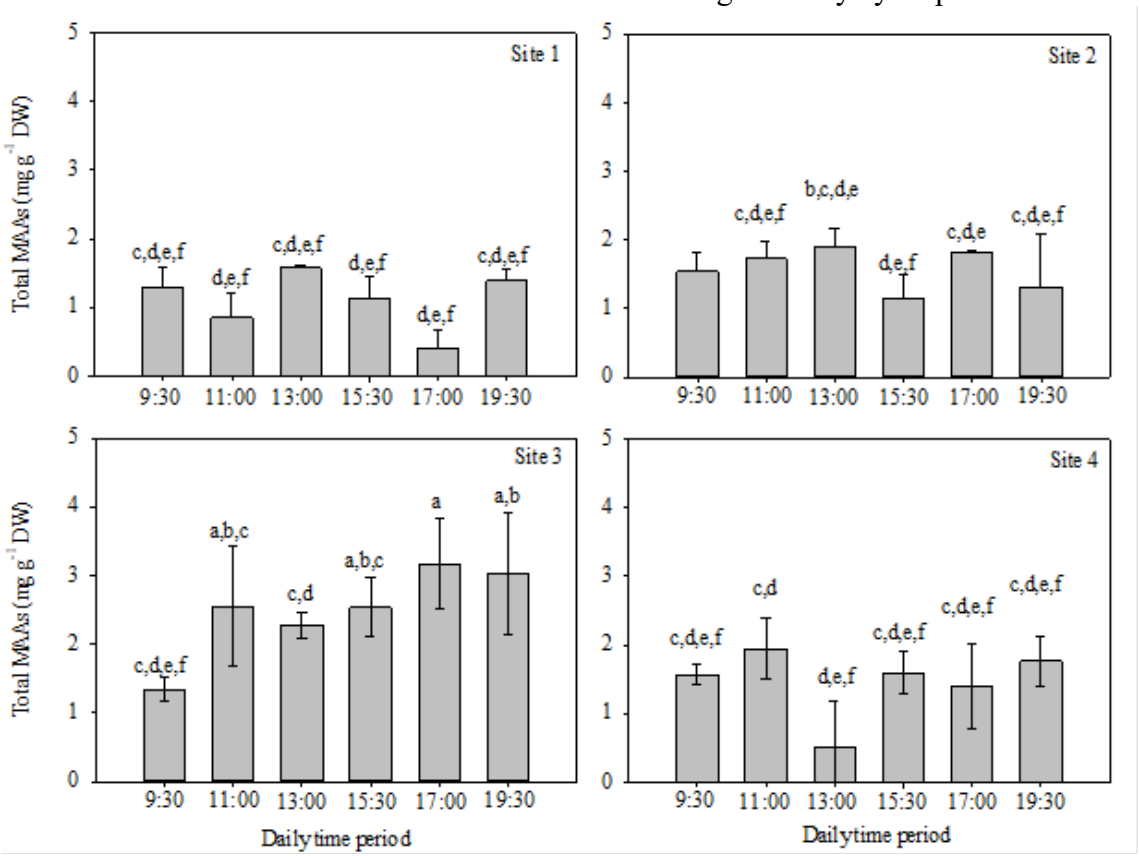

The results are expressed as mg of MAAs per gram of dry weight. Different letters indicate significant differences among the interaction between the sites of collection and the daily time period.

Figura 26. Relative composition (%) of Mycosporine-like amino acids (MAAs) detected in *Plocamium cartilagineum* extract in the four different sites during the daily cycle period.

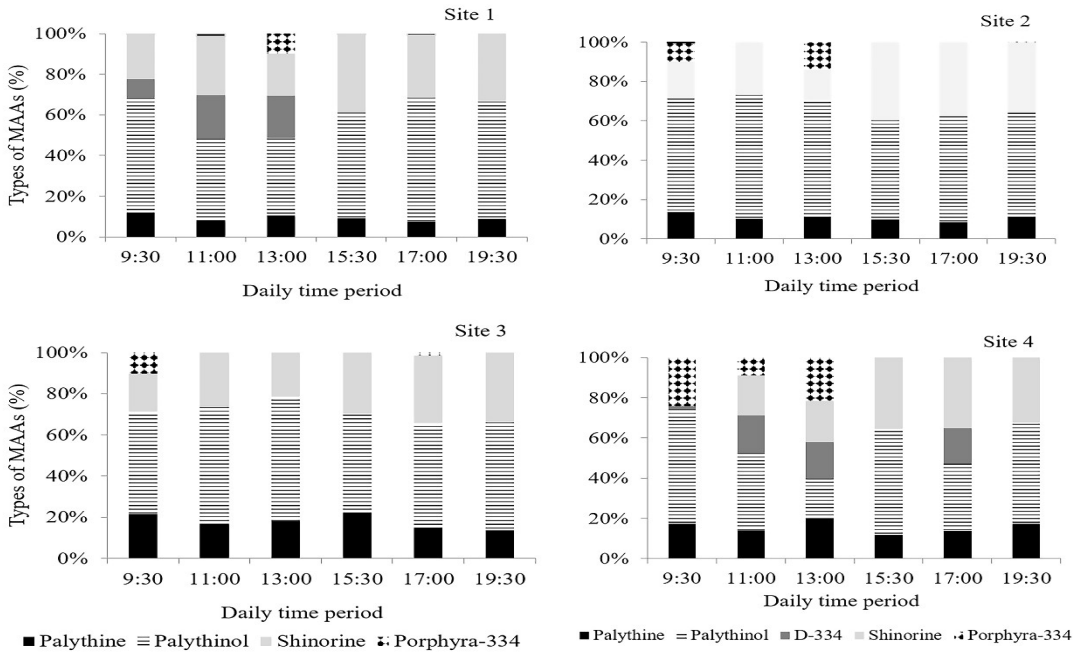

The analysis describes the levels of porphyra-334, shinorine, D-334, palythinol, palythine and asterina-330 of the samples.

Besides MAAs characterization by HPLC, these compounds were also identified by ESI-Mass spectrometry (Table 8). The results indicated the presence of more MAAs types on Site #4 than Site #1. Palythinol, palythine and asterina-330 were identified in algae from Site #1. This last MAA may be equivalent to mycosporine-2-glycine, palythine-threonine or mycosporine-methylamine:serine. In the Site #4, Asterina-330 to mycosporine-2-glycine, mycosporine-glutamine, palythine-serine, palythine and shinorine were identified.

Tabela 8. Mass spectrometry characterization of Mycosporine-like amino acids (MAAs) in *Plocamium cartilagineum* from Sites #1 and #4.

Site	Type of MAA	Molecular Formula	λ_{max} (nm)	Calculated m/z $[M+H]^+$	Observed m/z $[M+H]^+$
#1	Palythinol	$C_{13}H_{22}N_2O_6$	332	273.14450	273.14420
	Asterina-330	$C_{12}H_{20}N_2O_6$	330	289.13941	289.13901
	Palythine	$C_{10}H_{16}N_2O_5$	320	245.11320	245.11287
#4	Palythinol	$C_{13}H_{23}N_2O_6$	332	289.13941	289.13898
	Mycosporine-2-glycine	$C_{12}H_{18}N_2O_7$	331	303.11868	303.11838
	Mycosporine-glutamine	$C_{13}H_{20}N_2O_7$	310	317.13433	317.13385
	Palythine-Serine	$C_{11}H_{18}N_2O_6$	320	275.12376	275.12341
	Palythine	$C_{10}H_{16}N_2O_5$	320	245.11320	245.11284
	Shinorine	$C_{13}H_{20}N_2O_8$	333	333.12924	333.12863

Relative composition (%) of Mycosporine-like amino acids (MAAs) detected in *Plocamium cartilagineum* extract in the four different sites during the daily cycle period.

ANOVA analysis (Table S6) indicated that antioxidant capacity was not significantly influenced neither by the independent factors (collection site and daily time period) nor the interaction between them. *P. cartilagineum* showed an average of antioxidant capacity equivalent to 38.04 % ± 12.06, regardless of the place or time of collection.

Pearson's correlation (Table S8) analysis indicated a positive correlation between chlorophyll *a* and phycoerythrin ($r = 0.3993$, $p = 0.001$). Otherwise, a negative correlation was evident between Chl *a* and ETR ($r = -0.3639$, $p = 0.002$).

The simple linear regression analysis (Table S9), performed among the dependent variables and independent factors (environmental PAR, UV-A radiation and seawater temperature) evidenced a positive relation between PAR and ETR ($adjR^2 = 0.92$, $p = 0.00$) and a negative relation between PAR and Chl *a* ($adjR^2 = 0.08$, $p = 0.008$). Otherwise, UV-A radiation positively affected ETR ($adjR^2 = 0.68$, $p = 0.00$), synthesis of MAAs ($adjR^2 = 0.05$, $p = 0.02$), and negatively affected Chl *a* ($adjR^2 = 005$, $p = 0.02$). The temperature was associated to the positive modulation of ETR ($adjR^2 = 0.23$, $p = 0.001$), and negative modulation of Chl *a* ($adjR^2 = 0.15$, $p = 0.001$) and PE ($adjR^2 = 0.04$, $p = 0.05$). Positive correlations were observed between biochemical compounds and antioxidant capacity in the short-term (daily) variations.

3.5 DISCUSSION

Macroalgae are organisms with a high diversity and complexity, and over the evolution time they have developed the ability to adapt and colonize places with different conditions in order to survive. The adaptations mechanisms indicate a high plasticity among these organisms, including *Plocamium cartilagineum,* a shade-adapted algae that also responds to an increasing in radiation (JONES, 2019). Our manuscript, containing data about a field study performed with *P. cartilagineum* during a daily cycle, helps to elucidate the short-term variations developed by the species as a response to different light environments.

The measurement of photosynthetic activity is an important indicator of seaweed physiological condition, and allows to identify if it is submitted to stress conditions (LÓPEZ-FIGUEROA et al., 2006). The *in situ* ETR can be related to different destinations of photosynthetic reactions: For example, the reduction of NADPH which is used to fixing C at Calvin Cycle, the Mehler reaction to reduce impact of reactive oxygen species, and even the assimilation of nutrient by activation of nitrite reductase activity. These combined reactions will allow the macroalgae to have a higher growth rate or productivity in a specific period of time (VANLERBERGHE et al., 2020). In the case of our study, *in situ* ETR were much higher in the Sites #3 and #4, and strongly associated with PAR and UV-A radiation.

The ETR data observed under solar radiation increase at light curve measured at Sites #1 and #4 results may indicate the acclimation of those thalli, as the ETR increased similarly in both places with the same pattern until irradiance levels close to 500 μmol photons $m^{-2} \cdot s^{-1}$. Possible photoinhibition could be detected in *P. cartilagineum* only at Site #1, where ETR values sharply decreased when samples received the highest irradiance. When radiation exposure exceeds to the capacity of the macroalgae to conduct electrons, it may result on dynamic or chronic photoinhibition in order to reduce the damage caused by the light, or in extreme situations, it may suffer photodamage, associated to damage of antenna components and/or regulation mechanisms of the D1 protein present on PSII reaction centers (GÓMEZ et al., 1998).

The *in-situ* measurements in the field under the natural environmental conditions affecting photosynthesis, i.e. irradiance, temperature, hydrodynamic forcing, among others, are very valuable since they give us information on the daily variations of photosynthetic capacity or maximal efficiency in the complex scenario of the underwater field. In contrast, in laboratory, the measurement of rapid light curves under controlled conditions, but under

artificial light i.e. blue or red light, give us information on the potential values of photosynthetic parameters as ETR_{max}, α_{ETR}, $E_{k,}$ or NPQ_{max} under the conditions stablished in laboratory. The maximal ETR values are very different to the maximal values reached in the field (FIGUEROA et al., 2021). This is a key point if we want to use the ETR data to estimate carbon assimilation and C sequestration in order to calculate the contribution of macroalgae on C sink in a climate change scenario (FIGUEROA et al., 2021; FIGUEROA; CONDE-´ ALVAREZ; GÓMEZ, 2003). Previous works have shown in both micro- and macroalgae great differences between in situ and ex-situ (laboratory) measurements of in vivo chlorophyll *a* measurement (FIGUEROA et al., 2014; JEREZ et al., 2016; LONGSTAFF et al., 2002) i.e. ETR values under *in situ* conditions are 2-3 times higher than ETR_{max} values reached in Rapid Light Curves (RLC) conducted under red or blue light. The differences have been attributed to the differences in the light spectrum, polychromatic under solar radiation and only blue or red light under laboratory. In addition, it is necessary to consider the differences in the measurement procedure. In the underwater natural environment, the seaweeds are fixed in the substrate and they are moved by the hydrodynamic forcing whereas in a cuvette measurement system the macroalgae are in a fixed position without movement. Thus, the light field is more varied under natural conditions than that in the seaweed immersed in a cuvette i.e orthogonal light exposure. In addition, Figueroa et al (2021) observed that the *in situ* (solar radiation) yield and ETR_{max} were higher in free floating thallus in a tank (Yield measured by using Diving PAM) compared to thallus fixed in the tank (YII measured by using Monitoring PAM). The differences in ETR values can be attributed to the different solar exposure i.e., free floating thallus moved by air in the tank received less daily integrated irradiance and light quality can be enriched in green light due to shade effect of the seaweed in the tank compared to fixed with water flow through system receiving full solar spectra and higher irradiance. The measurement of *in vivo* chlorophyll *a* fluorescence in the field gives us reliable data on the photosynthetic capacity under natural conditions and the contribution of macroalgae to C sink can be better estimated than the measurement conducted under laboratory conditions.

The production and accumulation of photosynthetic pigments are other mechanism used by seaweed as for acclimation of photosynthesis to irradiance change but also as protection against photooxidative damage. Higher absolute content and changes in the rates PE/Chl *a* indicates photoacclimatation of antenna complex. In general, we observed a lower concentration of accessory pigments in thalli exposed to higher light intensities, mechanism developed to reduce light absorption and the damage of the excess of light (HÄDER;

FIGUEROA, 1997). Linear regression analysis also confirms the negative relation between Chl *a* and quantity/quality of the light, indicating a reduction on Chl *a* content with the increasing of PAR and UV-A radiation. The authors also described a negative correlation between PAR and Chl *a* content in many symbiotic algae in corals. In our study, *P. cartilagineum* showed a positive relationship of ETR with temperature. Similarly, it also evidenced a positive correlation between temperature and the photosynthetic response in *Grateloupia doryphora*. A review from Davison (1991) explains this relation by the possible reduction of carbon fixation by Rubisco, due to the potential of temperature on enzyme activity limitation, and an increasing on photorespiration.

In the case of *P. cartilagineum* from our study, both chlorophyll *a* and phycoerythrin showed a short-term diurnal fluctuation, which is associated with the environmental radiation, although these oscillations were not very acute. According to Betancor et al. (2015) a low variation in the accessory pigment content may be associated to an adaptation to the environmental conditions. Flores-Moya et al. (1998) observed a lower content of Chl *a* on *Rissoella verruculosa* at 14:00h, coinciding with the maximum irradiance of the day. López-Figueroa (1991) also observed a decrease on phycoerythrin content at the end of the day in *Chondrus crispus*. The author affirms that the light changes at the beginning and at the end of the day, it is noticed by the seaweed as "photomorphogenic signals" that control the synthesis of pigments during the day regulated photomorphogenic photoreceptors.

One of the most relevant strategies of photoprotection approach developed by some seaweeds exposed to higher light intensity including UVR , mainly in red macroalgae, is the production of UV-absorbing compounds, such as mycosporine-like amino acids (FIGUEROA et al., 2010; TAIRA et al., 2004). These nitrogenous compounds, which absorb UV radiation, also present anti-aging, antioxidant and anti-inflammatory activities, which makes them good candidates to the development of cosmetic and pharmaceutical products (VEGA et al., 2021). It is known that the production of MAAs is influenced by the quantity and quality of the radiation received. Although the regression analysis did not show influence of the amount of PAR in MAAs concentration, the UV-A radiation showed to be a factor of positive influence on MAAs production in *P. cartilagineum*, a fact observed in Site #3 and #4, which presented the highest doses of UV-A during the daily cycle. Figueroa et al. (2003), evaluating the total content of MAAs in *Porphyra leucosticta*, evidenced significant differences between the species from shade and from illuminated sites, with these compounds being dose and wavelength-dependent process. Karsten and Wiencke (1999) also showed a MAA

accumulation when the red macroalgae *Palmaria palmata* was transported from 3m depth to 0.2m depth with a higher incidence of UV-A. Navarro et al. (2021), studying *Mazzaella laminarioides* under laboratory conditions during a daily cycle, verified that the MAAs production is positively correlated with the radiation dose. The authors also describe a maximum content of MAAs at 13:00h under PAR+UV-A and PAR+UV-A+UV-B associated to different content of NO_3^-. In our study, besides Site #3, that shows an increasing pattern of MAAs in *P. cartilagineum* during the daily cycle, we could not observe a clear pattern of MAAs content throughout the day. Taira et al. (2004) associate a higher production of MAAs in the dinoflagellate *Scrippsiella sweeneyae* in the first six hours of the day light and infer that the synthesis of these molecules is associated not only with environmental factors but also with internal factors, such as cell cycle.

More than 30 types of MAAs have been described in literature and their chemical characteristics implies on the different roles they may play. MAAs present antioxidant capacity with differences among them (DE LA COBA et al., 2009a; WADA; SAKAMOTO; MATSUGO, 2013, 2015). The major MAA constituent of *P. cartilagineum* on this paper was palythinol. Besides photoprotection, MAAs may present a high antioxidant capacity (VEGA et al., 2021). Antioxidant capacity of purified aqueous extracts of MAAs, porphyra-334 plus shinorine, asterina-330 plus palythine, shinorine and mycosporine-glycine) was analyzed (DE LA COBA et al., 2009a). The scavenging potential of hydrosoluble radicals (ABTS), the antioxidant activity in lipid medium (β-carotene / linoleate bleaching method), and the scavenging capacity of superoxide radicals (pyrogallol autooxidation assay) were evaluated. Mycosporine-glycine presented the highest activity in all pH tested, followed by asterina-330 + palythine, while porphyra 334 + shinorine and shinorine showed scarce activity of hydrosoluble free radical scavenging, whereas asterina-330 + palythine showed high activity for inhibition of β-carotene oxidation relative to vitamin E and superoxide radical scavenging whilst the activity of porphyra-334 + shinorine and shinorine was moderate.

On the other hand, *in vivo* analysis of the cutaneous UV-protective properties of other MAAs has also been performed by De la Coba (2009b) for porphyra-334 and shinorine isolated from *Pyropia rosengurttii*. They showed that the galenic formulation containing porphyra-334 and shinorine (ratio 88:12) applied topically at a concentration of 2 $mg \cdot cm^{-2}$ (the dorsal skin of the SkhR-1 H female, albino, hairless mice prevented UV-induced clinical and histopathological damage including erythema, edema, SBC formation, skinfold thickening and other typical structural and morphological alterations observed in non-UV-

protected skin biopsies. De la Coba et al. (2009b) also showed that porphyra-334 plus shinorine counteracted the biochemical changes in UV-exposed skin by maintaining the expression of the heat shock protein Hsp70, a potential biomarker of acute UV damage, and the antioxidant defense system through an effective protection against the strong decrease in the activity of antioxidant enzymes, superoxide dismutase and catalase.

According to these results, the MAA photoprotection potential in cosmetic creams can be considered high due to a double function: (1) UV chemical screening with high efficiency for UV-B and UV-A regions of the solar spectrum; (2) high photo- and thermostability; and (3) their antioxidant capacity (DE LA COBA et al., 2009b; VEGA et al., 2021).

The ORAC methodology performed by Torres et al. (2018) evidenced the potential of 5 MAAs (palythinol, porphyra-334, shinorine, palythine and asterine-330) on inhibit lipid peroxidation, finding lower IC_{50} values for MAAs than the commercial synthetic antioxidant BHT. A study from Ngoennet et al. (2018) indicates the antioxidant capacity of the MAAs mycosporine-2-glycine, porphyra-334 and shinorine by $ABTS^{+}$ method, obtaining IC_{50} values equivalent to 40, 94 and 133 μM, respectively. Although those values are slightly higher than the control Trolox (10 μM), it indicates a potential of these natural molecules when compared to a synthetic one. In the case of this study with *P. cartilagineum*, ABTS method was not able to indicate a significant antioxidant variation during the daily period. However, as palythinol was the main MAA detected and it already was associated with the antioxidant role, we cannot discard that this MAA is providing this photoprotective strategy to *P. cartilagineum*.

In summary, the photosynthetic parameters and the accumulation of pigments and Mycosporine-like amino acids in *P. cartilagineum* are directly influenced by environmental factors, as irradiance, radiation quality, and temperature. Daily fluctuations on biocompound content are also evidenced indicating a high plasticity of these macroalgae during the daily cycle.

Acknowledgements

The study was financed by the Project NAZCA (P20-004589 by Government of Andalusia. The authors thank the Coordenação de Aperfeiçoamento de Pessoal de Nível Superior – Brasil

(CAPES) – Project CAPES-PRINT n° 88887.194792/2018-00 and Conselho Nacional de Pesquisa-Brasil (CNPq) – PDE n°200591/2014-2. The technical assitance by David López Paniagua is thankful.

CAPÍTULO 3

Manuscript submitted to *Algal Research*

Photomorphogenic and biochemical effects of radiation and nitrate availability on the red algae *Plocamium cartilagineum* (L.) Dixon.

Bruna Rodrigues Moreira[a,*], Julia Vega[b], Marta García-Sánchez[b], Cristina González Fernández[b], Antonio Avilés Benítez[b], Jose Bonomi-Barufi[a], Félix L. Figueroa[b]

[a] *Programa de Pós-graduação em Biociências e Biotecnologia, Laboratório de Ficologia, Departamento de Botânica, Universidade Federal de Santa Catarina, 88040-900 Florianópolis, Brazil*

*Correspondent author: bruna.rm01@gmail.com

[b] *Universidad de Málaga, Instituto Andaluz de Biotecnología y Desarrollo Azul (IBYDA), Centro Experimental Grice Hutchinson. Lomas de San Julián, 2, 29004 Málaga., Spain*

3.6 ABSTRACT

Photomorphogenic responses occurs in algae through the action of non-photosynthetic photoreceptors detecting different wavelengths ranges in the UV and visible region of the spectra. This radiation stimulus triggers different photomorphogenic and biochemical responses that helps algae acclimation and homeostasis. To understand the responses triggered by photoreceptors in *Plocamium cartilagineum* an experimental design based in the saturation of photosynthesis by Amber light and supplementation by different light qualities detected by potential photoreceptors was conducted. Thalli were submitted to (Amber, Amber + UV-A, Amber + Blue and Amber + Green under two nitrate levels, 60 and 240 μM). The experiment comprised to an innovative experimental design able to simulate the pattern of a daily cycle in a fully automated system. To evaluate possible modulations in *P. cartilagineum* thalli, photosynthetic and biochemical parameters were measured after 7 and 14 days of experiment. In addition, photosynthetic performance was also followed at days 1, 5, 8 and 12, during different daily times. As the main goal was to evaluate photomorphogenic responses, the photosynthetic performance did suffer only slightly variations. Nitrate assimilation was higher in the treatments containing blue and green light as complementary radiation, fact possible associated with an increase of nitrate reductase activity. Photosynthetic pigments were affected in distinct patterns over the two weeks, being mostly influenced by UV and Blue radiations with the highest nitrate concentration. Mycosporine-like amino acids production was also enhanced by those conditions, highlighting the increasing of shinorine content of thalli under blue radiation with 240 μM of nitrate at day 7, possibly associated to the modulation of a blue photoreceptor. The increase in the content bioactive compounds in the short-term by specific light qualities under optimal photosynthetic performance showed a biotechnological strategy to increase the level of high value bioactive compounds from algae.

Keywords: innovative experimental design, photoreceptors, mycosporine-like amino acids, red macroalgae.

3.7 INTRODUCTION

Sunlight plays a key role in the development of photosynthetic organisms. The photosynthetic active radiation (PAR) is captured by an antenna complex of algae and transferred to photosystem II (PSII), releasing an electrons flow on the electrons transport chain. The photosynthetic photochemical reactions driven by this electron flow can regulate nitrate assimilation, carbon fixation, antioxidant responses, among others, in algal metabolism due to the use the photosynthetic ATP and NADPH in the assimilation processes (CARDONA; SHAO; NIXON, 2018). However, besides photosynthesis, light is also involved in physiological responses triggered by non-photosynthetic photoreceptors. Photoreceptors are light-sensitive proteins, capable of monitoring continuously the light and trigger signal transduction chains that generate cellular and molecular responses (KIANIANMOMENI; HALLMANN, 2014). Those photoreceptors are associated with the control of the photoperiodism, photomorphogenesis and phototropism, responding to light signals depending on the quantity and quality of the signal. It also varies among the different groups of macroalgae (ROCKWELL et al., 2014; RÜDIGER; LÓPEZ-FIGUEROA, 1992).

Different photoreceptor groups have been described in plants and algae, including phytochromes, cryptochromes, phototropins, photoactive yellow protein, blue and UV-light receptors (HEGEMANN; FUHRMANN; KATERIYA, 2001). *Chlamydomonas*, a green microalga, possess at least three types of rhodopsin-like receptors associated with other proteins and carotenoid vesicles, organized into a light-perception system. The rhodopsin photoreceptors are light gated ion channels which can modulate the beating pattern of the flagella, driving the algae in the light direction and consequently improving photosynthesis and survival (LUCK; HEGEMANN, 2017; SINESHCHEKOV; JUNG; SPUDICH, 2002) .*Euglena* spp. also present an eyespot formed by photoreceptors and carotenoids (KATO et al., 2020). Phytochrome like proteins were detected by monoclonal antibodies in different macroalgae (LINDEMANN et al., 1989; LÓPEZ-FIGUEROA et al., 1990).

Changes in the light pattern of a daily cycle are also noticed by photoreceptors, promoting changes in pigment content and photoacclimation of micro and macroalgae. López Figueroa & Niell (LOPEZ-FIGUEROA; PEREZ; NIELL, 1989; LOPEZ-FIGUEROA;

NIELL, 1989) and López Figueroa (1990) suggested the production of chlorophyll and phycobiliproteins mediated by the stimulation phytochromes or phytochrome-like receptor by giving pulses of red and far-red radiation in macroalgae including red algae as *Corallina elongata and Porphyra umbilicalis* .

Furthermore, it is also known that blue and UV- photoreceptors trigger the production of photoprotective compounds in macroalgae (ALLORENT; PETROUTSOS, 2017; SCHNEIDER et al., 2020b). Among them, mycosporine like amino acids can be highlighted. Around 30 types of MAAs have been identified on algae, and those molecules are considered a mechanism of photoprotection, absorbing UV radiation and avoiding photodamage (VEGA et al., 2021).

Besides radiation, nutrient availability plays an important role on photosynthetic and photomorphogenic responses of algae. A study carried out by López- Figueroa et al. (2021) indicates an increasing of ETR_{max} values on *Ulva rigida* when thalli are cultivated under nitrate supply, also reducing photoinhibition under high solar radiation exposition. Many authors suggests that the combination of radiation and nutrient may also results in interesting modulations, as for example, the study performed by Bonomi-Barufi et al. (2012), that identified a photoprotection effect of the NO_3^- on *Gracilaria tenuistipitata,* reducing the negative effects of UV radiation by synthetizing a higher content of mycosporine-like amino acids. Figueroa et al. (2010) evidenced a positive effect of N-supply on photosynthesis of *Gracilaria conferta* due to the increasing of phycoerythrin and phycocyanin synthesis, under UV exposition. Blue light is also described for increasing nitrate absorption by stimulating nitrate reductase and glutamine synthetase activities, enhancing amino acids and pigments production (HADER et al., 1996).

Experimental designs have varied for investigating photomorphogenic light effects in algal or plant responses. Since the first studies with lettuce determining phytochrome activity in seed germination, other efforts have been done since then (BORTHWICK et al., 1954). Some authors simply exposed the algae to continuous and fixed amounts of light, fitting photoperiodic switching on and off (AGUILERA et al., 2000; FIGUEROA; AGUILERA; NIELL, 1995; KORBEE; FIGUEROA; AGUILERA, 2005). Different photoperiods can also serve as a strategy to modulate physiological and biochemical responses (BONOMI BARUFI; FIGUEROA; PLASTINO, 2015). Other studies complemented PAR radiation with low intensity levels for stimulating photoreceptors beside photosynthesis. After, the strategy of saturating photosynthesis with yellow low pressure sodium lamp (SOX light) with Amber

color was employed, ensuring the low amounts of other monochromatic lights to induce responses of the algae (PAGELS et al., 2020; SCHNEIDER et al., 2020b, 2022). However, none of these studies focused on variation of light intensity following the light daily available, simulating a dial light increase/decrease in laboratory regulated conditions.

Plocamium cartilagineum (Plocamiaceae) is a red macroalgae, found in intertidal and subtidal zones in tropical and temperate areas around the world, that awakens a great biotechnological interest due to its high chemical complexity. *P. cartilagineum* produces compounds like proteins, lipids, organic acids, halogenated compounds, polysaccharides, terpenes, pigments and mycosporine-like amino acids (MOREIRA et al., 2022; VALENTÃO et al., 2010). Those molecules extracted from *P. cartilagineum* are reported by many authors as antioxidant, photoprotective, virucidal, insecticide, anticancer molecules, among others (HARDEN et al., 2009; KNOTT, 2016; MOREIRA et al., 2022; SABRY et al., 2017). All those mentioned bioactivities stand *P. cartilagineum* as a potential alga to be cultivated and used by pharmaceutical, cosmetic and nutraceutical industries. Moreover, novelty cultivation strategies may be employed to enhance the production of specific compounds, as for example, by photoreceptors stimulation using distinct quality and quantity of radiation.

This paper aimed to cultivate *Plocamium cartilagineum* under the influence of different radiation treatments associated with two nitrogen concentrations. The experiment was performed with an innovative design using climatic controlled chambers, simulating a daily cycle pattern and its light fluctuation. The goals of the experiment were to evaluate and comprehend photosynthetic and biochemical performance of algae thalli submitted to different treatments during two weeks.

3.8 MATERIAL AND METHODS

3.8.1 Biological Material and acclimation

The red macroalga *Plocamium cartilagineum* (Linnaeus) P.S.Dixon (Plocamiales, Rhodophyta) was recollected at La Herradura Beach, Granada, Spain (36°44'17"N, 3°45'01"W) on January, 2022. Algae was quickly transported to the Instituto de Biotecnología y Desarrollo Azul (IBYDA) in Malaga city (36°43′12″ N, 4°25′13″ O) where the experiment was conducted. Algae thalli were manually cleaned for debris and epiphytes. Acclimatation was performed submitting *P. cartilagineum* to an irradiance equivalent to 20 μmol m^{-2} s^{-1} of amber radiation (λ=590 nm) using an Amber lamp provided by LEDs, in seawater produced by marine salt in distilled water supplemented with 50 μM of potassium nitrate and 3 μM of sodium phosphate dibasic, at 18 °C, during a week. All acclimation processes and the experiment were conducted in an Aralab Climatic Chamber (FITOCLIMA 25000 PLH).

3.8.2 Experimental design

For the experiment, 3 g L^{-1} of fresh *P. cartilagineum* were placed into polymethylmethacrylate cylinders transparent to UV-radiation. To evaluate the potential effect of light quality and nutrient availability on photosynthetic performance and biochemical properties, *P. cartilagineum* was submitted to 4 different types of radiation provided by LEDs: Amber (λmax 590 nm), Amber + UV-A (λmax 365 nm), Amber + Blue (λmax 420 nm) and Amber + Green (λmax 520 nm); two concentrations of potassium nitrate (60 μM and 240 μM) and 3 μM of sodium phosphate dibasic, during 2 weeks. These treatments configured an initial N:P ratio of 20:1 and 80:1, respectively. The water of the cylinders was changed at 1st and 7th day of the experiment, followed by nutrient addition. Water samples were obtained at different interval periods for evaluating nutrient uptake by the algae (see details below). In this sense, the experiment consisted of the exposure of *P. cartilagineum* to 8 different treatments with 3 replicates in each one. The experiment was designed to simulate the pattern of a sunny day without clouds, with an increase of the radiation until midday, in a photoperiod of 12:12, hereafter considered from 9:00 to 21:00 as light period. Amber was used as

saturating photosynthetic light in all treatments. In this way, when the light was switched on, at 9:00, it was increased till 20 μmol m^{-2} s^{-1} at 9:30 and remained at this irradiance for one hour (9:30 – 10:30), when an increment of 20 μmol m^{-2} s^{-1} was provided during 30 min, achieving 40 μmol m^{-2} s^{-1} at 11:00 and remaining at this intensity for 3 next hours, when a new increment of Amber light was produced, reaching 80 μmol m^{-2} s^{-1} at 14:30h remaining in this quantity for one hour. Then, from 15:30 to 16:00, the irradiance was decreased gradually till reach again 40 μmol m^{-2} s^{-1}. Again, the samples remained receiving this amount of light for the subsequent 3 hours, and from 19:00 to 19:30, a new gradual drop was applied, till the value of 20 μmol m^{-2} s^{-1}. Samples received this irradiance for one hour, and at 20:30 the system started automatically to switch off the light, decreasing from 20 to zero during 30 min. Then, from 21:00 to 9:00 of the next day, samples remained in darkness. Total daily Amber doses was 251.5 kJ m^{-2}. The irradiance values chosen for the experiment were determined previously incubating algal thalli into diverse increasing Amber irradiances for 5 min. Electron transport rate (ETR) was determined as described below and light curves were fitted to a model of Eilers and Peters (1989), ensuring the determination of saturating irradiance (see details of this procedure below). In that case, the value found was close to 95 μmol m^{-2} s^{-1} and we opted to utilize a value a little bit lower as the maximal one along the daily dial cycle. Besides Amber, three groups were exposed to complementary radiation (UV, Blue, Green) from 12:00 to 18:00. In this sense, complementary radiation of 8 μmol m^{-2} s^{-1} initially was provided from 12:00 to 14:00, and then doubled gradually from 30 min until reach 16 μmol m^{-2} s^{-1}, remaining in this total for one hour (14:30 to 15:30). So, complementary irradiance also was decreased by the half back to 8 μmol m^{-2} s^{-1}, remaining in this quantity for more two hours and switched off at 18:00 (Figure 27). Total daily doses were 358.75 kJ m^{-2} for Amber + UV-A, 398.61 kJ m^{-2} for Amber + Blue, and 357.19 kJ m^{-2} for Amber + Green treatments.

Figura 27. Experimental design performed on the Aralab Bioclimatic camara. A. Representative scheme of the experimental design containing the different radiation qualities and intensities. Amber was employed during the whole daily cycle and is represented by yellow color, meanwhile complementary radiations are restricted to certain period of the day and are represented by violet
(UV-A), blue and green. B. Relative absorption spectrum of the lamps employed in the experiment. C. Total daily doses (kJ m^{-2}) of each treatment employed in the experiment

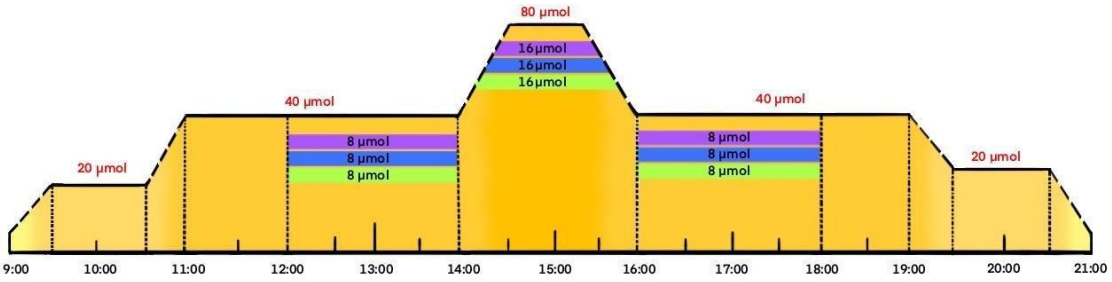

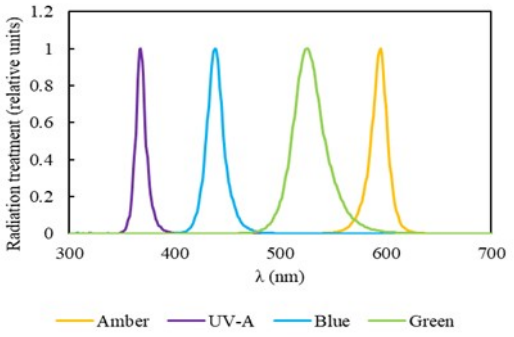

Treatment	Daily doses (kJ m^{-2})
Amber	251.50
Amber + UV-A	358.75
Amber + Blue	398.61
Amber + Green	357.19

3.8.3 Photosynthetic performance

Photosynthetic parameters were measured during the experiment by *in vivo* chlorophyll *a* fluorescence using a Mini-PAM (Walz, Effeltrich, Germany). Effective quantum yield (Y(II)), and maximum quantum yield (F_v/F_m) of photosystem II were assessed as described by Figueroa et al. (2014) at days 1, 5, 8 and 12, in four different periods throughout the day: 8:20 (F_v/F_m), 9:45, 15:00 and 18:20h.

Data obtained at the last three times from the algae in the experimental vessels were Y(II), and were used to calculate in situ electron transport rates. Rapid Light Curves (RLC) were performed on the 1st, 7th and 14th days in the period from 9:00 to 14:00h, using the Mini-PAM fluorometer connected to the WinControl software. During this interval, radiation treatments remained constant to avoid interference on the test due to the variation of

irradiances. Algal samples from each treatment were acclimated during 15 minutes in darkness and subsequently exposed to the following increasing irradiances: 0, 25, 45, 66, 90, 125, 190, 285, 420, 625, 845, 1150, and 1500 μmol photons m^{-2}. s^{-1} of red actinic light. After incubation of each irradiance the samples received a saturation pulse. Electron transport rates (ETR) were calculated according to the following equation:

$$ETR = Y(II) * E * A * 0.15$$

Where, Y(II) correspond to effective quantum yield of PSII; E correspond to the irradiance to which algae was submitted; 0.15 is equivalent to the factor to adjust the irradiance captured and used by photosystem II (PSII) by red macroalgae; A is referent to the absorptance calculated by the following equation according to Grzymski et al. (1997) and Figueroa et al. (2003):

$$A = 1 - \frac{E_F}{E_T}$$

Where, E_F corresponds to the irradiance transmitted throughout algae thalli and E_T is the total irradiance, measured with the LICOR radiometer.

3.8.4 Nutrient assimilation

Nutrient uptake efficiency (NUE) was calculated for nitrate and phosphate considering all conditions evaluated in this experiment. To evaluate nutrient assimilation by algae, water samples were taken as soon as the nutrients were added at day 1 (after adding the nutrients), at day 7 and at day 14 (before water changing and nutrient addition), and frozen at -80 °C for further analysis. The remaining content of each nutrient in the water was quantified as described by Grasshoff et al. (1999), using a segmented flow analyzer (SFA; Seal Analytical autoanalyzer QuAAtro). NUE was calculated as described by Massocato et al. (2022) using the following formula:

$$NUE(\%) = 100 - \left(\frac{C_{sample}\, x\, 100}{C_{initial}} \right)$$

where, C_{sample} represents the nutrient concentration on the water sample for each treatment and $C_{initial}$ the initial nutrient concentration added to each treatment.

3.8.5 Photosynthetic pigments

In order to determine photosynthetic pigments, we used distinct extracts. For Chl *a* quantification, 15 mg of dry algae were macerated with 2 mL of acetone 90% previously prepared with 10% of a saturated solution of $C_4Mg_4O_{12}$. The mixture was extracted overnight, at 4 °C in darkness. At the end of the process, the mixture was centrifuged for 10 min, at 4 °C and 10 000 rpm. Chl *a* content on acetonic extracts was calculated according methodology of Ritchie (2008), as described in the equation:

$$Chl\,a\left(\mu g\,mL^{-1}\right)=11.4711*\left(A_{664}-A_{750}\right)-1.6841*\left(A_{691}-A_{750}\right)$$

For phycoerythrin (PE) and phycocyanin (PC), the extracts were prepared by macerating 15 mg of dry algae with 2 mL of sodium phosphate buffer pH 6.8. The mixture was incubated overnight, and subsequently centrifuged during 10 min, at 4 °C and 10 000 rpm. R-PE and R-PC on aqueous extracts were quantified according methodology described by Wiley & Neefus (SAMPATH-WILEY; NEEFUS, 2007), described in the following equations:

$$R-PE\left(mg\,mL^{-1}\right)=0.1247\left(A_{564}-A_{730}\right)-0.4583\left(A_{618}-A_{730}\right)$$

$$R-PC\left(mg\,mL^{-1}\right)=0.154\left(A_{618}-A_{730}\right)$$

3.8.6 Phenolic compounds

The quantification of phenolic compounds was performed using the same aqueous extract employed for phycobiliproteins quantification, described on item 2.5. After extraction, the content of phenolic compounds was measured using the methodology of Folin-Ciocalteau (1927). The reaction was carried out by mixing 100 µL of algal extract with 700 µL of distilled water, 50 µL of Folin-Ciocalteau reagent and lastly, 150 µL of 20% sodium

carbonate (Na_2CO_3), which starts the reaction. The mixture was incubated for 2 hours at 4 °C. After incubation time the absorbance was measured at 760 nm. The results are expressed in mg equivalent of phloroglucinol (Ph) per gram of algal dry weight (DW), and were calculated based on a phloroglucinol (6-hydroxy-2, 5, 7, 8-tetramethylchroman-2-carboxylic acid) calibration curve, using the following linear fitting: $y=0.0641x + 0.0174$ ($r^2 = 0.99$).

3.8.7 Mycosporine-like amino acids

Mycosporine-like amino acids (MAAs) were extracted by grinding 15 mg of algae dry biomass with 1 mL of 20% methanol. The mixture was incubated for 2 hours at 45 °C. After incubation time, the mixture was centrifuged for 10 min, at 10 000 rpm. The supernatant was collected and submitted to dry in a vacuum concentrator (Speed-Vac SPD210, Thermo Scientific, Waltham, MA, USA). The dry extract was resuspended in 1 mL of methanol HPLC grade and filtered through a 0.2 µm membrane filter. MAAs analysis were performed using ultra high performance liquid chromatography uHPLC (1260 Agilent InfinityLab Series, Santa Clara, CA, USA) according to the methodology described by Korbee-Peinado et al. (2004). The mobile phase used to MAAs separation was composed by aqueous methanol 2.5% (v/v) and acetic acid 0.1% (v/v) in water. 30 µL of each sample was injected in a C8 chromatographic column. Flow rate was set as 0.5 mL. min^{-1} in a run time of 20 min per sample. MAAs peaks were detected in a photodiode detector at 320 and 330 nm.

3.8.8 Statistical Analysis

Factorial ANOVA (analysis of variance) were applied for the data obtained at day 7 and at day 14 independently. The independent factors used in ANOVA were radiation treatment and nitrate concentration. Student- Newman-Keuls (SNK) post-hoc test was used to identify the correlation among the responses, considering significance level of $p < 0.05$. All statistical analyses were conducted using Statistica 7.0 (StatSoft. Inc.) and graphs were created using Prisma software.

3.9 RESULTS

The photosynthetic parameters of *P. cartilagineum* submitted to the different treatments are presented in Table 9 and Fig. S8. The experiment performed in this paper was designed aiming to promote photoreceptors modulation stimulated by low irradiance of different light qualities (UVA, Blue or Green) under similar photosynthetic rate provided by Amber light under saturated irradiance for photosynthesis. Data derived from rapid light curves (Table 9) performed on days 1, 7 and 14 of the experiment, evidenced a stability on the most photosynthetic parameters, with some slight variability. At day 7, any of the photosynthetic parameters were affected by the treatments evaluated. Although Anova (Table S10) indicated that F_v/F_m was affected by the interaction between radiation and nitrate concentration, Newman-Keuls post-hoc test did not detect any variation among the treatments. So, it was found an average of 0.531 ± 0.06 for F_v/F_m, 0.063 ± 0.02 for α_{ETR}, 6.1 ± 1.0 for ETR_{max} and 115.5 ± 73.1 for E_k. At day 14 is possible to note that F_v/F_m and α_{ETR} did not presented significative difference among the treatments, with an average of 0.511 ± 0.06 and 0.076 ± 0.01, respectively. The E_k values observed at day 14 were affected only by nutrient concentration, being observed higher values of E_k on treatments containing 240 µM of nitrate than on treatments containing 60 µM. Significative differences were observed on the ETR_{max} , being the highest values detected on thalli submitted to Amber + Blue (240 µM of nitrate) and Amber (60 µM of nitrate), corresponding respectively to 8.0 ± 1.5 and 7.7 ± 0.9 µmoL electrons m^{-2} s^{-1}, and the lowest value on thalli under Amber + Green (60 µM of nitrate) treatment, corresponding to 4.6 ± 0.7 µmoL electrons m^{-2} s^{-1}.

Fig. S8 presents *in situ* ETR measured throughout the day during the experiment. *P. cartilagineum*. In general, it is possible to observe a similar in situ ETR variation during the experimental period. Anova data (Table S11) indicates that different radiations have not significatively influenced *in situ* ETR in all days evaluated. It was observed in specific daily periods, on day 1 at 18:20, day 5 at 09:45 and 18:20 and day 12 at 09:45, a slightly reduction on *in situ* ETR on treatments containing 240 µM of nitrate when compared to those with 60 µM of nitrate

Tabela 9. Photosynthetic parameters of *Plocamium cartilagineum* submitted to different radiation treatments (Amber, Amber + UV, Amber + Blue and Amber + Green) and nitrate concentrations (60 µM and 240 µM) at days 7 and 14 of the experiment, obtained from Rapid Light Curves.

Treatments			F_v/F_m	α_{ETR}	ETR_{max}	E_k
Time	Radiation	NO_3				
Initial	-	-	0.474 ± 0.07	0.054 ± 0.01	4.2 ± 0.7	79.3 ± 5.3
7 days	Amber	60	0.506 ± 0.05	0.054. ± 0.03	5.4 ± 1.4	64.3 ± 8.6
	Amber	240	0.536 ± 0.07	0.07 ± 0.01	6.2 ± 0.2	83.3 ± 8.1
	Amber + UV-A	60	0.526 ± 0.05	0.053 ± 0.02	6.4 ± 0.9	108.3 ± 29.1
	Amber + UV-A	240	0.498 ± 0.07	0.067 ± 0.02	5.8 ± 0.6	88.7 ± 15.2
	Amber + Blue	60	0.492 ± 0.04	0.058 ± 0.03	6.3 ± 1.1	82.5 ± 21.6
	Amber + Blue	240	0.589 ± 0.04	0.072 ± 0.01	6.9 ± 1.1	96.7 ± 23.5
	Amber + Green	60	0.603 ± 0.01	0.076 ± 0.01	6.4 ± 0.9	85.3 ± 17.9
	Amber + Green	240	0.500 ± 0.02	0.048 ± 0.01	6.4 ± 0.4	162.5 ± 12.5
14 days	Amber	60	0.527 ± 0.03	0.082 ± 0.01	7.7 ± 0.9[a]	94.1 ± 3.4
	Amber	240	0.466 ± 0.06	0.068 ± 0.01	6.0 ± 0.4[a,b]	88.6 ± 12.2
	Amber + UV-A	60	0.492 ± 0.03	0.081 ± 0.01	7.3 ± 1.4[a,b]	89.7 ± 19.2
	Amber + UV-A	240	0.500 ± 0.05	0.070 ± 0.01	7.2 ± 0.7[a,b]	102.7 ± 13.6
	Amber + Blue	60	0.480 ± 0.06	0.088 ± 0.02	6.5 ± 1.7[a,b]	77.6 ± 30.0
	Amber + Blue	240	0.536 ± 0.06	0.074 ± 0.01	8.0 ± 1.5[a]	109.8 ± 29.1
	Amber + Green	60	0.551 ± 0.02	0.070 ± 0.01	4.6 ± 0.7[b]	65.7 ± 7.5
	Amber + Green	240	0.534 ± 0.10	0.073 ± 0.02	7.5 ± 0.7[a,b]	105.5 ± 18.4

Data is mean +/- SD. Different letters indicate significatively differences among αETR, ETRmax, Ek and Fv/Fm independently.

Nutrient uptake efficiency (NUE) of *P. cartilagineum* for both nitrate and phosphate are presented in Figure 28. In the first week of the experiment (Figure 28A), algae thalli cultivated in salt water containing 60 µM of nitrate presented the highest nutrient uptake efficiency (NUE), incorporating 76.1 ± 24.5 % of nitrate available, which is equivalent to around 45.6 µM of nitrate. In the second week (Figure 28B), it was observed an interaction between nitrate availability and the radiation treatments employed. The efficiency of nitrate uptake was also higher in algae grown with 60 µM of nitrate. Furthermore, it is possible to notice that using 240 µM of nitrate, algae grown under treatments containing Amber + Blue and Amber + Green radiation exhibited a higher nitrate uptake when compared to algae grown using only Amber and Amber + UV-A radiation. Phosphate uptake was not affected by any factors during the first week, presenting an average of 39.5 ± 8.1 % phosphate incorporation

(Table S12). During the second week (Figure 28C), algae grown using 240 µM of nitrate absorbed more phosphate than those cultivated using 60 µM of nitrate.

Figura 28. Nutrient uptake efficiency determined on *Plocamium cartilagineum* thalli cultivated under the influence of different treatments

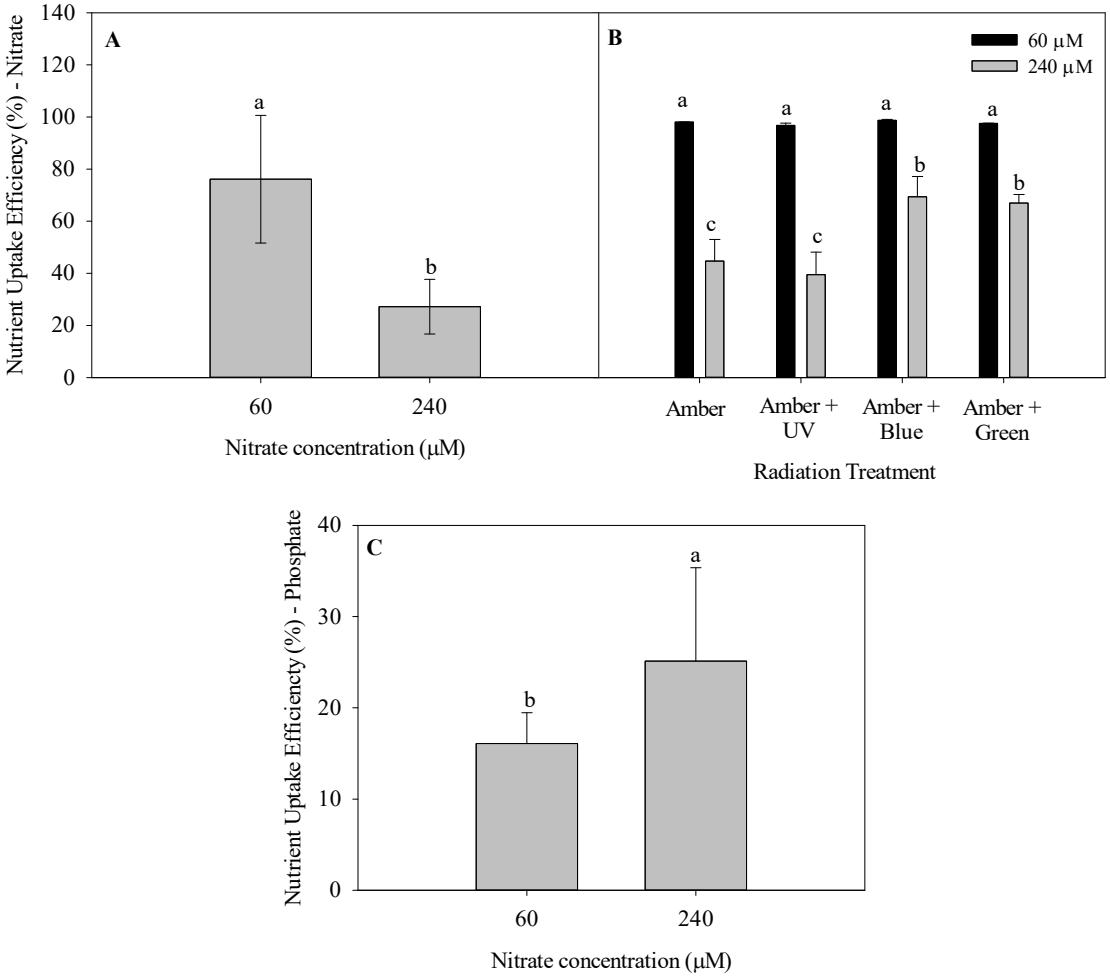

A – Nitrate uptake efficiency on day 7 on algae cultivated using different nitrate concentration; B- Nitrate uptake efficiency on day 14 on *P. cartilagineum* thalli cultivated under different radiation treatments and nitrate concentration; C- Phosphate uptake efficiency of *P. cartilagineum* thalli on day 14 using different nitrate concentration. Different letters indicate significant differences among the treatments at days 7 and 14.

The pigment contents of *P. cartilagineum* (chlorophyll *a* (Chl *a*), phycoerythrin (PE) and phycocyanin (PC) contents) after 7 and 14 days of experiment are presented in Figure 29. The production of the three pigment groups exhibited different patterns in the two weeks of the experiment. Chl *a* content was influenced by radiation treatments during the first week and by nitrate concentration in the second one (Table S12 and S13). The highest contents of

Chl *a* at day 7 were detected in algae thalli under Amber + UV and Amber + Blue treatments, reaching the values of 637.3 ± 39. 6 and 612.1 ± 61.9 µg. g DW^{-1}, respectively. On day 14, algae grown with 240 µM of nitrate exhibited a higher content of Chl *a* (597 ± 134.4 µg. g DW^{-1}) than algae grown with 60 µM of nitrate (423 ± 153.3 µg. g DW^{-1}).

Figura 29. Photosynthetic pigments determined in *Plocamium cartilagineum* thalli on the different experimental treatments

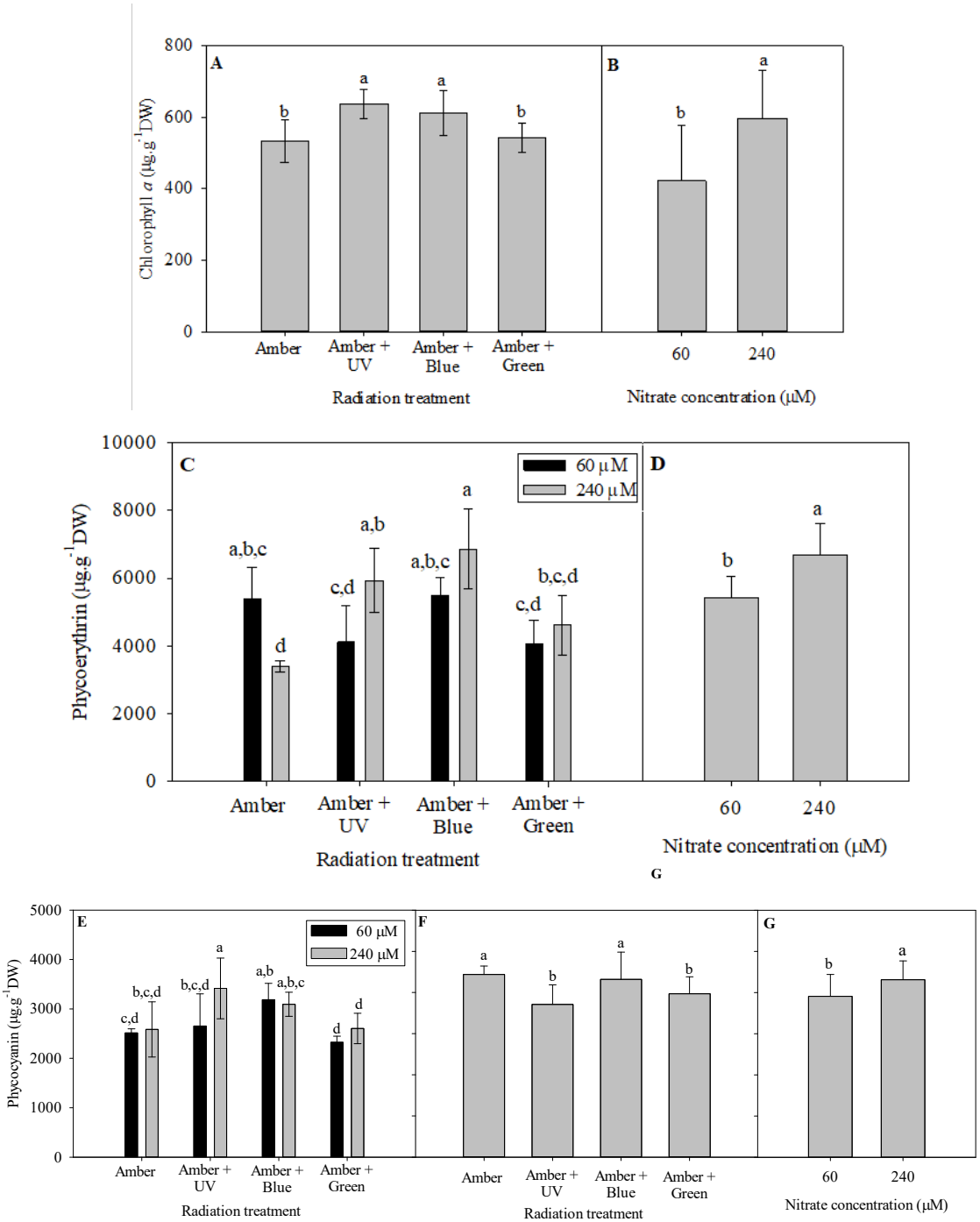

Chlorophyll a content on algae thalli at day 7 (A) influenced by radiation treatments and at day 14 influenced by nitrate concentration (B); Phycoerythrin content on algae thalli at day 7 (C) influenced by the interaction between radiation treatment and nitrate concentration and at day 14 (D) influenced by nitrate concentration; Phycocyanin content on algae thalli at day 7 (E) influenced by the interaction between radiation treatment and nitrate concentration and at day 14, being F the content of PE influenced by radiation treatment and G by nitrate concentration, independently. Different letters indicate significant differences ($p < 0.05$) among the treatments at distinct times.

There is not a clear pattern in the production of phycoerythrin (PE) on algae thalli from day 7 (Figure 29C). The interaction of radiation treatment and nitrate concentration evidenced a higher content of PE in Amber (60 μM of nitrate) when compared to Amber (240 μM of nitrate). On the other hand, the highest nitrate concentration increased PE production when using Amber + UV radiation and Amber + Blue. At day 14, the pigment production was enhanced using 240 μM of nitrate (6674 ± 938 μg. g^{-1} DW). Regarding PC content, at day 7 only the use of 240 μM of nitrate combined with Amber + UV radiation increased PC content compared with the use of 60 μM of nitrate. On day 14, it was observed the effect of radiation treatments (Figure 29F) and nitrate concentration (Figure 29G) independently. The use of Amber and Amber + Blue stimulated PC production, as well the use of 240 μM of nitrate.

Polyphenol content at day 7, represented in Figure 30, was influenced by the interaction between radiation treatment and the nitrate concentration (Table S12). It can be noticed that *P. cartilagineum* exhibited higher polyphenol content when submitted to Amber + Blue, than in the other three treatments. The combination of Amber + Blue radiation was the most effective treatment to stimulate the production of phenolic compounds in both nitrate concentrations. Although ANOVA analysis at day 14 (Table S13) indicates a significative difference on polyphenol content influenced by radiation treatment, the post-hoc analysis did not confirm the pattern.

Figura 30. Phenolic compounds measured in *Plocamium cartilagineum* thalli at day 7 of the experiment resulted from the interaction between radiation treatment and nitrate concentration.

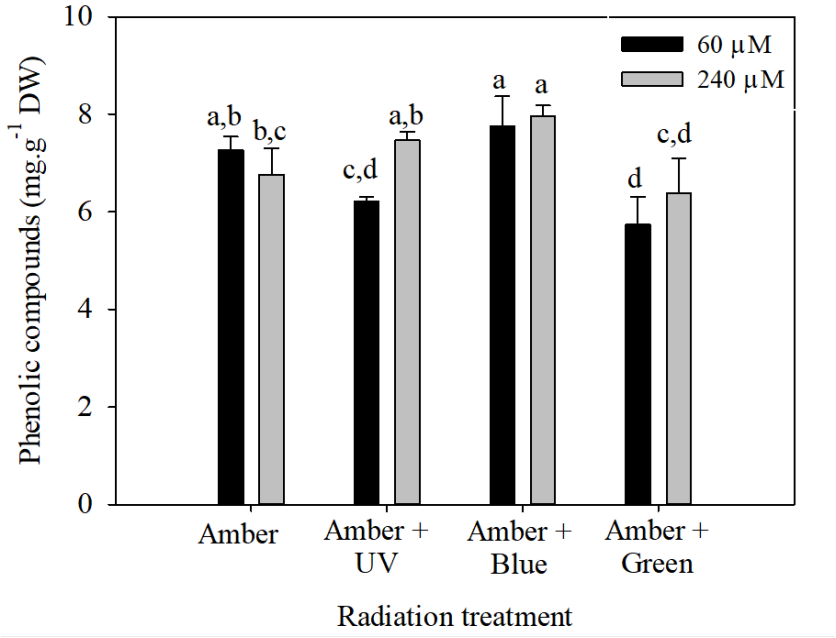

Different letters indicate significant differences ($p < 0.05$) among the treatments at distinct times.

Nutrient concentration and radiation treatment influenced significatively the level of total MAAs in both weeks of the experiment (Table S12 and S13). The highest concentration of MAAs was detected in *P. cartilagineum*, corresponding to 2.4 ± 0.5 mg. g^{-1} DW, cultivated under Amber + UV radiation and 240 µM of nitrate (Figure 31). This cultivation condition was more efficient to stimulate MAAs production/accumulation than all of the other treatments, except for algae cultivated under Amber + Blue containing also 240 µM of nitrate.

Figura 31. Total mycosporine-like amino acids on *Plocamium cartilagineum* thalli submitted to different treatments.

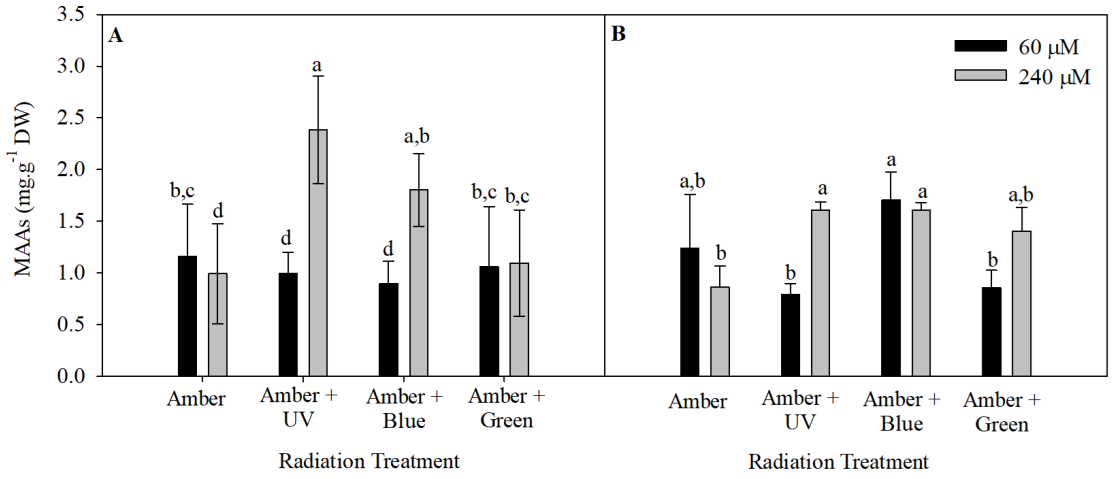

A indicate MAAs content on thalli at day 7, influenced by radiation treatment and B indicate MAAs content on day 14, influenced by the interaction between radiation treatment and nitrate concentration. Different letters indicate significant differences ($p < 0.05$) among the treatments at distinct times.

Among different MAAs found in *P. cartilagineum*, we were able to identify and quantify, by using HPLC chromatograms associated with their specific standards, the following: Palythine, traces of Asterine-330 and Shinorine. There were also observed two unidentified peaks, with similar retention times, absorbing UV radiation at 332 nm. Figure 32 exhibits the fluctuation of shinorine levels during the two weeks of the experiment. Analysis of variance (Table S14) indicated that shinorine concentration was directly influenced by the interaction between radiation and time and also by radiation and nitrate concentration, independently. Regarding the first interaction (Figure 32), the highest contents of shinorine were detected on the treatments using Amber + Blue at day 7, Amber at day 14 and Amber + Green at day 14. Those three values were statistically higher than the initial concentrations measured at 1, indicating that those treatments increased the production of this MAA. Figure 33B evidenced that Amber + Blue associated to a higher nitrate availability increased shinorine when compared to the other treatments evaluated. An increasing on shinorine was also observed on thalli submitted to Amber + UV radiation containing 240 µM of nitrate when compared to those from 60 µM. Both treatments, Amber + Blue and Amber + UV, both with 240 µM of nitrate, increased 4.7 and 2.8 times, respectively, the content of shinorine when compared to thalli from the first day of the experiment (0.06 ± 0.04 mg g^{-1} DW)

Figura 32. Shinorine levels detected on *P. cartilagineum* thalli submitted to the different treatments

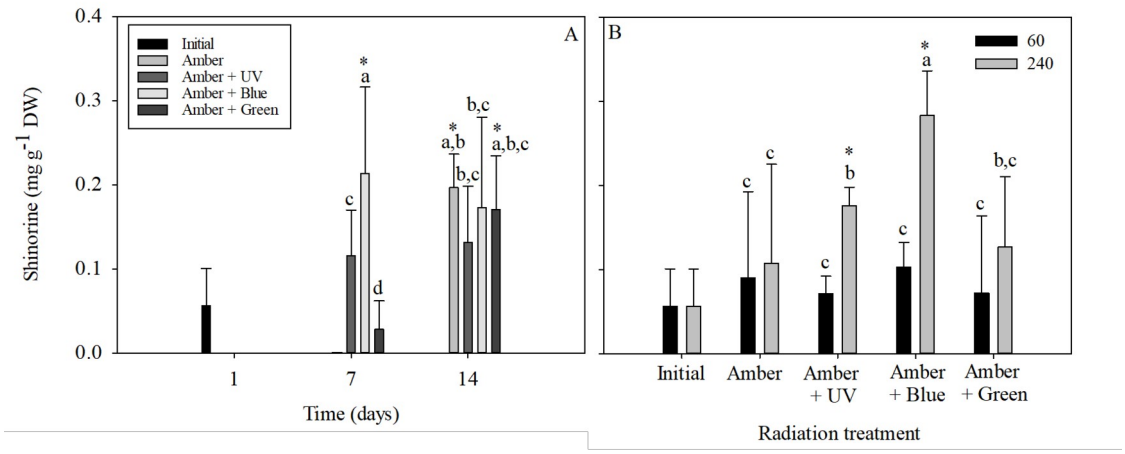

A, shinorine levels resulted from the interaction between radiation and time, and B, shinorine levels resulted from the interaction between radiation and nitrate concentration. Different letters indicate significant differences among the treatments. * indicates significant difference from the initial samples using T-student test.

3.10 DISCUSSION

In this paper, an innovative experimental design was chosen to evaluate the influence of radiation treatments and nutrient concentration on *Plocamium cartilagineum* thalli during 2 weeks. Our study employed the use of Aralab bioclimatic rooms which allows the simulation of an entire daily cycle pattern in an automated system. This methodology helps to elucidate how algae develop acclimation mechanisms in order to survive to different environmental changes throughout the day, including photomorphogenic responses. Furthermore, the automated systems facilitate the execution of longer experiments with controlled conditions. The dial mechanism allows the algae to receive gradually irradiances along the day period. Then, acclimation procedures associated to gradual light increment and decrease can be properly considered here.

Most studies about the influence of daily cycle variations comprise field studies under solar radiation (FIGUEROA et al., 2003; FLORES-MOYA et al., 1999; HADER et al., 1996). Although some of these studies are performed during a longer period, the measurements require a complex infrastructure and are subject to adverse conditions such as the presence of clouds and heatwaves for example. Another important fact is that as the sun emits a broad spectrum of radiation, it would be impossible to fully comprehend the action of specific photoreceptors. That is the reason we chose to use Amber as photosynthetic radiation,

the same strategy used by other authors (CASTRO-VARELA et al., 2021; GHEDIFA et al., 2021; SCHNEIDER et al., 2022; THOMAS; DICKINSON, 1979).

Considering the complementary radiation, UV-A, blue and green, it is estimated that low fluences varying from 1 to 20 μmol photons m^{-2} s^{-1} are enough to activate photoreceptors (LÓPEZ-FIGUEROA, 1991; PETROUTSOS et al., 2016; RÜDIGER; LÓPEZ-FIGUEROA, 1992). Although some variability was noticed on photosynthetic parameters, we did not observe huge differences on them, as previously planned in the experimental design. This fact was planned in order to maintain photosynthesis rate, using Amber as photosynthetic radiation, and on the other hand to stimulate the action of photomorphogenic photoreceptors by adding the complementary radiation (SCHNEIDER et al., 2020b) to stimulated genes mediated by a cAMP in transduction chain (SEGOVIA et al., 2001; SEGOVIA; GORDILLO; FIGUEROA, 2003). The absence of significant differences on F_v/F_m values indicates that *P. cartilagineum* did not suffer photoinhibition by the treatment's exposition.

Regarding pigment content, UV and blue were the most efficient radiation to stimulate chlorophyll production at the first week of experiment, meanwhile, at the second week, just a higher nitrate concentration affected positively the pigment concentration. López-Figueroa and Niell (1990), studying *Ulva rigida*, *Corallina elongata*, *Plocamium cartilagineum* and *Porphyra umbilicalis* evidenced that continuous blue light exposition during 6 hours stimulated chlorophyll *a* synthesis. On the other hand, green and red lights were more efficient to stimulate phycoerythrin and phycocyanin respectively in the red algae studied. Ben Ghedifa et al. (2021) reported that green light stimulated both R-phycoerythrin and soluble proteins in the red alga *Gracilaria gracilis*. Thus, green light stimulated phycoerythrin a pigment with maximal absorption in green light (565 nm). However, in our study PE accumulation of *P. cartilagineum* was no stimulated by green light. It is noted that PE has other additional peak at 498 nm close to blue region of the spectra. We hypothesize that chlorophyll a and PE content regulation in *P. cartilagineum* is mainly determined by a Blue-receptor and indicates an ecological adaptation considering that in clear waters blue predominates with depth increasing. A high nitrogen availability may also result in the increase of phycobiliproteins and total proteins of the species, as found in our study. Previous studies already showed nitrogen regulation of biliprotein contents, such as López-Figueroa et al. (2010) Navarro et al. (2014a) and Yu et al. (2022).The increase of pigments by B light has related to the stimulation of nitrogen metabolism , both nitrate uptake and nitrate reduction by

nitrate reductase activity (FIGUEROA et al., 1995; FIGUEROA, 1996; LÓPEZ-FIGUEROA; RÜDIGER, 1991).

Many field studies and laboratory experiments, using constantly photoperiods, try to comprehend how the production of MAAs is affected by radiation and nutrient availability (BONOMI BARUFI et al., 2012; FIGUEROA et al., 2003; KORBEE; FIGUEROA; AGUILERA, 2005; SCHNEIDER et al., 2020b). The production of MAAs using systems able to simulate a fully daily cycle in laboratory still scarce. The Aralab bioclimatic room utilized in our manuscript allow a proper management of light quality and quantity along the photoperiod and this can be a good strategy for modulating responses regulated at short time (hours, for example). It is a great advantage provided by dial light regulation, and the strategy showed to be very useful with different responses found according to variation of irradiances.

The experiment indicated that the treatment Amber + Blue and Amber + UV-A radiations, associated with a high nitrate availability, enhanced the production of MAAs in *P. cartilagineum*. Korbee et al. (2005), studying *Porphyra leucosticta* under blue and white treatments, with a high source of nitrogen, also observed an increase in MAAs production. Studies indicate that blue radiation irradiation promotes nitrate incorporation, as well as stimulation of nitrate reductase and glutamine synthetase activities (HADER et al., 1996). Nitrate assimilation was incremented by blue and also by green complementary irradiances, when *P. cartilagineum* received more nutritional apport. However, this pattern was not evident when lower amount of N was available. Then, it is possible that stimulation of nitrate assimilation in *P. cartilagineum* is light-controlled only when more quantity of nutrient is available. Nutrient assimilation can be regulated by nutrient availability coupled to radiation quality, mainly through blue light photoreceptor (Cryptochromes). Additionally, UV and blue radiation have been reported by stimulating the action of photoreceptors by increasing total MAAs levels and the proportion of specific MAAs (KORBEE et al., 2004; KORBEE; FIGUEROA; AGUILERA, 2005; SCHNEIDER et al., 2020a).

An interesting achievement was the increasing of shinorine levels mainly in the 7th day under UV-A and Blue treatments. Krabs et al. (2004) suggests the action of one or two UV-A photoreceptors in the red alga *Chondrus crispus* modulating the production of shinorine in this species. They also noticed the same effect using blue light, a fact that may be correlated to the photoregulation of pterin synthesis, a chromophore presented in the UV-A/Blue photoreceptors.

The decrease of total MAA content after 14 days have already reported by other authors (ÁLVAREZ-GÓMEZ; KORBEE; FIGUEROA, 2019; NAVARRO et al., 2016). This decrease could be due to the photodegradation by UV long term exposure. However, analyzing the variation in MAA composition, it can be observed that certain MAAs decreased whereas other MAAs increased. In this study Shinorine is maintained high after 14 days under high nitrogen level, thus the nitrate is crucial to maintain high level of MAAs. Probably in the interconversion of MAAs in the pathway certain MAAs are favored under high nitrogen level compared to others. Interestingly, Navarro et al. (2014a) observed that during an ozone hole episode in sub Antarctic area in Chile i.e. increased UVB radiation that UVA absorbing MAAs as shinorine and palythine maintained similar level than that before ozone depletion whereas mycosporine-glycine an UVB absorbing MAA increased. Thus the proportion of different MAAs can change in the short term (hours and days) influenced by both UV radiation and nitrate availability (NAVARRO et al., 2014a, 2014b).

In conclusion, Blue and UV radiations coupled with higher availability of nitrogen showed to be relevant for regulating bioactive compounds of *P. cartilagineum*, mainly after 7 days. Thus, at biotechnological point of view, the harvest to extract bioactive compounds is more favorable at day 7 than that at day 14. This can have advantageous since it is possible to increase bioactive compounds production in the short term. MAAs and phycobiliproteins were significantly incremented with complementary radiation, indicating that photoreceptors-like cryptochromes can be acting in the photoregulation of the species metabolism. This is properly very relevant considering biotechnological approaches for eliciting compounds with valuable relevance for industrial perspective specially for cosmeceutical applications to design more environmentally and healthy friendly sunscreen (ROSIC et al., 2023; VEGA et al., 2021) , although cultivation of *Plocamium spp*. is still a great challenge to be achieved.

Acknowledgments

The authors thanks Pablo Castro Varela, Víctor Robles Carnero and María Girón Tena for the technical assistance to obtain biological material for experiments.

Funding

This work was supported by Coordenação de Aperfeiçoamento de Pessoal de Nível Superior – Brasil (CAPES) [grant numbers 88882.438333/2019-01] and the internalization

program CAPES-PRINT [grant numbers 88887.578926/2020-00]. The project was also supported by Junta de Andalucía, the projects (1) FACCO- UMA18-FEDER JA-162 and (2) NAZCA- PY20-00458-FR.

4 CAPÍTULO 4

Manuscript containing preliminary results. After completing experimental approaches, the manuscript will be submitted to the journal "*Carbohydrate Polymers"*.

Sulfated polysaccharide from *Plocamium cartilagineum*: its role on health and tumor cell toxicity

Bruna Rodrigues Moreira[1*], Pablo Castro Varela[2], Roberto Abdala Díaz[2], Marcelo Maraschin[3], José Bonomi-Barufi[1], Félix López Figueroa[2]

[1]Laboratório de Ficologia, Departamento de Botânica, Universidade Federal de Santa Catarina, Florianópolis 88049-900, SC, Brazil; *bruna.rm01@gmail.com (B.R.M.) – corresponding author; jose.bonomi@ufsc.br

[2]Universidad de Málaga, Instituto Andaluz de Biotecnología y Desarrollo Azul (IBYDA), Departamento de Ecología, Campus Universitario de Teatinos s/n - Centro Experimental Grice Hutchinson, Lomas de San Julián 2, 29004 Málaga, España; felixlfigueroa@uma.es, pablo.castro@uma.es, abdala@uma.es

[3]Laboratório de Morfogênese e Bioquímica Vegetal, Centro de Ciências Agrárias, Universidade Federal de Santa Catarina, 88034-000, Florianópolis, Brazil; mtocsy@gmail.com

4.1 ABSTRACT

Cancer is one of the major causes of death around the world. Furthermore, the standard treatments for the disease reduce life quality of the patients causing a lot of side effects. For these reasons, the search for new treatments that are effective and less aggressive for cancer are needed. Sulphated algae polysaccharides (SP) have been highlighted in this field due to their chemical composition and the promising cytotoxic effects, presenting high selectivity for cancer cells instead of health cells. In this study, we extracted and chemically characterized the sulphated polysaccharide from *Plocamium cartilagineum*. The possible cytotoxic effect of SP was assessed on two health cell lines and three cancer cell lines, and the selectivity index was presented. Gas-mass chromatography indicated that the SP extracted is composed mainly by the monosaccharide galactose. Elementary analysis and Fourier transform infrared evidenced the presence of sulphate groups on the polysaccharide. The SP from *P. cartilagineum* exhibited a high cytotoxicity on leukemia cells (inhibitory concentration = 0.15 ± 0.02 mg mL^{-1}), and also low cytotoxicity in the health cells, resulting in a high selectivity index. This index indicates that the SP is more selective to cancer cells than for health cells. With these results we conclude that the SP from *P. cartilagineum* was characterized for the first time, and it is a good candidate as an alternative therapeutic agent to be considered to the following tests to the development of a new pharmaceutical product.

Keywords: red macroalgae, sulphated polysaccharide, anticancer, characterization

4.2 INTRODUCTION

Cancer is a worldwide problem that presents a high socioeconomic impact. According to International Agency for Research on Cancer, 19.3 million new cases and 10 million cancer deaths were reported worldwide in 2020 (SUNG et al., 2021). In general, cancer's treatment comprises to a combination of different techniques depending on the type of cancer, the site of tumor and patient characteristics, including surgery, chemotherapy, radiotherapy and immunotherapy. The main goal of all these treatments is to kill tumoral cells without affecting healthy cells, that means, a selective treatment. Although the currently therapies present certain efficiency, the selectiveness is still a great challenge, because the nowadays therapies cause a range of adverse effects on the patient. For this reason the search for alternative cancer treatments is extremely relevant (GUTIÉRREZ-RODRÍGUEZ et al., 2018; LEFRANC et al., 2019).

Marine algae are highlighted due to its high biodiversity and for being a rich source of biomolecules as for example vitamins, peptides, mycosporine-like amino acids, phenolic compounds and polysaccharides (APPELTANS et al., 2012; JIN et al., 2022). It is estimated that in 2018, around $ 10.5 billion was associated to drugs derived from marine sources around the world (RENGASAMY et al., 2020). Among those potential molecules, polysaccharides, mainly sulphated polysaccharides (SP), present a potential to be used as anticancer molecules. Their bioactivities depend directly on their monosaccharide composition, molecular weight and degree of sulfation (CUNHA; GRENHA, 2016).

Rhodophytes are an important economic source of polysaccharides, including commercial agar and carrageenan (USOV, 2011). Many studies indicate the potential of these polysaccharides as anticancer agents through different action mechanisms. Kappa-carrageenan isolated from *Hypnea musciformis* presents anti-proliferative effects on MCF-7 (Human breast cancer) and SH-SY5Y (Human neuroblastoma) cancer cell-lines but not against 3T3 (mouse fibroblast cell-line) (SOUZA et al., 2018). Castro-Varela et al. (CASTRO-VARELA et al., 2023) comparing neutral and acid (sulphated) polysaccharides extracted from *Sarcopeltis skottsbergii* concluded that the acid polysaccharide fraction was

more efficient than the neutral polysaccharides considering that acid fraction presented higher selective index, an index that indicates the preference to killing cancer cell lines rather than health cell lines. Commercial carrageenan (Sigma-Aldrich) and native carrageenan extracted from *Kappaphycus alvarezii* also present a good potential as anticancer agents against MCF-7 and HT-29 (human colon cancer) cell lines (SUGANYA et al., 2016). Porphyrans are also indicated as good candidates for anticancer activity (PRADHAN; ROUT; KI, 2023). The porphyran extracted from *Pyropia yezoensis* has shown cytotoxicity against HeLa (human cervical cancer cell line), Hep3B (human hepatic carcinoma cell line) and HL-7702 (Human normal liver cell line), exhibiting distinct inhibitory concentration (IC_{50}) levels depending on the molecular weight of the polysaccharide (HE et al., 2019).

Among red macroalgae group, *Plocamium* spp. are red macroalgae found in tropical and subtropical zones, and the species already investigated produces polysaccharides with interesting biological activities. Falshaw et al. (1999) extracted and characterized the SP from *Plocamium costatum,* mostly constituted by the monosaccharide galactan. Miller (1999) followed the characterization by defining the carbohydrate linkages using NRM analysis in the same species. Regarding the biological activities, Harden et al. (2009) describes the potential antiviral activity of SP extracted from *P. cartilagineum*, possible due to direct inactivation of the virus and by inhibiting virus attachment to cell surface. There is a lack of studies focusing in *P. cartilagineum* for entire structural characterization of its SP and anticancer activity. A study performed by Alves et al. (2016), indicated an antiproliferative effect of dichloromethane extract from *P. cartilagineum* against HEPG-2 cells, presenting an IC_{50} value around 1 mg mL^{-1}.

Considering all the facts mentioned before, the aim of this study was the chemical characterization of SP extracted from *P. cartilagineum*, and the evaluation the cytotoxic effect on healthy and tumoral cell lines.

4.3 MATERIALS AND METHODS

4.3.1 Algal material

Plocamium cartilagineum was collected at La Herradura Beach, situated in Granada, Spain (36°44'N, 3°45'W). The algae were kept in ice and transferred to the laboratory, where it was cleaned from epiphytes and debris. *P. cartilagineum* thalli were frozen at -80 °C during 24h and then lyophilized. Finally, the algae material was ground using a mixer until obtaining small particles.

4.3.2 Sulfated polysaccharide (SP) extraction and purification

The first step of the extraction corresponded to the removal of the pigments from the biomass. For the chlorophyll removal, 1g of lyophilized and milled *P. cartilagineum* was added to 30 mL of ethanol 80%, stirring during 1 hour. After this period of extraction, the mixture was centrifuged at 4000 rpm, 4 °C, during 10 minutes. The supernatant was discarded and the biomass submitted to the same process 3 times more until complete removal of chlorophyll. Phycobiliproteins were removed adding 30 mL of 0.1 phosphate buffer pH 6.5 to the biomass free of chlorophyll. The mixture was stirred during 10 minutes, followed by centrifugation at 4000 rpm, 4 °C, during 5 minutes. The supernatant was removed and the biomass precipitated submitted again to the same process. After pigment removal, the precipitated obtained was dissolved in 60 mL of distilled water and stirred during 1 hour under 90 °C. The mixture was centrifuged at 4000 rpm during 15 minutes. The supernatant was stored and the precipitated was submitted to the same process one more time to increase the efficiency of the process. At the end of the process both supernatants were mixed.

The selective precipitation of acid polysaccharides was performed adding 20 mL of 2% cetavlon for each 100 mL of supernatant. After precipitation, the polysaccharide was centrifuged at 4000 rpm during 20 minutes. The precipitate was dissolved in 6 ml of 4M sodium chloride solution, and posteriorly centrifuged at 4000 rpm during 15 minutes. The

process was repeated until the obtention of a white precipitate. Finally, to remove NaCl added to the polysaccharide extraction, the precipitated was dialyzed with ethanol absolute (1:1) overnight. After this period, the mixture was centrifuged at 4000 rpm during 15 minutes. Finally, it was added 2mL of ethanol absolute to the precipitate and frozen at -80 °C until further lyophilization.

4.3.3 Polysaccharide characterization

4.3.3.1 CHNS

Carbon, hydrogen, nitrogen and sulfur content was determined using the CNHS LECO-932 elemental analyzer (St. Joseph, MI, USA) in the Research Support Central Services (SCAI, University of Málaga, Málaga, Spain).

4.3.3.2 Gas chromatography-mass spectrometry (GC-MS)

To analyze the monosaccharide profile of the SP in GC-MS, the sample was previously treated with hydrolysis and derivatization. Briefly, 2 mg of the polysaccharide was added to 600 μL of HCl prepared in methanol 3N. The sample was heated during 24 h at 80 °C, and dried using a nitrogen gas flow at 50 °C (Stuart BlocK Heater, SBH200D/3). For derivatization the hydrolyzed sample was mixed with 300 μL of Trisil reactive (Pierce, Thermo), during 1 h at 80 °C. Following the sample was dried with the nitrogen gas flow, solubilized in 500 μL of hexane and centrifuged during 15 min. The supernatant was collected, dried and again solubilized in 150 μL of hexane.

GC/MS analysis was performed using a Trace GC gas chromatograph (Thermo Scientifics), Tri Plus autosampler and DSQ mass spectrometer quadrupole (Thermo Scientifics). For the analysis, 1 μL of the sample was injected in a chromatography column Zebrón ZB-5 (30 m x 0.25 mm ID x 0.25 μ df, Phenomenex). The temperature of the injector was 250 °C, with a gas flow equivalent to 1.2 mL/min. The initial temperature of the oven was set to 80 °C during 2 min, followed by gradient increasing of the temperature until reach 230 °C. Mass spectrometry (MS) analysis was performed using an ionization mode of electronic impact (EI) with 70 eV at 230 °C.

The results obtained were compared to monosaccharides standards and the National Institute of Standards and Technology (NIST 2014) library.

4.3.3.3 Fourier-Transform Infrared Spectroscopy (FTIR)

For FTIR analysis, the samples were prepared by mixing the polysaccharide and KBr (1% w/w) under a hydrostatic force of 15.0 tcm^{-2} for 3 minutes in a self-supporting pressed disks of 16 mm diameter. FTIR spectra of sulfated polysaccharide from *P. cartilagineum* was obtained using a Thermo Nicolet Avatar 360 IR spectrophotometer (Thermo Electron Inc., USA), scanning between 400 and 4000 cm^{-1}, with a resolution of 4 cm^{-1} and a DTGS (deuterated triglycine sulfate) detector. The data was analyzed using an OMNIC 7.2 software (bandwidth 50 cm^{-1}, enhancement factor 2.6).

4.3.4 Cell culture and maintenance

Cytotoxic effect of the polysaccharide was assessed against following 5 cell lines: HACAT - Immortalized human keratinocytes cell line (ATCC, USA), 1064SK - Normal human neonatal foreskin fibroblasts cell line (CIC-UGA, ES), HCT-116 - Human colon carcinoma cell line (ATCC, USA), U-937 - Human leukemia cell line (ATCC, USA) and G-361 - Human malignant melanoma cell line (ATCC, USA).

Before the cytotoxic evaluation, HACAT and G-361 were previously cultured using RPMI-1640 medium (BioWhittaker, ref. BE12-167F) supplemented with 10% fetal bovine serum (Biowest ref. S1810-500), 1% penicillin–streptomycin solution 100×, and 0.5% of amphotericin B. The cells 1064sk, U-937 and HCT-116 were previously cultured using Dulbecco's modified Eagle's medium (DMEM) (Capricorn Scientific, ref. DMEM-HPSTA) supplemented with 10% fetal bovine serum (Biowest, ref. S1810-500), 1% penicillin–streptomycin solution 100× (Capricorn Scientific, ref. PS-B), and 0.5% of amphotericin B (Biowest ref. L0009-100). The cells were kept under sub confluence at 37 °C in an incubator with controlled atmosphere supplied with 5% CO_2. Then, the cell cultivation was followed to maintain viable cells and ensure a sufficient quantity for performing the assays.

4.3.5 Cytotoxicity assay

The polysaccharide was previously prepared by mixing 5 mg of polysaccharide in 1 mL both on DMEM or RPMI culture medium, and incubated during at 37 °C during 30 minutes. After complete solubilization, the solution was diluted ranging from 0.009 to 5 mg mL^{-1}. The experiment was performed using 96-well plates, containing 10000 cell/well for 1064sk and 6000 cell/well to the other cell lines (HACAT, G-361, HCT-116 and U-937). The cells were incubated with the different polysaccharide concentrations during 72 hours in the atmosphere-controlled incubator, with 5% CO_2 at 37 °C. At the end of incubation period, 10 µL of the MTT solution (5 mg mL^{-1} in phosphate buffer) and 100 µL of culture medium was added to each well. The plates were incubated at 37 °C for 4 h, and finally 150 µL of 0.04 N HCl^{-2} propanol were added to solubilize formazan crystals. The absorbance was measured spectrophotometrically at 550 nm (Micro Plate Reader Synergy HTX, BIOTEK, USA). The results are expressed as half-maximal (50%) inhibitory concentration (IC_{50}), that corresponds to the amount of the compound required to inhibit 50% of viable cell number *in vitro* (ABDALA DÍAZ et al., 2019). The experiment was conducted in four replicates.

4.3.6 Selectivity Index

Selectivity index (SI) was calculated comparing the IC_{50} values obtained on the cytotoxic assay, according the following equation:

$$SI = \frac{IC_{50}\, health\, cells}{IC_{50}\, cancer\, cells}$$

4.3.7 Statistical analysis

IC_{50} values were expressed as mean ± standard deviation, using Statistic software.

4.3.8 Future analysis

The characterization results of the SP from *P. cartilagineum* exhibited in this manuscript are preliminary results. We want to improve the polysaccharide characterization

before submitting this manuscript to publication. Aiming to deep the knowledge about the SP obtained, we will perform two more replicates of each characterization analysis described before. Furthermore, an RMN of the polysaccharide will be performed as well as the determination of its molecular weight and sulphation degree.

4.4 RESULTS

4.4.1 Carbon, hydrogen, nitrogen and sulfur content (CHNS)

Table 10 presents the data of CHNS levels in the biomass and in the polysaccharide extracted from *P. cartilagineum*. Both biomass and polysaccharide showed a total of C higher than 20%. The algal biomass showed 4.6% of H, 4.3% of N and 3.1% of S. Meanwhile, polysaccharide was composed by 3.8% of H, 1.6%N and 3.3% of S.

Tabela 10. Descriptive amounts of total carbon, hydrogen, nitrogen, and sulfur content (%) in biomass and sulfated polysaccharide extracted from *P. cartilagineum*.

	Carbon	Hydrogen	Nitrogen	Sulfur
Biomass	28.2	4.6	4.3	3.1
Polysaccharide	25.9	3.8	1.6	3.3

Data was provided by only one replicate.

4.4.2 Gas chromatography-mass spectrometry (GC-MS)

Figure 33 exhibits the pattern of the monosaccharides identified in the *P. cartilagineum* polysaccharide using GC-MS technique. The mainly monosaccharide which composes the sulfated polysaccharide is galactose, corresponding to the peaks of 28.3, 29.1 and 29.3 minutes of retention. Using the area of the peaks, the percentage of all identified monosaccharides are presented in table 11. As mentioned before, galactose corresponds to the mainly monosaccharide of the sample (83.13%), followed by glucuronic acid (8.17%), glucose (3.12%) and xylose (2.18%). Rhamnose, ribose, mannose, fucose and arabinose were also identified in lower concentrations.

Figura 33. Gas chromatography-mass spectrometry (GC-MS) of sulfated polysaccharide extracted from *P. cartilagineum*

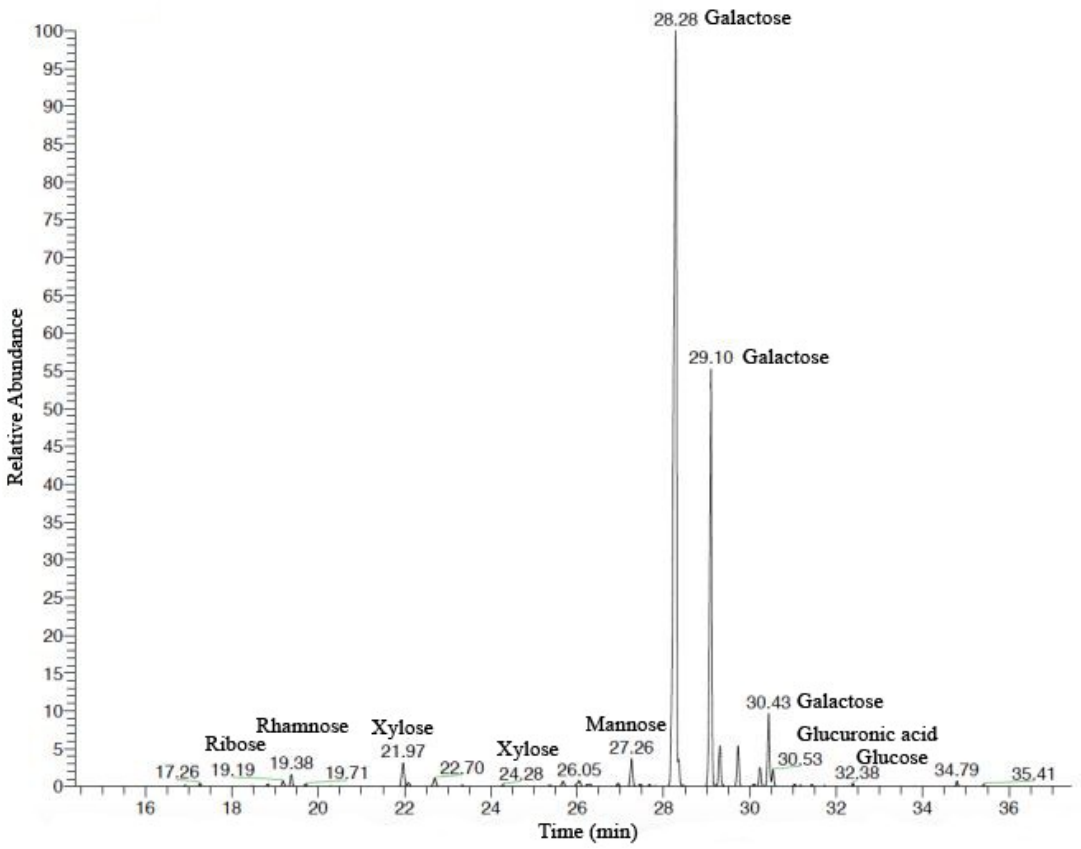

Tabela 11. Monosaccharide composition (%) of sulfated polysaccharide extracted from *Plocamium cartilagineum*.

Monosaccharide	**%**
Galactose	83.13
Glucuronic acid	8.17
Glucose	3.12
Xylose	2.18
Rhamnose	0.67
Ribose	0.40
Mannose	0.21
Fucose	0.06
Arabinose	0.06

4.4.3 Fourier-Transform Infrared Spectroscopy (FTIR)

Figure 34 exhibits the FTIR spectrum indicating distinct absorption bands characteristics of different functional groups. The broad bands observed around 3451 cm^{-1} and 2939 cm^{-1} corresponds respectively to the stretching vibration of hydroxyl (O–H) and alkyl (C–H) groups (CASTRO-VARELA et al., 2023; FALSHAW; FURNEAUX; MILLER, 1999). The sharp band observed around 1644 cm^{-1} correspond to carboxyl group ((C(=O) OH). Absorption bands around 1255 cm^{-1}, 1050 cm^{-1} and 849 cm^{-1} are all associated to the presence of sulphate groups, being respectively sulfate esters bonds (S=O), 3,6-anhydrogalactose (C–O) and a C–O–SO_4 bond in galactose C4 (SOUZA et al., 2018).

Figura 34. FTIR spectroscopy of the sulfated polysaccharide from *P. cartilagineum*

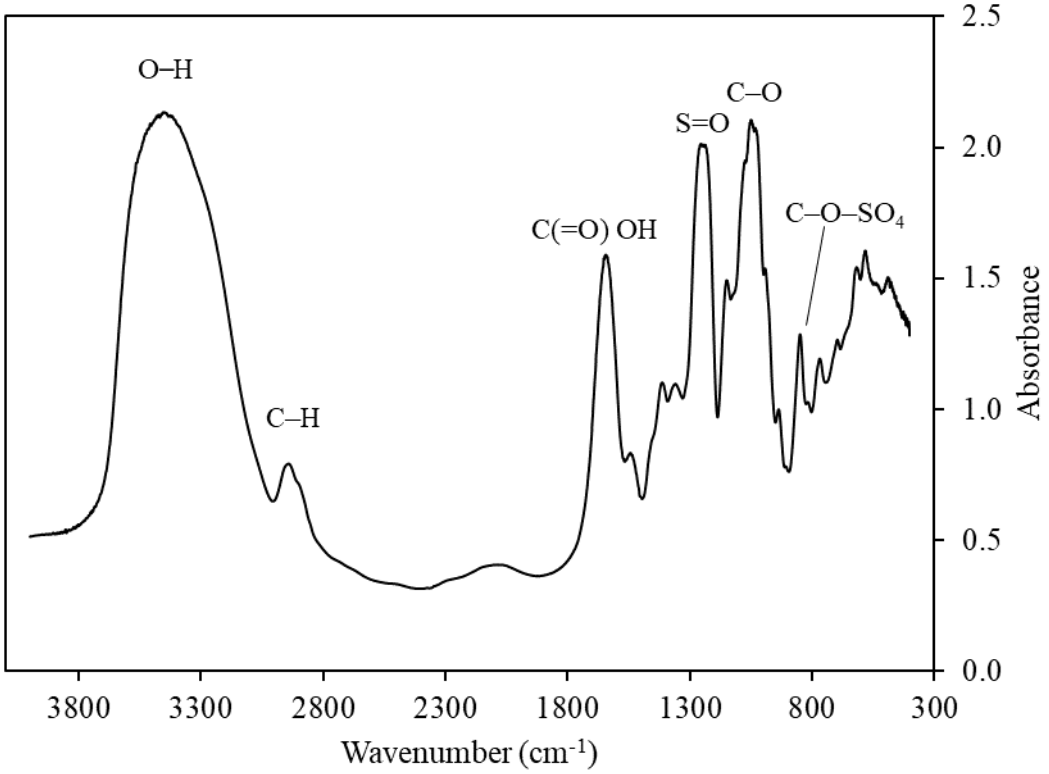

Letters over the peaks represents chemical bonds characteristics from each absorption band.

4.4.4 Cytotoxicity assay and Selectivity index

The cytotoxic activity caused by different concentrations of the polysaccharide (0.009 to 5 mg mL^{-1}) in healthy and tumoral cell lines is presented in Figure 35. Regarding healthy

cell lines, a higher IC_{50} was obtained for keratinocytes HACAT (2.37 ± 0.18 mg mL^{-1}) than for fibroblasts 1064sk (1.41 ± 0.49 mg mL^{-1}), both under 1 mg mL^{-1}. In tumoral cells it is possible to observe to distinct patterns. In G-361 and HCT-116, the polysaccharide did not exhibit a cytotoxic effect in the concentrations tested, therefore, it was not possible to determine IC_{50} on those cell lines. As the concentration of 5 mg mL^{-1} is high and the solubility of the polysaccharide is low, we chose not to try higher concentrations. On the other hand, the polysaccharide exhibited a significant cytotoxic effect on leukemia U-937 cell line in a dose-dependent manner, presenting an IC_{50} equivalent to 0.15 ± 0.02 mg mL^{-1}. As the SP was not cytotoxic for G-361 and HCT-116 the Selectivity index (SI) was calculated only for U-937 cells. Then, in the case of SI for HACAT/U-937, the value found was 15.8; by other side, the SI calculated for 1064sk/U-937 achieved the value of 9.41.

Figura 35. Inhibition (%) of cell survival submitted to different concentrations sulfated polysaccharide extracted from *P. cartilagineum*

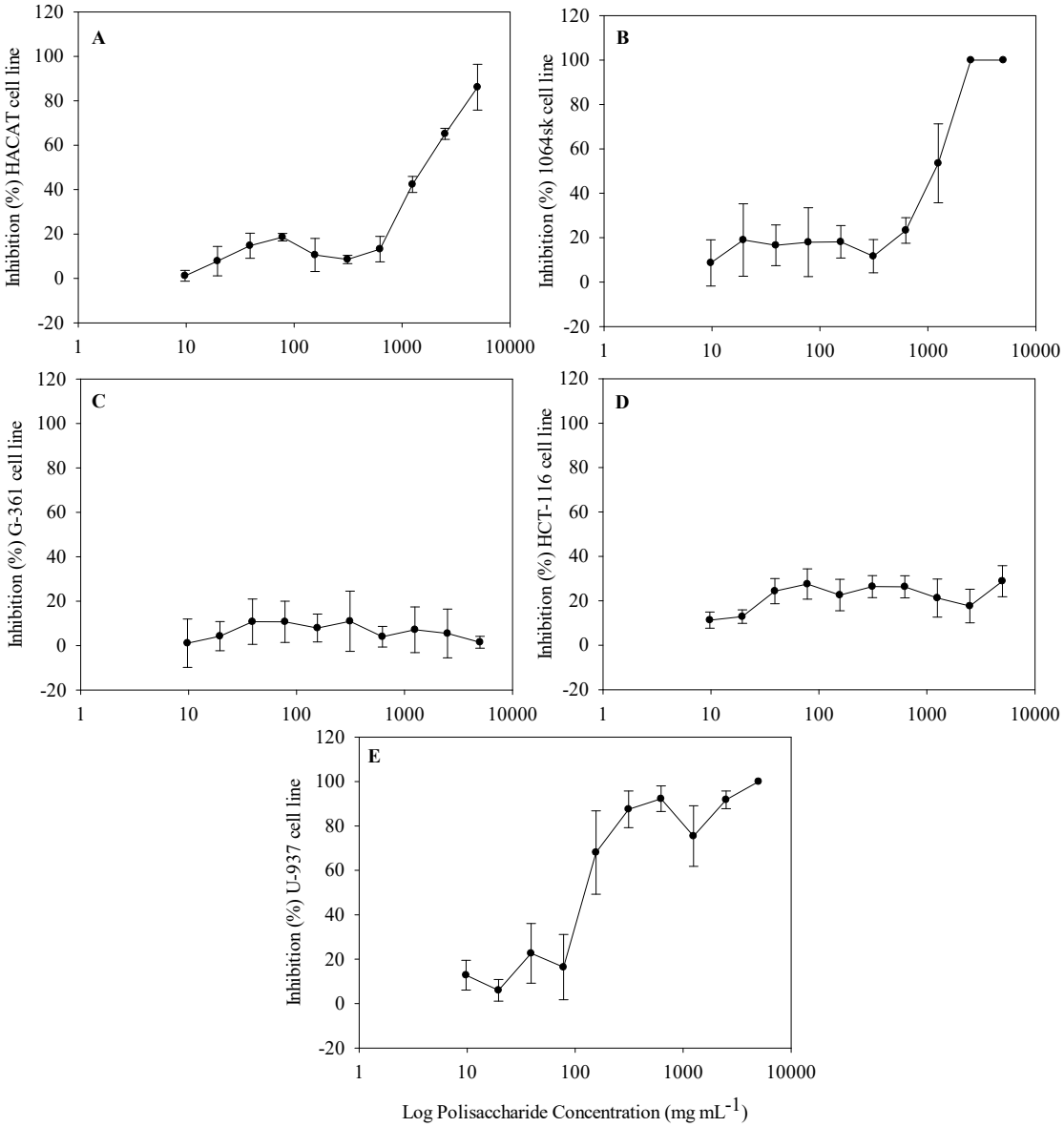

A- HACAT cell line, B- 1064sk cell line, C- G-361 cell line, D – HCT-116 cell line and E – U-937 cell line. The data are presented as mean ± SD (n=4).

4.5 DISCUSSION

Algal polysaccharides are very relevant for maintain algal structure and they are an interface between external and internal environments of algal cells, considering algal osmoregulation among other cellular strategies for algal survival. In this way, this manuscript characterized for the first time the SP of *Plocamium cartilagineum*, and also determined its cytotoxicity against human cell strains. Therefore, the perspective of biotechnological utilization of these SP can be highlighted as one of the most relevant contribution of this study.

Red macroalgae are an important source of polysaccharides, including carrageenans, agars, sulphated galactans, xylans, porphyran and floridean starch. The polysaccharide extracted in this study comprises to a sulphated galactan, as previously reported by Falshaw et. al (1999) and Miller (1999) in the specie *Plocamium costatum*. There was not found any publication describing the chemical structure of SP extracted from *P. cartilagineum*. SPs from *P. costatum* are constituted by 93% of galactose, 6% of xylose and 1% of 3,6-anhydrogalactose, fewer monosaccharides found in our study and presenting different proportions. *P. cartilagineum* showed a more heterogeneus and complex SP. As monosaccharide composition plays a fundamental role in biological activities, these differences detected may influence directly in the anticancer potential (HENTATI et al., 2020).

As mentioned before, the monosaccharides composition influence on biological activities, being the presence of uronic acid associated to a higher anticancer potential (JIN et al., 2017; MA et al., 2014). The degree of sulfation is another important chemical characteristic on the polysaccharides, and in general, the presence of sulphate groups enhances anticancer activity (TERUYA et al., 2007). A possible action mechanism for the anticancer potential of sulphate groups on tumor cells is the interaction between the sulphate groups and cationic proteins on cells surface (SHAO; CHEN; SUN, 2013)

As observed on the cytotoxic activity test, the survival of U-937 cells were strongly affected by the SP extracted from *P. cartilagineum*. Besides the cytotoxicity, the polysaccharide also showed to be selective, being toxic to the leukemia cell line (U-937) but not to the two healthy cell lines tested (HACAT and 1064sk). There is not a fully agreement about the best selectivity index, varying according to the authors. According to Peña-Morán et al. (2016), a compound has to present a selectivity index over to 10, to be considered as a

potential drug. On the other hand, Weerapreeyakul et al. (2012), consider a compound with an SI > 3 a high selective compound. Considering those facts, we consider the SP extracted from *P. cartilagineum* a selective compound to be consider as a promisor agent against leukemia U-937 cells.

Anticancer effect of polysaccharides may occur through different pathways. SP extracted from *Laurencia papillosa* induces a reduction on suppresses cell proliferation of MDA-MB-231 (human breast adenocarcinoma) cells by arresting cells to G1-phase and inducing apoptosis by inhibiting Blc-2 protein and enhancing the expression of Bax, resulting on the activation of caspase-3 pathway (MURAD et al., 2016). Fractioned κ-Carrageenan, a sulphated galactan, from *Kappaphycus alvarezii* may acting inducing mitochondrial-mediated apoptotic pathway in HCT-116 cells, upregulating caspase 3 and downregulating XIAP (RAMAN; DOBLE, 2015). Lajili et al. (2018) evidenced the cytotoxic effect of the SP extracted from *Laurencia obtuse* in monocytic leukemia cells (THP-1). The authors evidenced that the polysaccharide is able to induce the cells to enter in apoptosis. Furthermore, the SP also presented in vitro and in vivo antioxidant capacity, another protection mechanism against cancer. Besides the pharmacological approach, SPs can also be used as a nutraceutical compounds included in functional foods or supplements, in order to reduce tumor occurrence in humans (XU; HUANG; CHEONG, 2017).

5 DISCUSSÃO GERAL

Macroalgas são consideradas fontes promissoras de moléculas com atividades biológicas muito interessantes. A indústria de um modo geral está em constante busca por moléculas de origem natural que apresentem o mesmo ou melhor desempenho que compostos de origem sintética. No **capítulo I** deste trabalho, 14 extratos (aquosos e hidroetanólicos) de macroalgas vermelhas foram avaliados em relação à sua composição bioquímica e possíveis atividades antioxidante, fotoprotetora e de inibição da enzima colagenase. Neste último caso, relacionadas a um potencial antienvelhecimento.

Os espectros de absorção são ferramentas muito úteis para conhecer alguns padrões de compostos observados nas amostras. Os picos acentuados na região UV observados nas espécies *P. acanthophora* e *P. linearis* são indicativos de concentrações mais elevadas de MAAs (ÁLVAREZ-GÓMEZ; KORBEE; FIGUEROA, 2016), enquanto que os padrões observados na região visível das espécies *P. linearis*, *G. cornea* e *P. cartilagineum* são característicos das ficobiliproteínas.

Dentre as algas utilizadas, *P. acanthophora* e *P. linearis* foram as que mais se destacaram em relação a quantidade de compostos fenólicos e aminoácidos tipo micosporinas. Uma descoberta interessante foi a detecção das estruturas químicas correspondentes aos MAAs micosporina-glutamina, micosporina-2-glycina, palitina-serina e aplisiapalitina B. Mais análises químicas são necessárias para a confirmação da identificação de cada uma destas moléculas, pois estes MAAs não são normalmente descritos em espécies de macroalgas, sendo alguns deles citados somente uma vez na literatura em macroalgas (ORFANOUDAKI et al., 2019).

A análise de correlação de Pearson e a análise de componentes principais demonstraram uma forte correlação do conteúdo de compostos fenólicos e MAAs com o potencial para inibição da enzima colagenase. Vários estudos indicam o potencial inibitório de polifenóis ou extratos ricos em polifenóis em metaloproteinases (LOO et al., 2023; WEI et al., 2022; WITTENAUER et al., 2015), porém pouco se discute sobre o papel desempenhado por MAAs nesta atividade. Hartmann et al. (2015), através de simulações *in sílico* determinaram que atividade a anticolagenase de MAAs pode ocorrer por interações dos aminoácidos com a região P1′–P3′ do sítio catalítico da colagenase.

Os extratos aquosos, por apresentarem em geral melhores resultados bioquímicos do que os extratos hidroetanólicos e menor toxicidade, foram escolhidos para serem incorporados em uma formulação cosmética. A baixa toxicidade foi confirmada nos ensaios celulares com fibroblastos e queratinócitos. A adição dos extratos aquosos de *P. linearis* e *P. acanthophora* à formulação promoveu um aumento significativo nos fatores de proteção biológica quando comparados a formulação controle sem filtros físicos, indicando o potencial protetor destas formulações. O conjunto de atividades biológicas, capacidade antioxidante, inibição de colagenase e melhoria nos fatores de proteção biológica, faz com que os extratos de *P. linearis* e *P. acanthophora* se destaquem em relação a um potencial antienvelhecimento.

No **capítulo II** desta tese, foi realizado um experimento de campo para a avaliação dos mecanismos de fotoaclimatação de *P. cartilagineum*, observando-se talos de algas localizados em diferentes rochas, que estavam expostas a diferentes quantidades e qualidades de radiação. O experimento consistiu na análise de distintos fatores ao longo de um ciclo diário e durante este período foram avaliados os parâmetros fotossintetizantes e coletadas amostras para posterior análises bioquímicas.

Foram observados diferentes padrões das radiações PAR, UV-A e UV-B nos locais escolhidos, sendo os locais #3 e #4 os que apresentaram maiores valores de irradiância integrada. Outro ponto importante é que embora tenha sido observado um padrão lumínico semelhante nestes dois locais, o local #3 estava exposto a uma maior dose de UV-A que o local #4. Considerando os parâmetros fotossintetizantes, foi observada uma flutuação nos valores de ETR *in situ* durante o dia, fato correlacionado estatisticamente com as variações de luminosidade. Além disso o experimento de curva de luz, utilizando talos coletados nos locais #1 e #4, evidenciaram uma possível fotoinibição nos talos coletados no local #1 durante a exposição à maior intensidade luminosa. Este fato pode estar associado a um mecanismo de fotoaclimatação visto que o local #1 está situado em um local de sombra durante parte do dia e menores intensidades de PAR e UV-A.

Neste experimento foi observado que as algas situadas em locais com maior exposição solar apresentaram menores concentrações de pigmentos acessórios (clorofila e ficoeritrina). Este fato é considerado um mecanismo de fotoproteção visando reduzir a captação de luz e os danos causados pelo excesso de radiação (HÄDER; FIGUEROA, 1997). Também foi notada uma leve variação no conteúdo destes pigmentos ao longo do dia. Autores descrevem este fato também como um mecanismo fotoprotetor aonde ocorre uma regulação negativa da produção de pigmentos nos momentos de maior incidência solar (FLORES-

MOYA et al., 1998; LÓPEZ-FIGUEROA, 1991). Esta modulação é associada a modulação de fotorreceptores que percebem as variações no padrão de luminosidade, principalmente ao amanhecer e ao entardecer, controlando a produção de pigmentos ao longo do dia (HEGEMANN; FUHRMANN; KATERIYA, 2001; KIANIANMOMENI; HALLMANN, 2014).

Outro mecanismo de fotoproteção desenvolvido pelas algas, principalmente por algas vermelhas, é a produção de compostos que absorvam radiação UV, como por exemplo, aminoácidos tipo micosporinas (VEGA et al., 2020b). De um modo geral, a produção destes compostos depende tanto da quantidade como da qualidade de luz, bem como a disponibilidade de nitrogênio no meio em que se encontram (KORBEE; FIGUEROA; AGUILERA, 2005). Neste estudo, não foi observada uma correlação significativa entre a intensidade de PAR com a produção de MAAs. Em contrapartida a produção de MAAs está diretamente associada a intensidade de radiação UV-A presente no ambiente, não sendo verificado um padrão claro de variação destes compostos ao longo do dia. Resultados semelhantes foram obtidos por FIGUEROA et al. (2003), evidenciando a diferença na produção de MAAs em espécies de *Porphyra* situadas em locais com diferentes quantidades de irradiância.

Em resumo, foram observados diferentes mecanismos de fotoaclimatação desenvolvidos por *P. cartilagineum* associados a diferentes doses de PAR e UV-A. Estes mecanismos incluem modulação de parâmetros fotossintéticos, produção de pigmentos acessórios e compostos que absorvem radiação UV.

No **capítulo III** são apresentados os resultados obtidos em um experimento em laboratório realizado afim de se analisar possíveis modulações de fotorreceptores em *P. cartilagineum*. No estudo, a alga foi submetida a diferentes radiações e concentrações de nutrientes durante 14 dias. Durante o experimento foram acompanhados parâmetros fotossintetizantes e bioquímicos, a fim de se avaliar alterações decorrentes das condições experimentais.

O desenho do experimento utilizado para avaliar os parâmetros mencionados anteriormente foi idealizado a fim de se estimular a ação de fotorreceptores sem influenciar parâmetros fotossintéticos. Este fato foi realizado por meio da incubação das algas em luz âmbar em uma irradiância pré-determinada com valores próximos a irradiância de saturação da alga, associados a pequenas doses de radiações monocromáticas complementares, como proposto por outros autores (PAGELS et al., 2020; SCHNEIDER et al., 2020a, 2022).

A assimilação de nitrato por talos de *P. cartilagineum* foi estimulada pelas radiações complementares azul e verde, possivelmente associado a modulação da atividade da enzima nitrato redutase e glutamina sintetase, resultando em um possível aumento da síntese de aminoácidos e pigmentos acessórios (HADER et al., 1996).

Em relação aos pigmentos fotossintetizantes, na primeira semana de experimento evidenciou-se que as radiações UV e azul foram as mais eficientes para estimular a produção de clorofila *a* enquanto que a síntese da ficoeritrina foi estimulada também por estas duas radiações, associadas a uma maior disponibilidade de nitrato. Um estudo de López-Figueroa & Niell (1990) evidenciou o efeito positivo da luz azul na produção de clorofila *a* e luz verde e vermelha na síntese de ficoeritrina e ficocianina, respectivamente.

O mesmo padrão foi observado para a produção dos MAAs, sendo a produção destes influenciada positivamente pelas radiações azul e UV e alta concentração de nitrogênio, na primeira semana. A quantificação do MAA shinorina também evidenciou uma maior eficiência da radiação azul na primeira semana em estimular a síntese deste MAA. Korbee e colaboradores (2004) também observaram o papel da luz azul, bem como da luz branca, associada a elevadas fontes de nitrogênio, na estimulação da síntese de MAAs. Krabs e colaboradores (2004) sugerem a ação de fotorreceptores de luz azul na alga *Condrus crispus* modulando a síntese de shinorina.

Como pontos principais deste trabalho destacam-se o desenho inovativo utilizado, com o incremento gradual da radiação simulando o padrão lumínico de um ciclo diário. Além disso, as radiações UV-A e azul, associadas a uma maior concentração de nitrato, foram as mais eficientes para estimular a produção de compostos em *P. cartilagineum.*

O **capítulo IV** apresenta a caracterização química e a atividade citotóxica *in vitro* do polissacarídeo sulfatado extraído de *P. cartilagineum*. Os dados apresentados neste trabalho correspondem a resultados parciais e que serão complementados posteriormente com análises químicas de determinação do peso molecular, grau de sulfatação e ressonância magnética nuclear.

Tanto a análise de componentes elementar quanto os dados de FTIR comprovam a extração de polissacarídeos que contem em sua composição enxofre, associados a grupos sulfatados. A análise de GC-MS evidenciou os monossacarídeos presentes na amostra, indicando que o polissacarídeo extraído é composto majoritariamente por galactose, sendo este portando uma galactana sulfatada. Além de galactose foram detectadas maiores quantidades de ácido glucurônico, glicose e xilose. A composição de monossacarídeos e o

grau de sulfatação são considerados fatores determinantes na atividade biológica da molécula, sendo que de um modo geral, um maior grau de sulfatação e a presença de ácido urônico em sua estrutura, potencializa sua atividade antitumoral (CASTRO-VARELA et al., 2023; CUNHA; GRENHA, 2016).

A busca constante por novos agentes antitumorais que causem menos efeitos colaterais que os tratamentos convencionais é de suma importância para a indústria farmacêutica. O polissacarídeo extraído de *P. cartilagineum* demonstrou alta toxicidade para células de leucemia humana (U-937). Ao mesmo tempo, o polissacarídeo testado não apresentou toxicidade celular em células saudáveis de tecido epitelial (1064sK e HACAT), apresentando altos índices de seletividade em relação a estas células.

6 CONCLUSÕES GERAIS

No **Capítulo I,** os extratos aquosos se destacaram em relação aos extratos hidroetanólicos, além de serem considerados menos tóxicos. As algas *P. acanthophora* e *P. linearis* foram as que mais se destacaram em relação a seu conteúdo de MAAs e compostos fenólicos nos extratos, sendo estes fortemente correlacionados a atividade inibitória da enzima colagenase. Além disso a adição dos extratos aquosos destas duas algas melhorou a capacidade protetora das formulações em relação aos efeitos biológicos de proteção, sendo ótimas candidatas ao desenvolvimento de produtos antienvelhecimento.

Os **Capítulos II e III** evidenciaram mecanismos de fotoaclimatação desenvolvidos pela espécie *P. cartilagineum* em diferentes condições, sendo estas analisadas em condições ambientais naturais e em laboratório, respectivamente. No capítulo II, observou-se que espécies expostas a maiores irradiâncias de PAR e UV-A apresentam menor quantidade de pigmentos fotossintetizantes e maior acúmulo de compostos que absorvem UV, como os MAAs. Diferenças nos parâmetros fotossintetizantes também foram observados nos talos situados em diferentes locais. Em contrapartida apenas algumas significativas foram alterações foram observadas ao longo do ciclo diário. No capítulo III, a adição de luzes complementares não afetou significativamente os parâmetros fotossintéticos, que se mantiveram estáveis durante as duas semanas, com pequenas exceções. As radiações azul e verde estimularam a incorporação de nitrato na segunda semana do experimento, enquanto que em geral, as radiações UV e azul foram as mais eficientes para estimular a produção de compostos, associadas a concentração de mais alta de nitrato.

No **Capítulo IV,** a caracterização química evidenciou que o polissacarídeo extraído de *P. cartilagineum* é um polissacarídeo sulfatado composto majoritariamente por galactose, contendo também quantidades significativas de ácido glucurônico, glicose e xilose. O polissacarídeo de *P. cartilagineum* apresentou alto índice de seletividade, apresentando elevada toxicidade celular para células de leucemia humana e baixa toxicidade celular para células saudáveis de tecido epitelial.

Em resumo, foi possível concluir que as macroalgas vermelhas são fontes promissoras de moléculas com diferentes atividades biológicas, enfatizando a capacidade de

reagir frente à colagenase e às células tumorais. Os estudos realizados nesta tese destacaram este potencial com a extração de moléculas com capacidade antioxidante, potencial fotoprotetor, potencial para inibição de enzimas e atividade antitumoral, indicando que estas moléculas podem ser exploradas biotecnologicamente para o desenvolvimento de produtos em vários segmentos da indústria. Conhecer os parâmetros ecofisiológicos é interessante pois ajuda a compreender mecanismos de fotoaclimatação destas algas em ambientes naturais, auxiliando na transferência do conhecimento para o cultivo em laboratório, visando estimular a produção das moléculas de interesse e aumentar a escala de produção destas algas.

7 REFERÊNCIAS

ABDALA-DÍAZ, R. T. et al. Daily and seasonal variations of optimum quantum yield and phenolic compounds in Cystoseira tamariscifolia (Phaeophyta). **Marine Biology**, v. 148, n. 3, p. 459–465, jan. 2006.

ABDALA DÍAZ, R. T. et al. Immunomodulatory and Antioxidant Activities of Sulfated Polysaccharides from Laminaria ochroleuca, Porphyra umbilicalis, and Gelidium corneum. **Marine Biotechnology**, v. 21, n. 4, p. 577–587, 15 ago. 2019.

ABDO, J. M.; SOPKO, N. A.; MILNER, S. M. The applied anatomy of human skin: A model for regeneration. **Wound Medicine**, v. 28, p. 100179, 1 mar. 2020.

ABDULRAHMAN, R. M. The effects of light on vitamin D level in human serum during laboratory processing. **Journal of King Saud University**, v. 35, p. 102602, 2023.

AGUILERA, J. et al. Light quality effect on photosynthesis and efficiency of carbon assimilation in the red alga Porphyra leucosticta. **Journal of Plant Physiology**, v. 157, n. 1, p. 86–92, 1 jul. 2000.

ALLORENT, G.; PETROUTSOS, D. Photoreceptor-dependent regulation of photoprotection. **Current Opinion in Plant Biology**, v. 37, p. 102–108, 1 jun. 2017.

ÁLVAREZ-GÓMEZ, F. et al. UV Photoprotection, Cytotoxicity and Immunology Capacity of Red Algae Extracts. **Molecules**, v. 24, p. 2–16, 2019.

ÁLVAREZ-GÓMEZ, F.; KORBEE, N.; FIGUEROA, F. L. Analysis of antioxidant capacity and bioactive compounds in marine macroalgal and lichenic extracts using different solvents and evaluation methods. **Ciencias marinas**, v. 42, n. 4, p. 271–288, 2016.

ÁLVAREZ-GÓMEZ, F.; KORBEE, N.; FIGUEROA, F. L. Effects of UV Radiation on Photosynthesis, Antioxidant Capacity and the Accumulation of Bioactive Compounds in Gracilariopsis longissima, Hydropuntia cornea and Halopithys incurva (Rhodophyta). **Journal of Phycology**, v. 55, n. 6, p. 1258–1273, 1 dez. 2019.

ALVES, C. et al. High cytotoxicity and anti-proliferative activity of algae extracts on an in vitro model of human hepatocellular carcinoma. **Springer Plus**, v. 5, p. 1339, 2016.

ANTONIOU, C. et al. Photoaging: Prevention and topical treatments. **American Journal of Clinical Dermatology**, v. 11, n. 2, p. 95–102, 26 ago. 2010.

APPELTANS, W. et al. Article The Magnitude of Global Marine Species Diversity. **Current Biology**, v. 22, p. 2189–2202, 2012.

ARISTEO PEÑA-MORÁN, O. et al. Cytotoxicity, Post-Treatment Recovery, and Selectivity Analysis of Naturally Occurring Podophyllotoxins from Bursera fagaroides var. fagaroides on Breast Cancer Cell Lines. **Molecules**, v. 21, p. 1–15, 2016.

ASHOKKUMAR, V. et al. Technological advances in the production of carotenoids and their applications-A critical review. **Bioresource Technology**, v. 367, p. 128215, 2023.

BARCELÓ-VILLALOBOS, M. et al. Production of Mycosporine-Like Amino Acids from Gracilaria vermiculophylla (Rhodophyta) Cultured Through One Year in an Integrated Multi-trophic Aquaculture (IMTA) System. **Marine Biotechnology**, v. 19, n. 3, p. 246–254, 1 jun. 2017.

BARROS, M. P. et al. Temporal mismatch between induction of superoxide dismutase and ascorbate peroxidase correlates with high H 2 O 2 concentration in seawater from clofibrate-treated red algae Kappaphycus alvarezii. **Archives of Biochemistry and Biophysics**, v. 420, p. 161–168, 2003.

BETANCOR, S. et al. Photosynthetic performance and photoprotection of Cystoseira humilis (Phaeophyceae) and Digenea simplex (Rhodophyceae) in an intertidal rock pool. **Aquatic Botany**, v. 121, p. 16–25, 1 fev. 2015.

BHATIA, S. et al. Immuno-modulation effect of sulphated polysaccharide (porphyran) from Porphyra vietnamensis. **International Journal of Biological Macromolecules**, v. 57, p. 50–56, 1 jun. 2013.

BONOMI BARUFI, J. et al. Nitrate reduces the negative effect of UV radiation on photosynthesis and pigmentation in Gracilaria tenuistipitata (Rhodophyta): the photoprotection role of mycosporine-like amino acids. **Phycologia**, v. 51, p. 636–648, 2012.

BONOMI BARUFI, J.; FIGUEROA, F. L.; PLASTINO, E. M. Effects of light quality on reproduction, growth and pigment content of Gracilaria birdiae (Rhodophyta: Gracilariales) ; Efectos de la calidad de luz en la reproducción, crecimiento y contenido pigmentario de Gracilaria birdiae (Rhodophyta: Gracilariales). v. 79, n. 1, p. 15–24, 2015.

BORTHWICK, H. A. et al. Action of Light on Lettuce-Seed Germination. **https://doi.org/10.1086/335817**, v. 115, n. 3, p. 205–225, mar. 1954.

BOTTALICO, A.; ALONGI, G.; PERRONE, C. Macroalgal diversity of Santa Cesarea-Castro (Salento Peninsula, southeastern Italy). **Anales del Jardin Botanico de Madrid**, v. 73, n. 2, 2016.

BRADFORD, M. M. A rapid and sensitive method for the quantitation of microgram quantities of protein utilizing the principle of protein-dye binding. **Analytical Biochemistry**, v. 72, n. 1–2, p. 248–254, 7 maio 1976.

BRIANI, B. et al. The influence of environmental features in the content of mycosporine-like amino acids in red marine algae along the Brazilian coast. **Journal of Phycology**, v. 54, n. 3, p. 380–390, 1 jun. 2018.

CARDONA, T.; SHAO, S.; NIXON, P. J. Enhancing photosynthesis in plants: the light reactions. **Essays in Biochemistry**, v. 62, p. 85–94, 2018.

CARMO, J. DE O. DOS S. **Tratamento tópico com friedelina acelera a cicatrização de feridas cutâneas em camundongos diabéticos e induz a atividade de fibroblastos in vitro**. [s.l.] Universidade Federal de Alagoas, 2019.

CARVALHO DE QUEIROZ, J. L. et al. Encapsulation techniques perfect the antioxidant action of carotenoids: A systematic review of how this effect is promoted. **Food Chemistry**, v. 385, 2022.

CASTRO-VARELA, P. et al. A sequential recovery extraction and biological activity of water-soluble sulfated polysaccharides from the polar red macroalgae Sarcopeltis skottsbergii. **Algal Research**, v. 73, p. 103160, 2023.

CASTRO-VARELA, P. A. et al. Photobiological Effects on Biochemical Composition in Porphyridium cruentum (Rhodophyta) with a Biotechnological Application. **Photochemistry and Photobiology**, v. 97, n. 5, p. 1032–1042, 1 set. 2021.

CHAVES-PEÑA, P. et al. Quantitative and Qualitative HPLC Analysis of Mycosporine-Like Amino Acids Extracted in Distilled Water for Cosmetical Uses in Four Rhodophyta. **Marine Drugs**, v. 18, n. 1, p. 27, 28 dez. 2019.

CHEN, H. et al. Extraction of sulfated agar from Gracilaria lemaneiformis using hydrogen peroxide-assisted enzymatic method. 2019.

CHEN, X. W. et al. Antioxidant activity of sulfated Porphyra yezoensis polysaccharides and their regulating effect on calcium oxalate crystal growth. **Materials Science and Engineering: C**, v. 128, p. 112338, 1 set. 2021.

CHIEN, A. L. et al. Effect of Age, Gender, and Sun Exposure on Ethnic Skin Photoaging: Evidence Gathered Using a New Photonumeric Scale. **Journal of the National Medical Association**, v. 110, n. 2, p. 176–181, 1 abr. 2018.

CHOI, D. Y. et al. Antioxidant properties of natural polyphenols and their therapeutic potentials for Alzheimer's disease. **Brain Research Bulletin**, v. 87, n. 2–3, p. 144–153, 10

fev. 2012.

CHOI, Y. H. et al. Mycosporine-Like Amino Acids Promote Wound Healing through Focal Adhesion Kinase (FAK) and Mitogen-Activated Protein Kinases (MAP Kinases) Signaling Pathway in Keratinocytes. **Marine drugs**, v. 13, n. 12, p. 7055–7066, 1 dez. 2015.

CHRAPUSTA, E. et al. **Mycosporine-Like Amino Acids: Potential health and beauty ingredients**. **Marine Drugs**, 2017.

CONDE-ÁLVAREZ, R. M. et al. Photosynthetic performance and pigment content in the aquatic liverwort Riella helicophylla under natural solar irradiance and solar irradiance without ultraviolet light. **Aquatic Botany**, v. 73, n. 1, p. 47–61, 1 maio 2002.

CONDE, F. R.; CHURIO, M. S.; PREVITALI, C. M. Experimental study of the excited-state properties and photostability of the mycosporine-like amino acid palythine in aqueous solution. **Photochemical and Photobiological Sciences**, v. 6, n. 6, p. 669–674, 1 jun. 2007.

CORTÉS, H. et al. Alterations in mental health and quality of life in patients with skin disorders: a narrative review. **International Journal of Dermatology**, 2021.

COTAS, J. et al. Seaweed Phenolics: From Extraction to Applications. **Marine Drugs**, v. 18, p. 384–411, 2020.

CRUZ, S.; SERÔDIO, J. Relationship of rapid light curves of variable fluorescence to photoacclimation and non-photochemical quenching in a benthic diatom. **Aquatic Botany**, v. 88, n. 3, p. 256–264, abr. 2008.

CUNHA, L.; GRENHA, A. Sulfated Seaweed Polysaccharides as Multifunctional Materials in Drug Delivery Applications. **Marine drugs**, v. 14, n. 3, p. 42, 2016.

DAGNINO-LEONE, J. et al. Phycobiliproteins: Structural aspects, functional characteristics, and biotechnological perspectives. **Computational and Structural Biotechnology Journal**, v. 20, p. 1506–1527, 1 jan. 2022.

DAVISON, I. R. **Environmental effects on algal photosynthensis**. **J. Phyc.**, 1991.

DE LA COBA, F. et al. Antioxidant activity of mycosporine-like amino acids isolated from three red macroalgae and one marine lichen. **Journal of Applied Phycology**, v. 21, n. 2, p. 161–169, 21 abr. 2009a.

DE LA COBA, F. et al. Prevention of the ultraviolet effects on clinical and histopathological changes, as well as the heat shock protein-70 expression in mouse skin by topical application of algal UV-absorbing compounds. **Journal of dermatological science**, v. 55, n. 3, p. 161–169, set. 2009b.

DE LA COBA, F. et al. UVA and UVB Photoprotective Capabilities of Topical Formulations

Containing Mycosporine-like Amino Acids (MAAs) through Different Biological Effective Protection Factors (BEPFs). **Marine Drugs**, v. 17, n. 1, p. 55, 14 jan. 2019.

DENG, W. et al. AODB: A comprehensive database for antioxidants including small molecules, peptides and proteins. **Food Chemistry**, v. 418, p. 135992, 30 ago. 2023.

DIEHL, N. et al. Stress metabolite pattern in the eulittoral red alga Pyropia plicata (Bangiales) in New Zealand – mycosporine-like amino acids and heterosides. **Journal of Experimental Marine Biology and Ecology**, v. 510, p. 23–30, 1 jan. 2019.

EILERS, P. H. C.; PEETERS, J. C. H. A model for the relationship between light intensity and the rate of photosynthesis in phytoplankton. **Ecological Modelling**, v. 42, n. 3–4, p. 199–215, 1 set. 1988.

FALSHAW, R.; FURNEAUX, R. H.; MILLER, I. J. The backbone structure of the sulfated galactan from Plocamium costatum (C. Agardh) Hook. f. et Harv. (Plocamiaceae, Rhodophyta). **Botanica Marina**, v. 42, n. 5, p. 431–435, 10 set. 1999.

FAYAD, S. et al. Simultaneous elastase-, hyaluronidase- and collagenase-capillary electrophoresis based assay. Application to evaluate the bioactivity of the red alga Jania rubens. **Analytica Chimica Acta**, v. 1020, p. 134–141, 22 ago. 2018.

FERRERO, L. et al. Importance of substrate roughness for in vitro sun protection Assessment. **International Journal of Cosmetic Science**, v. 29, n. 1, p. 59–59, 1 fev. 2007.

FIGUEROA, F. et al. Growth, pigment synthesis and nitrogen assimilation in the red alga Porphyra sp. (Bangiales, Rhodophyta) under blue and red light. **Scientia Marina**, 1995.

FIGUEROA, F. L. Effects of light quality on Nitrate reductase and Glutamine synthetase activities in the red alga Porphyra leucosticta Thur in Le Jol. and other macroalgae-. **Scientia Marina**, v. 60, p. 163–170, 1996.

FIGUEROA, F. L. et al. Effects of solar radiation on photoinhibition and pigmentation in the red alga Porphyra leucosticta. **Marine Ecology Progress Series**, v. 151, p. 81–90, 1997.

FIGUEROA, F. L. et al. Effects of short-term irradiation on photoinhibition and accumulation of mycosporine-like amino acids in sun and shade species of the red algal genus Porphyra. **Journal of Photochemistry and Photobiology B: Biology**, v. 69, n. 1, p. 21–30, 1 jan. 2003.

FIGUEROA, F. L. et al. Accumulation of mycosporine-like amino acids in asparagopsis armata grown in tanks with fishpond effluents of gilthead sea bream, sparus aurata. **Journal of the World Aquaculture Society**, v. 39, n. 5, p. 692–699, 2008.

FIGUEROA, F. L. et al. Acclimation of Red Sea macroalgae to solar radiation: Photosynthesis and thallus absorptance. **Aquatic Biology**, v. 7, n. 1–2, p. 159–172, 2009.

FIGUEROA, F. L. et al. Effect of nutrient supply on photosynthesis and pigmentation to short-term stress (UV radiation) in Gracilaria conferta (Rhodophyta). **Marine Pollution Bulletin**, v. 60, n. 10, p. 1768–1778, 2010.

FIGUEROA, F. L. et al. Continuous monitoring of in vivo chlorophyll a fluorescence in ulva rigida (Chlorophyta) submitted to different CO2, nutrient and temperature regimes. **Aquatic Biology**, v. 22, p. 195–212, 20 nov. 2014.

FIGUEROA, F. L. et al. Short-term effects of increased CO2, nitrate and temperature on photosynthetic activity in Ulva rigida (Chlorophyta) estimated by different pulse amplitude modulated fluorometers and oxygen evolution. **Journal of experimental botany**, v. 72, n. 2, p. 491–509, 2 fev. 2021.

FIGUEROA, F. L.; AGUILERA, J.; NIELL, F. X. Red and blue light regulation of growth and photosynthetic metabolism in Porphyra umbilicalis (Bangiales, Rhodophyta). **European Journal of Phycology**, v. 30, n. 1, p. 11–18, 1995.

FIGUEROA, F. L.; CONDE-´ ALVAREZ, R.; GÓMEZ, I. Relations between electron transport rates determined by pulse amplitude modulated chlorophyll fluorescence and oxygen evolution in macroalgae under different light conditions. **Photosynthesis Research**, v. 75, p. 259–275, 2003.

FIGUEROA, F. L.; CONDE-ÁLVAREZ, R.; GÓMEZ, I. Relations between electron transport rates determined by pulse amplitude modulated chlorophyll fluorescence and oxygen evolution in macroalgae under different light conditions. **Photosynthesis Research**, v. 75, n. 3, p. 259–275, 2003.

FIGUEROA, F. L.; DOMÍNGUEZ-GONZÁLEZ, B.; KORBEE, N. Vulnerability and acclimation to increased UVB radiation in three intertidal macroalgae of different morpho-functional groups. **Marine environmental research**, v. 97, p. 30–38, 2014.

FIGUEROA, F. L.; GÓMEZ, I. Photosynthetic acclimation to solar UV radiation of marine red algae from the warm-temperate coast of southern Spain: A review. **Journal of Applied Phycology**, v. 13, p. 235–248, 2001.

FLINT, L. H. Light in Relation to Dormancy and Germination in Lettuce Seed on JSTOR. **Science**, v. 80, n. 2063, p. 38–40, 1934.

FLINT, L. H.; MCALISTER, E. D. WAVELENGTHS OF RADIATION IN THE VISIBLE SPECTRUM INHIBITING THE GERMINATION OF LIGHT-SENSITIVE LETTUCE SEED. **Smithsonian Miscellaneous Collections**, v. 94, n. 5, p. 1–12, 1935.

FLORES-MOYA, A. et al. Effects of solar radiation on the endemic Mediterranean red alga

Rissoella verruculosa: photosynthetic performance, pigment content and the activities of enzymes related to nutrient uptake. **New Phytologist**, v. 139, n. 4, p. 673–683, 1 ago. 1998.

FLORES-MOYA, A. et al. Involvement of solar UV-B radiation in recovery of inhibited photosynthesis in the brown alga Dictyota dichotoma (Hudson) Lamouroux. **Journal of Photochemistry and Photobiology B: Biology**, v. 49, n. 2–3, p. 129–135, 1 abr. 1999.

FOLIN, O.; CIOCALTEU, V. ON TYROSINE AND TRYPTOPHANE DETERMINATIONS IN PROTEINS. **Journal of Biological Chemistry**, v. 73, n. 2, p. 627–648, 1927.

FRANCO, D. et al. Polyphenols from plant materials: Extraction and antioxidant power. **Electronic Journal of Environmental, Agricultural and Food Chemistry**, v. 7, n. 8, p. 3210–3216, 2008.

GANGULY, B.; HOTA, M.; PRADHAN, J. Skin Aging: Implications of UV Radiation, Reactive Oxygen Species and Natural Antioxidants. 19 set. 2021.

GENTY, B.; BRIANTAIS, J. M.; BAKER, N. R. The relationship between the quantum yield of photosynthetic electron transport and quenching of chlorophyll fluorescence. **Biochimica et Biophysica Acta (BBA) - General Subjects**, v. 990, n. 1, p. 87–92, 27 jan. 1989.

GHEDIFA, A. BEN et al. Effects of light quality on the photosynthetic activity and biochemical composition of Gracilaria gracilis (Rhodophyta). **Journal of Applied Phycology**, v. 33, p. 3413–3425, 2021.

GNAIGER, E.; BITTERLICH, G. Proximate biochemical composition and caloric content calculated from elemental CHN analysis: a stoichiometric concept. **Oecologia 1984 62:3**, v. 62, n. 3, p. 289–298, jun. 1984.

GÓMEZ, I. et al. Effects of solar radiation on photosynthesis, UV-absorbing compounds and enzyme activities of the green alga Dasycladus vermicularis from southern Spain. **Journal of Photochemistry and Photobiology B: Biology**, v. 47, n. 1, p. 46–57, 1 nov. 1998.

GRASSHOFF, K.; KREMLING, K.; EHRHARDT, M. **Methods of Seawater Analysis**. [s.l: s.n.].

GRZYMSKI, J.; JOHNSEN, G.; SAKSHAUG, E. THE SIGNIFICANCE OF INTRACELLULAR SELF-SHADING ON THE BIOOPTICAL PROPERTIES OF BROWN, RED, AND GREEN MACROALGAE1. **Journal of Phycology**, v. 33, n. 3, p. 408–414, 1 jun. 1997.

GU, Y. et al. Biomarkers, oxidative stress and autophagy in skin aging. **Ageing Research Reviews**, v. 59, p. 101036, 1 maio 2020.

GUIRY, M. . **AlgaeBase**.

GUTIÉRREZ-RODRÍGUEZ, A. G. et al. Anticancer activity of seaweeds. **Drug Discovery Today**, v. 23, n. 2, 2018.

HADER, D. P. et al. Photosynthetic oxygen production and PAM fluorescence in the brown alga Padina pavonica measured in the field under solar radiation. **Marine Biology**, v. 127, p. 61–66, 1996.

HÄDER, D. P.; FIGUEROA, F. L. Photoecophysiology of Marine Macroalgae. **Photochemistry and Photobiology**, v. 66, n. 1, p. 1–14, 1997.

HARDEN, E. A. et al. Virucidal activity of polysaccharide extracts from four algal species against herpes simplex virus. **Antiviral Research**, v. 83, n. 3, p. 282–289, 1 set. 2009.

HARTMANN, A. et al. Inhibition of Collagenase by Mycosporine-like Amino Acids from Marine Sources. **Planta Medica**, v. 81, n. 10, p. 813–820, 2015.

HE, D. et al. Antitumor bioactivity of porphyran extracted from Pyropia yezoensis Chonsoo2 on human cancer cell lines. Journal of the Science of Food and Agriculture | 10.1002/jsfa.9954. **Journal of the Science of Food and Agriculture**, v. 99, n. 15, p. 6722–6730, 2019.

HEGEMANN, P.; FUHRMANN, M.; KATERIYA, S. Algal Sensory Photoreceptors. **J. Phycol**, v. 37, p. 668–676, 2001.

HENTATI, F. et al. Bioactive Polysaccharides from Seaweeds. **Molecules**, v. 25, p. 3152, 2020.

HOYER, K. et al. Photoprotective substances in Antarctic macroalgae and their variation with respect to depth distribution, different tissues and developmental stages. **Marine Ecology Progress Series**, v. 211, p. 117–129, 14 fev. 2001.

HUOVINEN, P. et al. Ultraviolet-absorbing mycosporine-like amino acids in red macroalgae from Chile. **Botanica Marina**, v. 47, n. 1, p. 21–29, 26 fev. 2004.

HUOVINEN, P. et al. The role of ammonium in photoprotection against high irradiance in the red alga Grateloupia lanceola. **Aquatic Botany**, v. 84, p. 308–316, 2006.

ITA, K. Anatomy of the human skin. **Transdermal Drug Delivery**, p. 9–18, 1 jan. 2020.

JEREZ, C. G. et al. Chlorella fusca (Chlorophyta) grown in thin-layer cascades: Estimation of biomass productivity by in-vivo chlorophyll a fluorescence monitoring. **Algal Research**, v. 17, p. 21–30, 1 jul. 2016.

JI, Y.; GAO, K. Effects of climate change factors on marine macroalgae: A review. In: **Advances in Marine Biology**. [s.l.] Academic Press, 2021. v. 88p. 91–136.

JIMENEZ-LOPEZ, C. et al. Main bioactive phenolic compounds in marine algae and their mechanisms of action supporting potential health benefits. **Food Chemistry**, v. 341, p. 128262, 30 mar. 2021.

JIMÉNEZ, C. et al. Effects of solar radiation on photosynthesis and photoinhibition in red macrophytes from an intertidal system of southern Spain. **Botanica Marina**, v. 41, n. 3, p. 329–338, 1 jan. 1998.

JIN, H. et al. An Overview of Antitumour Activity of Polysaccharides. **Molecules 2022, Vol. 27, Page 8083**, v. 27, n. 22, p. 8083, 21 nov. 2022.

JIN, W. et al. The structure-activity relationship between polysaccharides from Sargassum thunbergii and anti-tumor activity. **International Journal of Biological Macromolecules**, v. 105, p. 686–692, 1 dez. 2017.

JOHNSEN, G.; SAKSHAUG, E. Biooptical characteristics of PSII and PSI in 33 species (13 pigment groups) of marine phytoplankton, and the relevance for pulse-amplitude-modulated and fast-repetition-rate fluorometry1. **Journal of Phycology**, v. 43, n. 6, p. 1236–1251, 1 dez. 2007.

JONES, J. M. K. Seasonal growth and photoinhibition in Plocamium cartilagineum (Rhodophyta) off the Isle of Man. **https://doi.org/10.2216/i0031-8884-26-1-88.1**, v. 26, n. 1, p. 88–99, mar. 2019.

JUNQUEIRA, L. C.; CARNEIRO, J. Pele e anexos. In: ABRAHAMSOHN, P. (Ed.). **Histologia básica**. 13. ed. [s.l.] Guanabara Koogan, 2018. p. 1216–1267.

KARSTEN, U.; WIENCKE, C. Factors controlling the formation of UV-absorbing mycosporine-like amino acids in the marine red alga Palmaria palmata from Spitsbergen (Norway). **Journal of Plant Physiology**, v. 155, n. 3, p. 407–415, 1999.

KATO, S. et al. Carotenoids in the eyespot apparatus are required for triggering phototaxis in Euglena gracilis. **The Plant Journal**, v. 101, n. 5, p. 1091–1102, 1 mar. 2020.

KIANIANMOMENI, A.; HALLMANN, A. Algal photoreceptors: In vivo functions and potential applications. **Planta**, v. 239, n. 1, p. 1–26, jan. 2014.

KLIGMAN, L. H. Photoaging. Manifestations, prevention, and treatment. **Dermatologic Clinics**, v. 4, n. 3, p. 517–528, 1986.

KNOTT, M. G. A review of secondary metabolites isolated from Plocamium species worldwide. **International Science and Technology Journal of Namibia**, v. 6, p. 75–93, 2016.

KORBEE, N. et al. Ammonium and UV radiation stimulate the accumulation of mycosporine-

like amino acids in Porphyra columbina(Rhodophyta)from Patagonia, Argentina. **Journal of Phycology**, v. 40, p. 248–259, 2004.

KORBEE, N.; FIGUEROA, F. L.; AGUILERA, J. Effect of light quality on the accumulation of photosynthetic pigments, proteins and mycosporine-like amino acids in the red alga Porphyra leucosticta (Bangiales, Rhodophyta). **Journal of Photochemistry and Photobiology B: Biology**, v. 80, n. 2, p. 71–78, 1 ago. 2005.

KORBEE, N.; FIGUEROA, F. L.; AGUILERA, J. Accumulation of mycosporine-like amino acids (MAAs): biosynthesis, photocontrol and ecophysiological functions. **Revista Chilena De Historia Natural**, v. 79, n. 1, p. 119–132, 2006.

KOTTKE, T. et al. Cryptochrome photoreceptors in green algae: Unexpected versatility of mechanisms and functions. **Journal of Plant Physiology**, v. 217, p. 4–14, 1 out. 2017.

KRÄBS, G.; WATANABE, M.; WIENCKE, C. A Monochromatic Action Spectrum for the Photoinduction of the UV-Absorbing Mycosporine-like Amino Acid Shinorine in the Red Alga Chondrus crispus¶. **Photochemistry and Photobiology**, v. 79, n. 6, p. 515, 2004.

KROMKAMP, J. C.; FORSTER, R. M. The use of variable fluorescence measurements in aquatic ecosystems: Differences between multiple and single turnover measuring protocols and suggested terminology. **European Journal of Phycology**, v. 38, n. 2, p. 103–112, maio 2003.

LAI-CHEONG, J. E.; MCGRATH, J. A. Structure and function of skin, hair and nails. **Medicine**, v. 49, n. 6, p. 337–342, 1 jun. 2021.

LAJILI, S. et al. Characterization of sulfated polysaccharide from Laurencia obtusa and its apoptotic, gastroprotective and antioxidant activities. 2018.

LEANDRO, A.; PEREIRA, L.; GONÇALVES, A. M. M. Diverse applications of marine macroalgae. **Marine Drugs**, v. 18, n. 1, 2020.

LEFRANC, F. et al. Algae metabolites: from in vitro growth inhibitory effects to promising anticancer activity. 2019.

LEISTER, D. Enhancing the light reactions of photosynthesis: Strategies, controversies, and perspectives. **Molecular Plant**, v. 16, n. 1, p. 4–22, 2 jan. 2023.

LI, W. et al. Phycobiliproteins: Molecular structure, production, applications, and prospects. **Biotechnology Advances**, v. 37, n. 2, p. 340–353, 1 mar. 2019.

LINDEMANN, P. et al. Detection of a phytochrome -like protein in macroalgae. **Botanica Acta**, v. 102, p. 178–180, 1989.

LIU, M.; HANSEN, P. E.; LIN, X. Bromophenols in Marine Algae and Their Bioactivities.

Marine Drugs 2011, Vol. 9, Pages 1273-1292, v. 9, n. 7, p. 1273–1292, 22 jul. 2011.

LONG, X. et al. Insights on preparation, structure and activities of Gracilaria lemaneiformis polysaccharide. **Food Chemistry: X**, v. 12, p. 100153, 30 dez. 2021.

LONGSTAFF, B. J. et al. An in situ study of photosynthetic oxygen exchange and electron transport rate in the marine macroalga Ulva lactuca (Chlorophyta). **Photosynthesis Research**, v. 74, n. 3, p. 281–293, 2002.

LOO, Y. C. et al. Development on potential skin anti-aging agents of Cosmos caudatus Kunth via inhibition of collagenase, MMP-1 and MMP-3 activities. **Phytomedicine**, v. 110, p. 154643, 1 fev. 2023.

LÓPEZ-FIGUEROA, F. et al. Detection of Some Conserved Domains in Phytochrome-like Proteins from Algae. **Journal of Plant Physiology**, v. 136, n. 4, p. 484–487, 1 jul. 1990.

LÓPEZ-FIGUEROA, F. et al. The use of chlorophyll fluorescence for monitoring photosynthetic condition of two tank-cultivated red macroalgae using fishpond effluents. **Botanica Marina**, v. 49, p. 275–282, 2006.

LÓPEZ-FIGUEROA, F.; NIELL, F. X. Effects of light quality on chlorophyll and biliprotein accumulation in seaweeds. **Marine Biology**, v. 104, n. 2, p. 321–327, jun. 1990.

LOPEZ-FIGUEROA, F.; PEREZ, R.; NIELL, F. X. Effects of red and far-red light pulses on the chlorophyll and biliprotein accumulation in the red alga Corallina elongata. **Journal of Photochemistry and Photobiology B: Biology**, v. 4, n. 2, p. 185–193, 1 nov. 1989.

LÓPEZ-FIGUEROA, F. Red, green and blue light photoreceptors controlling chlorophyll a, biliprotein and total protein synthesis in the red alga Chondrus crispus. **British Phycological Society**, p. 383–393, 1991.

LÓPEZ-FIGUEROA, F. Diurnal Variation in Pigment Content in Porphyra laciniata and Chondrus crispus and its Relation to the Diurnal Changes of Underwater Light Quality and Quantity. **Marine Ecology**, v. 13, n. 4, p. 285–305, 1 dez. 1992.

LOPEZ-FIGUEROA, F.; NIELL, F. X. Red-light and blue-light photoreceptors controlling chlorophyll a synthesis in the red alga Porphyra umbilicalis and in the green alga Ulva rigida. **Physiologia Plantarum**, v. 76, n. 3, p. 391–397, 1989.

LÓPEZ-FIGUEROA, F.; RÜDIGER, W. Stimulation of nitrate net uptake and reduction by red and blue light and reversion by far-red light in the green alga Ulva rigida. **Journal of Phycology**, v. 27, n. 3, p. 389–394, 1 jun. 1991.

LUCK, M.; HEGEMANN, P. The two parallel photocycles of the Chlamydomonas sensory photoreceptor histidine kinase rhodopsin 1. **Journal of Plant Physiology**, v. 217, p. 77–84, 1

out. 2017.

LV, J. et al. Protective roles of mesenchymal stem cells on skin photoaging: A narrative review. **Tissue and Cell**, v. 76, p. 101746, 1 jun. 2022.

MA, G. et al. Purification, characterization and antitumor activity of polysaccharides from Pleurotus eryngii residue. **Carbohydrate Polymers**, v. 114, p. 297–305, 2014.

MACHADO, M. et al. Amino Acid Profile and Protein Quality Assessment of Macroalgae Produced in an Integrated Multi-Trophic Aquaculture System. **Foods**, v. 9, p. 1–15, 2020.

MANCINI-FILHO, J.; VIDAL-NOVOA, A.; SILVA, A. M. O. Antioxidant properties of algal components and fractions. **Functional Ingredients from Algae for Foods and Nutraceuticals**, p. 255–286, 2013.

MARQUARDT, R. et al. Light acclimation strategies of three commercially important red algal species. 2009.

MASSOCATO, T. F. et al. Growth, biofiltration and photosynthetic performance of Ulva spp. cultivated in fishpond effluents: An outdoor study. **Frontiers in Marine Science**, v. 9, p. 1550, 2 set. 2022.

MAZEPA, E. et al. Structural characteristics of native and chemically sulfated polysaccharides from seaweed and their antimelanoma effects. **Carbohydrate Polymers**, v. 289, p. 119436, 1 ago. 2022.

MCCABE, M. C. et al. Alterations in extracellular matrix composition during aging and photoaging of the skin. **Matrix Biology Plus**, v. 8, p. 100041, 1 nov. 2020.

MELO, R. et al. Temporal and spatial variation of seaweed biomass and assemblages in Northwest Portugal. **Journal of Sea Research**, v. 174, p. 102079, 1 ago. 2021.

MILLER, I. J. Further evaluation of the structure of the polysaccharide from Plocamium costatum with the use of set theory. **Hydrobiologia**, v. 398, p. 385–389, 1999.

MORA HUERTAS, A. C. et al. Molecular-level insights into aging processes of skin elastin. **Biochimie**, v. 128–129, p. 163–173, 1 set. 2016.

MORAIS, R. P. et al. Skin interaction, permeation, and toxicity of silica nanoparticles: Challenges and recent therapeutic and cosmetic advances. **International Journal of Pharmaceutics**, v. 614, p. 121439, 25 fev. 2022.

MOREIRA, B. R. et al. Antioxidant and anti-photoaging properties of red marine macroalgae: Screening of bioactive molecules for cosmeceutical applications. **Algal Research**, v. 68, p. 102893, nov. 2022.

MURAD, H. et al. Induction of G1-phase cell cycle arrest and apoptosis pathway in MDA-

MB-231 human breast cancer cells by sulfated polysaccharide extracted from Laurencia papillosa. **Cancer Cell International**, v. 16, n. 1, p. 1–11, 26 maio 2016.

NASSAR, C. **Macroalgas marinhas do Brasil: guia de campo das principais espécies**. Technical ed. [s.l: s.n.].

NAVARRO, N. et al. Short-term variations of mycosporine-like amino acids in the carrageenan-producing red macroalga Mazzaella laminarioides (Gigartinales, Rhodophyta) are related to nitrate availability. **Journal of Applied Phycology**, v. 33, n. 4, p. 2537–2546, 1 ago. 2021.

NAVARRO, N. P. et al. The effects of NO 3 supply on mazzaella laminarioides (rhodophyta, gigartinales) from southern chile. **Photochemistry and Photobiology**, v. 90, n. 6, p. 1299–1307, 2014a.

NAVARRO, N. P. et al. Short-term effects of solar UV radiation and NO3- supply on the accumulation of mycosporine-like amino acids in Pyropia columbina (Bangiales, Rhodophyta) under spring ozone depletion in the sub-Antarctic region, Chile. **Botanica Marina**, v. 57, n. 1, p. 9–20, 2014b.

NAVARRO, N. P. et al. Differential responses of tetrasporophytes and gametophytes of Mazzaella laminarioides (Gigartinales, Rhodophyta) under solar UV radiation. **Journal of Phycology**, v. 52, n. 3, p. 451–462, 1 jun. 2016.

NAVARRO, N. P. et al. Mycosporine-like amino acids from red algae to develop natural UV sunscreens. In: **Sunscreens: Source, Formulations, Efficacy and Recommendations**. [s.l: s.n.]. p. 99–129.

NGO, D. H.; KIM, S. K. Sulfated polysaccharides as bioactive agents from marine algae. **International Journal of Biological Macromolecules**, v. 62, p. 70–75, 1 nov. 2013.

NGOENNET, S. et al. A Method for the Isolation and Characterization of Mycosporine-Like Amino Acids from Cyanobacteria. **methods and protocols**, v. 1, n. 46, p. 1–15, 2018.

NIGAM, S. et al. Perspective on the Therapeutic Applications of Algal Polysaccharides. **Journal of Polymers and the Environment**, v. 30, p. 785–809, 2022.

ORFANOUDAKI, M. et al. Chemical profiling of mycosporine-like amino acids in twenty-three red algal species. **Journal of Phycology**, v. 55, n. 2, p. 393–403, abr. 2019.

OROIAN, M.; ESCRICHE, I. Antioxidants: Characterization, natural sources, extraction and analysis. **Food Research International**, v. 74, p. 10–36, 1 ago. 2015.

PAGELS, F. et al. Light regulating metabolic responses of Cyanobium sp. (Cyanobacteria). **Fundamental and Applied Limnology**, v. 193, n. 4, p. 285–297, 29 jun. 2020.

PANDEL, R. et al. Skin Photoaging and the Role of Antioxidants in Its Prevention. **Article ID**, v. 2013, p. 11, 2013.

PEINADO, N. K. et al. Ammonium and UV radiation stimulate the accumulation of mycosporine-like amino acids in Porphyra columbina (Rhodophyta) from Patagonia, Argentina. **Journal of Phycology**, v. 40, n. 2, p. 248–259, abr. 2004.

PEREIRA, D. T. et al. Effects of ultraviolet radiation on the morphophysiology of the macroalga Pyropia acanthophora var. brasiliensis (Rhodophyta, Bangiales) cultivated at high concentrations of nitrate. **Acta Physiologiae Plantarum**, v. 42, p. 61, 2020.

PEREIRA, L.; MESQUITA, J. F. Population studies and carrageenan properties of Chondracanthus teedei var. lusitanicus (Gigartinaceae, Rhodophyta). **Journal of Applied Phycology**, v. 16, p. 369–383, 2004.

PERES, P. S. et al. Photoaging and chronological aging profile: Understanding oxidation of the skin. **Journal of Photochemistry and Photobiology B: Biology**, v. 103, n. 2, p. 93–97, 3 maio 2011.

PÉREZ-SÁNCHEZ, A. et al. Nutraceuticals for Skin Care: A Comprehensive Review of Human Clinical Studies. **Nutrients**, v. 10, n. 4, 1 abr. 2018.

PESSOA, A. F. M. **A administração sistêmica e tópica de vitaminas antioxidantes acelera a cicatrização de feridas cutâneas em camundongos diabéticos**. [s.l.] Universidade de São Paulo, 2014.

PETROUTSOS, D. et al. A blue-light photoreceptor mediates the feedback regulation of photosynthesis. **Nature**, v. 537, n. 7621, p. 563–566, set. 2016.

PITTAYAPRUEK, P. et al. Molecular Sciences Role of Matrix Metalloproteinases in Photoaging and Photocarcinogenesis. 2016.

PLAZA, M. et al. Screening for bioactive compounds from algae. **Journal of Pharmaceutical and Biomedical Analysis**, v. 51, n. 2, p. 450–455, 20 jan. 2010.

PRADHAN, B.; ROUT, L.; KI, J.-S. Immunomodulatory and anti-inflammatory and anticancer activities of porphyran, a sulfated galactan. **Carbohydrate Polymers**, v. 301, p. 120326, 2023.

PROUTSOS, N. et al. PAR and UVA composition of global solar radiation at a high altitude Mediterranean forest site. **Atmospheric Research**, v. 269, p. 106039, 1 maio 2022.

QUAN, T. et al. Matrix-degrading metalloproteinases in photoaging. **Journal of Investigative Dermatology Symposium Proceedings**, v. 14, n. 1, p. 20–24, 2009.

QUINTANO, E. et al. Depth influence on biochemical performance and thallus size of the red

alga Gelidium corneum. **Marine Ecology**, v. 39, n. 1, 1 fev. 2018.

RALPH, P. J.; GADEMANN, R. Rapid light curves: A powerful tool to assess photosynthetic activity. **Aquatic Botany**, v. 82, n. 3, p. 222–237, 1 jul. 2005.

RAMAN, M.; DOBLE, M. κ-Carrageenan from marine red algae, Kappaphycus alvarezii-A functional food to prevent colon carcinogenesis. 2015.

RANGEL, K. C. et al. Assessment of the photoprotective potential and toxicity of Antarctic red macroalgae extracts from Curdiea racovitzae and Iridaea cordata for cosmetic use. **Algal Research**, v. 50, p. 101984, 1 set. 2020.

RE, R. et al. Antioxidant activity applying an improved ABTS radical cation decolorization assay. **Free Radical Biology and Medicine**, v. 26, n. 9–10, p. 1231–1237, 1 maio 1999.

REALI, N. **Efeitos de filtros solares sobre a comunidade fitoplanctônica**. [s.l.] Universidade Federal de Santa Catarina, 2023.

REINOSA, J. J. et al. Enhancement of UV absorption behavior in ZnO–TiO2 composites. **Boletín de la Sociedad Española de Cerámica y Vidrio**, v. 55, n. 2, p. 55–62, 1 mar. 2016.

RENGASAMY, K. R. et al. Bioactive compounds in seaweeds: An overview of their biological properties and safety. **Food and Chemical Toxicology**, v. 135, p. 111013, 1 jan. 2020.

RESENDE, D. I. S. P. et al. Trends in the use of marine ingredients in anti-aging cosmetics. **Algal Research**, v. 55, p. 102273, 1 maio 2021.

RITCHIE, R. J. Universal chlorophyll equations for estimating chlorophylls a, b, c, and d and total chlorophylls in natural assemblages of photosynthetic organisms using acetone, methanol, or ethanol solvents. **Photosynthetica**, v. 46, n. 1, p. 115–126, mar. 2008.

ROCKWELL, N. C. et al. Eukaryotic algal phytochromes span the visible spectrum. **Proceedings of the National Academy of Sciences of the United States of America**, v. 111, n. 10, p. 3871–3876, 11 mar. 2014.

RODRIGUES, R. D. P. et al. Application of protic ionic liquids in the microwave-assisted extraction of phycobiliproteins from Arthrospira platensis with antioxidant activity. **Separation and Purification Technology**, v. 252, p. 117448, 1 dez. 2020.

ROSIC, N. et al. Exploring Mycosporine-like Amino Acid UV-Absorbing Natural Products for a New Generation of Environmentally Friendly Sunscreens. **Marine Drugs 2023, Vol. 21, Page 253**, v. 21, n. 4, p. 253, 19 abr. 2023.

ROSIC, N. N. **Mycosporine-like amino acids: Making the foundation for organic personalised sunscreens**. **Marine Drugs**, 2019.

RÜDIGER, W.; LÓPEZ-FIGUEROA, F. PHOTORECEPTORS IN ALGAE. **Photochemistry and Photobiology**, v. 55, n. 6, p. 949–954, 1 jun. 1992.

SABEENA FARVIN, K. H.; JACOBSEN, C. Phenolic compounds and antioxidant activities of selected species of seaweeds from Danish coast. **Food Chemistry**, v. 138, n. 2–3, p. 1670–1681, 1 jun. 2013.

SABRY, O. M. M. et al. Cytotoxic halogenated monoterpenes from Plocamium cartilagineum. **Natural Product Research**, v. 31, n. 3, p. 261–267, 2017.

SAMPATH-WILEY, P.; NEEFUS, C. D. An improved method for estimating R-phycoerythrin and R-phycocyanin contents from crude aqueous extracts of Porphyra (Bangiales, Rhodophyta). **Journal of Applied Phycology**, v. 19, n. 2, p. 123–129, abr. 2007.

SCHMID, D. et al. Mycosporine-like amino acids: natural UV-screening compounds from red algae to protect the skin against photoaging. 2003.

SCHNEIDER, G. et al. Physiological and biochemical responses driven by different UV-visible radiation in: Osmundea pinnatifida (Hudson) Stackhouse (Rhodophyta). **Photochemical and Photobiological Sciences**, v. 19, n. 12, p. 1650–1664, 2020a.

SCHNEIDER, G. et al. Photoprotection properties of marine photosynthetic organisms grown in high ultraviolet exposure areas: Cosmeceutical applications. **Algal Research**, v. 49, 1 ago. 2020b.

SCHNEIDER, G. et al. Effects of UV–visible radiation on growth, photosynthesis, pigment accumulation and UV-absorbing compounds in the red macroalga Gracilaria cornea (Gracilariales, Rhodophyta). **Algal Research**, v. 64, n. February, p. 3–10, 2022.

SEGOVIA, M. et al. Light regulation of cyclic-AMP levels in the red macroalga Porphyra leucosticta. **Journal of photochemistry and photobiology. B, Biology**, v. 64, n. 1, p. 69–74, 1 nov. 2001.

SEGOVIA, M.; GORDILLO, F. J. L.; FIGUEROA, F. L. Cyclic-AMP levels in the lichen Evernia prunastri are modulated by light quantity and quality. **Journal of Photochemistry and Photobiology B: Biology**, v. 70, n. 3, p. 145–151, 1 jul. 2003.

SEN, S.; MALLICK, N. Mycosporine-like amino acids: Algal metabolites shaping the safety and sustainability profiles of commercial sunscreens. **Algal Research**, v. 58, p. 102425, 1 out. 2021.

SHAO, P.; CHEN, X.; SUN, P. In vitro antioxidant and antitumor activities of different sulfated polysaccharides isolated from three algae. **International Journal of Biological Macromolecules**, v. 62, p. 155–161, 2013.

SINESHCHEKOV, O. A.; JUNG, K. H.; SPUDICH, J. L. Two rhodopsins mediate phototaxis to low- and high-intensity light in Chlamydomonas reinhardtii. **Proceedings of the National Academy of Sciences of the United States of America**, v. 99, n. 13, p. 8689–8694, 25 jun. 2002.

SONANI, R. R.; RASTOGI, R. P.; MADAMWAR, D. Natural Antioxidants From Algae: A Therapeutic Perspective. **Algal Green Chemistry: Recent Progress in Biotechnology**, p. 91–120, 1 jan. 2017.

SOUZA, R. B. et al. In vitro activities of kappa-carrageenan isolated from red marine alga Hypnea musciformis: Antimicrobial, anticancer and neuroprotective potential. 2018.

SUGANYA, A. M. et al. Pharmacological importance of sulphated polysaccharide carrageenan from red seaweed Kappaphycus alvarezii in comparison with commercial carrageenan. **Biomedice and pharmacotherapy**, v. 84, p. 1300–1312, 2016.

SUH, S. S. et al. Anti-inflammation activities of mycosporine-like amino acids (MAAs) in response to UV radiation suggest potential anti-skin aging activity. **Marine Drugs**, v. 12, n. 10, p. 5174–5187, 14 out. 2014.

SUNG, H. et al. Global Cancer Statistics 2020: GLOBOCAN Estimates of Incidence and Mortality Worldwide for 36 Cancers in 185 Countries. **CA: A Cancer Journal for Clinicians**, v. 71, n. 3, p. 209–249, maio 2021.

SUWAL, S. et al. Effects of high hydrostatic pressure and polysaccharidases on the extraction of antioxidant compounds from red macroalgae, Palmaria palmata and Solieria chordalis. **Journal of Food Engineering**, v. 252, p. 53–59, 1 jul. 2019.

TAIRA, H. et al. Daily variation in cellular content of UV-absorbing compounds mycosporine-like amino acids in the marine dinoflagellate Scrippsiella sweeneyae. **Journal of Photochemistry and Photobiology B: Biology**, v. 75, n. 3, p. 145–155, 2004.

TANVEER, M. A.; RASHID, H.; TASDUQ, S. A. Molecular basis of skin photoaging and therapeutic interventions by plant-derived natural product ingredients: A comprehensive review. 2023.

TERUYA, T. et al. Anti-proliferative activity of oversulfated fucoidan from commercially cultured Cladosiphon okamuranus TOKIDA in U937 cells. **International Journal of Biological Macromolecules**, v. 41, n. 3, p. 221–226, 1 ago. 2007.

THOMAS, B.; DICKINSON, H. G. Evidence for Two Photoreceptors Controlling Growth in De-etiolated Seedlings. **Planta**, v. 146, n. 5, p. 545–550, 1979.

TORRES, P. et al. Comparative analysis of in vitro antioxidant capacities of mycosporine-like

amino acids (MAAs). **Algal Research**, v. 34, p. 57–67, 1 set. 2018.

TSUJINO, I.; SAITO, T. Studies on the compounds specific for each group of marine algae. I : Presence of characteristic ultraviolet absorbing material in Rhodophyceae. **BULLETIN OF THE FACULTY OF FISHERIES**, v. 12, p. 49–58, 1961.

USOV, A. I. Polysaccharides of the red algae. **Advances in Carbohydrate Chemistry and Biochemistry**, v. 65, p. 115–217, 1 jan. 2011.

V. BRITO, T. et al. Sulfated polysaccharide from the marine algae Hypnea musciformis inhibits TNBS-induced intestinal damage in rats. **Carbohydrate Polymers**, v. 151, p. 957–964, 20 out. 2016.

VALENTÃO, P. et al. Codium tomentosum and Plocamium cartilagineum: Chemistry and antioxidant potential. **Food Chemistry**, v. 119, p. 1359–1368, 2010.

VAN KOOTEN, O.; SNEL, J. F. H. The use of chlorophyll fluorescence nomenclature in plant stress physiology. **Photosynthesis Research**, v. 25, p. 147–150, 1990.

VANLERBERGHE, G. C. et al. Photosynthesis, respiration and growth: A carbon and energy balancing act for alternative oxidase. **Mitochondrion**, v. 52, p. 197–211, 1 maio 2020.

VEGA, J. ; et al. Isolation of Mycosporine-like Amino Acids from Red Macroalgae and a Marine Lichen by High-Performance Countercurrent Chromatography: A Strategy to Obtain Biological UV-Filters. **Marine Drugs**, v. 21, n. 6, p. 357, 10 jun. 2023.

VEGA, J. et al. Antioxidant activity of extracts from marine macroalgae, wild-collected and cultivated, in an integrated multi-trophic aquaculture system. **Aquaculture**, v. 522, p. 735088, 30 maio 2020a.

VEGA, J. et al. Cyanobacteria and Red Macroalgae as Potential Sources of Antioxidants and UV Radiation-Absorbing Compounds for Cosmeceutical Applications. **Marine drugs**, v. 18, n. 12, 21 dez. 2020b.

VEGA, J. et al. Mycosporine-like amino acids from red macroalgae: Uv-photoprotectors with potential cosmeceutical applications. **Applied Sciences (Switzerland)**, v. 11, n. 11, 2021.

WADA, N.; SAKAMOTO, T.; MATSUGO, S. Multiple Roles of Photosynthetic and Sunscreen Pigments in Cyanobacteria Focusing on the Oxidative Stress. **Metabolites**, v. 3, n. 2, p. 463, 30 maio 2013.

WADA, N.; SAKAMOTO, T.; MATSUGO, S. Mycosporine-Like Amino Acids and Their Derivatives as Natural Antioxidants. **Antioxidants**, v. 4, n. 3, p. 603–646, 7 set. 2015.

WANG, P. et al. Structural and compositional characteristics of hybrid carrageenans from red algae Chondracanthus chamissoi. **Carbohydrate Polymers**, v. 89, n. 3, p. 914–919, 1 jul.

2012.

WEERAPREEYAKUL, N. et al. Evaluation of the anticancer potential of six herbs against a hepatoma cell line. **Chinese Medicine (United Kingdom)**, v. 7, n. 1, p. 1–7, 10 jun. 2012.

WEI, L. et al. Antioxidant properties, anti- SARS-CoV-2 study, collagenase and elastase inhibition effects, anti-human lung cancer potential of some phenolic compounds. **Journal of the Indian Chemical Society**, v. 99, n. 4, p. 100416, 1 abr. 2022.

WHITE, A. J.; CRITCHLEY, C. Rapid light curves: A new fluorescence method to assess the state of the photosynthetic apparatus. **Photosynthesis Research**, v. 59, p. 63–72, 1999.

WIDOWATI, W. et al. Antioxidant and anti aging assays of Oryza sativa extracts, vanillin and coumaric acid. **Journal of Natural Remedies**, v. 16, n. 3, p. 88–99, 1 jul. 2016.

WITTENAUER, J. et al. Inhibitory effects of polyphenols from grape pomace extract on collagenase and elastase activity. **Fitoterapia**, v. 101, p. 179–187, 1 mar. 2015.

WU, Q. et al. Effects of physicochemical factors and in vitro gastrointestinal digestion on antioxidant activity of R-phycoerythrin from red algae Bangia fusco-purpurea. **International Journal of Food Science & Technology**, v. 50, n. 6, p. 1445–1451, 1 jun. 2015.

WU, Q.; KRAUSS, S.; VETTER, W. Occurrence and fate studies (sunlight exposure and stable carbon isotope analysis) of the halogenated natural product MHC-1 and its producer Plocamium cartilagineum. **Science of The Total Environment**, v. 736, p. 139680, 20 set. 2020.

XU, S.-Y.; HUANG, X.; CHEONG, K.-L. Recent Advances in Marine Algae Polysaccharides: Isolation, Structure, and Activities. **Marine drugs**, v. 15, p. 388, 2017.

YANG, C. Y. et al. Reinforcement learning strategies in cancer chemotherapy treatments: A review. **Computer Methods and Programs in Biomedicine**, v. 229, p. 107280, 1 fev. 2023.

YAO, W. et al. Advances in anti-cancer effects and underlying mechanisms of marine algae polysaccharides. **International Journal of Biological Macromolecules**, v. 221, p. 472–485, 30 nov. 2022.

YU, D. et al. Nitrogen assimilation-associated enzymes and nitrogen use efficiency of Pyropia yezoensis (Rhodophyta) in nitrate-sufficient conditions. **Algal Research**, v. 64, p. 102682, 1 maio 2022.

YU, Y. et al. Biological activities and pharmaceutical applications of polysaccharide from natural resources: A review. **Carbohydrate Polymers**, v. 183, p. 91–101, 1 mar. 2018.

YUBERO-SERRANO, E. M. et al. Coenzyme Q10 as an Antioxidant in the Elderly. **Aging: Oxidative Stress and Dietary Antioxidants**, p. 109–117, 1 jan. 2014.

ZAREKARIZI, A.; HOFFMANN, L.; BURRITT, D. J. The potential of manipulating light for the commercial production of carotenoids from algae. **Algal Research**, v. 71, p. 103047, 2023.

ZIMMER, T. B. R.; MENDONÇA, C. R. B.; ZAMBIAZI, R. C. Methods of protection and application of carotenoids in foods - A bibliographic review. **Food Bioscience**, v. 48, p. 2212–4292, 2022.

ANEXO A – MATERIAL SUPLEMENTAR (CAPÍTULO 1)

Tabela S1. Phycoerythrin and Phycocyanin levels measured on aqueous and hydroalcoholic extracts of the sex red macroalgae species. Results are expressed in mg of the compound per gram of dry weight. The species *Plocamium cartilagineum* was sampled in two sites: La Herradura (LH) and Tarifa (TA). Different letters indicate significant differences between aqueous and hydroethanolic extracts, according to a Tukey test ($p < 0.05$).

	Phycoerythrin (mg g^{-1})		**Phycocyanin (mg g^{-1})**	
	Aqueous	Hydroethanolic	Aqueous	Hydroethanolic
Phycocalidia acanthophora	$1.91^{a} \pm 0.25$	0	$0.4^{a} \pm 0.29$	$0.26^{a} \pm 0.03$
Porphyra linearis	$7.0^{a} \pm 0.12$	0	$6.94^{a} \pm 0.2$	$0.19^{b} \pm 0.02$
Condracanthus teedei	$0.14^{a} \pm 0.04$	0	$0.37^{a} \pm 0.004$	$0.03^{b} \pm 0.01$
Gracilaria cornea	$7.92^{a} \pm 0.38$	0	$0.37^{a} \pm 0.04$	$0.18^{b} \pm 0.02$
Osmundea pinnatifida	0	0	$0.06^{a} \pm 0.003$	$0.04^{a} \pm 0.01$
***Plocamium cartilagineum* (TA)**	0	0	$0.06^{a} \pm 0.01$	0
***Plocamium cartilagineum* (LH)**	$2.01^{a} \pm 0.13$	0	$0.12^{a} \pm 0.01$	$0.02^{b} \pm 0.01$

Tabela S2. Unifactorial ANOVA effect for Yield of extraction, $ABTS^{+}$, catalase activity, polyphenols content, collagenase inhibition, phycoerythrin and phycocyanin contents in different solvents (aqueous and hydroethanolic solution).

	Yield		$ABTS^{+}$		Catalase		Polyphenols		Collagenase inhibition		Phycoerythrin		Phycocyanin	
	F	P	F	P	F	p	F	p	F	p	F	p	F	p
Phycocalidia acanthophora	**71.6**	**0.00**	**17.2**	**0.01**	**127.8**	**0.00**	**7.97**	**0.05**	**12.2**	**0.03**	**170.2**	**0.00**	0.71	0.45
Porphyra linearis	**566.0**	**0.00**	**1944.8**	**0.00**	**1412.9**	**0.00**	**131.0**	**0.00**	**48.4**	**0.00**	**9785.6**	**0.00**	**3496.9**	**0.00**
Condracanthus teedei	**303.3**	**0.00**	**89.5**	**0.00**	**178.5**	**0.00**	**18.4**	**0.01**	2.5	0.19	**30.29**	**0.01**	**3098.9**	**0.00**
Gracilaria cornea	**17.7**	**0.01**	**67.1**	**0.00**	n.d.	n.d.	**130.6**	**0.00**	4.5	0.10	**1386.5**	**0.00**	**46.9**	**0.00**
Osmundea pinnatifida	**29.6**	**0.01**	4.7	0.10	**67.2**	**0.00**	1.2	0.34	**10.2**	**0.03**	n.d.	n.d.	5.8	0.07
Plocamium cartilagineum (TA)	**38.6**	**0.00**	0.2	0.64	**43.0**	**0.00**	0.5	0.50	2.9	0.16	n.d.	n.d.	**335.3**	**0.00**
Plocamium cartilagineum (LH)	**35.4**	**0.00**	**8.1**	**0.05**	n.d.	n.d.	**249.7**	**0.00**	**22.93**	**0.01**	**745.8**	**0.00**	**170.2**	**0.00**

The significance differences ($p < 0.05$) are shown in bold. N.d. means that no activity was detected for this sample

Tabela S3. Unifactorial ANOVA effect for total Mycosporine-like amino acids (MAAs) contents in different solvents (aqueous and 20% methanolic solution). The significance differences ($p < 0.05$) are shown in bold. N.d. means that no activity was detected for this sample

	Total MAAs	
	F	p
Phycocalidia acanthophora	**173.9**	**0.00**
Porphyra linearis	**16.9**	**0.01**
Condracanthus teedei	**9.0**	**0.04**
Gracilaria cornea	0.5	0.53
Osmundea pinnatifida	1.9	0.24
Plocamium cartilagineum (TA)	**33.6**	**0.00**
Plocamium cartilagineum (LH)	**75.5**	**0.00**

Figura S1. ESI-MS spectra of MAA peaks detected on aqueous extracts of *Phycocalidia acanthophora*. The following spectra correspond respectively to aplysyapalythine B, asterine-330, $C_{13}H_{20}N_2O_5$, $C_{13}H_{22}N_2O_6$, mycosporine-glutamine, palythine and Porphyra-334.

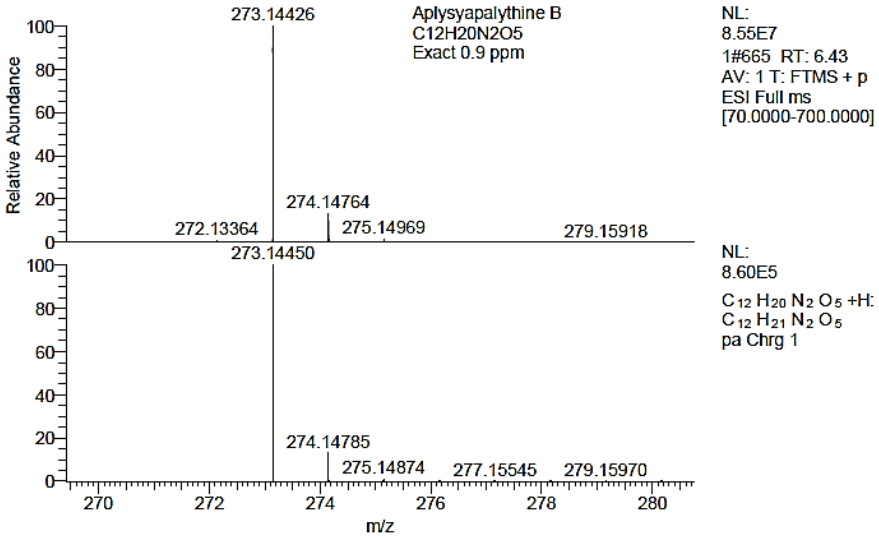
273.14426
Aplysyapalythine B
C12H20N2O5
Exact 0.9 ppm
NL:
8.55E7
1#665 RT: 6.43
AV: 1 T: FTMS + p
ESI Full ms
[70.0000-700.0000]
Relative Abundance
274.14764
272.13364
275.14969
279.15918
273.14450
NL:
8.60E5
C12 H20 N2 O5 +H:
C12 H21 N2 O5
pa Chrg 1
274.14785
275.14874
277.15545
279.15970
m/z

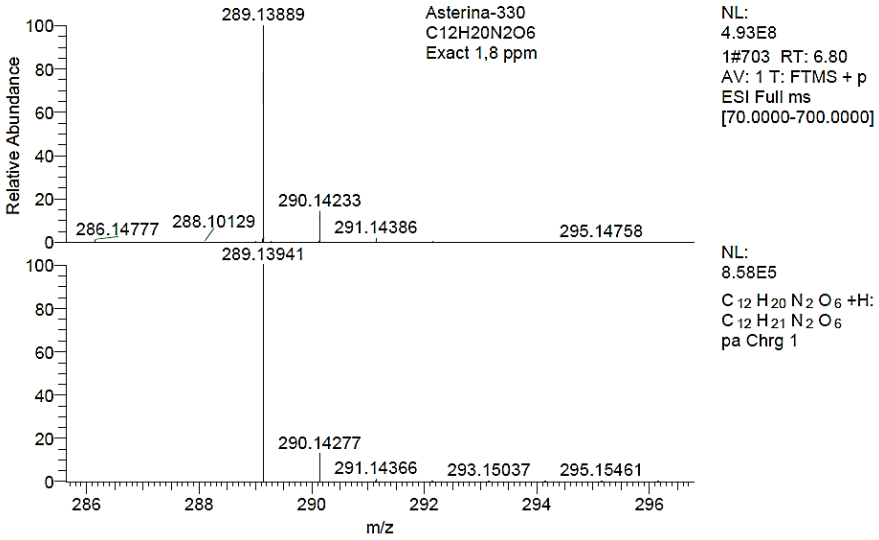
289.13889
Asterina-330
C12H20N2O6
Exact 1,8 ppm
NL:
4.93E8
1#703 RT: 6.80
AV: 1 T: FTMS + p
ESI Full ms
[70.0000-700.0000]
Relative Abundance
290.14233
286.14777
288.10129
291.14386
295.14758
289.13941
NL:
8.58E5
C12 H20 N2 O6 +H:
C12 H21 N2 O6
pa Chrg 1
290.14277
291.14366
293.15037
295.15461
m/z

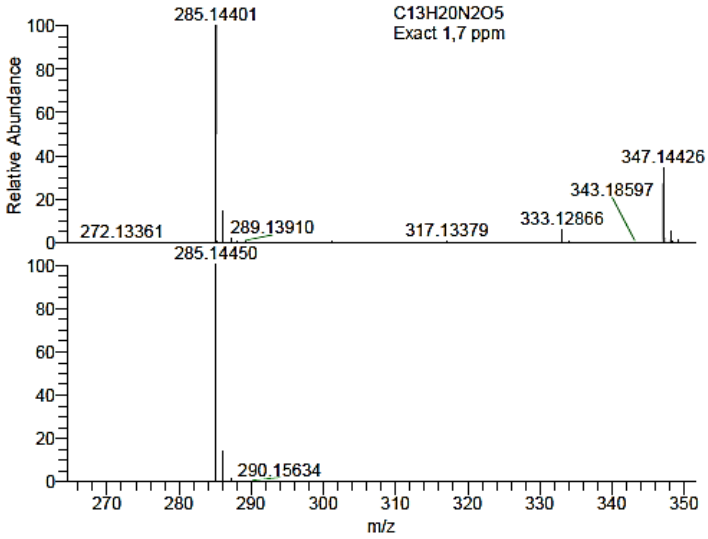
285.14401
C13H20N2O5
Exact 1,7 ppm
NL:
8.67E8
1#617 RT: 5.97
AV: 1 T: FTMS + p
ESI Full ms
[70.0000-700.0000]
Relative Abundance
347.14426
343.18597
272.13361
289.13910
317.13379
333.12866
285.14450
NL:
8.51E5
C13 H20 N2 O5 +H:
C13 H21 N2 O5
pa Chrg 1
290.15634
m/z

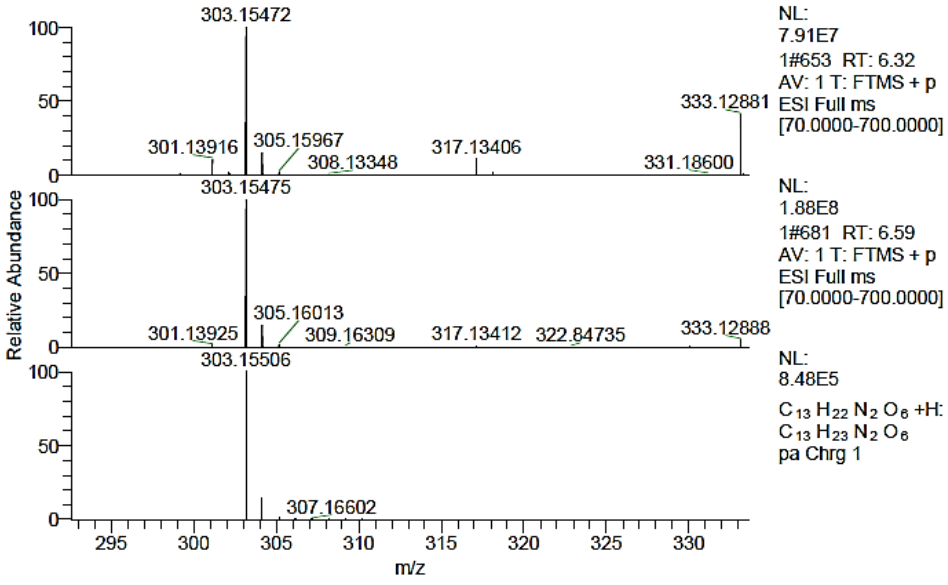
303.15472
NL:
7.91E7
1#653 RT: 6.32
AV: 1 T: FTMS + p
ESI Full ms
[70.0000-700.0000]
333.12881
301.13916
305.15967
308.13348
317.13406
331.18600
303.15475
NL:
1.88E8
1#681 RT: 6.59
AV: 1 T: FTMS + p
ESI Full ms
[70.0000-700.0000]
Relative Abundance
305.16013
301.13925
309.16309
317.13412
322.84735
333.12888
303.15506
NL:
8.48E5
C13 H22 N2 O6 +H:
C13 H23 N2 O6
pa Chrg 1
307.16602
m/z

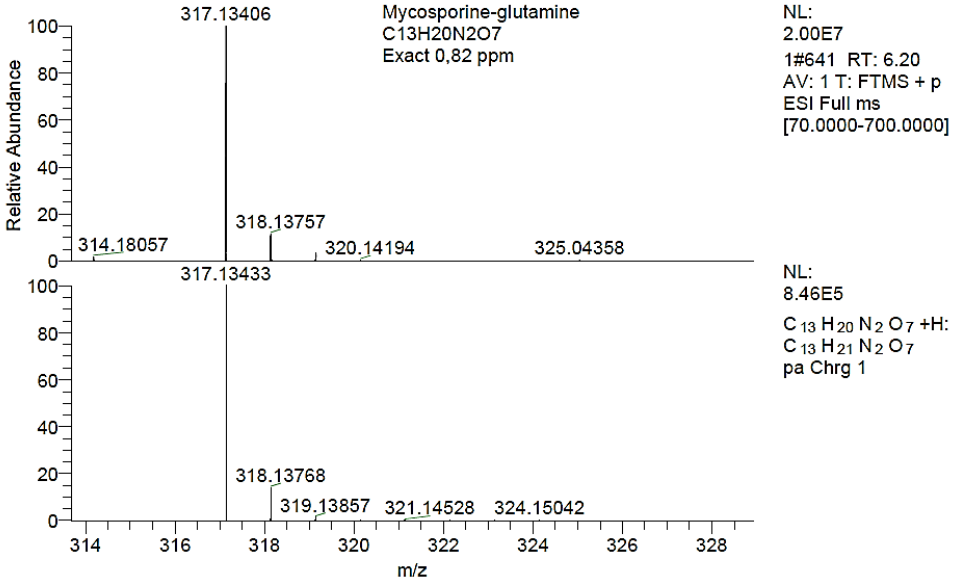
317.13406
Mycosporine-glutamine
C13H20N2O7
Exact 0,82 ppm
NL:
2.00E7
1#641 RT: 6.20
AV: 1 T: FTMS + p
ESI Full ms
[70.0000-700.0000]
Relative Abundance
318.13757
314.18057
320.14194
325.04358
317.13433
NL:
8.46E5
C13 H20 N2 O7 +H:
C13 H21 N2 O7
pa Chrg 1
318.13768
319.13857
321.14528
324.15042
m/z

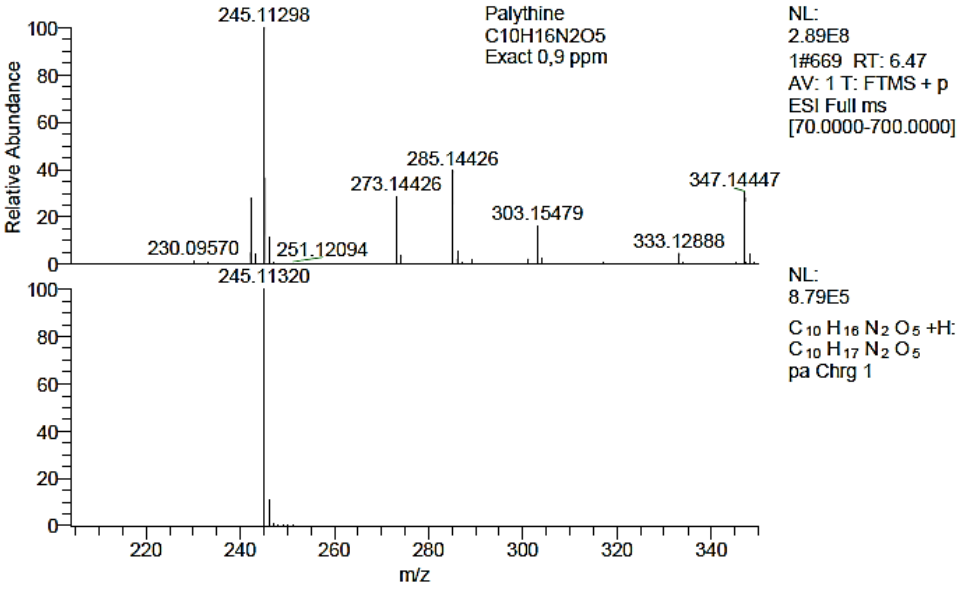
245.11298
Palythine
C10H16N2O5
Exact 0,9 ppm
NL:
2.89E8
1#669 RT: 6.47
AV: 1 T: FTMS + p
ESI Full ms
[70.0000-700.0000]
Relative Abundance
285.14426
273.14426
347.14447
303.15479
230.09570
251.12094
333.12888
245.11320
NL:
8.79E5
C10 H16 N2 O5 +H:
C10 H17 N2 O5
pa Chrg 1
m/z

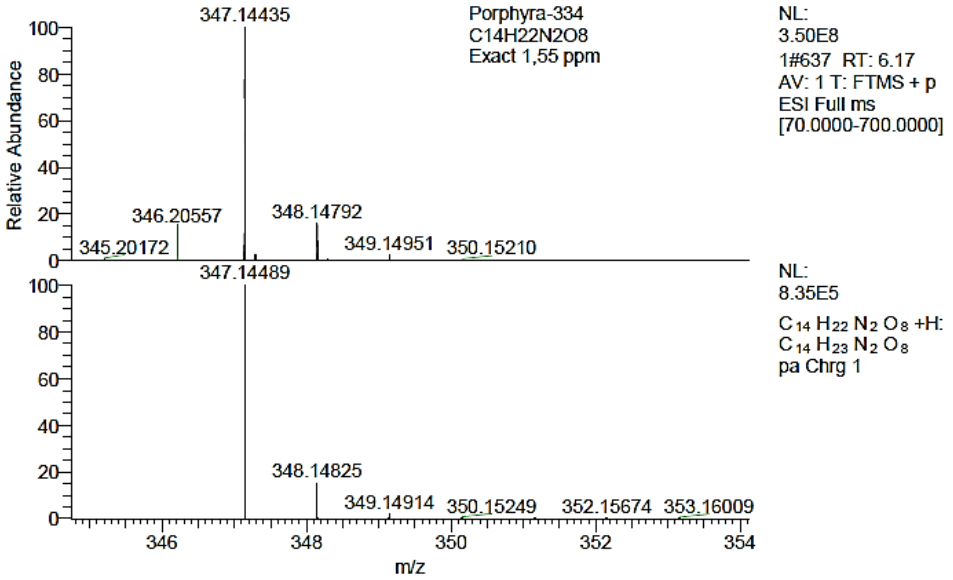
347.14435
Porphyra-334
C14H22N2O8
Exact 1,55 ppm
NL:
3.50E8
1#637 RT: 6.17
AV: 1 T: FTMS + p
ESI Full ms
[70.0000-700.0000]
Relative Abundance
346.20557
348.14792
345.20172
349.14951
350.15210
347.14489
NL:
8.35E5
C14 H22 N2 O8 +H:
C14 H23 N2 O8
pa Chrg 1
348.14825
349.14914
350.15249
352.15674
353.16009
m/z

Figura S2. ESI-MS spectra of MAA peaks detected on aqueous extracts of *Porphyra linearis*. The following spectra correspond respectively to aplysyapalythine B, $C_{13}H_{20}N_2O_5$, $C_{13}H_{22}N_2O_6$, mycosporine-glutamine, $C_{12}H_{20}N_2O_6$, palythine, shinorine and Porphyra-334.

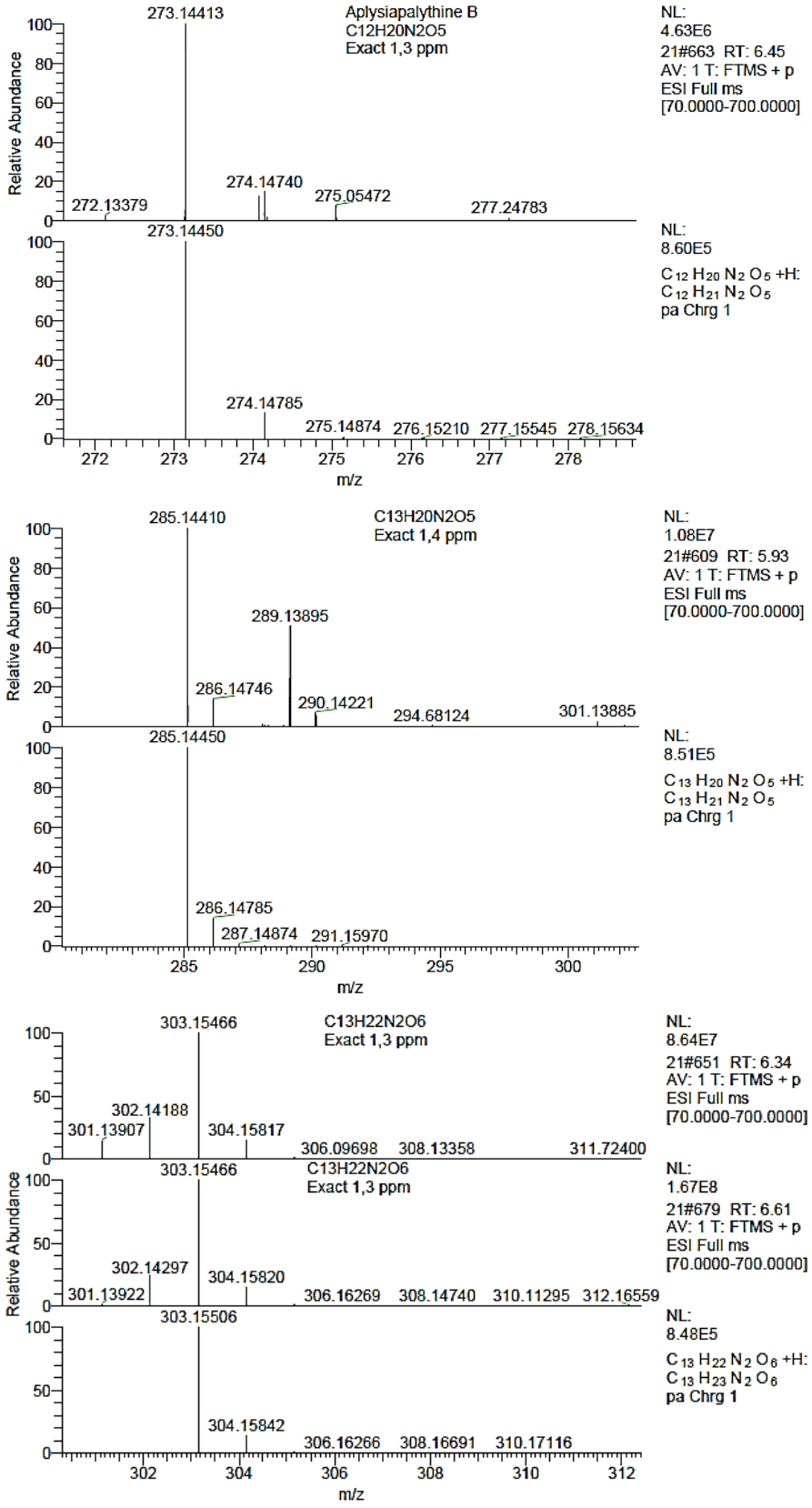

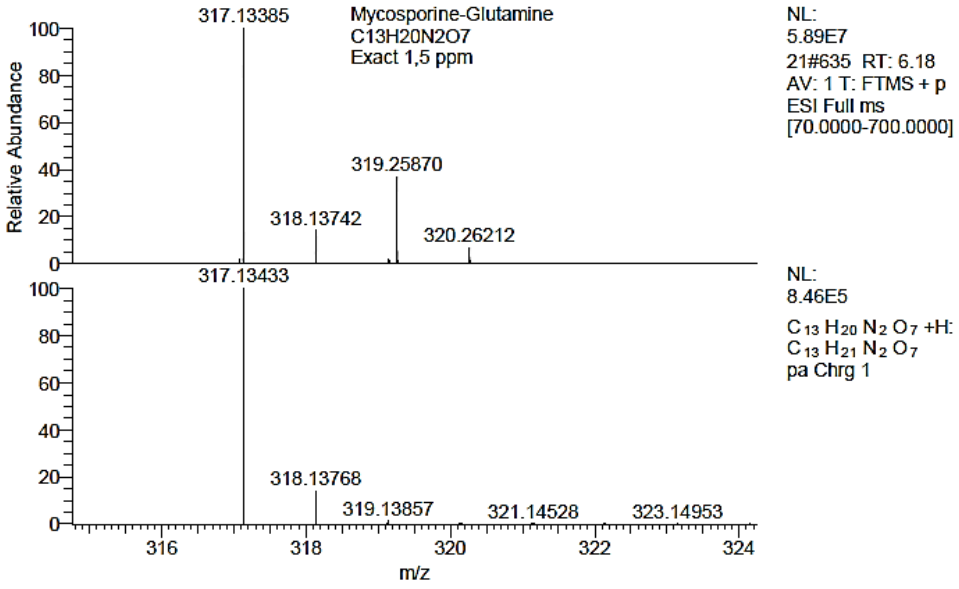
317.13385
Mycosporine-Glutamine
C13H20N2O7
Exact 1,5 ppm
NL:
5.89E7
21#635 RT: 6.18
AV: 1 T: FTMS + p
ESI Full ms
[70.0000-700.0000]
319.25870
318.13742
320.26212
Relative Abundance
317.13433
NL:
8.46E5
C13 H20 N2 O7 +H:
C13 H21 N2 O7
pa Chrg 1
318.13768
319.13857
321.14528
323.14953
316
318
320
322
324
m/z

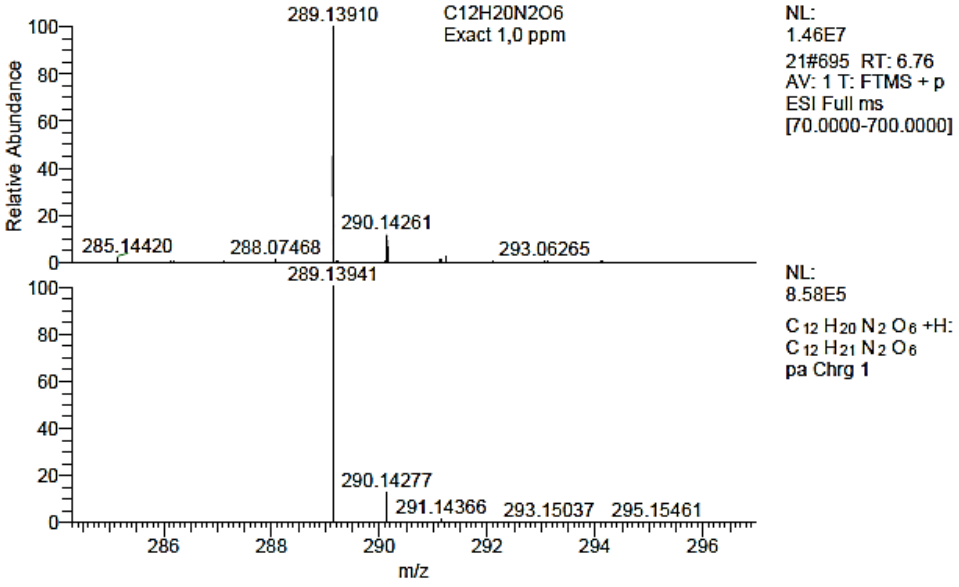
289.13910
C12H20N2O6
Exact 1,0 ppm
NL:
1.46E7
21#695 RT: 6.76
AV: 1 T: FTMS + p
ESI Full ms
[70.0000-700.0000]
290.14261
285.14420
288.07468
293.06265
Relative Abundance
289.13941
NL:
8.58E5
C12 H20 N2 O6 +H:
C12 H21 N2 O6
pa Chrg 1
290.14277
291.14366
293.15037
295.15461
286
288
290
292
294
296
m/z

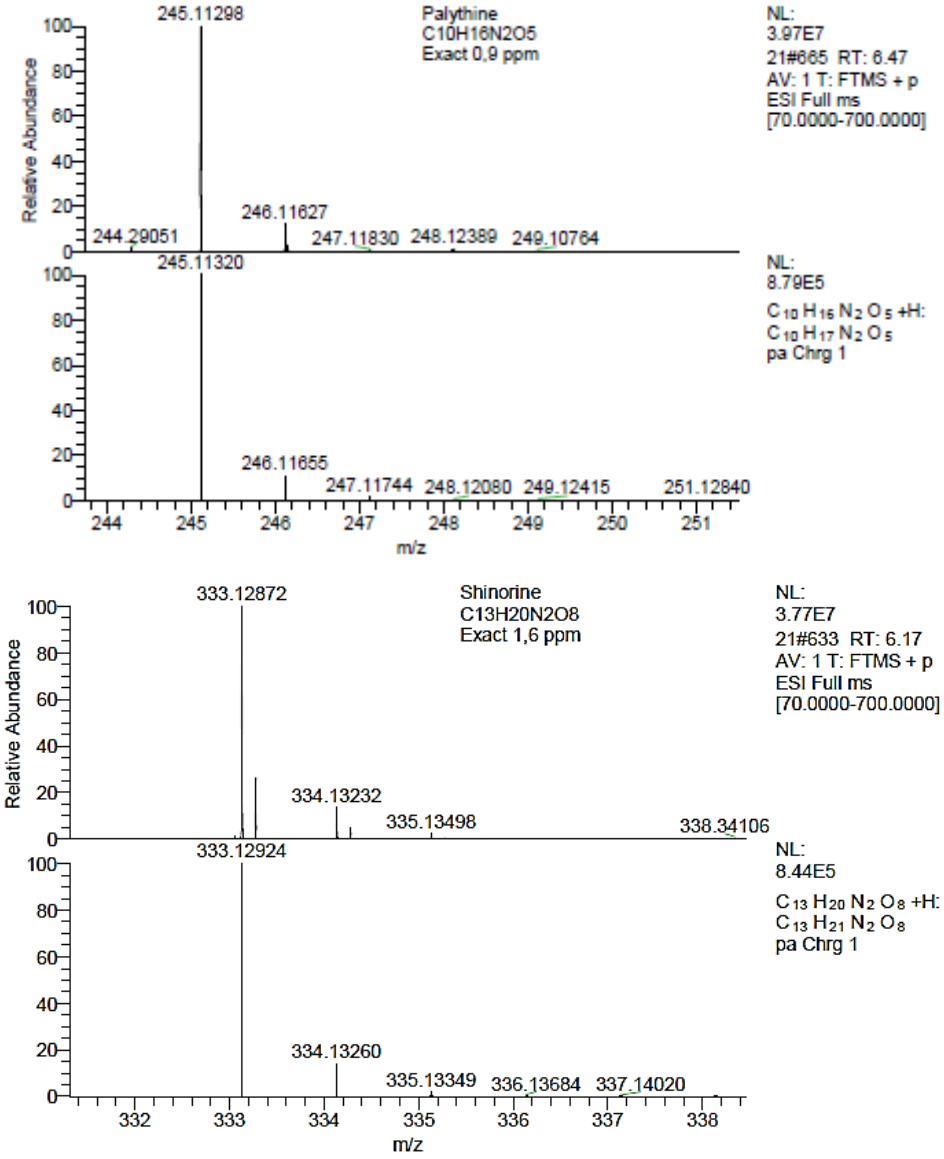
245.11298
Palythine
C10H16N2O5
Exact 0,9 ppm
NL:
3.97E7
21#665 RT: 6.47
AV: 1 T: FTMS + p
ESI Full ms
[70.0000-700.0000]
Relative Abundance
246.11627
244.29051
247.11830
248.12389
249.10764
245.11320
NL:
8.79E5
C10 H16 N2 O5 +H:
C10 H17 N2 O5
pa Chrg 1
246.11655
247.11744
248.12080
249.12415
251.12840
m/z
333.12872
Shinorine
C13H20N2O8
Exact 1,6 ppm
NL:
3.77E7
21#633 RT: 6.17
AV: 1 T: FTMS + p
ESI Full ms
[70.0000-700.0000]
334.13232
335.13498
338.34106
333.12924
NL:
8.44E5
C13 H20 N2 O8 +H:
C13 H21 N2 O8
pa Chrg 1
334.13260
335.13349
336.13684
337.14020

Figura S3. ESI-MS spectra of MAA peaks detected on aqueous extracts of *Condracanthus teedei*. The following spectra correspond respectively to mycosporine-glutamine, $C_{12}H_{20}N_2O_6$, palythine, shinorine, mycosporine-2-glycine and porphyra-334.

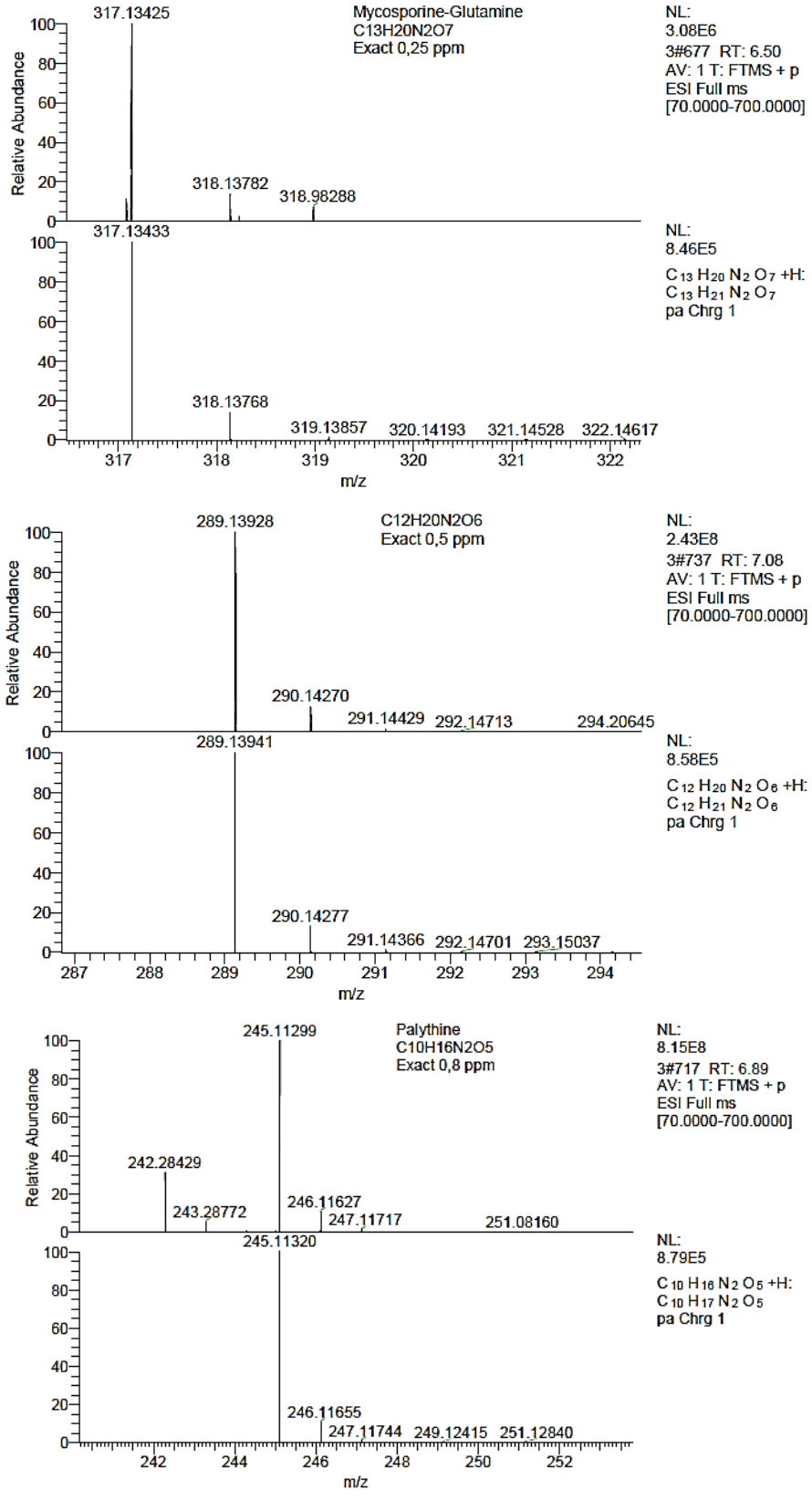

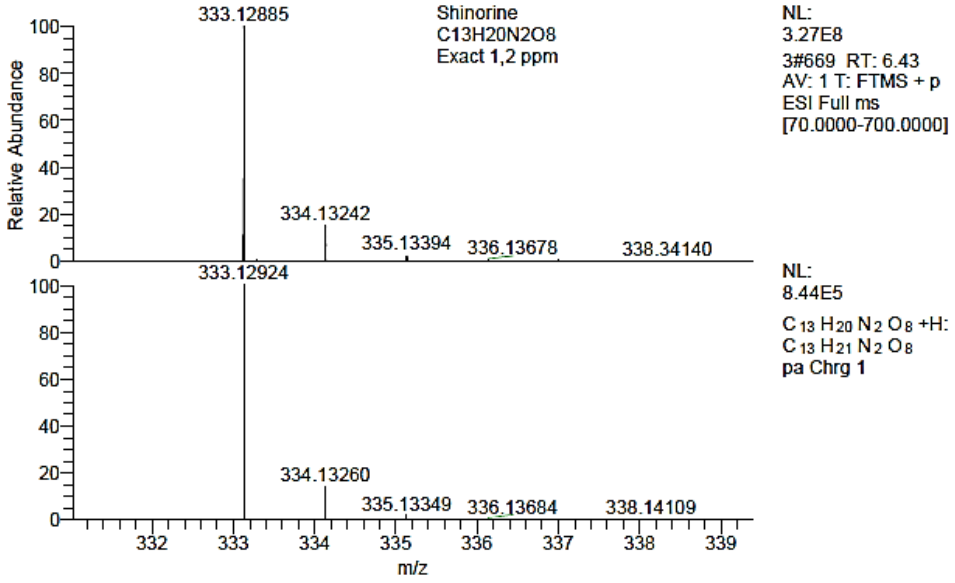
333.12885
Shinorine
C13H20N2O8
Exact 1,2 ppm
NL:
3.27E8
3#669 RT: 6.43
AV: 1 T: FTMS + p
ESI Full ms
[70.0000-700.0000]
Relative Abundance
334.13242
335.13394
336.13678
338.34140
333.12924
NL:
8.44E5
C 13 H 20 N 2 O 8 +H:
C 13 H 21 N 2 O 8
pa Chrg 1
334.13260
335.13349
336.13684
338.14109
m/z

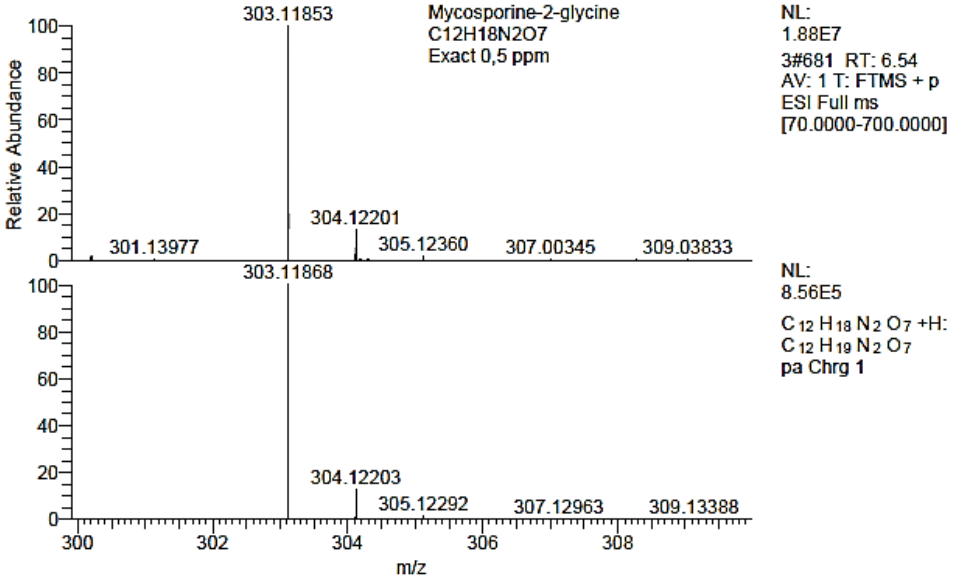
303.11853
Mycosporine-2-glycine
C12H18N2O7
Exact 0,5 ppm
NL:
1.88E7
3#681 RT: 6.54
AV: 1 T: FTMS + p
ESI Full ms
[70.0000-700.0000]
Relative Abundance
304.12201
301.13977
305.12360
307.00345
309.03833
303.11868
NL:
8.56E5
C 12 H 18 N 2 O 7 +H:
C 12 H 19 N 2 O 7
pa Chrg 1
304.12203
305.12292
307.12963
309.13388
m/z

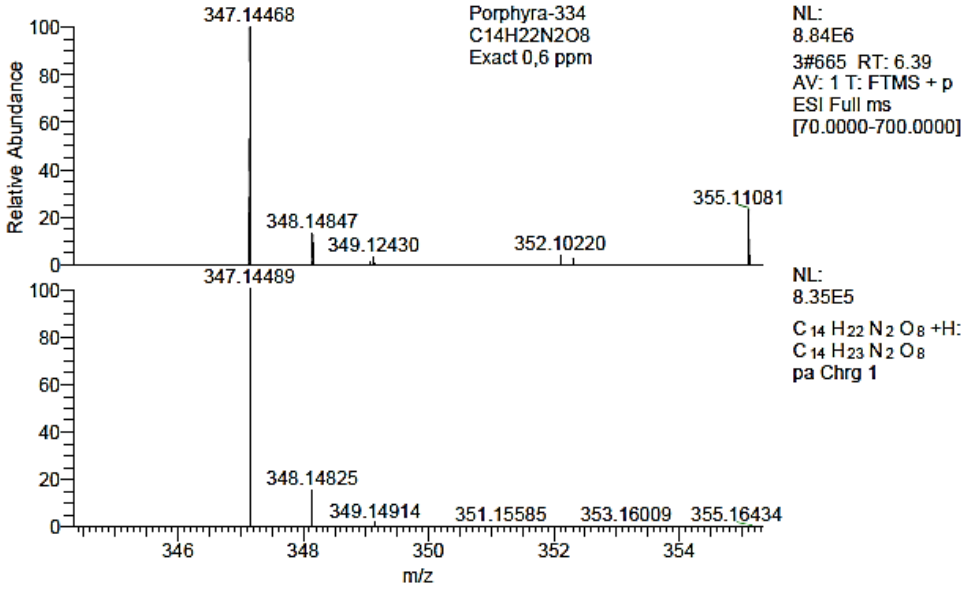
347.14468
Porphyra-334
C14H22N2O8
Exact 0,6 ppm
NL:
8.84E6
3#665 RT: 6.39
AV: 1 T: FTMS + p
ESI Full ms
[70.0000-700.0000]
Relative Abundance
355.11081
348.14847
349.12430
352.10220
347.14489
NL:
8.35E5
C 14 H 22 N 2 O 8 +H:
C 14 H 23 N 2 O 8
pa Chrg 1
348.14825
349.14914
351.15585
353.16009
355.16434
m/z

Figura S4. ESI-MS spectra of MAA peaks detected on aqueous extracts of *Gracilaria cornea*. The following spectra correspond respectively to $C_{13}H_{20}N_2O_5$, $C_{13}H_{22}N_2O_6$, $C_{12}H_{20}N_2O_6$, and palythine.

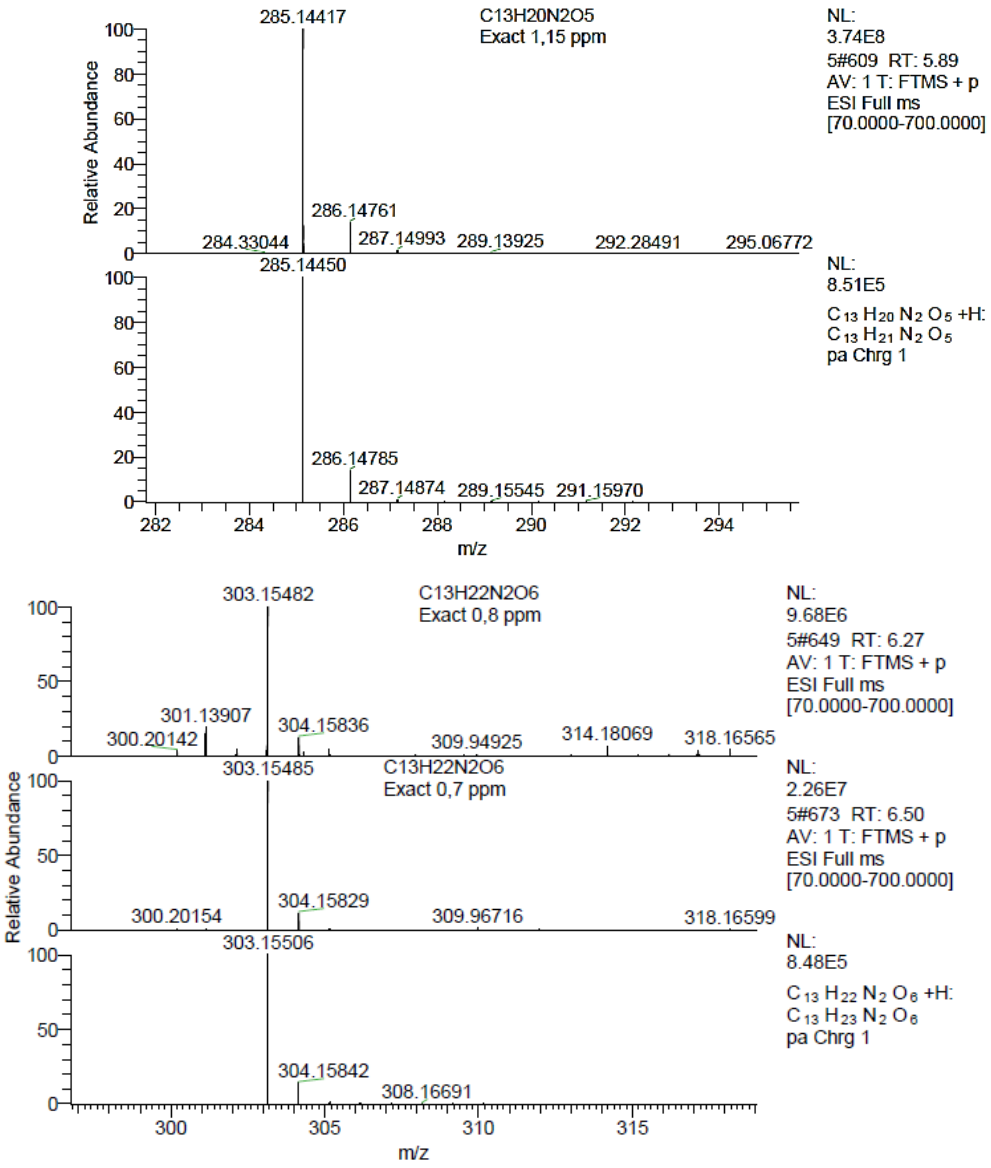

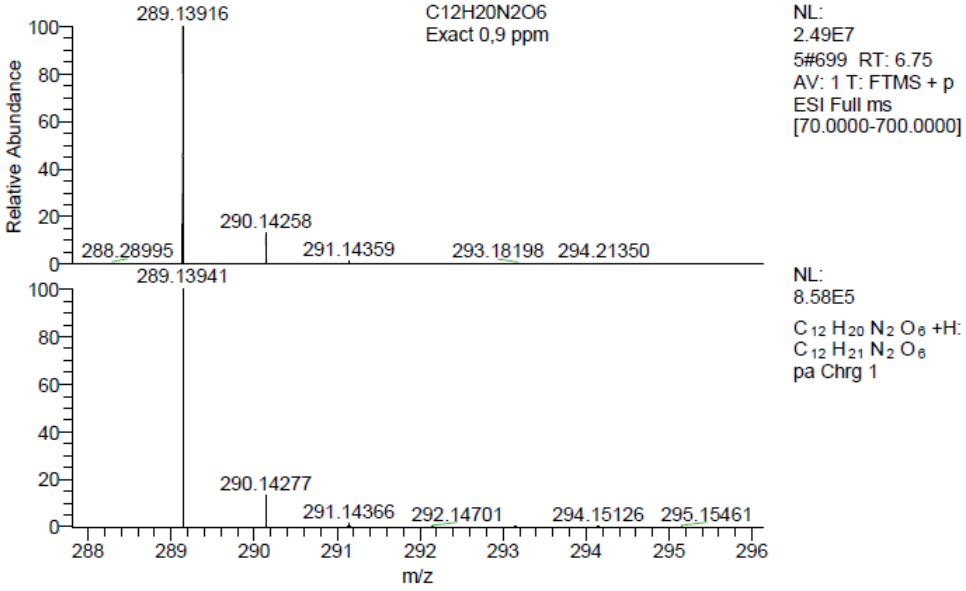
289.13916
C12H20N2O6
Exact 0,9 ppm
NL:
2.49E7
5#699 RT: 6.75
AV: 1 T: FTMS + p
ESI Full ms
[70.0000-700.0000]
Relative Abundance
290.14258
288.28995
291.14359
293.18198
294.21350
289.13941
NL:
8.58E5
C12 H20 N2 O6 +H:
C12 H21 N2 O6
pa Chrg 1
290.14277
291.14366
292.14701
294.15126
295.15461
m/z

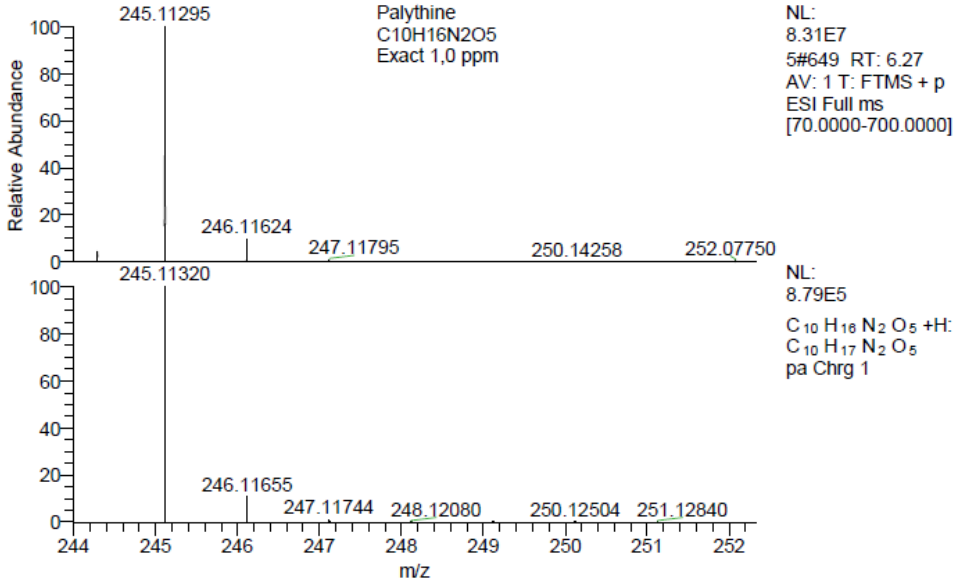
245.11295
Palythine
C10H16N2O5
Exact 1,0 ppm
NL:
8.31E7
5#649 RT: 6.27
AV: 1 T: FTMS + p
ESI Full ms
[70.0000-700.0000]
Relative Abundance
246.11624
247.11795
250.14258
252.07750
245.11320
NL:
8.79E5
C10 H16 N2 O5 +H:
C10 H17 N2 O5
pa Chrg 1
246.11655
247.11744
248.12080
250.12504
251.12840
m/z

Figura S5. ESI-MS spectra of MAA peaks detected on aqueous extracts of *Osmundea pinnatifida*. The following spectra correspond respectively to aplysiapalythine B $C_{13}H_{22}N_2O_6$, $C_{12}H_{20}N_2O_6$, and palythine.

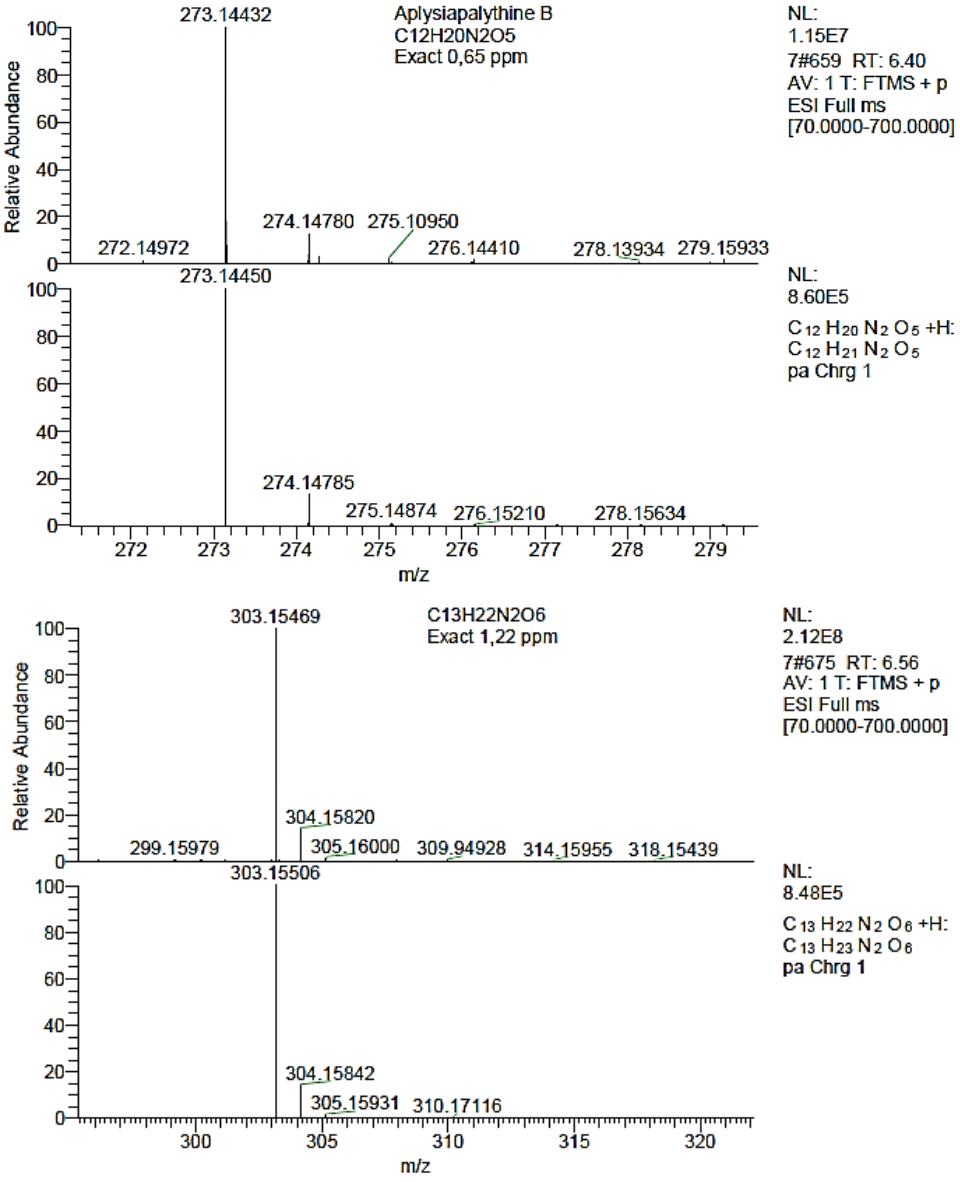

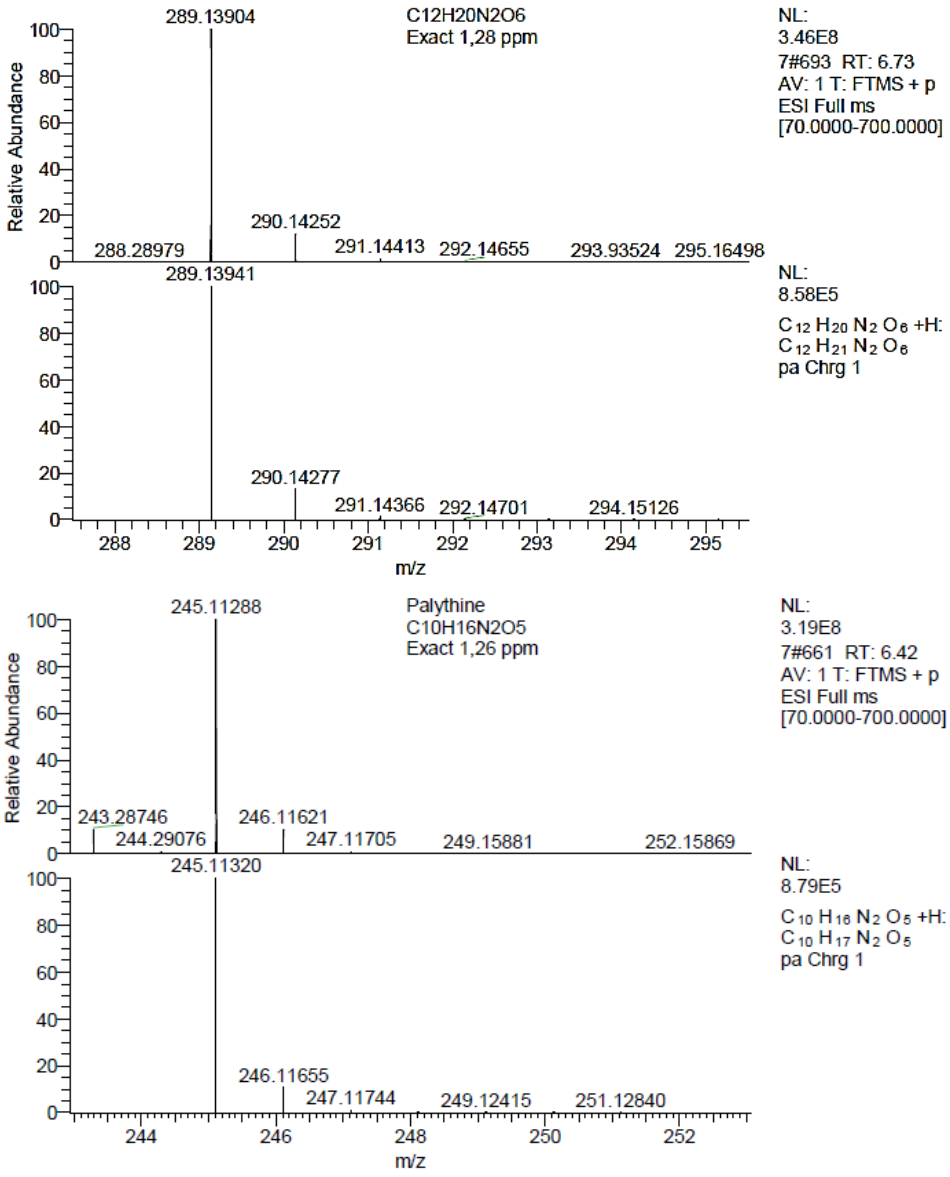
289.13904
C12H20N2O6
Exact 1,28 ppm
NL:
3.46E8
7#693 RT: 6.73
AV: 1 T: FTMS + p
ESI Full ms
[70.0000-700.0000]
Relative Abundance
290.14252
288.28979
291.14413
292.14655
293.93524
295.16498
289.13941
NL:
8.58E5
C12 H20 N2 O6 +H:
C12 H21 N2 O6
pa Chrg 1
290.14277
291.14366
292.14701
294.15126
m/z
245.11288
Palythine
C10H16N2O5
Exact 1,26 ppm
NL:
3.19E8
7#661 RT: 6.42
AV: 1 T: FTMS + p
ESI Full ms
[70.0000-700.0000]
Relative Abundance
243.28746
244.29076
246.11621
247.11705
249.15881
252.15869
245.11320
NL:
8.79E5
C10 H16 N2 O5 +H:
C10 H17 N2 O5
pa Chrg 1
246.11655
247.11744
249.12415
251.12840
m/z

Figura S6. ESI-MS spectra of MAA peaks detected on aqueous extracts of *Plocamium cartilagineum* (TA). The following spectra correspond respectively to $C_{13}H_{22}N_2O_6$, mycosporine-glutamine, $C_{12}H_{20}N_2O_6$, palythine, shinorine and palythine-serine.

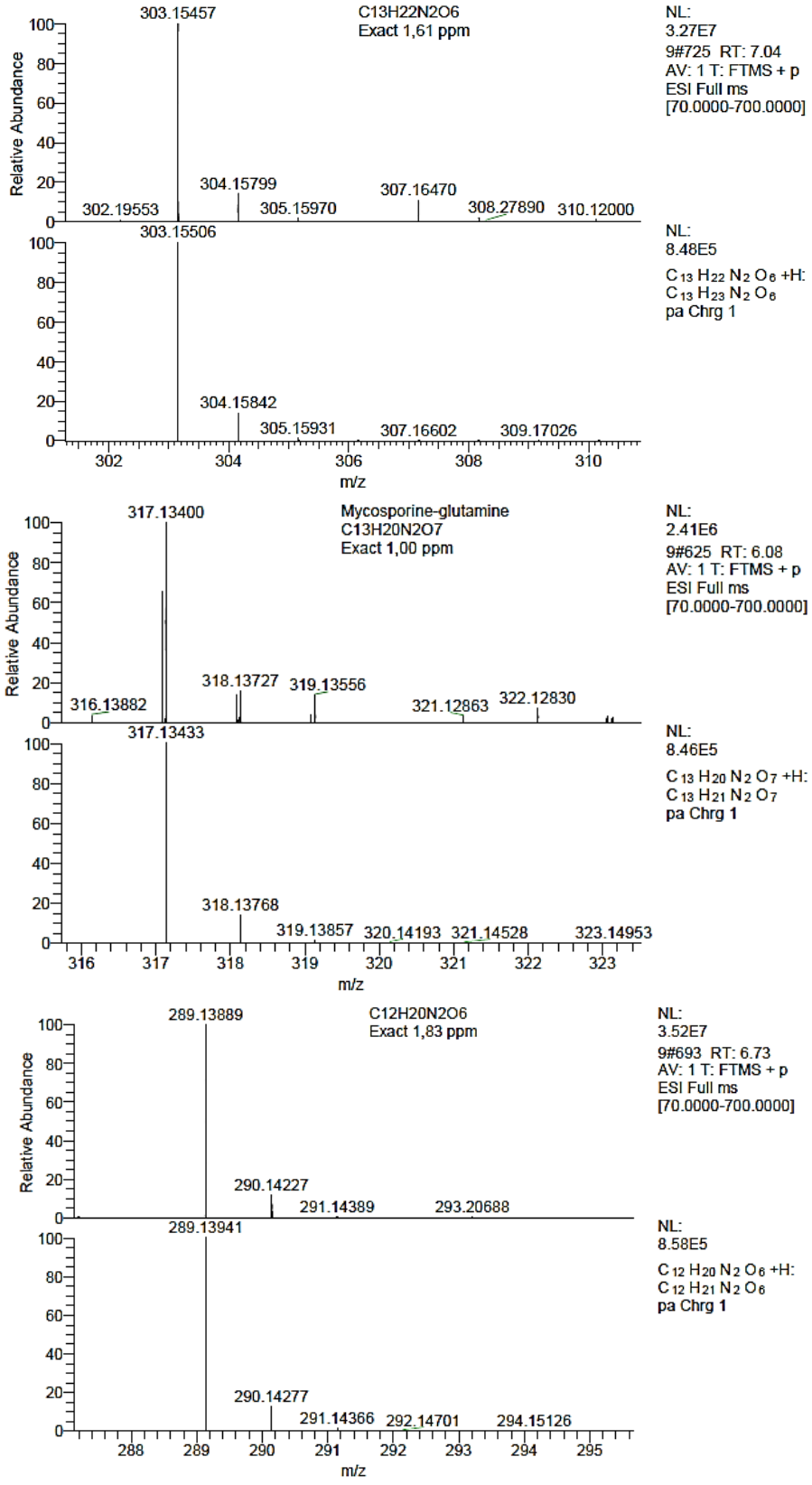

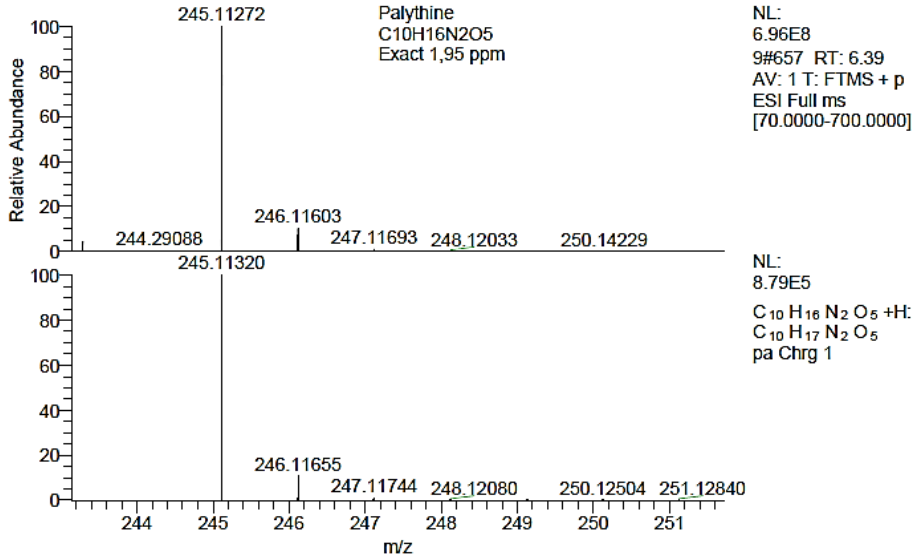
245.11272
Palythine
C10H16N2O5
Exact 1,95 ppm
NL:
6.96E8
9#657 RT: 6.39
AV: 1 T: FTMS + p
ESI Full ms
[70.0000-700.0000]
Relative Abundance
244.29088
246.11603
247.11693
248.12033
250.14229
245.11320
NL:
8.79E5
C10 H16 N2 O5 +H:
C10 H17 N2 O5
pa Chrg 1
246.11655
247.11744
248.12080
250.12504
251.12840
m/z

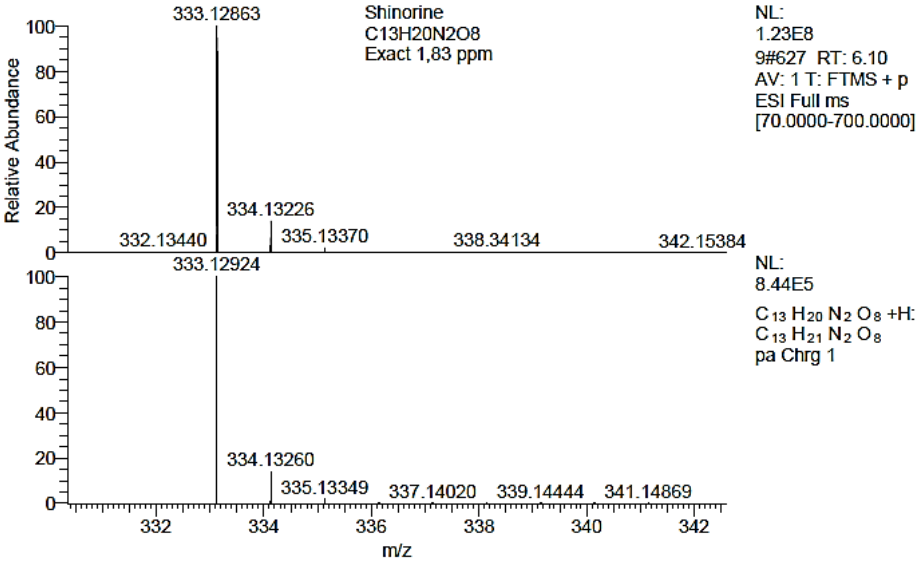
333.12863
Shinorine
C13H20N2O8
Exact 1,83 ppm
NL:
1.23E8
9#627 RT: 6.10
AV: 1 T: FTMS + p
ESI Full ms
[70.0000-700.0000]
Relative Abundance
332.13440
334.13226
335.13370
338.34134
342.15384
333.12924
NL:
8.44E5
C13 H20 N2 O8 +H:
C13 H21 N2 O8
pa Chrg 1
334.13260
335.13349
337.14020
339.14444
341.14869
m/z

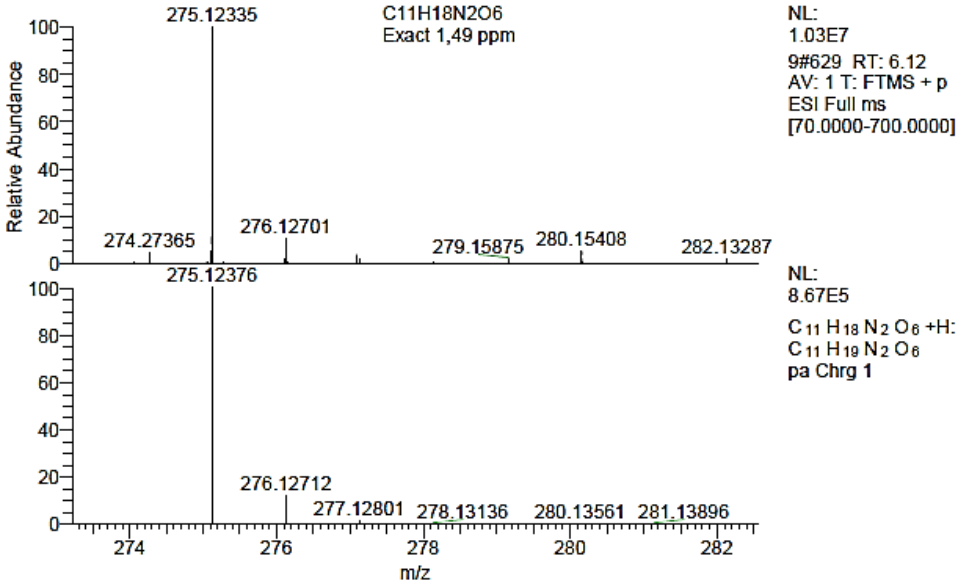
275.12335
C11H18N2O6
Exact 1,49 ppm
NL:
1.03E7
9#629 RT: 6.12
AV: 1 T: FTMS + p
ESI Full ms
[70.0000-700.0000]
Relative Abundance
274.27365
276.12701
279.15875
280.15408
282.13287
275.12376
NL:
8.67E5
C11 H18 N2 O6 +H:
C11 H19 N2 O6
pa Chrg 1
276.12712
277.12801
278.13136
280.13561
281.13896
m/z

Figura S7. ESI-MS spectra of MAA peaks detected on aqueous extracts of *Plocamium cartilagineum* (LH). The following spectra correspond respectively to mycosporine-glutamine, $C_{12}H_{20}N_2O_6$, palythine, shinorine, mycosporine-2-glycine and palythine-serine.

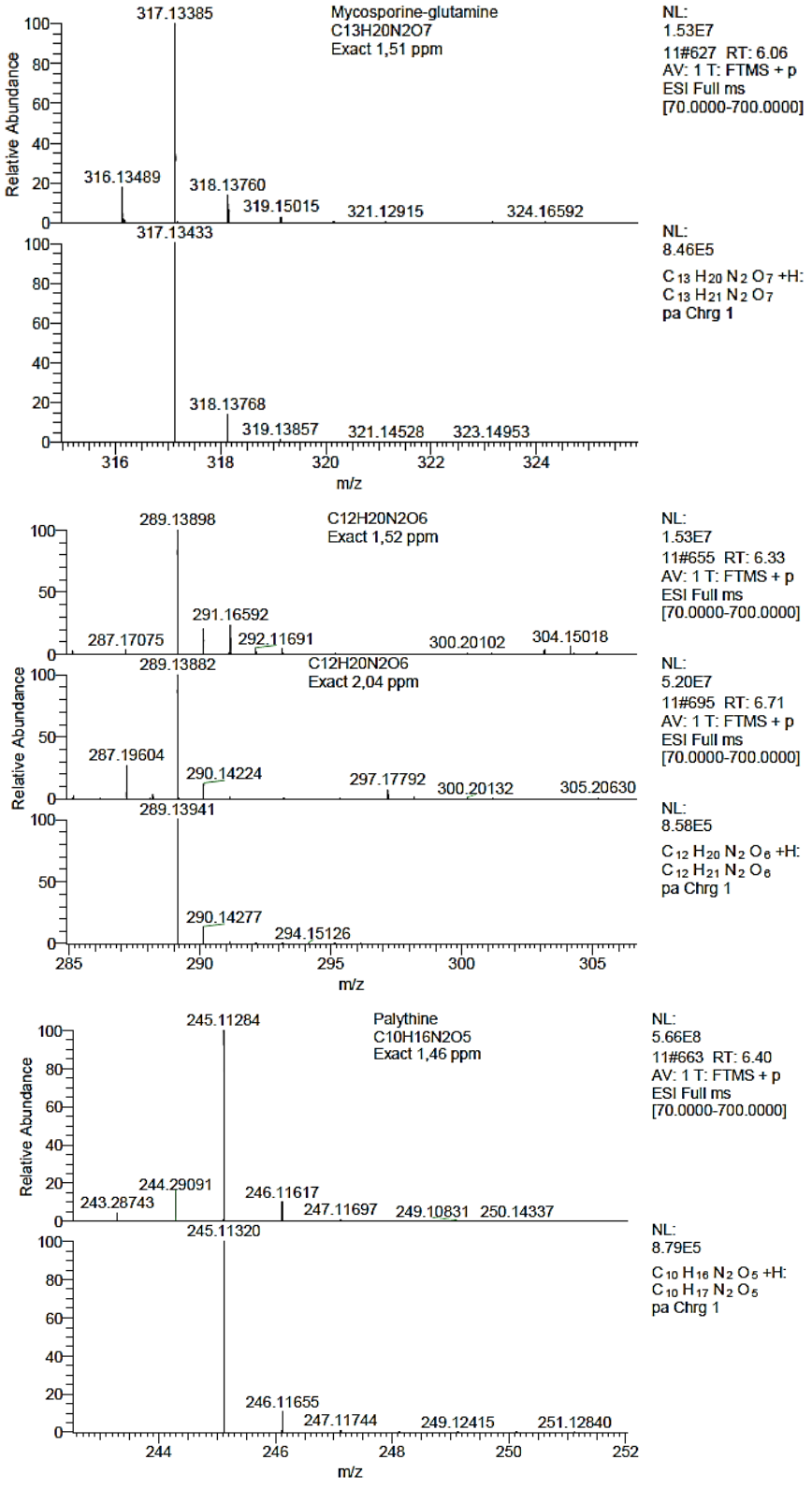

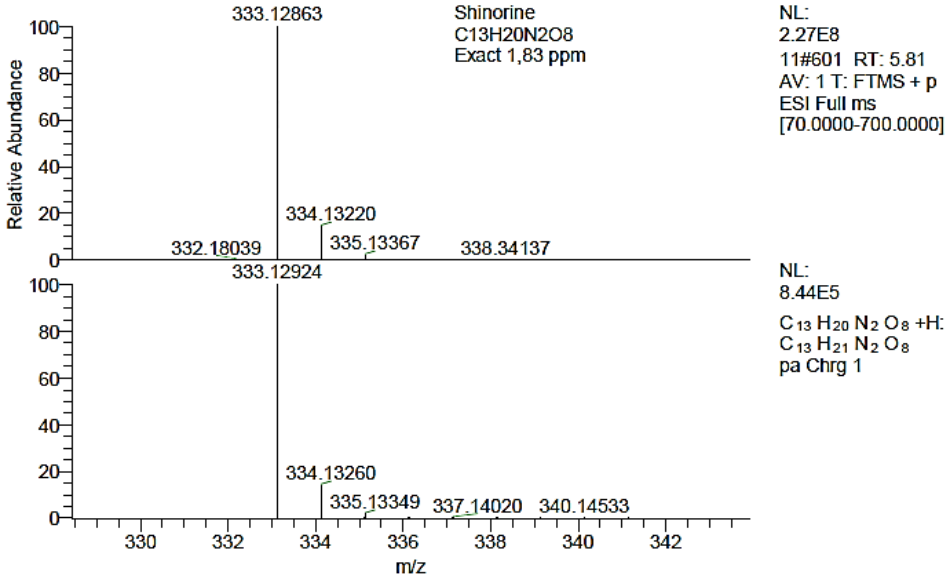
333.12863
Shinorine
C13H20N2O8
Exact 1,83 ppm
NL:
2.27E8
11#601 RT: 5.81
AV: 1 T: FTMS + p
ESI Full ms
[70.0000-700.0000]
Relative Abundance
334.13220
332.18039
335.13367
338.34137
333.12924
NL:
8.44E5
C13 H20 N2 O8 +H:
C13 H21 N2 O8
pa Chrg 1
334.13260
335.13349
337.14020
340.14533
m/z

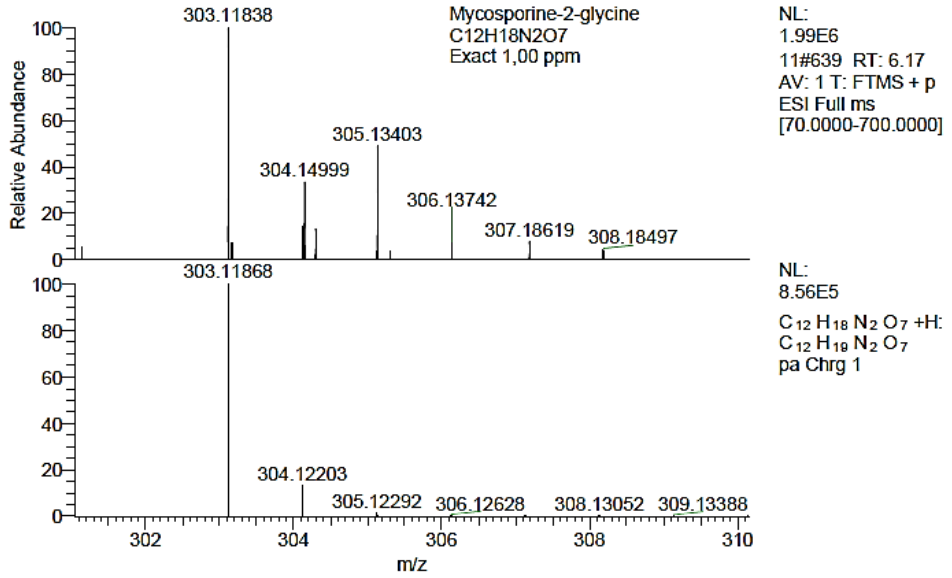
303.11838
Mycosporine-2-glycine
C12H18N2O7
Exact 1,00 ppm
NL:
1.99E6
11#639 RT: 6.17
AV: 1 T: FTMS + p
ESI Full ms
[70.0000-700.0000]
Relative Abundance
305.13403
304.14999
306.13742
307.18619
308.18497
303.11868
NL:
8.56E5
C12 H18 N2 O7 +H:
C12 H19 N2 O7
pa Chrg 1
304.12203
305.12292
306.12628
308.13052
309.13388
m/z

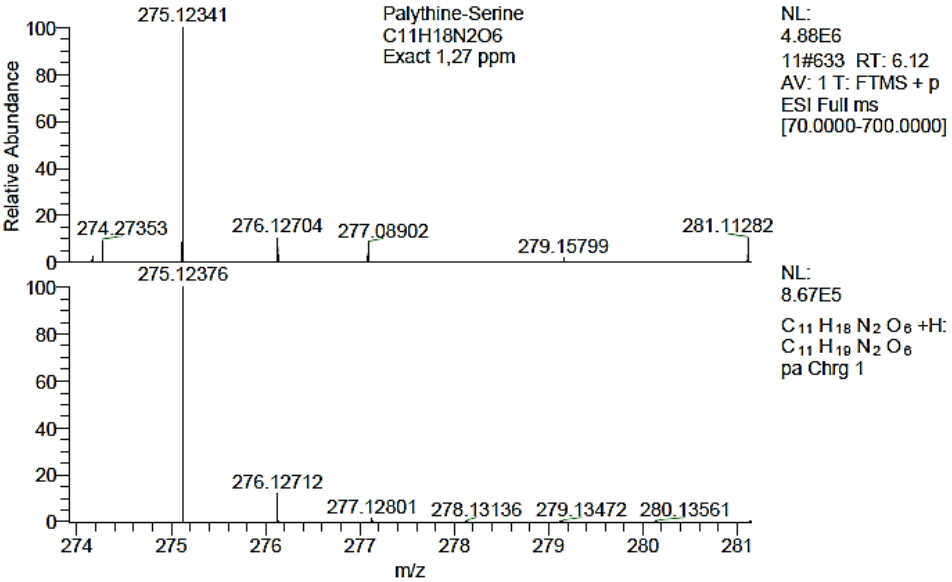
275.12341
Palythine-Serine
C11H18N2O6
Exact 1,27 ppm
NL:
4.88E6
11#633 RT: 6.12
AV: 1 T: FTMS + p
ESI Full ms
[70.0000-700.0000]
Relative Abundance
274.27353
276.12704
277.08902
279.15799
281.11282
275.12376
NL:
8.67E5
C11 H18 N2 O6 +H:
C11 H19 N2 O6
pa Chrg 1
276.12712
277.12801
278.13136
279.13472
280.13561
m/z

Tabela S4. Pearson's correlation among ABTS and total contents of polyphenols, collagenase inhibition activity, total MAAs content, phycoerythrin and phycocyanin of aqueous extracts of the red macroalgae in study.

	Polyphenol	Total MAAs	Collagenase inhibition	R-PE	PC
$ABTS^{+}$	**0.7513**	**0.7385**	**0.5557**	**0.7281**	**0.8963**
	p=0.000	**p=0.000**	**p=0.009**	**p=0.000**	**p=0.000**
Polyphenol		**0.7804**	**0.6809**	**0.5753**	**0.8248**
		p=0.000	**p=0.001**	**p=0.006**	**p=0.000**
Total MAAs			**0.9409**	**0.4434**	**0.7869**
			p=0.000	**p=0.044**	**p=0.000**
Collagenase inhibition				0.3934	**0.7026**
				p=0.078	**p=0.000**
R-PE					**0.6664**
					p=0.001

Significant values considered as a $p < 0.05$ are shown in bold. Mycosporine-Like amino acids as MAA. R-Phycoerythrin as R-PE. Phycocyanin as PC.

Tabela S5. Pearson's correlation among ABTS, polyphenol content, collagenase inhibition activity, phycoerythrin and phycocyanin of hydroethanolic extracts of the red macroalgae species studied.

	Polyphenols	Collagenase inhibition	R-PE	PC
$ABTS^{+}$	0.0486	**0.5128**	0.2258	0.0826
	p=0.834	**p=0.017**	p=0.325	p=0.722
Polyphenols		0.3757	-0.1597	**0.5678**
		p=0.093	p=0.489	**p=0.007**
Collagenase inhibition			0.1958	**0.5978**
			p=0.395	**p=0.004**
R-PE				0.3692
				p=0.100

Significant values considered as a $p < 0.05$ are shown in bold. R-Phycoerythrin as R-PE. Phycocyanin as PC.

ANEXO B – MATERIAL SUPLEMENTAR (CAPÍTULO 2)

Tabela S6. ANOVA factorial evaluating the significant differences of the effects of environmental light and time (six different times along daylight period).

Parameter	Factors	SS	Degr. of Freedom	MS	F	P
ETR	Site of collection	70123	3	23374.4	180.722	**< 0.001**
	Time	55740	5	111481	86.193	**< 0.001**
	Site x Time	45841	15	3056.1	23.628	**< 0.001**
Total MAAs	Site of collection	16.8862	3	5.6287.	25.8794	**< 0.001**
	Time	1.6838	5	0.3368	1.5483	0.1928
	Site x Time	13.1542	15	0.8769	4.0320	**< 0.001**
Chl *a*	Site of collection	195002	3	65001	21.1931	**< 0.001**
	Time	143372	5	28674	9.3491	**< 0.001**
	Site x Time	36125	15	2408	0.7852	0.6868
PE	Site of collection	1742893	3	580964	8.377	**< 0.001**
	Time	1436130	5	287226	4.141	**< 0.001**
	Site x Time	1906050	15	127070	1.832	0.0573
AC	Site of collection	749.8	3	249.9	2.0898	0.1139
	Time	657.7	5	131.5	1.0998	0.3729
	Site x Time	3171.8	15	211.5	1.7680	0.0687

Tabela S7. Photosynthetic parameters extracted from the light curves performed using *P. cartilagineum* from sites 1 and 4.

	Site 1	Site 4
F_v/F_m*	0.48 ± 0.04 [b]	0.62 ± 0.03 [a]

α_{ETR}	0.079 ± 0.022	0.077 ± 0.021
ETR_{max}	28.65 ± 14.56	46.03 ± 12.94
E_K	436.0 ± 379.9	670.4 ± 329.8

Tabela S8. Pearson's correlation between Electron Transport Rate (ETR), Mycosporine-like amino acids (MAAs), Chlorophyll *a* (Chl *a*), Phycoerythrin (PE) and Antioxidant capacity (AC). Significance level at $p < 0.05$.

	MAAs	Chl *a*	PE	AC
ETR	0.145	**-0.364**	0.123	-0.044
	p=0.224	**p=0.002**	p=0.304	p=0.716
MAAs		-0.188	-0.165	-0.137
		p=0.114	p=0.167	p=0.250
Chl *a*			**0.399**	-0.196
			p=0.001	p=0.098
PE				-0.097
				p=0.419

Tabela S9. Simple linear regression analysis results of dependent parameters of *P. cartilagineum* in response to PAR, UV-A and temperature.

Variable PAR	Intercept Mean	SD	Slope Mean	SD	R^2	p

ETR	1.30	±	2.37	0.07	±	0.00	0.93	0.00
MAAs	1.53	±	0.13	0.00	±	0.00	0.01	0.29
Chlorophyll *a*	181.48	±	14.23	-0.04	±	0.01	0.11	0.01
Phycoerythrin	1121.12	±	60.23	-0.04	±	0	0.01	0.49
Antioxidant capacity	38.71	±	2.11	0	±	0.00	0.00	0.66
Variable UV-A	Intercept Mean		SD	Slope Mean		SD	R^2	p
ETR	16.97	±	4.43	1145.07	±	92.09	0.69	0.00
MAAs	1.46	±	0.12	5.71	±	2.44	0.07	0.02
Chlorophyll *a*	171.79	±	13.07	-643.23	±	271.81	0.07	0.02
Phycoerythrin	1110.43	±	54.45	-629.83	±	1131.92	0.01	0.58
Antioxidant capacity	37.71	±	1.91	10.37	±	39.71	0.00	0.79
Variable Temperature	Intercept Mean		SD	Slope Mean		SD	R^2	p
ETR	-168.52	±	48.31	11.19	±	2.42	0.23	0.00
MAAs	0.58	±	0.84	0.05	±	0.04	0.02	0.21
Chlorophyll *a*	465.75	±	86.62	-15.85	±	4.34	0.16	0.00
Phycoerythrin	1822.84	±	369.84	-36.92	±	18.5	0.05	0.05
Antioxidant capacity	30.56	±	13.26	0.38	±	0.66	0.01	0.57

ANEXO C – MATERIAL SUPLEMENTAR (CAPÍTULO 3)

Tabela S10. Multifactorial ANOVA effects for photosynthetic parameters extracted from Rapid Light Curves, including Fv/Fm, αETR, ETR_{max} and saturation irradience (E_k), for day 7 and day 14, independently. Significative differences are shown in red ($p < 0.05$).

Day	Parameter	Factors	Degr. F	SS	MS	F	P
7	Fv/Fm	Radiation	3	0.006	0.002	0.80	0.511
		Nutrient	1	0.000	0.000	0.00	0.962
		Radiation * Nutrient	3	0.033	0.011	4.41	0.019
	Aetr	Radiation	3	0.000	0.000	0.07	0.973
		Nutrient	1	0.000	0.000	0.39	0.541
		Radiation * Nutrient	3	0.002	0.001	1.63	0.222
	ETR_{max}	Radiation	3	1.024	0.341	0.30	0.828
		Nutrient	1	1.051	1.051	0.91	0.354
		Radiation * Nutrient	3	3.974	1.325	1.15	0.360
	E_k	Radiation	3	2260	753.4	0.12	0.945
		Nutrient	1	4387	4387	0.71	0.410
		Radiation * Nutrient	3	17903	5968	0.97	0.430
14	Fv/Fm	Radiation	3	0.009	0.003	0.88	0.470
		Nutrient	1	0.000	0.000	0.02	0.881
		Radiation * Nutrient	3	0.011	0.004	1.10	0.378
	αETR	Radiation	3	0.000	0.000	0.75	0.540
		Nutrient	1	0.001	0.001	4.41	0.052
		Radiation * Nutrient	3	0.000	0.000	0.81	0.508
	ETR_{max}	Radiation	3	5.780	1.927	1.59	0.232
		Nutrient	1	2.475	2.475	2.04	0.173
		Radiation * Nutrient	3	17.41	5.805	4.78	0.015
	E_k	Radiation	3	376.4	125.5	0.35	0.788
		Nutrient	1	2368	2367	6.65	0.020
		Radiation * Nutrient	3	1857	619.1	1.74	0.200

Figura S8. *In situ* Electron transport rate (ETR) measured in *P. cartilagineum* thalli throughout the day, at 08:20, 09:45, 15:00 and 18:20, at day 1, 5, 8 and 12 of the experiment. Results are expressed in µmoL electrons m^{-2} s^{-2}.

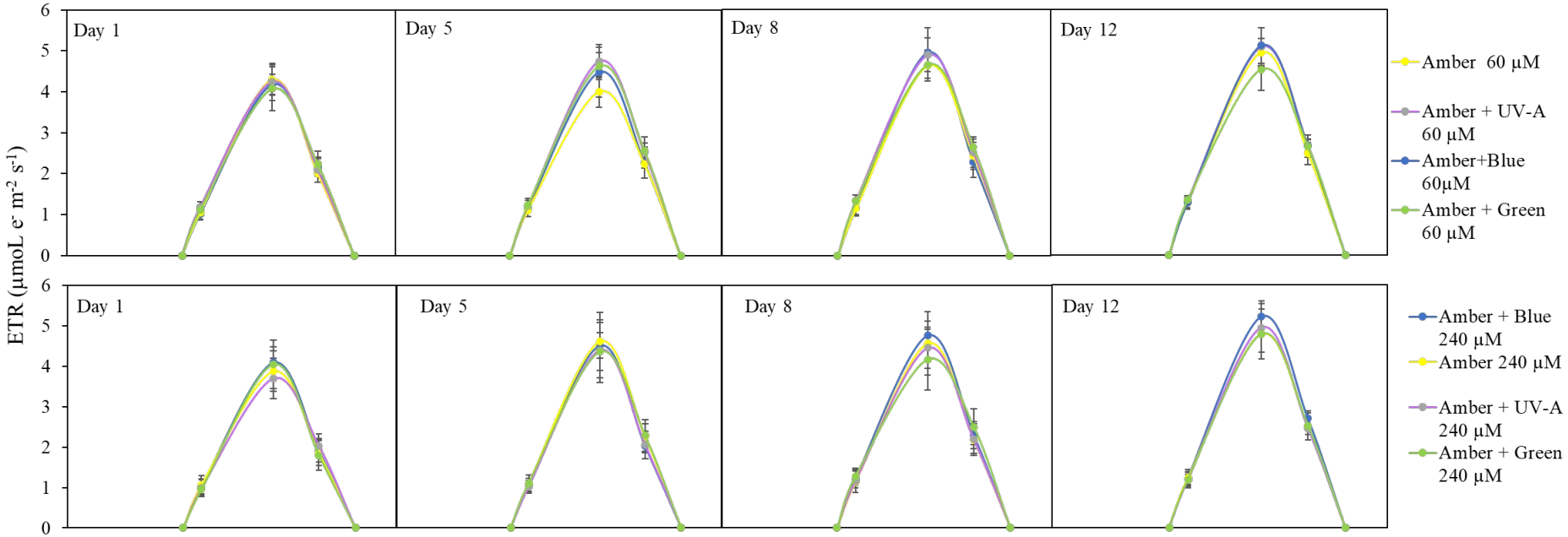

Different colors represent the different treatments: yellow is amber, violet is amber +UV, blue is amber + blue and green is amber+ green.

Tabela S11. Multifactorial ANOVA effect for $ETR_{in\ situ}$ at days 1, 5, 8 and 14, with measurements at 09:45, 15:00 and 18:20

Day	Hour	Factors	Degr. F	SS	MS	F	P
1	09:45	Radiation	3	0.017	0.006	0.43	0.737
		Nutrient	1	0.042	0.042	3.10	0.098
		Radiation * Nutrient	3	0.043	0.014	1.06	0.394
	15:00	Radiation	3	0.069	0.023	0.23	0.875
		Nutrient	1	0.407	0.407	4.07	0.061
		Radiation * Nutrient	3	0.252	0.084	0.84	0.493
	18:20	Radiation	3	0.053	0.018	0.41	0.751
		Nutrient	1	0.295	0.295	6.75	0.019
		Radiation * Nutrient	3	0.084	0.028	0.64	0.598
5	09:45	Radiation	3	0.025	0.008	0.66	0.588
		Nutrient	1	0.066	0.066	5.32	0.035
		Radiation * Nutrient	3	0.026	0.009	0.69	0.574
	15:00	Radiation	3	0.2039	0.068	0.44	0.730
		Nutrient	1	0.000	0.000	0.00	0.986
		Radiation * Nutrient	3	0.845	0.282	1.81	0.187
	18:20	Radiation	3	0.194	0.065	1.73	0.201
		Nutrient	1	0.314	0.314	8.39	0.011
		Radiation * Nutrient	3	0.186	0.062	1.66	0.216
8	09:45	Radiation	3	0.076	0.025	1.32	0.303
		Nutrient	1	0.011	0.011	0.58	0.458
		Radiation * Nutrient	3	0.049	0.016	0.86	0.481
	15:00	Radiation	3	0.690	0.230	1.87	0.176
		Nutrient	1	0.384	0.384	3.12	0.097
		Radiation * Nutrient	3	0.239	0.080	0.65	0.596
	18:20	Radiation	3	0.276	0.092	1.59	0.232
		Nutrient	1	0.236	0.236	4.07	0.061
		Radiation * Nutrient	3	0.070	0.023	0.40	0.752
12	09:45	Radiation	3	0.001	0.000	0.03	0.992
		Nutrient	1	0.068	0.068	6.21	0.024
		Radiation * Nutrient	3	0.017	0.006	0.53	0.670
	15:00	Radiation	3	0.834	0.278	3.13	0.055
		Nutrient	1	0.003	0.003	0.03	0.861
		Radiation * Nutrient	3	0.182	0.061	0.68	0.576
	18:20	Radiation	3	0.094	0.031	1.11	0.374
		Nutrient	1	0.029	0.029	1.03	0.325
		Radiation * Nutrient	3	0.079	0.026	0.93	0.449

Significative differences are shown in red ($p < 0.05$).

Tabela S12. Multifactorial ANOVA effect for NO_3 absorption, PO_4 absorption, Chlorophyll *a* (Chl a), Phycorythrin (PE), Phycocyanin (PC) and Mycosporine-like amino acids (MAAs) in *Plocamium cartilagineum* thalli at Day 7 of the experiment. The significant differences ($p < 0.05$) are shown in red.

Parameter	Factors	Degr. of Freedom	SS	MS	F	P
NO_3^- Absorption	Radiation	3	1939.5	646.5	2.83	0.07
	Nutrient	1	14357.7	14357.7	62.79	0.001
	Radiation* Nutrient	3	2206.5	735.5	3.22	0.051
PO_4^{3-} Absorption	Radiation	3	89.2	29.72	0.46	0.71
	Nutrient	1	32.7	32.67	0.51	0.486
	Radiation* Nutrient	3	361.9	120.66	1.87	0.175
Chl *a*	Radiation	3	47314	15771	5.09	0.011
	Nutrient	1	2185	2185	0.71	0.413
	Radiation* Nutrient	3	706	235	0.08	0.972
Phenolic compounds	Radiation	3	9.735	3.245	15.43	0.001
	Nutrient	1	0.958	0.958	4.56	0.048
	Radiation* Nutrient	3	2.451	0.817	3.89	0.029
PE	Radiation	3	1320485	440161	5.94	0.006
	Nutrient	1	1154720	115472	1.56	0.230
	Radiation* Nutrient	3	1296220	432073	5.83	0.007
PC	Radiation	3	1712348	570783	4.49	0.019
	Nutrient	1	705942	705942	5.56	0.031
	Radiation* Nutrient	3	1299810	433270	3.41	0.043
MAAs	Radiation	3	1.506	0.502	2.55	0.092
	Nutrient	1	1.750	1.750	8.88	0.009
	Radiation* Nutrient	3	2.421	0.807	4.09	0.025

Tabela S13. Multifactorial ANOVA effect for NO_3 absorption, PO_4 absorption, Chlorophyll *a* (Chl a), Phycorythrin (PE), Phycocyanin (PC) and Mycosporine-like amino acids (MAAs) in *Plocamium cartilagineum* thalli at Day 14 of the experiment. The significant differences ($p < 0.05$) are shown in red.

Parameter	Factors	Degr. of Freedom	SS	MS	F	P
NO_3^- Absorption	Radiation	3	1121.8	373.9	13.78	0.001
	Nutrient	1	10895.1	10895.1	401.7	0.000
	Radiation * Nutrient	3	976.4	325.5	12.00	0.001
PO_4^{3-} Absorption	Radiation	3	294.16	98.05	2.44	0.102
	Nutrient	1	490.01	490.01	12.19	0.003
	Radiation * Nutrient	3	337.33	112.44	2.80	0.074
Chl a	Radiation	3	114343	38114	1.89	0.171
	Nutrient	1	181264	181264	9.01	0.008
	Radiation * Nutrient	3	20913	6971	0.35	0.792
Phenolic compounds	Radiation	3	3.842	1.28	3.72	0.033
	Nutrient	1	1.209	1.21	3.51	0.079
	Radiation * Nutrient	3	0.740	0.25	0.72	0.556
PE	Radiation	3	3600722	1200241	2.55	0.092
	Nutrient	1	9385258	9385258	19.92	0.001
	Radiation * Nutrient	3	2774444	924815	1.96	0.160
PC	Radiation	3	496320	165440	3.90	0.029
	Nutrient	1	242496	242496	5.72	0.029
	Radiation * Nutrient	3	174263	58088	1.37	0.287
MAAs	Radiation	3	1.328	0.44	7.24	0.003
	Nutrient	1	0.301	0.30	4.89	0.042
	Radiation * Nutrient	3	1.373	0.46	7.48	0.002

Tabela S14. Multifactorial ANOVA effect for shinorine levels in *Plocamium cartilagineum* thalli at days 1, 7 and 14.

Parameter	Factors	Degr. of Freedom	SS	MS	F	P
Shinorine	Radiation	3	0.052	0.0174	9.69	0.0001
	Nutrient	1	0.082	0.082	45.41	0.0001
	Time	1	0.062	0.062	34.36	0.0001
	Radiation * Nutrient	3	0.032	0.011	5.87	0.003
	Radiation * Time	3	0.129	0.043	23.87	0.0001
	Nutrient * Time	1	0.000	0.000	0.02	0.899
	Radiation * Nutrient * Time	3	0.002	0.001	0.42	0.740

The significant differences ($p < 0.05$) are shown in red.